# Measuring and Modelling Autophagic Flux

by

André du Toit

*Dissertation presented for the degree of Doctor of Philosophy of Science (Biochemistry) in the Faculty of Science at Stellenbosch University*

Supervisor: Prof. B. Loos

Co-supervisor: Prof. J.-H. S. Hofmeyr

April 2019

Stellenbosch University https://scholar.sun.ac.za

# Declaration

By submitting this dissertation electronically, I declare that the entirety of the work contained therein is my own, original work, that I am the sole author thereof (save to the extent explicitly otherwise stated), that reproduction and publication thereof by Stellenbosch University will not infringe any third party rights and that I have not previously in its entirety or in part submitted it for obtaining any qualification.

Date: December 2018 .....

Copyright © 2019 Stellenbosch University
All rights reserved.

Stellenbosch University https://scholar.sun.ac.za

# Acknowledgements

I would like to express my sincere gratitude to my supervisors, Prof Ben Loos and Prof Jannie Hofmeyr, for their mentorship, constant guidance and patience, and their acceptance of my dyslexia through their dedication in time and effort in improving my writing skills. I wish to thank the Departments of Physiological Sciences and Biochemistry, particularly the Disease Signalling Group (DSG), for fellowship and support. Further thanks to Dr Annadie Krygsman, Dr. Danzil Joseph, Mr. Noel Markgraaff, Mr. Ashwin Isaacs, Mrs. Lize Engelbrecht, Ms. Rozanne Adams and Ms. Dumisile Lumkwana for technical support as well as Prof Maryna Van De Venter at Nelson Mandela University (NMU) for providing access to their high content screening microscopy platform and for her technical support. I also wish to acknowledge Prof Noboru Mizushima for kindly providing GFP-LC3 MEF and HeLa cells used in this study. This work was supported by grants from the National Research Foundation. I wish to thank my parents and friends for their support. Finally, and most importantly, I would like to acknowledge the role of faith in God that provided strength throughout the duration of this project, as well as Aneeta Anne Sindhu for her love and support during the good and the bad.

Stellenbosch University https://scholar.sun.ac.za

This thesis is dedicated to God and Aneeta Anne Sindhu, as well as my family and my supervisors.

Stellenbosch University https://scholar.sun.ac.za

# Contents

Stellenbosch University https://scholar.sun.ac.za

Stellenbosch University https://scholar.sun.ac.za

Stellenbosch University https://scholar.sun.ac.za

Stellenbosch University https://scholar.sun.ac.za

# List of Figures

Stellenbosch University https://scholar.sun.ac.za

Stellenbosch University https://scholar.sun.ac.za

Stellenbosch University https://scholar.sun.ac.za

# List of Tables

Stellenbosch University https://scholar.sun.ac.za

# Nomenclature

### Abbreviations

3D: Three-dimensional

ACN: Acetonitrile

AGC: Automatic gain control

Beclin 1: BCL2 interacting protein 1

BSA: Bovine serum albumine

$CO_2$: Carbon dioxide

$dH_2O$: Distilled water

DMEM: Dulbecco's Modified Eagle Medium

DMSO: Dimethylsulfoxide

ECL: Enhanced chemiluminescence

EDTA: Ethylenediaminetetraacetic acid

ER: Endoplasmic recticulum

FA: Formic acid

FBS: Foetal bovine serum

GAPDH: Glyceraldehyde-3-phosphate dehydrogenase

GFP: Green fluorescent protein

HeLa GFP-LC3: HeLa stably expressing GFP-LC3

IgG: Immunoglobulin G

KCl: Potassium chloride

$KH_2PO_4$: Potassium dihydrogen phosphate

Stellenbosch University https://scholar.sun.ac.za



LAMP-2A: Lysosome-associated membrane protein-2A

LC3: Microtubule-associated protein 1 light chain 3

LC3-PE: Microtubule-associated light chain 3-phosphatidylethanolamine (LC3 II)

LCMS: Liquid chromatography mass spectrometry

LUT: Look up table LUT

MEF: Mouse embryonic fibroblast

MEF GFP-LC3: Mouse embryonic fibroblast stably expressing GFP-LC3

MMTS: Methyl-methanethiosulphonate

mTOR: Mechanistic target of rapamycin

$Na_2HPO_4$: Disodium hydrogen phosphate

$Na_3VO_4$: Sodium orthovanadate

NaCl: Sodium chloride

NaF: Sodium fluoride

p62: Nucleoporin p62 (SQSTM1)

PAGE: Polyacrylamide gel electrophoresis

PE: Phosphatidylethanolamine

PLL-g-PEG: Polylysine-grafted polyethyleneglycol

PMSF: Phenylmethylsulfonylfluoride

pmTOR: Phosphorylated mechanistic target of rapamycin

PVDF: Poly-vinylidene fluoride

PySCeS: Python Simulator for Cellular Systems

RIPA: Radio-immunoprecipitation

ROI: Region of interest

RT: Room temperature

SDS: Sodium dodecyl sulphate

SQSTM1: Sequestosome 1 (P62)

TBS-T: Tris-buffered saline and Tween 20

Stellenbosch University https://scholar.sun.ac.za



TCE: 2,2,2-Trichloroethanol

TCEP: Tris(carboxyethyl) phosphine

TEAB: Triethylammonium bicarbonate

TEM: Transmission electron microscopy

UVO: Ultra Violet Ozone

UVRAG: UV-radiation resistance-associated gene

**Units Of Measurements**

$\mu$s: microseconds

s: seconds

min: minute

h: hour

°C: degree Celsius

kDa: kilodalton

mm: millimeter

$\mu$m: micrometer

nm: nanometer

g: gram

mg: milligram

$\mu$g: microgram

l: litre

ml: millilitre

$\mu$l: microlitre

fl: femtolitre

M: molar

mM: milliomolar

$\mu$M: micromolar

nM: nanomolar

Stellenbosch University https://scholar.sun.ac.za



mW: milliWatt

### Model Abbreviations

$J$: Flux

$P$: Phagophores

$A$: Autophagosomes

$AL$: Autolysosomes

$AA$: Amino acids

$L$: Lysosomes

$mTOR$: Mechanistic target of rapamycin

$pmTOR$: Phosphorylated mechanistic target of rapamycin

### Coefficients

$C_v^J$: Flux-control coefficient

$C_v^n$: Concentration-control coefficient

$\varepsilon_n^v$: Species elasticity coefficient

### Model Variables

$J$: Autophagosome flux ($n_{\mathrm{A}}$/hr/cell)

$v_A$: Autophagosome synthesis rate ($n_{\mathrm{A}}$/hr/cell)

$\tau$: Transition time (hr)

$n_{\mathrm{species}}$: Species concentration (number/cell)

$A$: Autophagosomes ($n_{\mathrm{A}}$/cell)

$AL$: Autolysosomes ($n_{\mathrm{AL}}$/cell)

$L$: Lysosomes ($n_{\mathrm{L}}$/cell)

Stellenbosch University https://scholar.sun.ac.za

# Summary

**Introduction.** Autophagy is an evolutionarily-conserved cellular process of self-digestion, wherein cytoplasm and organelles are sequestered and delivered to lysosomes for degradation. Autophagy plays a vital role in maintaining cellular function and proteostasis through the recycling of cellular components; it generates the building blocks for *de novo* synthesis and substrates for energy generation during periods of nutrient deprivation. It also serves to protect cells against diverse pathologies by removing potentially harmful proteins and organelles. Autophagy has been linked to the progression of several diseases; the loss of autophagy function leads to the build up of toxic compounds, such as those associated with neurodegeneration, while enhanced autophagy activity contributes to the resistance of cancer against chemotherapeutic drugs. The role of autophagy in disease has made it an attractive therapeutic target for the treatment of several diseases. Clinical trials using autophagy modulators have already shown promising results. The success of autophagy-targeting therapies depends, however, on our ability to accurately measure autophagy and characterise autophagy modulators, as well as unravelling its role in disease both on a mechanistic (single cell) and a global (whole organ) level. We previously developed a fluorescence-based microscopy technique for accurately measuring autophagosome flux that showed great promise.

**Aims.** The first aim of this project was to validate the reliability and applicability of our approach to accurately measure autophagosome flux and autophagy intermediates. The second aim was to use this technique for the screening of several autophagy modulating-drugs and then, as our third aim, to identify novel biomarkers that could serve as indicators of autophagosome flux in a clinical setting. The

Stellenbosch University https://scholar.sun.ac.za



fourth aim was to use our approach to investigate the underlying mechanism of autophagy that could provide context for understanding the dynamic nature of autophagy. Our fifth aim, as an extension of our previous modelling efforts, was to perform supply and demand analysis to characterise the distribution of flux and concentration control of the autophagic steady state. Our final aim was to bridge the gap between *in vitro* and *ex vivo* by characterising the three-dimensional spatial organisation of autophagy pathway intermediates in brain tissue.

**Methods.** A fluorescence-based imaging approach was employed to measure autophagy variables in mouse embryonic fibroblasts (MEF) and HeLa cells that stably express GFP-LC3. Cells were cultured in the presence of an acidotrophic fluorescent dye that allows, in combination with GFP-LC3, the visualisation of autophagosomes, autolysosomes and lysosomes. We calculated the autophagosome flux as the initial rate of increase in the number of autophagosomes after inhibition of fusion between autophagosomes and lysosomes using bafilomycin $A_1$. We validated the reliability and applicability of this approach through a series of experiments: measuring autophagosome flux in autophagy-silenced cells, evaluating alternative probes, and comparing our approach to a recently-developed flux probe. Then we used this approach to screen several clinically relevant autophagy modulators and characterised their dose-response and time-response curves. Proteomic analysis was performed on MEF cells with autophagy being induced by 25% and 75% using rapamycin and spermidine to identify novel biomarkers of autophagosome flux. A partial-inhibition-of-fusion group was included to filter false positive markers. To investigate the underlying mechanism of autophagy we used our approach to (i) assess cytoplasmic cargo (volume) turnover by measuring autophagosome size and flux before and after induction with rapamycin, spermidine and FBS, (ii) determine changes in the tubulin-associated translocation rate and displacement of autophagosomes in response to induction with rapamycin and spermidine, and in response to partial inhibition with bafilomycin $A_1$, by acquiring an image series of MEF GFP-LC3 cells to analyse autophagosomal movement with TrackMate, and (iii) assess whether autophagosome flux changed in rela-

Stellenbosch University https://scholar.sun.ac.za



tion to cell size. For the supply and demand analysis the autophagic response to rapamycin induction was used to determine the demand elasticity coefficient and rate characteristics, while the supply elasticity coefficient and rate characteristics were determined by incrementally decreasing the rate of fusion of autophagosomes and lysosomes using bafilomycin $A_1$ and measuring the autophagy variables. Finally, brains were harvested from mice and polymerised in an acrylamide and paraformaldehyde solution. The hydrogel-tissue matrix was made transparent using a 3D-printed clearing station and stained for autophagy markers (LC3, p62 and LAMP2A). Tissue was imaged using a light-sheet and a confocal microscope.

**Results.** Our method quantified the autophagosome flux and the autophagy intermediates in a reliable and robust manner, and was able to detect small changes in autophagy activity, something that was not possible with the other flux probes. It proved to be suitable for high-throughput platforms and was flexible enough to accommodate a range of probes. Drug screening allowed for the characterisation of the dose response curve with high precision, demonstrating that it is possible to finely modulate autophagy. We identified several autophagosome flux markers, the majority being cytosolic proteins that decrease with increasing autophagosome flux. Moreover, proteomic analysis revealed that autophagy machinery proteins are not best suited as flux markers. We were able to shed light on the underlying mechanism of autophagy through a series of experiments that showed that (i) mTOR-dependent induction of autophagy modulates both autophagosome flux and autophagosome size, while mTOR-independent induction only modulates autophagosome flux, (ii) autophagosome flux increases in relation to cell size, and (iii) an increase in autophagosome flux leads to a decrease in the rate of autophagosome translocation. Supply and demand analysis revealed that the supply of autophagosomes (synthesis of autophagosomes) determines flux through the autophagy vesicular pathway while the demand of autophagosomes (their fusion with lysosomes) controls the homeostatic maintenance of autophagosomes under normal physiological conditions. Finally, we demonstrated it is possible to assess autophagy pathway intermediates in a three-dimensional neuroanatomical context.

Stellenbosch University https://scholar.sun.ac.za



**Conclusion.** Our approach quantifies autophagy variables in a robust and reliable manner and promises to be a technique of choice for characterising autophagy modulators. Biomarkers identified in this study could serve as a starting point for developing assays that can be used to measure autophagosome flux in a clinical setting. The data generated in our study of the autophagy system contributes to our understanding of autophagy as a whole and paves the way to the point where we will be able to finely modulate autophagy.

Stellenbosch University https://scholar.sun.ac.za

# Opsomming

**Inleiding.** Autofagie is 'n evolusionêr-bewaarde sellulêre proses van selfvertering, waarin sitoplasma en organelle in vesikels gesekwestreer word en na lisosome afgelewer word vir degradasie. Autofagie speel 'n belangrike rol in sellulêre funksie en proteostase deur die herwinning van sellulêre komponente; dit genereer beide boustene vir *de novo* sintese van proteïene en substrate vir energieproduksie gedurende periodes van voedingstoftekorte. Dit beskerm ook selle teen diverse siektetoestande deur die verwydering van potensieel skadelike proteïene en organelle. Autofagie is al geassosieer met verskeie siektes: 'n afname in autofagie degradasiekapasiteit lei tot die opbou van skadelike proteïene, soos diè geassosieer met neurodegenerasie, terwyl verhoogde autofagie-aktiwiteit bydra tot die robuustheid van kanker teenoor chemoterapeutiese middels. Hierdie eienskappe maak autofagie 'n aantreklike terapeutiese teiken vir die behandeling van verskeie siektes. Kliniese proewe wat van autofagiemoduleerders gebruik maak het alreeds goeie resultate getoon. Die sukses van autofagie-geteikende terapieë hang af van ons vermoë om autofagie akkuraat te meet en autofagiemoduleerders te karakteriseer, asook om autofagie se rol in siekte op 'n meganistiese (enkele sel) en 'n globale (hele orgaan) vlak te ontrafel. Ons het voorheen 'n fluoressensie-gebaseerde mikroskopiese tegniek om autofagosoomfluksie akkuraat te kan meet ontwikkel wat belowende resultate getoon het.

**Doel.** Die doel van hierdie projek was eerstens om die betroubaarheid en toepaslikheid van ons tegniek om die autofagosoomfluksie en sy intermediêre akkuraat te kan meet te bevestig. Die tweede doel was om dit te gebruik om verskeie autofagiemodulerende-middels te evalueer, en dan, as ons derde doel, om nuwe

Stellenbosch University https://scholar.sun.ac.za



merkers te identifiseer wat as meetbare aanwysers van autofagosoomfluksie in 'n kliniese omgewing te kan dien. Die vierde doel was om ons tegniek te gebruik om van die onderliggende autofagiese meganisme te ondersoek om ons begrip van die dinamiese aard van autofagie te verbeter. Ons vyfde doelwit, as uitbreiding van ons vorige modelleringspogings, was om 'n aanbod-aanvraag analise te doen op autofagie om die verspreiding van fluksie- en konsentrasiekontrole te karakteriseer. Laastens, met die doel om die gaping tussen *in vitro* en *ex vivo* te oorbrug, het ons 'n weefselverhelderingstegniek ge-evalueer om die 3-dimensionele organisasie van autofagie intermediêre in breinweefsel te karakteriseer.

**Metodes.** Fluoressensie-gebaseerde afbeelding is gebruik om autofagie veranderlikes in muis embrioniese fibroblaste (MEF) en HeLa selle wat stabiele GFP-LC3 uitdruk te meet. Selle is gekweek in die teenwoordigheid van 'n asidotrofiese fluoresserende kleurstof wat in kombinasie met GFP-LC3 die visualisering van autofagosome, autolisosome en lisosome moontlik maak. Die autofagosoomfluksie is bereken as die aanvanklike snelheid waarmee autofagosome toeneem na inhibisie van fusie van autofagosome en lisosome met bafilomisien. Die betroubaarheid en toepaslikheid van hierdie tegniek is bevestig deur autofagosoomfluksie te meet in selle waarin autofagie stilgemaak is, alternatiewe probes te evalueer, en ons benadering met 'n onlangs ontwikkelde fluksie-probe te evalueer. Daarna het ons die tegniek gebruik om verskeie klinies-relevante autofagiemoduleerders te evalueer en hul dosis- en tyd-responskurwes te karakteriseer. Proteomiese analise is uitgevoer op MEF selle waarvan die autofagosoomfluksie met 25% en 75% geinduseer is deur rapamisien en spermidien om nuwe merkers van autofagosoomfluksie te identifiseer. 'n Groep selle waarvan die fusie gedeeltelik met bafilomisien geinhibeer is is ingesluit om vals positiewes uit te filtreer. Om die onderliggende autofagiese meganisme te ondersoek het ons ons benadering gebruik om (i) die verandering in sitoplasmiese omset in respons op rapamisien, spermidien en FBS te bepaal deur autofagosoomgrootte en autofagosoomfluksie te meet voor en na induksie, (ii) die veranderinge in die tubulien-geassosieerde translokasietempo en verplasing van autofagosome te bepaal in respons op rapamisien, spermidien en bafilomisien

Stellenbosch University https://scholar.sun.ac.za



in MEF GFP-LC3 selle deur die verkryging van 'n beeldreeks om autofagosoom beweging met TrackMate te ontleed, en (iii) te bepaal of autofagosoomfluksie in verhouding tot selgrootte verander. Vir die aanbod-aanvraaganalise is die autofagie respons op rapamisien gebruik om die aanvraag elastisiteitskoeffisiënt en die aanvraag snelheidskarakteristiek van autofagosome te bepaal, terwyl die aanbod elastisiteitskoeffisiënt en aanbod-snelheidskarakteristiek bepaal is deur inkrementele inhibisie van fusie met bafilomisien en meting van die autofagie veranderlikes. Laastens is geïsoleerde muisbreine gepolimeriseer in 'n akrielamied en paraformaldehied-oplossing. Die hidrogel-weefselmatriks is deursigtig gemaak met behulp van 'n 3D-gedrukte skoonmaakstasie en gekleur vir autofagiemerkers (LC3, P62 en LAMP2A). Weefsel is afgebeeld deur gebruik te maak van 'n ligveld en 'n konfokale mikroskoop.

**Resultate.** Ons benadering kon autofagosoomfluksie en autofagie-intermediate op 'n betroubare en robuuste wyse kwantifiseer, en was in staat om klein veranderinge in autofagie aktiwiteit te bespeur, iets wat nie moontlik was met die ander fluksie-probes was nie. Dit is geskik vir hoë-deurset afbeeldingplatforms en kan 'n reeks probes akkommodeer. Ons kon met hoë akkuraatheid die dosis-responskurwes van autofagiese moduleerders karakteriseer, wat daarop wys dat dit moontlik is om autofagie fyn te kan moduleer. Ons het verskeie autofagosoomfluksiemerkers geïdentifiseer, waarvan die meerderheid sitosoliese proteïene was wat afneem met toenemende autofagosoomfluksie. Proteoomanalise het ook getoon dat die proteïene van die autofagie-masjinerie nie goeie fluksiemerkers is nie. Die autofagiestelsel se onderliggende meganisme is uitgelig deur 'n reeks eksperimente wat gewys het dat (i) mTOR-afhanklike induksie van autofagie beide autofagosoomfluksie en autofagosoomgrootte moduleer, terwyl mTOR-onafhanklike induksie slegs autofagosoomfluksie moduleer, (ii) autofagosoomfluksie toeneem met 'n toename in selgrootte, en (iii) 'n toename in autofagosoomfluksie lei tot 'n afname in die tempo van autofagosoomtranslokasie. Aanbod-aanvraaganalise het aangedui dat die aanbod van autofagosome (sintese van autofagosome) die fluksie deur die autofagiese vesikulêre pad bepaal, terwyl die aanvraag van autofagosome (fusie

Stellenbosch University https://scholar.sun.ac.za



met lisosome) die homeostatiese instandhouding van autofagosome onder normale fisiologiese toestande beheer. Laastens het ons gewys dat dit moontlik is om die autofagie-intermediate in 3-dimensionele neuro-anatomiese konteks te beskryf.

**Gevolgtrekking.** Ons benadering kwantifiseer autofagie veranderlikes op 'n robuuste en betroubare manier en blyk 'n goeie tegniek te wees vir die karakterisering van autofagiemoduleerders. Die autofagiese fluksiemerkers wat in hierdie studie geïdentifiseer is kan dien as 'n beginpunt vir die ontwikkeling van toetse wat effektief in 'n kliniese omgewing gebruik kan word om autofagosoomfluksie te assesseer. Die data uit hiedie studie dra by tot ons begrip van autofagie as geheel en stel ons in staat om autofagie fyn te moduleer.

Stellenbosch University https://scholar.sun.ac.za

# Chapter 1

# Introduction

Autophagy was first observed in the 1950's by Clark [39] and Novikoff [205] when they found partially-digested organelles in a double membrane vesicle. Later in 1960's de Duve and Wattiaux [44] coined the term autophagy and described the stepwise progression of the autophagy vesicles. Initially, the reason as to why a cell would digest parts of itself was perplexing, but as time progressed it became clear that autophagy serves as a cellular degradation system. With the advent of the twenty-first century, new molecular tools made it possible to unravel the molecular machinery of autophagy as well as its regulatory mechanisms. While yeast models revealed much of the molecular machinery involved in autophagy, it was mouse models that made the importance of its physiological role apparent. Under normal physiological conditions, autophagy serves as a homeostatic mechanism by removing unused and non-functional proteins and organelles, thereby maintaining cellular integrity. Even more so, it acts as an adaptive response to stress; for instance, during periods of starvation autophagy supplies amino acids for energy production by increasing protein degradation. On the other hand, the loss of autophagy activity can have detrimental effects, and is implicated in the progression of several diseases, most notably neurodegenerative diseases, due to the build-up of harmful proteins and organelles that would otherwise be degraded via autophagy. These attributes have led to autophagy being viewed as an attractive therapeutic target for treating diseases as well as promoting overall health.

Stellenbosch University https://scholar.sun.ac.za



Although preclinical trials of autophagy-targeting interventions have shown promising results, the success of autophagy-targeting therapies depends on several key factors. First, an in-depth understanding of the autophagy molecular machinery and its regulation, and how defects in autophagy contribute to disease pathology is required. Chapter 2 is an extensive literature review of the latter aspect. Second, being able to accurately measure autophagy activity in order to determine whether or not autophagic flux is too high or too low as well as to characterise autophagy-modulating drugs in both healthy and diseased cells is equally needed. There are a number of techniques used to assess autophagy that are discussed in Chapter 2. Although they often generate invaluable information about the internal workings of the autophagic machinery and its regulatory components, they are not well suited to measuring the autophagosome flux, which we have defined as the rate of flow through the pathway at steady state [168]. We previously described a fluorescence-based microscopy method for measuring the autophagosome flux in live cells [50]. As part of our aim of this study, we tested the reliability of our approach and compared it to other techniques. Using our approach we screened several clinical and autophagy modulating drugs, thereby paving the way forward for controlling autophagy activity. Despite the usefulness of our approach, employing it in a clinical setting will not be without its challenges, and therefore, as an additional study, we set out to identify novel autophagosome flux markers that could be easily assessed in a clinical setting. The results of these investigations are described in Chapter 4.

Despite a great deal being known about the individual processes involved in autophagy, its underlying mechanism remains poorly understood. This is in part due to the complexity of reactions involved in the autophagy process. In order to successfully exploit the autophagic system for therapeutic purposes, it is not only necessary to be able to numerically quantify autophagic flux, but also to be able to determine the degree of control each step exerts over the autophagic system. One of the ways of gaining this type of insight is to use a computational approach to interrogate complex networks such as autophagy by constructing a mathematical model of the autophagic system with which the dynamic and steady-

Stellenbosch University https://scholar.sun.ac.za



state behaviour of the system can be studied. In Chapter 2 we describe several important computational studies of autophagy and how they contribute to our understanding of its system properties. In Chapter 5 we describe the development of a kinetic model of autophagy that simulates the experimentally-determined time-course of the autophagic vesicles during the process of autophagy; this model is similar to the type of model used to study metabolism. The way we developed the model allowed us to associate the different steps in autophagy with different parts of the time-course. We also describe the results of an experimental supply and demand analysis to determine the distribution of the flux control of autophagy.

The link between autophagy and neurodegenerative diseases has lead to a considerable amount of research to develop autophagy targeting therapies to treat related diseases such as Alzheimer's disease. Yet, little is known about the distribution of autophagy activity or its pathway intermediates throughout the brain and how it impacts disease pathology in the three-dimensional neuroanatomical context. These type of insights would potentially aid in developing efficient autophagy targeting therapies. With this in mind, we assessed an advanced tissue-clearing technique, CLARITY, that captures cellular components *ex vivo* in a transparent hydrogel matrix for its ability to determine the organisational distribution of autophagy in the global context of the brain. In Chapter 6 we describe the development of a minimal tissue clearing station and imaging approach, and the data generated to assess its feasibility for characterisation of autophagy in the global perspective.

Chapter 7 is a general discussion that places our results in the context of related published work and maps out future studies that may build on the foundation laid by our study.

Stellenbosch University https://scholar.sun.ac.za

# Chapter 2

# Literature review

## 2.1 Introduction

Autophagy is an evolutionarily-conserved intracellular degradative process which plays a critical role in maintaining cellular function. It acts as a homeostatic mechanism that sequesters and degrades intracellular components such as proteins and organelles, thereby refreshing the cytoplasmic content by removing old, unused and potentially harmful, proteins and organelles. Autophagy is a multi-step process that is tightly regulated by a broad nutrient- and stress-sensing network. The induction of autophagy activates the recruitment of autophagy-related proteins (Atg) that partake in the formation and elongation of a cytoplasmic sequestering vesicle known as a phagophore. Once matured, the developing phagophore encapsulates cytoplasmic cargo into a double-membraned vesicle called an autophagosome, that fuses with lysosomes to form autolysosomes, in which the hydrolytic degradation of autophagic cargo occurs. The digestive products, mainly amino acids, are transported out of the autolysosome for recycling. Autophagy is a constitutively active process that plays different roles in the cell depending on the mode of activation. Constitutive (basal level) autophagy greatly contributes to maintaining quality control and protecting the cell from nutrient fluctuations, stress, and harmful proteins/organelles. In this way, autophagy preserves the cell's integrity, promoting cellular "health" and longevity. During periods of stress, such

Stellenbosch University https://scholar.sun.ac.za



as starvation, autophagy is upregulated and protects the cell by degrading proteins and organelles to be used as energy reserves [228]. Moreover, abnormally upregulated autophagy may result in autophagic cell death via the destruction of essential regulatory mechanisms that may impair cellular function to the extent of cellular demise [34].

Recent studies have shown that autophagy, or the lack thereof, contributes to the progression of several diseases, including neurodegenerative diseases and cancer. For instance, the reduction in autophagic degradative capacity leads to the build-up of deleterious protein aggregates in the neurons of Alzheimer's Disease (AD) patients [225], whereas in cancer, its upregulation is believed to contribute to the resistance of cancerous cells [282]. Current treatment strategies aim to exploit autophagy as a therapeutic target. Although in the last decade physiological and molecular studies have greatly contributed to our understanding of the basic molecular machinery involved in autophagy and its regulation, many details remain unexplored. Specifically, understanding the degree of control regulatory mechanisms have on autophagic activity could significantly impact drug development and treatment methods. In view of this, creating a mathematical model of the autophagic system could contribute greatly towards our understanding of the autophagic system, and may shed light on areas that are less accessible by conventional means, as well as aid in the process of developing enhanced therapeutic strategies.

In this review we aim to describe the autophagy process, from its molecular machinery to regulatory mechanisms, and its physiological role in maintaining cellular integrity. Also, the consequences of dysfunctional autophagy in organism development and its involvement in disease pathology will be discussed. With the aim to exploit autophagy for therapeutic purposes, we point out several key requirements for successfully modulate autophagy, one of which is understanding the dynamic nature of the autophagy process, which remains poorly understood. We will briefly review current techniques used in the field to measure autophagy activity and highlight some of their inherent challenges in unravelling the nature of the autophagy process.

Stellenbosch University https://scholar.sun.ac.za



Finally, we will review several computational models described in literature and how they contribute to understanding the underlining properties of the autophagy process. In recent years, a number of autophagic models have emerged that are used to investigate various aspects of the autophagic system. Some of these extensively model the autophagic regulatory mechanisms, i.e., the signalling pathways [121], whereas others only focus on the autophagic pathway, i.e., the vesicular machinery [22, 175]. The subject of this review is to discuss the use of several computational models described in literature, with the emphasis being on what is modelled (what is being investigated), the model itself (was it based on experimental data and how was it parameterised, and was it validated with independent experimental data), as well as how each model uniquely contributed to the field. Given that these mathematical frameworks model various aspects of the autophagic system, we will describe (in Section 2.6) the autophagy process mechanistically, in conjunction with published models of which we highlight key aspects.

## 2.2 The autophagy pathway

In all living organisms, cells are in a constant state of dynamic shifting to remove and replenish intracellular components in order to promote healthy growth and development, as well as to adapt to changes in both the micro- and macro-environment. The balance between cellular biosynthesis and intracellular degradation is crucial for maintaining cellular integrity. There are two major mechanisms by which intracellular proteins are degraded: the ubiquitin-proteasome pathway (UPS) and lysosomal proteolysis. The lysosomal pathway involves the sequestration and delivery of intracellular organelles/proteins to the lysosome where degradation and recycling occurs through the autophagic pathway. The lysosomal pathway can degrade both intra- and extracellular cargo. Extracellular proteins/cargo can be transported to lysosomes via endocytosis or selectively recruited and delivered to lysosomes via phagocytosis. Autophagy comprises three distinct variants: chaperone-mediated autophagy, microautophagy and macroautophagy. The most

Stellenbosch University https://scholar.sun.ac.za



prevalent form of autophagy is macroautophagy. Macroautophagy, hereafter referred to as autophagy, is generally considered to be a non-selective process, but recent evidence suggests that autophagy can also selectively target organelles and proteins for degradation. One such example is the process of mitophagy, where dysfunctional mitochondria are selectively targeted for degradation [220].

The autophagic pathway can be categorized into four distinct steps: initiation, nucleation, maturation and cargo delivery, and degradation (Fig. 2.1). The initiation process is regulated by an integrated network able to sense energy abundance, nutrient levels (amino acids) and stress, which, once initiated, involves the recruitment and coordination of more than 30 proteins known as the "core machinery" to the nucleation site. [160]. Scaffolding and lipidation proteins facilitate the elongation of the phagophore at the nucleation site. During the development of the phagophore, cytoplasmic cargo is engulfed. Once the growing phagophore has matured it is called an autophagosome. The autophagosome is transported to and fuses with a lysosome to form an autolysosome, in which the autophagic cargo is delivered and degraded by lysosomal enzymes. The digestive products, mainly amino acids, are released back into the cytoplasm for recycling. Several key proteins are involved in the regulation and formation of autophagosomes and the events that follow.

Stellenbosch University https://scholar.sun.ac.za






**Figure 2.1:** The autophagy pathway. Illustration of the four steps involved in the autophagy process: initiation, nucleation, maturation and cargo delivery and degradation. The autophagy process is initiated through intra- or extracellular stimuli that result in the recruitment of Atg proteins (greyed out) that bring about the nucleation of membrane forming the omegasome. The developing phagophore encapsulates cytoplasmic cargo in a double membrane vesicle termed an autophagosome. Once matured, it is transported along the microtubule network (greyed out) to lysosomes. The outer autophagosomal membrane fuses with lysosomes to form autolysosomes, in which the encapsulated cargo is degraded by lysosomal enzymes and released back into the cytoplasm for recycling.

Stellenbosch University https://scholar.sun.ac.za



### 2.2.1 The core machinery of autophagy

The core machinery proteins of autophagy can be grouped into several functional units that are responsible for the various steps involved in the autophagy process (Fig. 2.2). In this section we explore the mechanism of the induction and formation of the phagophore and the subsequent events involved in the autophagy process. It is important that an organism is able to increase or decrease autophagy efficiently in order to adapt to both intracellular and extracellular stress. One of the main regulators of autophagy is the mammalian target of rapamycin complex 1 (mTORC1), generally considered to be the master growth regulator that can suppress autophagosome synthesis [160]. mTORC1 forms hubs in several signalling pathways that integrate diverse nutritional and environmental cues, such as growth factors, energy levels, cellular stress, and amino acids. Moreover, AMP-activated protein kinase (AMPK), a cellular energy sensor, is activated by reduced ATP levels and the concomitant increase in the AMP level [103], which inactivates mTORC1 and directly induces autophagy [54, 131, 159] and the synthesis of Beclin1 [130]. These master regulators, as well as other regulatory proteins (discussed in more depth in section 2.2.2) all contribute to the multifaceted regulation of autophagy allowing for an integrated response to a wide array of metabolic perturbations as well as environmental cues.

**Induction, nucleation and the formation of the phagophore.** The formation of the phagophore is the first step in the autophagy process that facilitates encapsulation of cytoplasmic cargo. In mammalian cells phagophores are generally formed near the endoplasmic reticulum (ER)-mitochondria contact sites [12]. In response to stimuli, phagophore formation is initiated by the assembly and activation of a multi-protein complex which contains Atg13, Atg101, Unc-51-like kinase 1 (ULK1) and focal adhesion kinase family interacting protein of 200 kDa (FIP200, also known as RBCC1) at the Atg9-containing membrane. During periods of nutrient abundance, mTORC1 associates with the ULK1 complex and phosphorylates the conserved C-terminal domain (CTD) of ULK1 and Atg13, which inhibits the ULK1 complex. In contrast, the inhibition of mTORC1 through nutrient

Stellenbosch University https://scholar.sun.ac.za



deprivation results in its dissociation from the ULK1 complex, the subsequent autophosphorylation of ULK1 brought about by its conformational change allowing its kinase domain to autophosphorylate ULK as well as Atg13 and FIP200 [116]. Activation of this complex and phosphorylation of Atg9 initiates the elongation of the pre-autophagosomal membrane by incorporating phospholipids from various sources including, but not limited to, the mitochondria, ER, and recycled endosomes [155]. Although the exact source of the membrane remains debated, the formation of the phagophore requires the recruitment of the ULK1 complex and Atg14 [122], which facilitate the assembly of the autophagy specific class III phosphatidylinositol 3-kinase (PtdIns3K) complex [179], containing PtdIns3K itself, PtdIns3K catalytic subunit type 3 (PIK3C3, better known as VPS34), PtdIns3K regulatory subunit 4 (PI3KR4, better known as VPS15), Beclin1 (the mammalian homologue of Atg6/Vps30), Atg14 (also known as Barkor and Atg14L), nuclear receptor binding factor 2 (NRBF2), and UV radiation resistance-associated protein (UVRAG) [61, 106, 126, 127, 166, 170, 180, 244, 289]. The formation of the PI3K complex permits production of phosphatidylinositol-3-phosphate (PI3P) which allows for the targeting and recruitment of various other autophagy PI3P-binding proteins and members of the WIPI family [214]. Moreover, the activation of PtdIns3K complex promotes the formation of the Atg12-Atg5:Atg16L1 complex and the subsequent local lipidation of LC3, which is vital for elongation of the membrane and expansion of the developing autophagosome [246, 247]. The assembly of the Atg12-Atg5:Atg16L1 complex and lipidation of LC3 involves the ubiquitin-like enzymes Atg7, Atg3, Atg10 and Atg12-Atg5.

**Atg12–Atg5:Atg16L1 complex formation.** Atg7 is homologous to the ATP-binding and catalytic sites of the E1 ubiquitin activation enzyme that activates and transfers Atg12 to Atg10, a ubiquitin-like E2 conjugating enzyme that attaches it covalently to a lysine residue of Atg5 [68]. The conjugation of Atg12 to Atg5 is irreversible and does not require the substrate-specific E3 ligase ubiquitination process. Atg12–Atg5 then further complexes with Atg16L1 to form Atg12–Atg5:Atg16L1, which tetramerises by self-oligomerisation and acts as scaffolding by attaching to the developing autophagosome [89, 188].

Stellenbosch University https://scholar.sun.ac.za



**LC3 processing.** Cytoplasmic LC3 is first cleaved by Atg4 to expose the C-terminal glycine residue, which is then activated by Atg7 (similar to Atg12), and transferred to Atg3, a ubiquitin-like E2 conjugating enzyme, to form LC3-I. Atg12–Atg5 possesses a ubiquitin-like E3 conjugating site that conjugates LC3-I with phosphatidylethanolamine (PE) to form LC3-PE (also known as LC3-II) [82]. During periods of nutrient abundance the majority of LC3 remains in the cytosol. When autophagy is induced, endogenous cytoplasmic LC3 reserves are immediately mobilized, lipidated and incorporated into both the inner and outer membrane of the growing autophagosome [118]. Interestingly, it has been suggested that LC3 plays an important role in determining autophagosome membrane curvature, thereby aiding in the regulation of the size of the autophagosome [279]. The closing of the phagophore completes the maturation process, forming the double-membraned autophagosome structure in which engulfed cytoplasmic cargo resides. Although the exact mechanism remains elusive, GTPase RAB7A, a member of the RAS oncogene family (RAB7A), has been shown to be essential to the autophagosome maturation process [74, 110, 165].

Stellenbosch University https://scholar.sun.ac.za



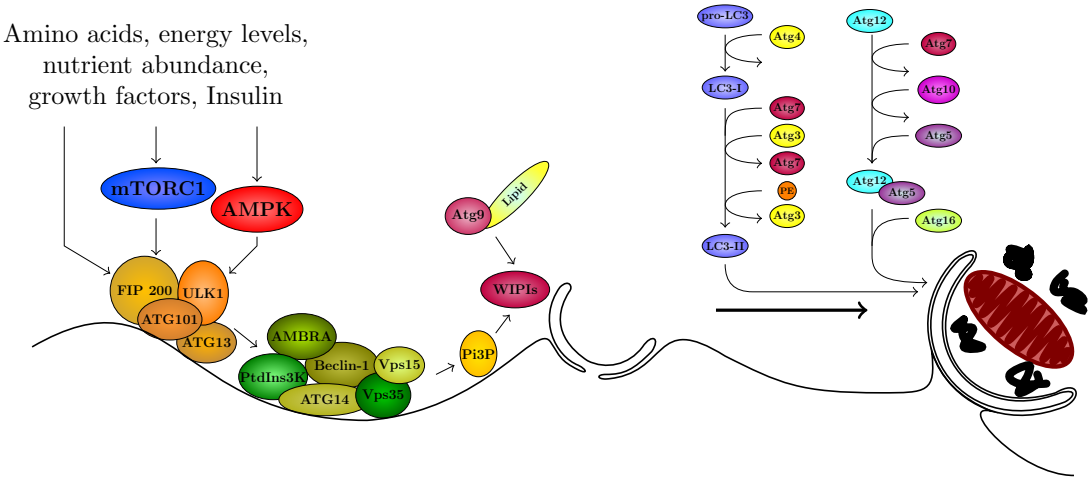


**Figure 2.2:** Autophagy regulatory complexes. Autophagy is regulated by a broad nutrient- and stress-sensing network that initiates the recruitment and activation of the ULK1 complex in response to metabolic cues. The ULK1 complex subsequently activates the PtdIns3K complex, which, together with WIPI and Atg9, establishes the omegasome. The growing phagophore requires the assembly of structural components, the Atg12-Atg5:Atg16L1 complex and lipidated LC3, to be incorporated into the membrane.

**Cargo recognition and selectivity.** Although in the past autophagy was generally considered to be a bulk degradation process, an increasing number of studies have described various forms of autophagy that selectively engulf cargo such as ribosomes (ribophagy) and protein aggregates (aggrephagy), or organelles such as mitochondria (mitophagy) and peroxisomes (pexophagy) [65, 193, 242, 261]. One of the first and best defined selective forms of autophagy is mitophagy, which is the selective sequestration of mitochondria for lysosomal degradation. Selective autophagy is facilitated via autophagy receptor proteins, which are proteins recognised by the autophagy machinery that mediate the binding of autophagy substrates to the developing autophagosome and thereby promote its degradation [242]. Many receptor proteins have been identified that are autophagy specific (HSPA8, for example, is the main receptor for endosomal microautophagy but not for chaperone-mediated autophagy [193, 261]), and they seem to be involved in the recognition of autophagy substrates, which gives rise to various sub-forms

Stellenbosch University https://scholar.sun.ac.za



of autophagy [62, 222]. Most of these receptors share an evolutionary-conserved LC3-interacting region (LIR) that transports autophagy substrates into close proximity of forming autophagosomes, enabling them to be sequestered. These include Atg19, Atg32, Atg34, BNIP3, BNIP3L, FUNDC1, NBR1, NDP52, OPTN, p62, PHB2, TAX1BP1 and TRIM5 [20, 36, 271]. Autophagy-specific receptor proteins often contain ubiquitin-binding domains that allow them to recruit ubiquitinated substrates to growing autophagosomes [125]. Furthermore, some receptors are able to bind to the Atg12-Atg5:Atg16L1 complex (e.g., p62 and OPTN) and stimulate conjugation of LC3 at the phagophore developing site [64]. Similarly, some proteins of the TRIM protein family that act as receptors can also interact with upstream components of the autophagy machinery, which include the ULK1 and VPS34 complexes [135, 136]. Considering the ability of TRIM proteins to interact with upstream regulatory components, it is conceivable that other autophagy receptors may also have regulatory functions aside from cargo recognition.

**Autophagosomes, the cargo carriers.** Autophagosomes are transient double-membraned vesicles that mediate the delivery of encapsulated cargo to lysosomes for degradation [236]. Autophagosomes share many proteins with the late stage of developing phagophores. The lack of hydrolytic enzymes in autophagosomes allows for the easy detection of autophagic substrates, ubiquitinated or non-ubiquitinated, and autophagy receptors [138]. LC3 protein is abundant on both the inner and outer membrane of developing autophagosomes. However, once matured, LC3 is efficiently removed by Atg4 from the surface of the outer membrane [155]. Once LC3 is removed, autophagosomes fuse with lysosomes, or late endosomes, delivering cargo for degradation.

**Fusion of autophagosomes with lysosomes delivers the autophagic cargo for degradation.** Once autophagosomes have matured they are able to fuse with either endosomes or lysosomes to form what is called an amphisome or autolysosome. The molecular machinery required for fusion involves many proteins, most of which are shared with the endocytic pathway [7, 8]. The fusion process is a critical step in the autophagy process and results in the delivery

Stellenbosch University https://scholar.sun.ac.za



of cargo to the lysosome for degradation; the exact underlying mechanism remains unclear, however. The fusion process is facilitated by the activation of the GTPase RAB7A [74, 110, 165], pleckstrin-homology and RUN domain-containing M1 (PLEKHM1) [182], the PI3P-binding protein tectonin beta-propeller repeat containing 1 (TECPR1) [30], inositol polyphosphate-5-phosphatase E (INPP5E) [88], ectopic P-granules autophagy protein 5 homolog (EPG5) [255], syntaxin 17 (STX17); soluble N-ethylmaleimide-sensitive factor activating protein receptor (SNARE) proteins [60, 107, 198], and homotypic-fusion and vacuole protein-sorting (HOPS) complexes [182]. The fusion of autophagosomes and lysosomes is mediated by the same machinery that is used in vacuole fusion. The fusion process requires lysosome-associated membrane protein 2 (LAMP2) and the small GTPase Rab7 [110, 250]. Moreover, lysosome-associated membrane protein 2 B (LAMP2B), Atg14 and the lipidated and phosphorylated forms of LC3 are also involved in the formation of autolysosomes [49, 59, 202, 273]. In addition, some of the regulatory and structural proteins involved in the formation can also regulate the fusion of autophagosomes with lysosomes. For instance, FYVE zinc finger together with coiled-coil domain-containing 1 (FYCO1) and sorting nexin 18 (SNX18), which are involved in the formation of autophagosomes, also participate in the interaction of autophagosomes with the cytoskeleton and their fusion with lysosomes [142, 207]. In contrast, Beclin1-interacting protein (RUBCN, better known as RUBICON) and VPS34 can negatively regulate the fusion between autophagosomes and lysosomes through the interaction with RUN [180].

**Autolysosomes and cargo degradation.** Autolysosomes are single-membrane organelles that form upon fusion between autophagosomes and lysosomes [141]. Autolysosomes contain lysosomal enzymes, as well as endo/lysosomal markers such as LAMP1, LAMP2, and the V-type ATPase. Autolysosomes have low levels of LC3-II since it is cleaved by Atg4 from the outer membrane and released into the cytosol; LC3-II in the inner membrane is degraded by lysosomal hydrolases [137, 141]. A recent study suggests that disassembly of the inner autophagosomal membrane may be supported by the Atg conjugation systems [259]. Upon

Stellenbosch University https://scholar.sun.ac.za



completion of the fusion process, the inner compartment of the autophagosome, containing the autophagic cargo, is exposed to lysosomal hydrolases such as proteinases A and B, and cathepsin B and L [251] in an acidic environment that is maintained through an ATP-dependent proton pump commonly known as V-type ATPase [186]. The exposure of the autophagic cargo to the hydrolases results in its degradation; the digestive products, mainly amino acids, are released back into the cytoplasm where they are available as nutrients during periods of starvation or as precursors for protein synthesis. Once the degradation of autophagy cargo is completed, autolysosomes regenerate to lysosomes through a process called autophagic lysosome reformation (ALR), whereby proto-lysosomal vesicles extrude from autolysosomes to regenerate the lysosome [284]. Interestingly, the ALR process is initiated by the reactivation of mTORC1 which in turn inhibits autophagy.

**Autophagy vesicle translocation.** Microtubules play a crucial role in the translocation of both Atg proteins, such as Atg9, as well as autophagic vesicles, particularly autophagosomes. The depolymerisation of microtubules by chemical intervention with nocodazole in primary rat hepatocytes has been shown to have a detrimental effect on autophagy function [143], and deacetylation of microtubules and tubulin by deacetylase HDAC6 has been shown to play a role in the autophagic degradation of polyglutamine aggregates [109, 208]. In mammalian cell lines autophagosomes are predominately formed in peripheral areas of the cell and actively transported towards the nuclear region of the cell where lysosomes are highly concentrated for efficient fusion and clearance of autophagic cargo. Possible 'kiss-and-run' events between autophagosomes and lysosomes may also occur where there is a partial transfer of vesicle content while the two vesicles still remain separate [111, 143]. The active transport of autophagosomes relies on the dynein and kinesin motor proteins that transport them along the microtubule network. Considering their role, it is not surprising that mutations in the dynein motor machinery impair autophagic clearance and lead to premature aggregate formation [217]. The microtubule network therefore plays an important role in the autophagy process, allowing it to proceed efficiently.

Stellenbosch University https://scholar.sun.ac.za



### 2.2.2 Metabolic regulation of autophagy

Autophagy is a tightly-regulated intracellular process that fulfils vital biological functions such as maintaining cellular integrity and adapting to stress by utilizing endogenous energy reserves during periods of starvation. Autophagy can respond rapidly to a wide range of metabolic and stress stimuli as a result of being regulated by an extensive intracellular nutrient and stress-sensing network. The aim of this section is to firstly discuss the metabolic triggers of autophagy, and secondly to discuss the cellular sensors that monitor the abundance of metabolites and regulate autophagy.

#### 2.2.2.1 Metabolic triggers of autophagy

Given that autophagy plays an important role in cellular metabolism, its up or down regulation in response to metabolic cues is essential. This is achieved by multiple metabolic sensing pathways that monitor key metabolites, such as amino acids and glucose, involved in energy production and protein synthesis. Moreover, autophagy can also be upregulated by the accumulation of metabolic by-products and toxic compounds in order to remove these potentially deleterious compounds. Here some of key metabolic triggers that regulate autophagy will be discussed.

**Adenosine triphosphate (ATP), the energy currency of the cell.** The "energy charge" — $([\text{ATP}] + 0.5[\text{ADP}])/([\text{AMP}] + [\text{ADP}] + [\text{ATP}])$ — is a measure of the energy status of the cell when an active adenylate kinase is present [10]. The energy charge decreases when ATP is not actively produced through either oxidative phosphorylation or glycolysis to meet the cellular demand, leading to the accumulation of ADP and AMP, respectively. The decrease in ATP and increase in AMP levels induce autophagy via AMPK by inhibiting the mTORC1 complex and directly activating the ULK1 complex [86]. AMPK is highly sensitive to fluctuations in AMP and ATP, and therefore plays a key role as a metabolic master switch that regulates several intracellular metabolic pathways. Activation of AMPK promotes ATP production by increasing the activity, and/or expression of proteins involved in catabolic processes, such as glycolysis, fatty acid oxidation,

Stellenbosch University https://scholar.sun.ac.za



ketogenesis, as well as autophagy. This upregulation leads to an increase in cytosolic protein degradation, and the release of amino acids for energy production. In contrast, inhibition of AMPK suppresses energy expenditure by effectively switching off biosynthetic pathways in order to preserve energy for essential metabolic reactions required for survival. Interestingly, since autophagy also requires ATP, a rapid reduction in ATP levels can result in a decrease in the energy charge below the critical limit and trigger cell death rather than an adaptive autophagic response [67]. Cells that predominantly depend on glycolysis for fuel are extremely sensitive to glucose fluctuations and can rapidly upregulate autophagy when glucose levels decrease [86]. In addition to AMPK regulation of autophagy, hexokinase II, which catalyses the first step of glycolysis by phosphorylating glucose, has also been shown to promote autophagy during periods of glucose withdrawal. Hexokinase II directly interacts with mTORC1 and inhibits its activity, consequently inducing autophagy [219]. Moreover, nicotinamide adenine dinucleotide (NAD), a coenzyme found in all living cells, exists in both a reduced (NADH) or oxidized ($NAD^+$) state and is an essential substrate in redox reactions in multiple metabolic pathways, especially in glycolysis and oxidative phosphorylation. During nutrient-poor conditions there is an accumulation of $NAD^+$, whilst NADH levels decrease. The consequent shift in the NADH/$NAD^+$ ratio can also induce autophagy through the activation of histone deacetylases of the sirtuin family [98]. In conclusion, glucose deprivation results in changes in ATP/AMP, NADH/$NAD^+$, and enzyme activity that can either directly or indirectly regulate autophagy through a multi-pronged network.

**Amino acids are basic building blocks of life.** Amino acids play a crucial role in almost all biological processes and are potent activators of autophagy. A reduction in amino acid availability results in the activation of the nutritional stress response. Even though amino acids are normally obtained from the extracellular environment, such as the blood stream during the fed state, they can also be supplied via the breakdown of endogenous proteins during periods of starvation through catabolic processes such as autophagy. Several mechanisms have been de-

Stellenbosch University https://scholar.sun.ac.za



scribed through which autophagy can be induced by the availability of amino acids. One such mechanism is through the Rag family of GTPases, together with the Ragulator complex on the lysosome membrane, which facilitates the amino acid-mediated mTOR recruitment to the lysosome surface where mTORC1 becomes activated in the absence of amino acids. Furthermore, autophagy can also be induced through the accumulation of uncharged tRNA resulting from the reduction of available intracellular amino acids. The accumulation of tRNA species activates Rag and consequently mTORC1. Moreover, a decline in amino acid levels results in the depletion of $\alpha$-ketoglutarate, which promotes autophagy together with the inhibition of prolyl hydroxylase [51]. The absence of certain amino acids, in particular leucine, glutamate, and glutamine, can reduce intracellular acetyl-CoA stores and induce autophagy by (de)acetylation of regulatory complexes [174]. Several other proteins have also been implicated in amino acid regulation of autophagy, including MAP4K3, phospholipase D, and PIK3C3; their exact involvement, however, remains uncertain. In summary, there are several mechanisms that contribute to an extensive intracellular amino acid-sensing network that strongly links amino acid levels to autophagy. However, the degree of control that each of these mechanisms has over the autophagy pathway is not known. All these amino acid sensing mechanisms contribute to the orchestration of autophagic responses to a shortage of amino acids.

**Acetyl coenzyme A (acetyl-CoA) is the central intermediate of many pathways.** Acetyl-CoA acts as an acetyl source for many biochemical reactions, such as protein acetylation and energy production. Studies have shown that over several hours of nutrient withdrawal there is a significant reduction in cytosolic acetyl-CoA levels alongside induction of autophagy [174]. Similar trends have been observed in several pharmacological studies where the inhibition of acetyl-CoA synthesis, either through direct inhibition or substrate limitations, is accompanied by the induction of autophagy [56]. In contrast, replenishment of intracellular acetyl-CoA levels seems to inhibit starvation-induced autophagy in both cell culture and mouse models [174]. Reduction of cytosolic acetyl-CoA appears to act as a stimu-

Stellenbosch University https://scholar.sun.ac.za



lator of autophagy. This is thought to be facilitated by acetyl-CoA, which acts as a donor of acetyl groups for acetyl transferases, which in turn regulate autophagic machinery components, either at the transcriptional level by modulation through histone acetylation, or at the post-translational level through protein acetylation [158, 174]. The modulation of biochemical reactions through transcription takes considerably longer than post-translational modifications, leading to autophagy's biphasic response to metabolic stress.

**Cellular stress: ammonia, hypoxia and reactive oxygen species.** Ammonia, a stress-inducing toxic by-product of amino acid catabolism, has been shown to activate autophagy [57]. In contrast to amino acid deprivation-induced autophagy, ammonia-induced autophagy does not rely on either mTORC1 inhibition [85] or ULK1 activation [32]. Harder *et al.* [85] have shown that ammonia-induced autophagy occurs alongside the activation of AMPK and the unfolded protein response (UPR). The UPR is a cellular stress response that is activated by an accumulation of unfolded or misfolded proteins in the lumen of the ER, resulting in their degradation. Since both autophagy and UPR are involved in the removal of potentially deleterious proteins, which could result from misfolding, it is not surprising that they occur alongside each other. The role of the UPR in autophagy induction is supported by studies demonstrating that elevated ER stress markers, such as DNA damage-inducible transcript 3 (also known as C/EBP homologous protein, CHOP) and heat shock 70 kDa protein 5 (HSPA5), are associated with UPR during ammonia treatment [85]. Interestingly, tumours have been shown to contain high autophagic activity, as well as generate high levels of ammonia due to an increase in glutamine catabolism via glutaminolysis. Therefore, increased autophagy resulting from elevated ammonia levels may play a role in protecting tumour cells [73].

Reactive oxygen species (ROS) play important roles in cell signalling and homeostasis [48]. Acute ROS exposure can lead to extensive cellular damage and cell death [31]. Although cells maintain tolerable levels of ROS, they are able to protect themselves from damage caused by rapid increases in mitochondrial ROS through

Stellenbosch University https://scholar.sun.ac.za



anti-oxidative strategies [31, 77]. It is well documented that ROS can induce autophagy [31]. Accumulation of ROS beyond tolerable levels induces autophagy by either activating nuclear factor kappa-light-chain-enhancer of activated B cells (NK-kB) - receptor for AGEs (RAGE) pathway, or by inhibiting mTORC1 [31].

Hypoxia is the condition where oxygen levels decrease below 1% (hypoxic stress). Hypoxia has been shown to have significant physiological effects during embryo development, but may also occur in pathological conditions such as muscle and brain injuries, cardiovascular ischaemia and tumours [69]. Studies show that hypoxia can induce autophagy [18, 24, 210, 258]. Oxygen deprivation activates hypoxia-inducible factor-1 (HIF-1) that promotes transcription of various genes and activates anti-apoptotic Bcl-2 adenovirus E1a 19 kDa interacting protein 3 (BNIP3) and Nix. Activation of HIF-1 decreases mitochondrial biogenesis and respiration, which promotes erythropoiesis and angiogenesis as adaptives response to counteract the dangerous effects of oxygen deficiency [288]. BNIP3 induces autophagy by competing with Beclin1 to bind with Bcl-2, which subsequently promotes the dissociation of Bcl-2 and Beclin1, thereby inducing autophagy. Moreover, hypoxia can induce autophagy through an HIF-1 independent pathway that involves the UPS, ER stress mechanisms, and AMPK [288].

#### 2.2.2.2 Metabolic sensors that initiate autophagy

It is critical to cell survival that autophagy can respond to a wide range of stressors in order to adapt to fluctuations in metabolites, extracellular signals, redox potentials and extracellular conditions. There are several mechanisms that contribute to a broad extracellular and/or intracellular nutrient- and stress-sensing network that can initiate the autophagic response. Here the best characterised metabolic/stress sensors, and how they contribute to the regulation of autophagy are discussed.

**AMP-activated protein kinase is a master energy regulator in cells.** AMPK is highly conserved in eukaryotes and plays a key role in maintaining cellular energy homeostasis. It monitors the energy status of the cell by sensing

Stellenbosch University https://scholar.sun.ac.za



fluctuations in the intracellular ratio between AMP/ADP and ATP ratio. AMPK is a heterotrimeric protein that is composed of a catalytic $\alpha$-subunit, a regulatory $\gamma$-subunit and a scaffolding $\beta$-subunit, all of which exist as multiple isoforms. AMPK activity is regulated by the binding of either AMP or ADP (with greater affinity for AMP) to the regulatory $\gamma$-subunit that prevents the dephosphorylation of the $\alpha$-subunit by blocking access of phosphatases to the threonine-172 residue, which activates AMPK when phosphorylated. In contrast, the binding of ATP to $\gamma$-subunit allows phosphatases to access the threonine residue [86]. Thus, a reduction in the energy charge brought about by a decrease in ATP levels, and an increase in AMP and ADP, will increase AMPK activity. The $\alpha$-subunit can be phosphorylated by serine/threonine kinase 11 (STK11, also known as LKB1), calcium/calmodulin-dependent protein kinase kinase 2 (CAMKK2), and mitogen-activated protein kinase kinase kinase 7 (MAP3K7, also known as TAK1) [86]. A recent study showed that MAP3K7 is required for the starvation-induced phosphorylation of AMPK and activation of autophagy in cancer cells *in vitro* [41], and in mouse hepatocytes *in vivo* [104]. AMPK induces autophagy through several mechanisms, with AMPK autophagic regulation via mTORC1 inhibition being the best studied example. AMPK phosphorylates Raptor and tuberous sclerosis complexes 1 and 2 (TSC1 and TSC2), which negatively regulate mTROC1 [133]. Furthermore, AMPK can act directly on core components of the autophagy machinery to phosphorylate and activate ULK1 and Beclin1 [131].

**mTORC1 is a central regulator of cellular processes.** mTORC1 plays a crucial role in the induction of autophagy. It is composed of five proteins, including mTOR itself, a regulatory-associated protein of mTOR (Raptor), mammalian lethal with SEC13 protein 8 (mLST8, also known as G$\beta$L), proline-rich Akt substrate of 40 kDa (AKT1S1, better known as PRAS40), and DEP (Dishevelled, Egl-10 and Pleckstrin domain), domain-containing mTOR-interacting protein (DEPTOR) [128, 129, 276], which is shared with the mammalian target of rapamycin complex 2 (mTORC2). mTOR is the catalytic unit of both complexes, which are structurally distinct from one another. mTORC also localizes

Stellenbosch University https://scholar.sun.ac.za



to different subcellular compartments and has different activation cues and function. mTORC1 functions as an energy-, nutrient- and redox sensor; its activity is regulated by amino acids, energy reserves, nutrient availability, growth factors, and oxidative stress. Its role is to control the translation of proteins in response to growth factors and stimuli in the presence of adequate nutrients for cell growth and proliferation [128].

Growth factors can activate mTORC1 via the receptor tyrosine kinase (RTK)-Akt/PKB signalling pathway, thereby inhibiting autophagy whilst promoting protein synthesis through the activation of ribosomal protein S6 kinase (RPS6K, also known as p70S6K) and eukaryotic translation initiation factor 4E binding protein 1 (EIF4EBP1) [237]. Activated mTORC1 can suppress autophagy by phosphorylating and inhibiting ULK1 [131], as well as Atg14 [286], AMBRA [201] and transcription elongation factor b (TFEb) [234]. Although AMPK acts as a master energy sensor that can directly induce autophagy, it is also able to negatively regulate mTORC1 by activating TSC1 and TSC2, which in turn inhibit mTORC1 [86]. Moreover, AMPK can phosphorylate RAPTOR, which suppresses mTORC1 activity, thus promoting autophagosome synthesis [86].

Amino acid availability serves as a positive regulator of mTORC1, which, when abundant, suppresses autophagy through various pathways, many of which remain elusive. Given that lysosomes represent the major site of protein degradation and amino acid recycling, they act as transient amino acid stores. Recent studies have shown that mTORC1 and its regulators Rheb and Rag GTPases are closely associated with the lysosomal surface [52]. The Rag GTPase complexes, together with p14, p18, and MP1 protein complex, form a regulatory scaffold on the surface membrane. This Ragulator-Rag complex acts as an amino acid-sensing system that exists on the lysosomal surface and is able to assess surface amino acid abundance within the lysosomal lumen, and therefore regulates mTORC1. The site of localisation still remains elusive and may reflect a currently unknown function of lysosomes to link with the abundance of intracellular amino acids [229]. Importantly, mTORC1 not only regulates lysosomal biogenesis and represses autophagy, but also functions as a general regulator of anabolic reactions [237]. Moreover,

Stellenbosch University https://scholar.sun.ac.za



$\alpha$-ketoglutarate, which is a glutaminolysis intermediate, is a potent activator of autophagy, even in the absence of amino acids, by means of a process which is thought to be mediated by the lysosomal RHEB-dependent pathway [52]. Interestingly, a recent study showed that a reduction in $\alpha$-ketoglutarate abundance extended life expectancy by inhibiting mTORC1, and consequently upregulating autophagy [33].

**Eukaryotic initiation factor 2 alpha (eIF2$\alpha$) phosphorylation.** eIF2$\alpha$ kinases are a family of evolutionarily conserved serine/threonine kinases that form part of the integrated stress response that limits protein synthesis together with the activation of autophagy [151]. PERK, a transmembrane protein kinase of the PEK family in the ER membrane, phosphorylates eIF2$\alpha$, initiating a series of events that decreases ER stress and inhibits general protein translation, whilst selectively translating specific stress-related proteins, including selective autophagy genes [87, 97]. The phosphorylation of eIF2$\alpha$ integrates various types of intra- and extracellular stress signals that include amino acid deprivation, osmotic stress and oxidative stress. Although the exact mechanism by which eIF2$\alpha$ contributes to autophagic induction remains unclear, several mechanisms have been proposed, including the notion that eIF2$\alpha$ affects the ER in such a manner that it promotes the physical formation of the omegasome [151]. It has also been suggested that that eIF2$\alpha$ stimulates autophagy through the transactivation of autophagy genes, such as ATF4 transcription factor which promotes LC3 expression [184]. Moreover, there is evidence to suggest that eIF2$\alpha$ subunits interact with the autophagy core machinery, although it is not clear whether or not they promote autophagy [17].

**Sirtuins and protein (de)acetylation.** Sirtuins are class III histone deacetylases that catalyse the deacetylation of protein substrates by sensing environmental stress [76]. In contrast to other deacetylases that hydrolase acetyl-lysine residues, sirtuin-mediated deacetylation requires $NAD^+$ hydrolysis for lysine deacetylation. Sirtuin 1 (SIRT1) is the best studied of the sirtuin deacetylases, which mainly reside within the nucleus where it is responsible for the deacetylation of histones, in

Stellenbosch University https://scholar.sun.ac.za



particular H1 and H2, as well as other proteins such as transcription factors [98]. Resveratrol, a plant-derived polyphenolic compound which has received much attention in recent years due to its wide-ranging health benefits, can activate SIRT1 and promote autophagy [153]. Although Atg5, Atg7, Atg12 and LC3 have been implicated in the SIRT1-induced autophagy cascade, the exact mechanism through which autophagy is induced by SIRT1 activation remains elusive [156]. A recent study suggests that SIRT1 is able to induce autophagy without the assistance of its transcriptional cascade [194]. This implies that SIRT1 can stimulate autophagy by either deacetylating proteins involved in autophagy, or by increasing the expression of Atg. Given that sirtuins form part of a broad intracellular network, it is not surprising that SIRT1 can be activated by factors other than $NAD^+$ [29]. For instance, a low caloric diet has been shown to stimulate SIRT1 activity, whereas a high-fat diet reduces SIRT1 activity [29].

The transfer of acetyl groups plays a major role in signalling cascades and the post-translational modification of proteins, including histones. Histone acetylation is involved in nuclear remodelling of chromatin that can either result in its condensation or expansion, thereby making genes accessible for translation. The intracellular pool of acetyl-CoA relates directly to the overall protein acetylation in a cell since the availability of acetyl-CoA, the sole donor of acetyl groups, determines the catalytic activity of several acetyltransferases [56, 174]. The availability of intracellular acetyl-CoA has been linked to autophagy activity [157]. The E1A-binding p300 protein (EP300), which acts as an intracellular acetyl-CoA sensor in response to the transition between a fed and unfed state, has been shown to play a major role in the regulation of autophagy by acetylating proteins of the core autophagic machinery, such as Atg5, Atg7, Atg12, and LC3, autophagic regulatory proteins such as AMPK, as well as non-Atg components required for autophagy such as tubulin [174]. Although EP300 is implicated in autophagy regulation, it is most likely that other acetyltransferases also play a role in autophagy regulation, which is evident in yeast studies [174]. Moreover, acetyltransferases form part of a broad intracellular autophagy regulating network that can inhibit or stimulate proteins that are involved in the autophagic pathway. For instance, AMPK can

Stellenbosch University https://scholar.sun.ac.za



activate MEC17 and inhibit EP300 activity [281]. Thus, the activation of AMPK results in the hyperacetylation of $\alpha$-tubulin, whilst inhibiting EP300 which seems to have pro-autophagy effects [173]. In summary, both acetylation and deacetylation of proteins can have either an inhibitory or inducing effect on autophagy.

**Cell-surface nutrient receptors.** Cell-surface nutrient receptors enable the cell to respond to extracellular metabolite changes, and to physiological cues from the brain and other organs. As an adaptive response to stress, autophagy has been linked to cell-surface receptor signalling cascades, but the exact signalling cascades involved remain unclear. It is speculated that the activation of these receptors result in increases of intracellular inositol-1,4,5,-triphosphate, diacylglycerol and cyclic AMP (cAMP), and are involved in autophagy regulation [269]. It has also been found that several G protein-coupled receptors (GPCRs) present on the cell surface assess nutrient availability in the extracellular microenvironment and can communicate with the autophagic machinery. Several cell-surface receptors have been identified, these include amino acid sensing receptors, $\gamma$-aminobutyric acid B receptor 1 (GABBR1), G protein-coupled receptor family C group 6 member A (GPRC6A), metabotropic glutamate receptors (mGluRs), calcium-sensing receptors (CASR), and free fatty acid receptors.

### 2.2.3 Conclusion

There are several nutrient-sensing networks that monitor extracellular and/or intracellular nutrient fluctuations and initiate an autophagic response. These sensing networks overlap in their signalling cascades, so facilitating a multi-prong regulation of autophagy. Moreover, since many of the proteins involved in the signalling cascade are expressed as isoforms in a tissue specific manner, such as the AMPK subunits, they contribute to differential regulation of autophagy throughout the whole organism.

Stellenbosch University https://scholar.sun.ac.za



## 2.3 The physiological role of autophagy

It is accepted that autophagy evolved as a degradation process. While it still continues to do so, its role has expanded and became a vital cellular process that acts as an adaptive response to starvation and metabolic fluctuations. As previously discussed, the autophagic machinery as well as its major regulatory mechanisms that promote autophagy during periods of stress allow cells to either adapt (in the case of nutrient poor conditions) or overcome (in the case of damaged organelles) these stresses. Moreover, by playing an important role in protein quality control and organism development, autophagy serves as more than just as an adaptive response. Here the physiological role of autophagy will be discussed.

**Protein quality control and its implications in organism development.** It is essential for cell growth and development that a fine balance between protein and organelle synthesis and degradation is maintained. Autophagy acts as a protein quality control mechanism that prevents further damage to cellular components by rapidly degrading proteins and compounds that can have deleterious effects on vital cellular functions. Intracellular proteins can be broadly grouped into two categories: short-lived and long-lived proteins [102, 123]. Although short-lived proteins constitute less than 1% of protein content, they account for nearly one-third of protein turnover due to their rapid degradation [123, 195]. It is widely accepted that the ubiquitin-proteasome system is responsible for the degradation of most short-lived proteins, while autophagy degrades long-lived proteins. In contrast to the selective degradation by the ubiquitin-proteasome system, autophagy randomly sequesters cytosolic proteins, which may also contain short-lived proteins in the growing autophagosome for degradation, albeit to a lesser degree. It is only recently that the importance of basal autophagy has come to light through knock-out studies implicating its role as a quality-control system necessary for organism development, particularly in hepatocytes and neuronal cells. Cell-specific differences in autophagy could possibly be attributed to the importance of quality control in non-dividing and post-mitotic cells, in comparison to rapidly dividing cells where abnormal constituents can be rapidly diluted out if they are not de-

Stellenbosch University https://scholar.sun.ac.za



graded.

The importance of basal autophagy was first observed in liver-specific Atg7 knock-out mice [148]. Mice developed multiple organ abnormalities, such as hepatomegaly [148]. A large accumulation of ubiquitin-positive aggregates was observed in these hepatocytes. Neonates from Atg5 and Atg7 knock-out mice showed minimal defects at birth, but had a reduced body size and exhibited suckling defects compared to their wild type counterparts [148, 152]. Methodical analysis of neonates revealed accumulation of ubiquitin-positive aggregates in hepatocytes and some regions of the brain compared to other tissues such as skeletal muscle and kidney [83], indicating that the importance of basal autophagy may be both cell- and tissue-specific. Further studies using neuronal specific Atg5 and Atg7 knock-outs highlighted the significance of basal autophagy in the development of the central nervous system leading to "neurodegeneration". Although these mice were born normally, they exhibited growth retardation and developed progressive motor and behavioural defects [83, 146]. Examination of the brain revealed partial loss of cerebellar neuronal cells and axonal swelling in various parts of the brain. Atg7 knock-out seemed to be more fatal in mice compared to Atg5 knock-out, suggesting that Atg7 may also serve functions other than autophagy in neurons, especially since it has been implicated in the activation of LC3 homologs such as $\gamma$-aminobutyric acid (GABA) protein family [266]. Moreover, inhibition of autophagy in glial cells led to the accumulation of ubiquitinated proteins and resulted in protein aggregate formation in the cytoplasm [83]. Therefore, it is possible that protein aggregation results from impaired protein turnover. This highlights the importance of basal autophagy in maintaining cellular integrity via the continuous clearance of proteins, thereby preventing the accumulation of abnormal proteins as well as protein aggregation.

**Nutrient depletion is one of the most potent inducers of autophagy.** Autophagy is characteristically induced upon starvation. During periods of starvation the energy-sensor network, which monitors intracellular ATP, amino acids and NADH levels, stimulates autophagy [151]. Upregulation of autophagy targets

Stellenbosch University https://scholar.sun.ac.za



energy endogenous reserves, such as cytoplasmic proteins, for degradation in order to supply amino acids for ATP synthesis, as well as the building blocks for essential anabolic reactions [239]. Studies have shown that cells with defective autophagic machinery are more susceptible to nutrient perturbation compared to their wild type counterparts [151]. Moreover, autophagy can be regulated and induced in a biphasic manner, first a rapid response to a stimulus that occurs within minutes or hours [194, 252], and then a protracted response that relies on the transcriptional regulation of Atg which occurs over several days to weeks [234, 268]. The rapid autophagy response does not involve *de novo* synthesis of proteins, but rather relies on the rapid mobilization of endogenous reserves upon induction by post-translational regulatory mechanisms such as phosphorylation and acetylation. In contrast, the protracted response modulates autophagy by regulating the expression of several kinases and proteins that form part of the autophagic core machinery, such as Atg1 and mTORC1 [17]. Protein expression is regulated by transcriptional regulators such as TFEB and by histone modification through acetylation which alters gene expression. Differences in the expression levels of these proteins result in stoichiometric changes in the pathways that can either result in signal amplification or reduction followed by a shift in the autophagic response.

**Autophagy occurs in all organs - albeit at specific activity.** Although most studies focus on investigating autophagy in neuronal and liver cells, autophagy occurs throughout the whole organism and is differentially induced by nutrient deprivation in a tissue-dependent manner [189]. It has been shown that the maximal autophagic activity is reached after 24 hr of nutrient deprivation, which is followed by a decrease in most tissues. However, in certain tissues, such as the heart and slow-twitching muscle, the rate of autophagy continues to accelerate after 24 hr. Interestingly, minimal autophagy activity was initially reported in the brain of mice during periods of food withdrawal [189], most likely because neuronal cells are nutritionally protected by peripheral organs. However, recent studies have shown that autophagy can be induced in neurons [3, 124]. Different

Stellenbosch University https://scholar.sun.ac.za



autophagy activity in different tissue/cell types is to be expected given that they differ in protein turnover and amino acid demand, which also links the expression of various isoforms of autophagic regulator and core proteins.

## 2.4 Autophagy and human disease

Autophagy is essential for the survival of cells/organisms and plays an essential role in differentiation and development. In the previous section the importance of basal autophagy in maintaining cellular integrity via the continuous clearance of proteins was discussed. Considering the importance of this pathway in promoting cellular health, it is not surprising that its dysfunction has been increasingly associated with pathology in recent years. The following section will discuss the consequence of autophagic dysfunction.

### 2.4.1 The lack of autophagy function has dire consequences in neurodegenerative diseases

The demand for autophagy differs among different cell types and may be particularly important in non-dividing cells, such as neurons [83, 146, 148, 149]. This is evident in neuronal-specific Atg5 and Beclin1 knock-out mice that survived the postnatal starvation period, during which they developed cumulative motor deficits and exhibited abnormal reflexes and excessive ubiquitin-positive inclusion bodies in their neuronal cells [83, 146]. The importance of autophagy in neuronal cells becomes more apparent under disease conditions. Recent studies indicate autophagy, in addition to the UPS, plays an indispensable role in maintaining protein quality control via the clearance of disease-related mutant proteins. For instance, Alzheimer's disease, a chronic neurodegenerative disease commonly associated with short-term memory loss and dementia, is characterised by the presence of senile plaques as a result of undegraded amyloid beta (A$\beta$) deposits predominantly in the cerebral cortex [105]. These plaques are a product of dysfunctional proteolytic cleavage of the amyloid precursor protein (APP) localised to the en-

Stellenbosch University https://scholar.sun.ac.za



docytic and secretory systems [203]. While under normal physiological conditions autophagosomes are actively formed in synapses and along neuritic processes and transported towards the peri-nuclear region for efficient clearance of autophagic cargo, in Alzheimer's disease patients the autophagosome maturation process and their retrograde transport becomes impaired, thereby resulting in extensive accumulation of autophagic vacuoles together with neuronal dystrophy [203]. The presence of both APP and its processing enzymes in these autophagosomes further exacerbates Alzheimer's disease pathology by increasing the substrate and enzyme interaction time and consequently the number of A$\beta$ plaques [285]. Another example is Parkinson's disease, a neurodegenerative disorder that predominately affects dopaminergic neurons in the substantia nigra region of the midbrain. Parkinson's disease is characterised by the continual loss of dopaminergic neurons, leading to motor-related complications such as tremors and rigidity. Although the exact cause remains unclear, several factors have been shown to be involved in the progression of Parkinson's disease. One such factor is the accumulation of $\alpha$-synuclein inclusion bodies termed Lewy Bodies in neurons. In contrast to healthy neurons which degrade $\alpha$-synuclein via chaperone-mediated autophagy, in Parkinson's disease neuronal cell mutant variants of $\alpha$-synuclein (A53T and A30P) bind to the lysosomal membrane receptor and prevent their degradation, as well as that of other substrates, all of which renders the cell more susceptible to cellular stress [43].

Several studies have shown that upregulation of autophagy with rapamycin [218, 218, 231], lithium chloride (LiCl) [197], spermidine [204, 204] or rilmenidine [224] conferred positive effects and slowed down the progression of neurodegeneration. In light of autophagy function, the leading hypotheses are that autophagy either indirectly suppresses aggregate formation by rapidly degrading aggregate prone proteins, or directly eliminates inclusion bodies or protein aggregates [21, 109]. Together with the autophagy machinery, autophagy receptor proteins, such as p62, have also been shown to play a crucial role by preventing spontaneous protein aggregate formation [147] through recognition and binding of aggregate prone proteins to LC3 in the autophagic sequestering vesicle, thereby

Stellenbosch University https://scholar.sun.ac.za



facilitating their degradation [21, 209]. However, it was recently proposed that protein aggregates may serve as a possible cytoprotective mechanism to overcome impaired protein turnover in autophagy compromised cells [9, 249] [83]. Nonetheless, the use of autophagy modulators has shown promising results in mouse models [197, 204, 204, 218, 218, 224, 231], paving the way forward for clinical trails. However, the fine control and assessment of autophagy remains a challenge.

### 2.4.2 Autophagy the double edged sword in cancer development

Autophagy has long been associated with the development of cancer, and it has been proposed that the role of autophagy varies among the different stages of the disease [23]. For instance, autophagy seems to act as a cancer-guarding mechanism during normal cell development by efficiently removing cancer causing agents, whilst already established tumours are able to exploit autophagic activity for protection against chemotherapeutic drugs [112, 177, 272]. Cancer is one of the first diseases to be genetically associated with autophagic dysfunction [177]. Several proteins involved in the autophagy process, such as Beclin1, Atg5 and UVRAG, have been reported to be linked to cancer formation [164, 215]. Reportedly, 40–75% of human breast, ovarian, and prostate cancer cases are caused by the monoallelic deletion of BECN1, which encodes the Beclin1 protein [2, 166], and abnormal expression levels of Beclin1 in tumours have been linked to poor prognosis [70, 277]. Beclin1 is the regulator of the PtdIns3K complex that is required for the initiation, nucleation, and assembly of the phagophore, and has biological roles in anti-apoptosis [38] and endocytic trafficking [254]. Studies have shown that heterozygous disruption of Beclin1 in mice resulted in decreased autophagy, rendering them more susceptible to the spontaneous development of tumours [215, 287]. This indicates a possible mechanistic role for Beclin1 in tumorigenesis.

Although the genetic link between cancer and autophagic dysregulation suggests that it may act as a tumour suppressor pathway, the exact underlying mechanisms remain unknown. Studies in autophagy-deficient yeast have shown an increase in the frequency of mitochondrial DNA mutations implying that basal

Stellenbosch University https://scholar.sun.ac.za



autophagy may have a role in preventing genotoxic stress and subsequent DNA damage [161, 177]. Beclin1 or Atg5 knockdown mice epithelial cells show increased DNA damage and tumorigenicity, supporting the role of Atg5 and Beclin1 in preserving genomic integrity via autophagy [177]. In fact, given that the primary role of autophagy is to promote cell survival and preserve cellular integrity, it indirectly functions as a tumour suppressor by preserving gene stability. Under conditions of metabolic stress, autophagy is also able to support tumour survival [243]. Understanding the pro-survival effects of autophagy is especially important since it could potentially contribute to chemotherapeutic resistance in tumours. Studies have shown that the inhibition of autophagy increases cytotoxicity of cancer chemotherapeutic agents and also increases their efficacy [1, 26]. Thus, the disruption of autophagy could serve as a therapeutic target to maximize the effects of cytotoxic drugs in cancer treatment.

### 2.4.3 Continuous cytoplasmic protein turnover keeps cells healthy

A feature of ageing cells is the accumulation of damaged proteins and organelles in parallel with an increase in cellular stress susceptibility, even in the absence of diseases. Build-up of damaged proteins and organelles, and the resultant formation and accumulation of inclusion bodies, can have deleterious effects, particularly in non-dividing and differentiated cells. It is worth noting that, compared with other cell types, non-dividing cells characteristically exhibit earlier functional decline with age [253]. Moreover, studies have shown that both macroautophagy and chaperone-mediated autophagy activity decreases with age [42, 46]. Therefore, it is conceivable that the cytoprotective role of autophagy is not only important for maintaining cellular integrity, as a short-term response to stress (hours to days), but that it also contributes to the overall longevity of the cell and/or organism. Interestingly, studies have shown that caloric restriction, which is known to induce autophagy, slows down the effects of ageing [90].

Stellenbosch University https://scholar.sun.ac.za



### 2.4.4 Autophagy's cytoprotective properties make it an ideal therapeutic target

Autophagy has become an attractive target in neurodegenerative diseases to clear toxic and damaging aggregate-prone proteins, and thereby promote cellular homeostasis. Whereas autophagy-modulating drugs conferred positive effects against neurodegeneration, in cancer the pharmacological inhibition of autophagy has been shown to improve the efficacy of chemotherapeutic drugs by disrupting autophagy's cytoprotective properties and thereby sensitising cancer cells [6, 26, 162]. Even more so, studies have expanded on this design and showed that first increasing autophagy before inhibiting it can further improve the efficacy of cancer therapies [243]. Preclinical trials have shown that autophagy-targeting interventions can increase the effects of cancer chemotherapeutic drugs [11, 40, 53, 275].

Despite these promising results there appears to be considerable confusion as to how autophagy-therapies should be developed and used for the treatment of several pathologies. The success of developing future autophagy-targeting therapies requires three main factors: one, to accurately measure autophagy; two, to characterise autophagy modulating drugs in cells and tissues; three, to unravel the role of autophagy in disease pathology in order to identify modulating targets. This would enable us to determine whether autophagy activity is too high or too low, and adjust it accordingly to achieve the desired effect. In the following section we will discuss the current methods used for monitoring autophagy, and how they are utilized to characterise autophagy modulating drugs.

Thus, better characterising autophagy modulating drugs would play an important role in developing autophagy-targeting therapies as it would allow us to determine various pharmacodynamic properties such as the minimum and maximum therapeutic dosage, the lethal dosage, as well as synergistic and antagonistic drug effects. This would allow for the fine manipulation of autophagy using minimal dosages to achieve the desired effect, whilst bypassing side effects. Moreover, computational modelling provides a unique platform to interrogate and unravel the system properties. Such an approach would deepen our understanding of the contribution of autophagy to maintaining cellular "health" and its role in disease

Stellenbosch University https://scholar.sun.ac.za



pathologies.

## 2.5 Current methods for monitoring autophagy

There have been rapid advances in the autophagy research field in the past decade, driven by new molecular tools ushered in by the turn of the century. Novel techniques such as genetic manipulation uncovered various proteins involved in autophagy and the importance of this pathway in cellular processes ranging from homeostasis to foetus/organism development. Many techniques were developed to assess autophagy over the years [138–140, 190, 283]. In this section routinely used techniques, including electron and fluorescence microscopy and biochemical assays will be discussed. In light of understanding the dynamic properties of autophagy, the inherent challenges that accompany these techniques, with emphasis on measuring autophagy vesicles and/or activity over time, will be highlighted. Such information about the autophagy process would be crucial for the development of reliable computational models to investigate the underlining system properties.

### 2.5.1 Biochemical assays

Western blot analysis is a widely-used analytical technique in molecular research to separate and detect specific proteins based on their molecular size. Generally, autophagic activity is assessed by measuring the abundance of key autophagic machinery proteins (e.g., LC3), or autophagic receptors (e.g., p62) to report on autophagic system/cargo progress. Traditionally, western blot analysis is performed in conjunction with EM to provide ultrastructural detail of autophagosomes.

**The most widely used technique to assess autophagic activity is by monitoring LC3 turnover.** LC3 has become a particularly attractive means for assessing autophagic activity due to its direct relation to autophagosome formation. LC3 has several homologues among which LC3A and LC3B are the most commonly assessed by western blot analysis. Endogenous LC3 usually yields two distinct bands after separation on a sodium dodecyl sulphate–polyacrylamide gel

Stellenbosch University https://scholar.sun.ac.za



electrophoresis (SDS-PAGE): the presence of one band represents LC3-I, which is cytosolic, and the presence of two bands represents LC3-II, which is confined to autophagosomes. The amount of LC3-II detected corresponds to the number of autophagosomes, or more accurately, the overall abundance of the autophagosomal membrane integrated with LC3-II [118]. LC3-I and LC3-II are detected on the membrane at a molecular mass of approximately 16 kDa and 14 kDa respectively. Although the true molecular mass of LC3-II is greater than that of LC3-I, the conjugation of LC3 with PE causes it to migrate faster than LC3-I in SDS-PAGE, presumably due to its extreme hydrophobicity. Not all LC3-II is localised to autophagosomal membranes, the genetical or pharmacological suppression of autophagy still results in a certain degree of LC3-II being generated, and consequently detected via biochemical assays [84, 96, 178]. Therefore, either FM or EM is used in conjunction with western blot analysis to accurately report autophagy activity.

Under normal conditions, LC3 undergoes a series of biochemical reactions to form LC3-II and becomes incorporated into the membrane of the growing autophagosome. The fusion of autophagosomes with lysosomes results in the degradation of LC3-II, and thereby maintains low levels of LC3-II. Treatment of cells with lysosomotropic agents, such as bafilomycin $A_1$ or chloroquine, results in the accumulation of autophagosomes and, consequently, LC3-II, since the de-acidification of lysosomes prevents the fusion of autophagosomes and lysosomes [251]. The difference in LC3-II levels, both in the presence and absence of lysosomal inhibitors, reflects the amount of LC3-II delivered to lysosomes for degradation. Therefore, the rate at which LC3-II accumulates is proportional to the rate of autophagosome turnover, and protein degradation, through autophagy, i.e., autophagy flux [140, 190, 226].

**Degradation of selective markers.** Recent studies have revealed a number of autophagy receptor proteins that facilitate the binding of specific substrates to the growing autophagosome, thereby facilitating its degradation [65]. These receptors are selectively incorporated into the autophagosome by associating with LC3 via

Stellenbosch University https://scholar.sun.ac.za



the LIR motif of the receptor, thereby bringing the substrates into close proximity of developing autophagosomes for sequestration, and consequently, degradation. Of these autophagy receptors, p62 was the first to be described and remains the best studied receptor protein. The total number of intracellular autophagy receptors, such as p62, correlates inversely with autophagic activity. Thus, a reduction in p62 abundance compared to basal conditions indicates an increase in autophagic flux. The recent discovery of novel autophagy receptors makes it a promising method not only to assess autophagic flux but also cargo specific degradation. However, using autophagy receptors for autophagic flux analysis should be performed with caution as they are transcriptionally regulated during autophagy which may result in the inaccurate interpretation of autophagic flux at any given time [89, 200].

**General protein degradation.** Long lived proteins are primarily degraded by autophagy. Isotope labelling has been used for many years to study metabolic fluxes, and assesses the make-up of biochemical pathways and networks. This technique was vital in the initial days of metabolic pathway analysis when the conversion of chemical compounds was tracked and traced by following the incorporation of heavy atoms into substrates to metabolic products. One of the more historical methods, developed in the 1970s, involves the monitoring of radio-labelled, long-lived proteins in cells over time [191]. The radioactive labelling of long-lived proteins involves culturing cells with isotope-labelled amino acids (commonly [$^{14}$C] or [$^{3}$H]-labelled leucine or valine) for several days, followed by short-term culturing in normal growth media in order to remove all radio-labelled short-lived proteins. The amount of radio-labelled amino acids released into the cytoplasm is quantified and gives an indication of autophagic flux. This technique provides precise numerical data that reflects the half-life of long-lived cellular proteins.

Stellenbosch University https://scholar.sun.ac.za



### 2.5.2 Electron microscopy

Electron microscopy (EM) is the most established method for monitoring autophagic vesicles, and is still considered the gold standard in autophagy research. Autophagy was first discovered in mammalian cells in the 1960s using EM whilst studying lysosomes [44]. Autophagosomes were first described as double-membraned structures that contain partially digested cytoplasmic content, such as mitochondria or ER. The high resolution of EM micrographs makes it relatively easy to identify autophagosomes given their unique morphological characteristics. In contrast, autolysosomes are more difficult to identify since the cargo is either partially or completely degraded and surrounded by a single membrane vesicle with no other obvious characteristics distinguishing it from other single-membraned vesicles.

One of the most notable advantages of EM is its high resolution compared to optical microscopy, which allows for ultra-structural characterisation and morphometric analysis of autophagic vesicles, such as dimensions and cargo analysis. EM is a well-established method in the field of autophagy research and continues to provide invaluable data in dissecting the autophagy process. However, a number of challenges exist when utilizing EM; for instance, due to the constraints of sample preparation, which include fixation and sectioning, it does not reflect the true dynamic nature of the autophagy process, but rather provides a snapshot of the intracellular composition at one particular time point and on a single z-axis plane. Therefore, the autophagic response cannot be monitored over time on a single cell level. Furthermore, sectioning and imaging of EM samples only reflects the autophagic vesicles visible in a single focal plane, which does not provide information of the autophagic system in its entirety and therefore leads to the reporting of underestimated vesicle numbers. Recent advances in EM technology allows the 3-dimensional imaging of EM embedded samples using serial block face EM [47]. Even though this does overcome previous limitations of imaging a single z layer using EM to some degree, it still remains a laborious task and does not allow for imaging of a single cell in a time dependent manner.

Stellenbosch University https://scholar.sun.ac.za



### 2.5.3 Fluorescence microscopy

Fluorescence microscopy (FM) is a technique that enables the visualization and localization of fluorescent proteins or probes in a cell that tag a specific protein of interest. When these probes are excited at a particular wavelength, they emit a fluorescence signal that is used to generate an image. FM has recently become a popular tool amongst scientists since it requires considerably less expertise to operate than EM to identify autophagic related structures. FM has a number of advantages which makes it one of the most popular cell and molecular biological research tools to study dynamic changes in the cell. Perhaps the biggest advantage is the possibility to track distinct organelles or molecules over time using different fluorophores simultaneously. Multicolour FM further enables us to assess possible interactions between organelles or molecules by observing colocalization, i.e., when two or more differently-labelled fluorescent molecules overlap. FM allows for the observation of the dynamic processes that drive this structural organisation in living cells in a non-invasive manner, making it an ideal tool to assess the autophagy process, the recruitment of Atg, the formation of autophagosomes, and their subsequent fusion with lysosomes. Moreover, FM allows for 3D characterization based on a 3D data stack acquired through the z-plane. In contrast to conventional EM, 3D FM allows for whole cell characterisation of the autophagic system.

In autophagy research the most common application of FM is to monitor LC3 tagged with a fluorescent protein, typically green fluorescent protein (GFP) or mCherry. LC3 undergoes ubiquitination-like processing and gets incorporated into the growing phagophore and forms part of the autophagosome membrane, which, after fusion with the lysosome, is cleaved from the autophagosomal outer membrane, whilst the inner membranous LC3 is degraded by lysosomal hydrolases. Therefore, FM enables the visualisation of LC3 structures either as a diffuse cytoplasmic pool or as puncta which mainly represent autophagosomes. However, studies have shown that GFP is not immediately quenched and therefore autophagosomes may only constitute a small fraction of GFP-positive puncta [50, 111]. Variations in the physical and chemical properties of fluorescence probes and the autophagic vesicles have also been used to investigate the step-by-step transfor-

Stellenbosch University https://scholar.sun.ac.za



mation of autophagic vesicles more accurately. One such example is the mCherry-GFP tandem construct, which has been adapted to overcome lysosomal quenching of GFP [191]. In neutral or slightly basic conditions GFP is a stably folded protein; however, under low pH conditions (such as inside the lysosomal milieu), GFP undergoes denaturing, and the fluorescence signal is quenched. In contrast, mCherry and other red fluorescence proteins (RFP) show increased fluorescence under acidic conditions, and can readily be detected in autolysosomes. Therefore, the differences in the nature of these two fluorescence proteins allow distinction between autophagosomes and autolysosomes as yellow and red puncta respectively, and also allow for the monitoring of autophagy over time [139, 191]. Similar, chemical properties of the autophagic vesicles have been skilfully used to distinguish between autophagosomes, autolysosomes and lysosomes using GFP-LC3 and fluorescent dyes [50]. These acidotrophic dyes accumulate in a low pH environment and emit a fluorescence signal. Therefore, the combination of GFP-LC3 present in autolysosomes (which would otherwise been reported as autophagosomes) and fluorescent dyes inside the acid lumen of autolysosomes allows for the detection of the different autophagy intermediates.

In addition to directly labelling and monitoring autophagy vesicles, there are a number of techniques with which to assess autophagy activity, or more accurately, its degradative capacity. One such technique indirectly assesses autophagy activity by measuring cytoplasmic protein turnover using photo-activatable proteins [144, 260]. These photo-activatable proteins are expressed in the cytoplasm; once activated, they emit a fluorescence signal which is measured over time. The rate of decay of the fluorescence signal can be used to indirectly assess autophagic degradation [260]. Another technique is the recently developed GFP-LC3-RFP-LC3ΔG autophagic flux probe by Kaizuka *et al.* [120] that measures autophagy activity based on the abundance of GFP-LC3 and RFP-LC3ΔG [120]. This probe relies on the endogenous Atg4 protease to cleave GFP-LC3-RFP-LC3ΔG into equal amounts of GFP-LC3 and RFP-LC3ΔG. While GFP-LC3 undergoes lipidation and is subsequently incorporated into the autophagy pathway where it is degraded, RFP-LC3ΔG is lipidated and thus resides stably in the cytoplasm where it can

Stellenbosch University https://scholar.sun.ac.za



serve as an internal control. The GFP/RFP ratio can therefore be used to estimate autophagic flux, although it does not measure the pool sizes of autophagic vesicles.

### 2.5.4 Conclusion

It is clear that many techniques have been developed to investigate various aspects of the autophagy process. Although these techniques have provided invaluable information on the autophagic system they are not without limitations; to achieve a more accurate assessment of autophagic activity the standard practice is therefore to use several of these methods in combination. With the aim of modelling the autophagy process, experimental measurements should reflect the dynamic nature of the autophagy process quantitatively. Arguably, the greatest advantage of FM is that it allows the autophagy process to be assessed in real time using fluorescently-tagged autophagy proteins, which provides a powerful tool for generating the quantitative real time data required to create autophagy models.

## 2.6 Computational modelling of autophagy

Autophagy is a complex process that involves the recruitment of more than 30 proteins in a highly orchestrated manner to give rise to autophagosomes, which then requires additional proteins, such as transport and fusion proteins, for efficient autophagic cargo clearance. While there have been considerable advances in developing ever more accurate tools to assess autophagy, unravelling, in a laboratory setting, the underlying mechanism of autophagy and its role in disease pathology is challenging due to the complexity of interactions and tools available to accurately measure autophagy. In conjunction with experimental studies, computational modelling is a powerful tool with which to investigate the system properties of autophagy. Here several autophagy models will be discussed with emphasis on the vesicular pathway and cargo degradation.

Stellenbosch University https://scholar.sun.ac.za



### 2.6.1 Autophagic flux is a measure of autophagic degradation activity

Autophagic flux is defined as a measure of autophagic degradation activity. This definition rightfully points to the meaning of flux, namely the rate of autophagic degradation. Taking into consideration the autophagy process - the encapsulation of cargo in double-membraned vesicles and the fusion thereof with lysosomes for the degradation of the cargo - we can distinguish between the vesicular machinery of the autophagic system, and the cargo that is being degraded within this system. The vesicular flux is the rate of flow along the vesicular pathway, whereas the cargo degradation is the rate at which the autophagy cargo itself is being degraded within the system. Together these two components form the autophagy process.

#### 2.6.1.1 Vesicular pathway - the stepwise transformation of the autophagic vesicles

The autophagic vesicular pathway starts with the formation of a phagophore, that, once matured into an autophagosome, fuses with lysosomes to form autolysosomes in which the autophagic cargo is degraded and recycled (Fig. 2.3). This stepwise transformation of the autophagic vesicles forms the 'core' network in autophagy vesicular models used in computational research.

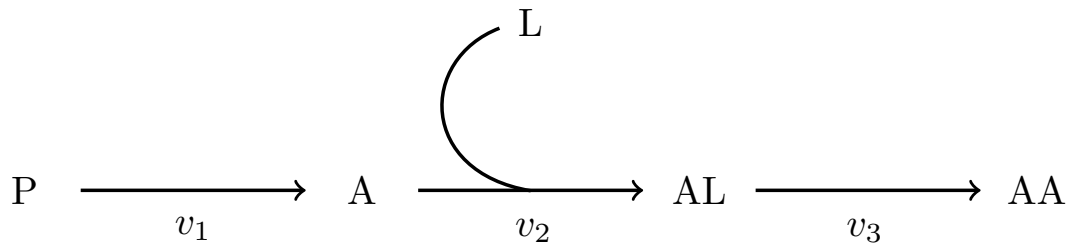


**Figure 2.3:** Network representation of the autophagy process: The minimal model describes autophagosome synthesis, fusion with lysosomes, and autophagosome breakdown with the release of amino acids.

Stellenbosch University https://scholar.sun.ac.za



**A computational model rooted in experimental data can provide a reliable platform for investigating autophagy in a cellular system.** The simplest approach in constructing a model would be to start with a minimal model of a system that can be systematically parameterised and expanded using experimental data. Martin *et al.* [175] were one of the first groups to construct a computational model of the autophagic vesicle dynamics using FM derived data. Their experimental work centred around the measurement of GFP-LC3-II positive autophagic vesicles over time in the absence and presence of autophagosome/lysosome fusion inhibitor, bafilomycin $A_1$. At basal levels, in the absence of lysosomal fusion inhibitor, the newly synthesised autophagosomes replenish the autophagosome pool whilst being degraded by lysosomes. The GFP moiety of the GFP-LC3-II fusion is pH sensitive and is quenched once delivered to the acidic lumen of the lysosome. Thus, GFP-LC3-II selectively labels phagophores and autophagosomes while it does not label autolysosomes. By completely inhibiting the fusion of autophagosomes and lysosomes, autophagosome synthesis continues unimpeded and the rate of accumulation of autophagosomes corresponds to the rate of autophagosome synthesis. The use of a lysosomal fusion inhibitor to tease out the rate of autophagosome synthesis was first described by Rubinsztein *et al.* [226] using western blot analysis of LC3-II. However, it only relates a relative increase, or decrease, in autophagosomal synthesis. Martin *et al.* [175] exploited FM to determine the rate of autophagosome synthesis by treating cells with a lysosomal fusion inhibitor and measuring the rate of autophagosome accumulation. The use of FM allowed them to generate quantitative data of the autophagic system in real time, which is necessary to construct a realistic model of autophagy.

Martin *et al.* [175] created a mechanistic and stochastic model of the autophagic vesicle dynamics consisting of a series of biochemical reactions that are involved in the formation of the phagophore, autophagosome maturation, and the degradation process. For modelling purposes, they considered all the proteins used in the model to be expressed at the same level and the parameters were determined by parameter fitting so that the number of autophagosomes and the rate of synthesis at steady state matched the experimentally observed values. They also

Stellenbosch University https://scholar.sun.ac.za



induced the autophagic system and incorporated it into the model by multiplying the input parameter with an induction constant to simulate the induction of autophagy. Analysis of the time course following induction of the autophagic system showed a lag in the increase of vesicle formation, which was also accounted for in the simulations. Sensitivity analysis of their model was performed to identify the parameters that were the most influential on the lag and found that the rate of recruitment of Atg12–Atg5-Atg16L1 scaffolding complex to the phagophore and LC3-I to Atg12–Atg5:Atg16L1 complex had the greatest effect. The Atg12–Atg5-Atg16L1 complex plays a key role in formation of autophagosomes by acting as a scaffolding protein in the growing autophagosome as well as partaking in the lipidation process of LC3 so that it can be incorporated. That the rate, and the amount, at which Atg12–Atg5-Atg16L1 is recruited would influence the size and the number of autophagosomes seems intuitive, but this is nevertheless a challenging aspect to assess experimentally. The model presented by Martin *et al.* [175] clearly shows how these factors contribute to the growing autophagosome. Simulations also demonstrated a positive correlation between LC3 levels and autophagosome size in cells when they incrementally increased the concentration of LC3 that resulted in an increase in the mean vesicle size. Their model prediction that LC3 plays a role in autophagosome curvature, and consequently size, is supported by yeast and mammalian studies [199, 279]. Moreover, the strength of computational modelling lies in its ability to generate testable predictions. Hence, Martin *et al.* [175] predicted the contribution of Atg9 to autophagosome size and showed that a reduction in Atg9 suppresses autophagy activity, a prediction that was supported by their Atg9 siRNA experimental data. Moreover, analysis of their experimental data suggests that vesicle turnover occurs at a rate proportional to the number of vesicles in a cell, and that autophagosome degradation occurs by means of a first order process. Therefore, the induction of autophagy would not only increase the rate of autophagosome synthesis, but also increased its rate of degradation. Since the number of lysosomes increases proportionally with autophagosomes, so will the number of encounters between lysosomes and autophagosomes and, concomitantly, the rate of autophagosome degradation. Therefore, if the lysosomes are

Stellenbosch University https://scholar.sun.ac.za



not limiting, the rate of autophagosome degradation follows from the law of mass action. Moreover, experimental data from Martin *et al.* [175] showed fluctuations in the number of autophagosomes as a result of the intrinsic noise in autophagosome dynamics, which was suggested to stem from a series of complex reactions required for the formation of the phagophore/autophagosome.

**Flux is the rate of flow along the vesicular pathway.** We recently published an approach that makes use of fusion inhibitors to measure the autophagosome flux, which we define as the rate of flow, i.e., the transformation of autophagic vesicles, along the vesicular pathway at steady state [50]. Our approach allows for the steady state characterisation of the autophagy system in terms of (i) its complete steady state pool size of the various autophagic intermediates ($n_{\mathrm{A}}$, $n_{\mathrm{AL}}$ and $n_{\mathrm{L}}$), (ii) the autophagosome flux, $J$ (autophagosome/hour/cell), and (iii) the transition time, $\tau$, for the respective autophagic vesicles pool ($\tau_{\mathrm{A}}$ and $\tau_{\mathrm{AL}}$). Our approach has several advantages: one, acquiring z-stacks generates an accurate measurement of the number of autophagic vesicles; two, using an acidotrophic LysoTracker, in combination with GFP-LC3, allows a distinction between autophagosomes and autolysosomes to be made; three, using small intervals to measure autophagosome accumulation after treatment with bafilomycin $\mathrm{A}_1$ at steady state produces more reliable flux data.

We constructed a computational model of autophagy (see Chapter 5), that successfully simulated the time-dependent behaviour of the autophagic system. Our modelling strategy was to start with a minimal model of autophagy using the simplest possible rate equations, and then to extend the network scheme and modify the kinetics parameters step by step in order to achieve a good fit to the experimental data. This approach allowed an in-depth understanding of the contribution of each part of the autophagic network to its time-dependent behaviour. Initially, all steps in the reaction network were described using first order rate equations, but to fit the simulated data to the experimental data more accurately the fusion step between autophagosome and lysosomes required a higher rate order to reflect the involvement of additional factors required in the fusion step. In our model the

Stellenbosch University https://scholar.sun.ac.za



fusion step is an oversimplification of a series of events required from the point of autophagosome maturation until complete fusion with lysosomes, which involves *inter alia* the active translocation of vesicles along the tubulin network as well as fusion proteins. The use of higher rate order is in contrast to Martin *et al.* [175], who described the degradation, or the turnover, of autophagosomes with a first-order rate equation. The reason for this may stem from the fact that they did not distinguish between autophagosomes and autolysosomes. Our data suggests that autophagosomes only constitute a small fraction of GFP-LC3 positive puncta, while the rest are autolysosomes, a conclusion which is also supported by Jahreiss *et al.* [111]. Thus, the turnover rate measured by Martin *et al.* [175] is more a representation of autolysosome degradation. Following induction with rapamycin there was an overall increase in GFP-LC3 positive puncta; with LysoTracker, however, we found that the number of autophagosomes remained unchanged while the number of autolysosomes greatly increased. This suggests that autophagosomes have a rather short half-life in the cell and are readily fused with lysosomes.

Our experimental data exhibited a lag in the autophagic response when it was induced, which was also reported Martin *et al.* [175]. We contributed this lag time to the signalling and recruitment of proteins upstream from the formation of the phagophore. In our model we simplified this very complicated procees by incorporating it into a single reaction step, namely the dephosphorylation of mTOR, which regulates the rate of autophagosome synthesis and, therefore, autophagosome flux. Since rapamycin targets mTOR, we simulated its inductive effect by changing the rate constant of the dephosphorylation of phospho-mTOR. In addition to the observed lag in autophagosomes response, the time course experiments also revealed that, following induction, there was an overshoot in the number of autophagosomes before they returne to their steady state number; this feature of the timecourse had not been previously reported. Although only a minimal model at this time, its distinction between autophagosomes and autolysosomes pool size and measurement of the flux at steady state, probably reflects the dynamic nature of the autophagic vesicular process more accurately than other models in the literature.

Stellenbosch University https://scholar.sun.ac.za



**The vesicular pathway: more than just free-floating intracellular vesicles.** Despite the illusion created by imaging techniques that autophagy vesicles are free-floating and move randomly within the cell, it is well established that they are actively translocated in an orderly manner from the site of synthesis along the microtubule network towards lysosomes [109, 143]. This transport process leads to a complex and integrated relationship between spatial regulation of autophagy vesicles and autophagy activity [150]. For instance, during periods of starvation lysosomes cluster in the perinuclear region, which is thought to promote fusion with autophagosomes. Indeed, autophagosomes are actively transported towards the perinuclear region bringing them into close proximity of lysosomes, thereby increasing the number of fusion events between lysosomes and autophagosomes. It is clear that the tubulin network plays an important role in the autophagic system [15, 143] and it is not surprising that it has been implicated in autophagy dysfunction and, consequently, disease progression [109]. The kinetic and thermodynamic properties of tubulin governs the density distribution of the tubulin network, which impacts the transport dynamics of autophagic vesicles and consequently autophagy function.

Börlin *et al.* [22] created an agent-based model (ABM) of autophagy to investigate the regulatory behaviour of spatio-temporal autophagy dynamics. Similar to the previously-mentioned modelling attempts by other groups, they parameterised their model using microscopy derived data from single cells. Börlin *et al.* [22] used mCherry-LC3B and GFP-RAB7 to make the important distinction between autophagosomes, autolysosomes and lysosomes, which they used to assess and model their spatio-temporal dynamics. Their 'core' model of autophagy closely resembled that of ours (see Chapter 5), but Börlin *et al.* [22] included autolysosome fusion with other autophagosomes, as well as their degradation when autolysosomes had reached the end of their lifetime. The ABM of Börlin *et al.* [22] made use of self-defined functions and hierarchical ordering of procedures to create a description of cellular processes; it simulated the temporal and spatial evolution of the autophagic system, where each individual agent (autophagic vesicles) was governed by its own parameter set that determined its behaviour and interaction with other

Stellenbosch University https://scholar.sun.ac.za



agents. Although ABMs are not commonly used for biological modelling, they have been used to capture emergent mitochondrial fusion and fission behaviour [211], and apoptotic death receptor dynamics [232]. For modelling, Bandyopadhyay *et al.* [16] assumed that phagophores and autolysosomes move randomly, while autophagosomes and lysosomes move directly towards or away from the nucleus, in a manner that simulates their active transport along the cytoskeleton at a rate that is independent of their size. The initial number of autophagosomes, lysosomes and autolysosomes was based on experimentally derived data, whereas all other parameters were generated using data-driven model parameter fitting of basal autophagic activity [16]. Earlier modelling attempts by Börlin *et al.* [22] demonstrated that their core model could not successfully simulate bafilomycin $A_1$ treated conditions. They suggested that after 3 hours bafilomycin $A_1$ treatment could have resulted in lysosomal inhibition, which prevented protein degradation and amino acid recycling, and thereby decreased mTOR activity and subsequently increased autophagy activity. Börlin *et al.* [22] integrated nutrient uptake and recycling in their model, so improving the accuracy of their simulation of autophagosome, autolysosome and lysosome numbers, as well as the spatial patterns and positioning of autophagic vesicles. Experimental data by Börlin *et al.* [22] showed that under starvation conditions the number of autophagosomes, autolysosomes and lysosomes increased, and surprisingly, that the number of autophagosomes decreased when cells were treated with a lysosomal fusion inhibitor. It would be expected that, following inhibition, the number of autophagosomes would increase, which indeed is the case and is at the centre of determining autophagic flux using western blot analysis and FM. It is possible that the decrease in autophagosomes results from the time scale in which the autophagic vesicles were measured following inhibition, since it is well documented that other degradation systems such as microautophagy and the UPS are upregulated to compensate for the lack of protein turnover as a result of dysfunctional autophagy [154, 267]. Therefore, dependency of protein turnover is shifted away from autophagy and proceeds at a lower rate, so decreasing the number of autophagosomes. However, this notion remains to be verified. The incorporation of spatio-temporal autophagy dynamics

Stellenbosch University https://scholar.sun.ac.za



is a step forward in building autophagy models.

#### 2.6.1.2 Cargo degradation and its implications in protein quality control

In the past autophagy was generally considered to be a non-specific process that involves the random engulfment of cytoplasmic material. However, autophagy can also selectively clear specific cellular components such as mitochondria (mitophagy), lipids (lipophagy) and ribosomes (ribophagy) [65]. Selective targeting of proteins/organelles is brought about by adapter proteins that facilitate the encapsulation of target proteins/organelles in the growing autophagosome. Because of the inherent difficulties in studying cargo degradation and the selective nature of autophagy experimentally, only a few studies have attempted to model these processes. Although it is possible to indirectly assess superfluous cargo degradation on the basis of autophagosome size and autophagosome flux, it has been the time-honoured technique of using radio-labelled isotopes in track and trace experiments that has generated data that has proved useful for modelling the cargo degradation.

The Choi research group used assays with radio-labelled amino acids and metabolic inert sugars, as well as ATP assays, to create a model that could be used to investigate the implications of autophagy for cellular quality control through cytoplasmic turnover [78–81]. They measured [$^{14}$C]-sucrose recovered from whole cell lysates and autophagosomes to assess cytoplasmic sequestration, while [$^{14}$C]-lactose and its hydrolytic product, [$^{14}$C]-sucrose, were used to assess intra-autolysosomal hydrolysis. Combined with [$^{14}$C]-valine to determine rates of protein synthesis and degradation, these experiments generated a rather unique data set of autophagy and its implications for the cytoplasmic protein content. In their 'core' model, the autophagy process was divided into several steps: autophagosome synthesis, autolysosome formation, and intra-lysosomal hydrolysis, where intracellular ATP and amino acids were considered to be the key molecules in the model that bridged between protein/organelle synthesis and autophagic/non-autophagic degradation. Although their network does include the vesicular pathway, the au-

Stellenbosch University https://scholar.sun.ac.za



thors focused on creating a model that characterised the relationship between autophagy activity and the corresponding cellular change. With that in mind, a model of intracellular ATP and amino acids dependency was constructed, in which the autophagic substrates included normal and abnormal/damaged proteins, each sequestered at different rates. The end products of autophagic degradation, mostly amino acids, can then be used to either generate new proteins or to produce ATP, whilst the generation of new proteins also requires ATP.

**Role of autophagy in cellular quality control.** To investigate the role of autophagy in protein/organelle quality control in response to perturbation of cellular damage, Han *et al.* [78] manipulated the deterioration rate of proteins in their model. Their simulations revealed a nonlinear relationship between damaged and normal proteins/organelles degradation [78]. Whilst the degradation of proteins/organelles increased proportionally with the accumulation of proteins/organelles, damaged proteins/organelles were exponentially degraded once a threshold was reached. Han *et al.* [78] attributed this to the affinity of adaptor proteins for the targeted proteins/organelles. Based on their results they concluded, in accordance with the literature, that during periods of too low autophagy activity the system loses the ability to maintain protein quality control, whilst induction of autophagy improves cellular protein/organelle quality. Based on their model, the authors concluded that the control over autophagic degradative capacity resides with autophagosome synthesis rather than autolysosome formation and the degradation of its cargo, and similar findings have also been reported by the other groups [22, 175].

#### 2.6.1.3 Vesicular pathway and cargo degradation contribute to the autophagic activity

Autophagy, in particular the lack thereof, has been implicated in several diseases, and has given rise to multiple hypotheses as to how autophagy contributes to disease progression. Some of the strongest suggestions include: (i) the inability of the developing phagophore to sequester (toxic) proteins, (ii) impaired translocation

Stellenbosch University https://scholar.sun.ac.za



of autophagosomes, and (iii) fusion with lysosomes and dysfunctional lysosomal hydrolase activity [100, 113, 227]. Although we have up to now discussed the autophagy process as separate components, i.e., the vesicular pathway and cargo degradation, it is in reality a single pathway in which both components proceed alongside each other. Although both the vesicular pathway and cargo degradation are driven by their own molecular machinery, they do share some proteins, but it is nevertheless reasonable to assume that it would be possible to differentially regulate the two components to achieve the desired goal. For instance, an increase in general cytoplasmic cargo sequestration and degradation without changing autophagosome flux can be achieved by increasing autophagosome size by enhancing LC3 or Atg14 expression levels. Similarly, an improvement in the clearance of specific proteins/organelles without affecting general cytoplasmic proteins can be achieved by increasing adaptor proteins, whilst the vesicular pathway flux remains unchanged. Insight into the unique interplay between the two components, as well as other non-autophagy components such as the tubulin network, could aid in the design of autophagy-related therapies through the identification of novel protein targets.

### 2.6.2 Modelling autophagy in a cell population

The end goal of these models is to further our understanding of autophagy and its pro-survival role so as to best exploit it for therapeutic purposes. However, most of the models described here focus on autophagy at a single cell level, whilst neglecting its broader impact. For instance, during periods of starvation autophagy is upregulated to supply amino acids for energy production in order to sustain the cell; amino acids can, however, also be released into the extracellular environment to support neighbouring cells, thereby contributing to the pro-survival effects of autophagy on a tissue level. Although we are far from modelling autophagy on such a systemic level, it is worth noting work done by Jin and Lei [114] who created a model of the effects of nutrient dynamics and autophagy on cell population growth in response to starvation. Their model is within a population growth framework, similar to those models used in ecology to study animal population patterns, to

Stellenbosch University https://scholar.sun.ac.za



simulate yeast growth during periods of high and low nutrient abundance, and to investigate the effects of autophagy on yeast population growth dynamics. For modelling purposes they considered yeast cells that can be either in a normal growth phase or in an induced autophagy phase in a container with a fixed volume that is supplied with nutrients at a constant rate whilst nutrients are lost. Induced autophagy cells were considered not to proliferate since growth arrest generally accompanies high autophagic activity, but they were nevertheless able to revert back to the normal growth phase. Analysis of the mathematical framework highlighted the importance of cell/population survival through the secretion of nutrients by cells undergoing high autophagic activity when there is no access to external environmental nutrients. Although the mathematical framework presented by Jin and Lei [114] is a general model with non-specific molecular level regulation, it is biologically plausible and could be used in a robust manner with different types of cells. Expansion of such models to include different cell/tissue could potentially serve as a starting point for understanding autophagy on a systemic level.

### 2.6.3 Conclusion

The models presented here represent the minimal models in their respective fields, making use of a variety of modelling platforms and computational tools. They contribute to the foundations of a formal framework that could be developed further to include more of the known molecular machinery involved in autophagy. To comprehensively model the autophagic pathway requires the incorporation of multiple autophagy proteins, ranging from the signalling pathways to recruitment of structural proteins involved in the growing autophagosomes and their translocation, as well as the fusion of autophagosomes and lysosomes. The increased complexity of such a model would require reaction networks consisting of a large number of proteins with their interactions, post-translational modifications and sub-cellular localisation. These models would need to be able to simulate the processes over a fast and slow time scale (i.e., hours to days) as well as be able to generate and test predictions relevant to the global consequences of autophagy, particularly in disease scenarios. Moreover, possibly the most important feature of a computational

Stellenbosch University https://scholar.sun.ac.za



model is that it can be used to generate novel experimentally-testable hypotheses. Ultimately one hopes that such models could be to be used in personalised medicine where they could assist in developing patient specific therapies to achieve maximal drug efficiency with minimal side effects.

Stellenbosch University https://scholar.sun.ac.za

# Chapter 3

# General Laboratory Methods and Materials

## 3.1 General laboratory consumables

Sterile disposable 5 mL (SPL, # 91005), 10 mL (SPL, # 91010) and 25 mL (SPL, # 91025) serological pipettes with pipette control (Pipetteman, PIPETBOY) were used to transfer large liquid volumes and for cell culturing purposes. Disposable pipette tips, 10 $\mu$L (Pipetman, # D10), 200 $\mu$L (Pipetman, # D200) and 1000 $\mu$L (Pipetman, # D1000), and disposable filter pipette tips, 200 $\mu$L (QSP, # TF140-200) and 1000 $\mu$L (QSP, # TF140-100) with Pipetman P20, P200, and P1000 (Pipetman Starter Kit) were used for cell culturing and general liquid handling. Solutions and cell lysates were stored in either micro-centrifuge tubes, 0.5 mL (Citotest, # 4610-1820), 1 mL (Citotest, # 4610-1816) and 2 mL (Citotest, # 4610-1815), or in Falcon® tubes, 15 mL (Biocom Biotech, # 50025) or 50 mL Falcon® tube (Biocom Biotech, # 50050).

## 3.2 Cell culturing protocol

Mouse Embryonic Fibroblast (MEF) and HeLa cells stably expressing GFP light chain 3 (LC3) protein (a kind gift from Prof. Noboru Mizushima, Tokyo Univer-

Stellenbosch University https://scholar.sun.ac.za



sity, Japan) and wild type MEF cells (a kind gift from Dr. Robea Ballo, University of Cape Town, South Africa) were cultured in Dulbecco's modified Eagle's medium (DMEM) (Life Technologies, # 41965-039) supplemented with 10% fetal bovine serum (FBS) (Biochrom, # S0615), 1% Penicillin-Streptomycin (Life Technologies, # 15240-062) and maintained in a humidified atmosphere in the presence of 5% $CO_2$ at 37°C. The sub-culturing of cells involved trypsinisation to dissociate adherent cells from the flask surface; culture medium was removed, and cells were washed with 0.01 M sterile phosphate buffered saline (PBS) (137 mM sodium chloride (NaCl) (Sigma, # S7653), 10 mM phosphate (disodium hydrogen phosphate ($Na_2HPO_4$) (Merck, # NIST2186II) and potassium dihydrogen phosphate ($KH_2PO_4$) (Merck, # NIST200B)) and 2.7 mM potassium chloride (KCl) (Sigma, # P9541), adjusted to pH 7.4) and trypsinised (0.25% Trypsin-EDTA), (Life Technologies, # 25200-072). Following the detachment of cells from flask surface (3–5 min), the trypsin was then transferred to a 15 mL Falcon® tube and culture medium was added to the cell suspension at a 2:1 ratio. The cell suspension was then centrifuged (Eppendorf Centrifuge 5804R) at 1500 rpm for three min at room temperature (RT). The supernatant was then discarded, and cells re-suspended in fresh culture medium. Cells were reseeded in tissue culture flasks, either a T25 (Porvair, # 500030), T75 (Porvair, # 500029) or T175 (Porvair, # 500028) depending on cell culturing needs. For further experimental purposes, cells were maintained in a humidified incubator (Sheb Lab) supplied with 100% carbon dioxide (Afrox, # 201-RC), or reseeded in petri-dishes (Sterlin, # 90032), 8-chamber cover slip-based dishes CatnumNunc Lab-Tek155411, or on micro-patterned slides.

## 3.3 Western blot analysis

**Protein extraction.** Culture medium was rapidly removed using a Vacusafe aspirator (Integra) and rinsed twice with cold PBS. A volume of 150 $\mu$L of RIPA buffer (50 mM Tris (Sigma, # D6750), 1% NP-40 (Sigma, # 74382), 1% sodium dodecyl sulphate (SDS) (Sigma, # L3771), 0.25% sodium-deoxycholate (Sigma,

Stellenbosch University https://scholar.sun.ac.za



# 30970), 150 mM NaCl, 1 mM ethylenediaminetetraacetic acid (EDTA) (Sigma-Aldrich, # E6758), 1 mM phenylmethylsulfonyl fluoride (PMSF) (Sigma, # P7626), 1 mM sodium orthovanadate ($Na_3VO_4$) (Sigma, # S6508), 1 mM sodium fluoride (NaF) (Sigma, # S7920), 1 $\mu$g/mL leupeptin (Sigma, # L9783), 1 $\mu$g/mL aprotonin (Sigma, # A6279), 1 $\mu$g/mL benzamidine (Sigma, # B6506), 10 $\mu$g/mL pepstatin (Sigma, # P4265), adjusted to pH 7.4) was added to the flasks or petri-dishes, and cells were removed from the surface using a cell scraper (Porvair, # 500034). Cell lysates were then collected in microcentrifuge tubes and sonicated using a Mixsonic (S-4000) for 4 sec with an amplitude setting of 4 on ice. Once the foam had subsided, cell lysates were centrifuged at 8000 rpm at 4°C for 10 min using a Spectrafuge 16M centrifuge and the supernatant was then collected and stored at -80°C for further analysis.

**Protein concentration determination.** The determination of sample protein concentration was performed using the Bradford protein assay. In brief, a protein standard curve was established using bovine serum albumin (BSA) (Roche, # 10 735 078 001) dissolved RIPA buffer. The BSA concentrations ranged from 0 to 4 mg/mL. The protein standards were incubated with the Bradford reagent (0.005% Coomassie Brilliant blue (Sigma, # B0770), 5% methanol (Sigma, # 34860), 10% phosphoric acid (Sigma, # W290017)) for five min in the dark and the absorbance values were measured with a universal microplate reader (EL800) at a wavelength of 595 nm. The absorbance value for 0 $\mu$g/$\mu$L was subtracted from the absorbance value of the protein standard concentration range. The standard curve was generated by plotting the absorbance values against protein concentration. Lysates were incubated with the Bradford reagent for five min in the dark and the absorbance value was determined by subtracting 0 $\mu$g/$\mu$L from the measured absorbance value of the lysate at 595 nm. The protein concentration of the lysates were determined by reading it off the standard curve.

**Western blot analysis.** For western blotting, 40 $\mu$g of total protein was mixed with Laemmli's buffer (6.5 mM Tris, 2% SDS, 5% $\beta$-mercaptoethanol (Sigma, # M6250), 10% glycerol (Sigma, # G5516), 0.01% bromophenol blue (Sigma, #

Stellenbosch University https://scholar.sun.ac.za



B0126), adjusted to pH 6.8) at a 2:1 volume ratio, and boiled for five min at 95°C. Protein separation was performed on a 12% TGX™FastCast™acrylamide gel (Bio-Rad, # 161-0174). TGX® FastCast™acrylamide gels were prepared according to the manufacturer's instructions with the addition of 2,2,2-trichloroethanol (TCE) (Sigma, # T54801) to final concentration of 0.625%. After completion of the protein separation, gels were activated using the ChemiDoc™MP System pre-programmed gel activation protocol. Thereafter proteins were transferred onto Immobilon® FL polyvinylidene difluoride (PVDF) membrane (MilliQ, # IPFL00010) as follows: the PVDF membrane was dipped in methanol and then equilibrated in Towbin buffer (25 mM Tris, 192 mM glycine (Sigma, # G8898), 20% methanol, pH 8.3) for five min. The acrylamide gel was placed on top of the PVDF membrane and sandwiched between two blotting filter papers (Bio-Rad, # 170-3955) equilibrated in Towbin buffer. The proteins were then electro-transferred to the membrane using the Trans-Blot® Turbo™(Bio-Rad, # 170-4155) system according to the manufacturer's instructions using the standard pre-programmed transfer protocol for mixed protein weights. Following protein transfer, membranes were washed with TBS-T (137 mM NaCl, 20 mM Tris, 0.1% Tween-20 (Sigma, # P1379), pH 7.6) for five min and blocked with 5% milk in TBS-T for 1 hour to prevent non-specific binding sites on the membranes. The membranes were then washed with TBS-T three times for five min and incubated with primary antibodies overnight at 4°C in TBS-T solution. Recommended dilutions of the following primary antibodies were used for mouse monoclonal anti-APG5 (Santa Cruz, # SC-133158) and rabbit polyclonal anti-LAMP2 (Abcam, # ab18528). Membranes were rinsed with TBS-T three times for five min and then incubated with either peroxidase linked to anti-mouse IgG (Sigma, # A9044) or to anti-rabbit IgG (Sigma, # A0545) in TBS-T solution for one hour at room temperature. Membranes were rinsed with TBS-T three times for five min, exposed to Clarity™Western ECL substrate and visualized using the ChemiDoc™MP System according to the manufacturer's instructions.

Stellenbosch University https://scholar.sun.ac.za



## 3.4 Proteomics

Proteomic analysis was performed on MEF-GFP cells treated with; rapamycin (20 nM and 100 nM), spermidine (50 nM and 500 nM), 10 nM bafilomycin $A_1$. A control group was also included. Label-free protein quantification on the six groups, which consisted of three biological replicates, was performed by The Center for Proteomic & Genomic Research based in Cape Town, South Africa.

**Protein extraction and quantification.** Lysates were collected as described in Section 3.3 and the total protein for each sample was quantified using the QuantiPro BCA Assay Kit (Sigma, # QPBCA) according to the manufacturer's instructions.

**Tube and Filter Passivation.** The 30kDA weight cut-off (MWCO) centrifugal filters and collection tubes (Millipore) were covered in a 5% TWEEN-20 (Thermo Fisher Scientific, # P1362) solution and incubated overnight on a shaker at room temperature. The centrifugal filters and collection tubes were removed and rinsed with MilliQ water, and then covered with MilliQ water prior to incubation on a shaker for 30 min. The MilliQ water was refreshed with MilliQ water, and then incubated for 30 min on a shaker for a total of three times.

**Tryptic Digestion.** A total of 100 $\mu$g protein from each sample was transferred in a 1.5 mL LoBind Eppendorf tube (Sigma, # Z666505) and reduced for 1 h at 60°C with 10% of the sample volume of 50 mM tris(carboxyethyl) phosphine (TCEP) (Fluka, # 646547). Thereafter, SDS concentration was diluted with urea-triethyl ammonium bicarbonate buffer (8 M urea (Sigma, # U5128), 100 mM (TEAB) (Sigma, # T7408)) to 0.5%. Samples were placed on a passivated centrifugal filter and concentrated down to 30 $\mu$L by centrifugation at 13000 g. The retentate was alkylated using 100 $\mu$L 15 mM methyl methanethiosulphonate (MMTS) (Sigma, # 208795) in urea-TEAB buffer for 15 min at 20°C. The buffer was replaced with 350 $\mu$L of 8 M urea in 100 mM TEAB buffer and centrifuged at 13000 g to reduce the volume to 30 $\mu$L. The retentate was washed a further five

Stellenbosch University https://scholar.sun.ac.za



times with 100 $\mu$L urea-TEAB buffer followed with centrifugation to completely remove SDS. The retentate was then washed twice with 100 $\mu$L 100 mM TEAB followed with centrifugation at 13000 g to reduce urea concentration. Proteins were digested by adding Sequencing Grade Modified Trypsin (Promega,#PRV5111) in 100 mM TEAB with a ratio of 50:1 protein:trypsin and then incubated for 18 h at 37°C. Peptides were collected in a passivated collection tube by centrifugation at 13000 g, washed twice using MilliQ water, followed by centrifugation at 13000 g. Samples were then dried and re-suspended in 0.1% trifluoroacetic acid (TFA) (Sigma, # T6508).

**LCMS.** Liquid chromatography–mass spectrometry (LCMS) analysis was performed with a Q-Exactive quadrupole-Orbitrap mass spectrometer coupled with a Dionex Ultimate 3000 nano-HPLC system (Thermo Fisher Scientific). Peptides were dissolved in 0.1% formic acid (FA) (Sigma, # 56302), 2% acetonitrile (ACN) (Burdick & Jackson, # BJLC015CS) and loaded on a C18 trap column (300 $\mu$m x 5 mm x 5 $\mu$m, Thermo Fisher Scientific). A C18 PepAcclaim column (75 $\mu$m x 25 cm x 2 $\mu$m, Thermo Fisher Scientific) was used for chromatographic separation. The solvents used were solvent A: LC water (Burdick & Jackson, # BJLC365), 0.1% FA, and solvent B: ACN, 0.1% FA. A multi-step gradient for peptide separation was generated at 250 $nl$/min as follows: time change 42 min, gradient change: 8–20% solvent B; time change 10 min, gradient change: 20–3% solvent B. Column was then washed for 10 min with 80% solvent B, and then re-equilibrated with 2% solvent B for 15 min. The mass spectrometer was operated in positive ion mode with a capillary temperature of 320°C. The applied electrospray voltage was 1.95 kV. Details of data acquisition are shown in the table 3.1.

**Data analysis.** The relative protein quantification was determined using Progenesis QI (Nonlinear) and was based on three biological replicates per condition using non-conflicting peptides. Data processing included peak picking, run alignment and normalisation. For protein identification, a UniProt sourced *Mus musculus* reference proteome (10090) was downloaded on 26/11/2016 from www.uniprot.org. The following protein markers were identified using a custom Python script based

Stellenbosch University https://scholar.sun.ac.za



**Table 3.1:** Data acquisition using Q-Exactive quadrupole-Orbitrap mass spectrometer coupled with a Dionex Ultimate 3000 nano-HPLC system.

| **Full Scan** | |
|---|---|
| Resolution | 70,000 (@ m/z 200) |
| AGC target value | $3x10^6$ |
| Scan range | 350-2000 m/z |
| Maximal injection time (ms) | 100 |
| Data-dependent MS/MS | |
| Inclusion | Off |
| Resolution | 17,500 (@ m/z 200) |
| AGC target value | $1x10^5$ |
| Maximal injection time (ms) | 50 |
| Loop Count | 15 |
| Isolation window width (Da) | 3 |
| NCE (%) | 27 |
| **Data-dependent Settings** | |
| Underfill ratio (%) | 1 |
| Charge exclusion | 1, 7, 8, >8 |
| Peptide match | Preferred |
| Exclusion isotopes | On |
| Dynamic exclusion (s) | 60 |

on their relation to the change in autophagosome flux: proteins that increase with increasing autophagosome flux, proteins that decrease with increasing autophagosome flux, proteins that remain constant irrespective of the change in autophagosome flux, and proteins that are involved in the autophagic process (Atg proteins, transporting proteins, etc.).

Stellenbosch University https://scholar.sun.ac.za



## 3.5 Micro-patterning

Micro-patterning has become a popular technique that has recently received particular interest in cell biology. The micron-size patterns allow for the study of cell sensitivity to fine spatial cues and provide a means to standardize cell shapes. Moreover, it immobilizes migratory cells, which allows for high-throughput screening over long periods of time. The protocol described here, adapted from Carpi *et al.* [28], is a lithographic-based method for printing micro-patterns on a glass with extra-cellular matrix proteins to promote cell adhesion. The backdrop is filled with polylysine grafted polyethyleneglycol (PLL-g-PEG) that creates a non-adhesive surface preventing cells from attaching. Fig. 3.1 illustrates the micro-patterning process with representative images. A quartz photomask is required to serve as the pattern template for transferring patterns onto the PLL-g-PEG layer which is then filled with attachment proteins. A GDSII layout file was created using the Python platform and gdsCAD 0.4.5 package of the pattern to be etched into the chrome mask. The chrome mask was manufactured by Delta Mask, Toppan, Netherlands.

**Glass silanization and passivation.** The glass coverslip was washed with 70% Ethanol and dried using a dry-oven. Thereafter the coverslip was illuminated with a deep UV lamp (185 nm) for 10 min using a UVO cleaner (Jelight, model 18). The distance used was dependent on the UVO model; here the coverslip was placed 1 cm from the UV lamp. The coverslip was then placed on top of a 30–150 $\mu$L drop of PLL-g-PEG solution (0.1 mg/mL PLL(20)-g[3.5]-PEG(2) (Surface Solutions, Zurich), 10 mM Hepes (Sigma, # H3375), adjusted to pH 7.4) on a sheet of parafilm with the activated face in contact with the PLL-g-PEG. The coverslip was incubated with the PLL-g-PEG solution for 1 hr at room temperature. Thereafter, the coverslip was washed for two min in PBS and then rinsed for two min in Millipore water.

**UV illumination and protein attachment.** The photomask was washed with 70% ethanol and dried with absorption paper. The non-chrome side of the pho-

Stellenbosch University https://scholar.sun.ac.za



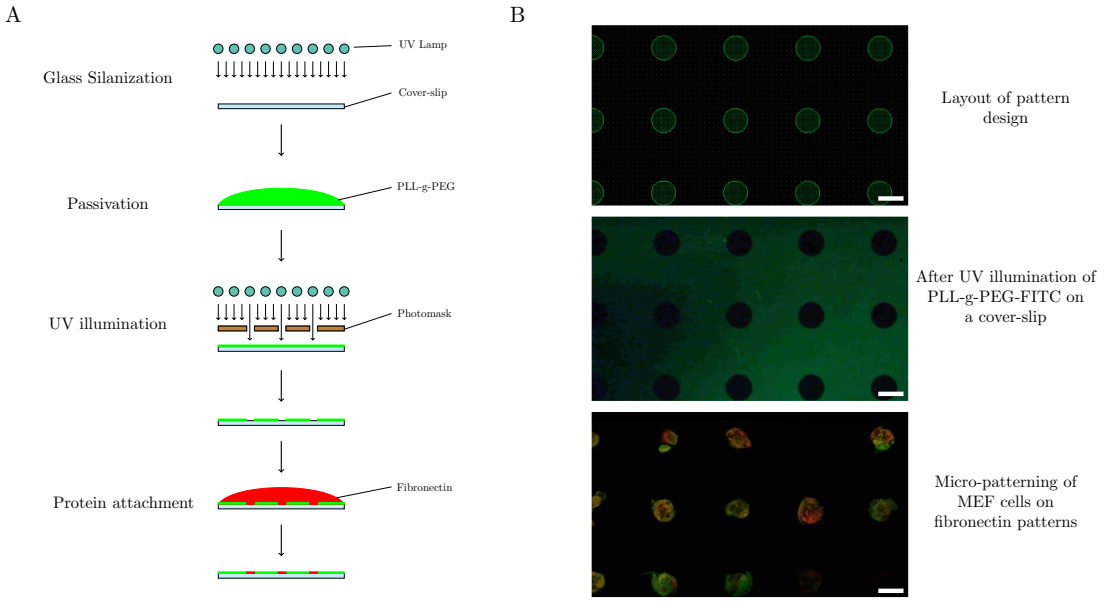


**Figure 3.1:** Micro-pattern on glass using deep UV. A) Illustration showing the micro-patterning process. B) Top, layout design of the patterns to be printed on the cover-slips; Middle, a micrograph of PLL-g-PEG-FITC on a cover-slip after UV illumination; Bottom, micro-patterning of MEF cells on fibronectin patterns. Cells were expressing GFP-LC3 and stained with LysoTracker Red. Scale bar 50 $\mu$m.

tomask was silanated by placing it with chrome side facing down in the UVO cleaner and illuminating it for 10 min. The photomask was left to cool, and then 5 $\mu$L Millipore water was placed on the non-chrome of the mask. The coverslip with the activated face was then placed on the drop of Millipore water in contact with the photomask. Excess water was removed using absorbent paper. The photomask was placed with its chrome side towards the lamp in the UVO cleaner and illuminated for 10 min. The mask was left to cool down and then submerged in Millipore water with chrome side facing down (the coverslip facing upwards) until the coverslip spontaneously floated. The coverslip was carefully removed to avoid scratching the mask and placed on a 30–100 $\mu$L drop of 25 $\mu$g/mL of fibronectin solution on parafilm with the illuminated surface in contact with the solution and incubated for 2 hrs at room temperature. Thereafter, the coverslip was washed for two min in Millipore water. *At this point, the coverslip was ready for use.* The

Stellenbosch University https://scholar.sun.ac.za



coverslip was dried overnight at 4°C and glued to our self-fabricated microscope slide.

**Seeding of the cells.** Cells were harvested by trypsinization as described in 3.2. Approximately 1000 cells were added to each well-containing culture medium and placed in the incubator for 1–2 hrs to allow the cells to attach. Once cells started to adhere on the patterns, the unattached cells were washed away using culture medium.

## 3.6 Fluorescence imaging

**General microscopy settings.** Live cell imaging was performed using a Carl Zeiss (Oberkochen, Germany) confocal microscope equipped with a humidified chamber at 37°C supplemented with 5% $CO_2$. The raw image stacks/series was acquired using a high NA objective (Olympus Plan APO N 60x/1.42 Oil/0.17/FN26.5) using an Argon multiline laser 25 mW at 488 nm and Diode 405 nm CW/PS and 633 nm laser as a light source with a GaAsP detector. Laser power and master gain were chosen for 405 nm (LysoTracker blue), 488 nm (GFP), 514 nm (LysoTracker red) and 633 nm (SiR Tubulin) to ensure an optimal signal/noise ratio with minimal pixel saturation. Track filters were set as follows; LysoTracker blue: 410–471 nm, GFP: 490–597 nm, LysoTracker red: 566–690 nm and SiR Tubulin: 638–759 nm.

**Z-stack image acquisition of a whole cell.** Raw image stacks were acquired to quantify the total number of autophagosomes, autolysosomes and lysosomes in cells. The image frames were acquired using a 60x objective with 0.75–1 $\mu$m step width between the individual image frames.

**Time lapse image series acquisition.** An image series was acquired to track autophagosome trafficking behaviour under various treatment conditions. The image series was acquired using a 60x objective with 20 image acquisition cycles in 15 sec intervals. A fast scanning speed (pixel dwell time of 0.02 $\mu$s) was used

Stellenbosch University https://scholar.sun.ac.za



to acquire time lapses of tubulin network and autophagy vesicles behaviour so as not to bleach fluorophores and induce phototoxicity in cells.

## 3.7 Image analysis

Images were processed using ZEN 2011 imaging software (Carl Zeiss) and the maximum intensity projections exported to Fiji (https://fiji.sc/)). Images were deconvolved using the Deconvolution Lab plug-in (http://bigwww.epfl.ch/) of Fiji to further improve the signal to background noise ratio.

**Counting autophagy intermediates.** The number of autophagosomes was assessed by subtracting the red channel (LysoTracker positive puncta) from the green channel (GFP positive puncta) and then using the "analyse particle" function to count the number of remaining puncta in Fiji. Similarly, lysosomes were counted by subtracting the green channel from the red channel and the number of remaining puncta was determined using the "analyse particle" function. The number of autolysosomes was determined by counting the number of puncta in the red channel and then subtracting the number of lysosomes. In the case of high background noise, Fiji "click count" function was used to assess the number of puncta.

**Puncta tracking.** The green channel was processed by setting threshold limits on the image histogram such that only autophagosomes were visible—the green fluorescence signal from the autolysosomes is weaker than that of autophagosomes. Image series were analysed using "TrackMate" plug-in [256] in Fiji.

## 3.8 Statistics

Statistical analysis was performed with TIBCO Statistica 13 software using a one-way ANOVA with the Fisher LSD post-test. Significance was indicated at $p < 0.05$.

Stellenbosch University https://scholar.sun.ac.za

# Chapter 4

# Autophagosome flux

Autophagosome flux is defined as the rate of flow along the vesicular pathway of the autophagy system [168]. We developed a method that allows for the quantification of the autophagosome flux ($J$) and the steady-state number of autophagy intermediates per cell: autophagosomes ($n_{\mathrm{A}}$), autolysosomes ($n_{\mathrm{AL}}$) and lysosomes ($n_{\mathrm{L}}$). $J$ is measured by inhibiting fusion of autophagosome and lysosome at steady state and calculated from the subsequent initial rate of $n_{\mathrm{A}}$ accumulation [50]. The autophagic steady-state variables ($J$, $n_{\mathrm{A}}$, $n_{\mathrm{AL}}$ and $n_{\mathrm{L}}$) can be used to derive several other useful autophagy variables: the transit time, $\tau$, which is the time required to clear the pool of a particular autophagic vesicle, and the flux derivatives $J_{\mathrm{vol}}$, the rate at which the cytoplasm is being encapsulated and delivered to lysosomes for degradation, and $J_{\mathrm{mem}}$, the rate at which the cellular membrane is being utilised by the autophagy machinery for autophagosome synthesis.

This chapter describes experiments that assess the reliability of our technique, and how our approach has been used to screen several autophagy-modulating drugs and to investigate the underlying mechanism of autophagy. In the first section, we will assess the reliability and applicability of our approach by measuring $J$ in autophagy-deficient cells (negative control) and using alternative lysosomal probes when characterising autophagy variables. We also compare our approach to a recently-developed ratiometric autophagy flux probe. Next, we use our approach to screen selected autophagy modulating drugs to characterise the dose-dependent

Stellenbosch University https://scholar.sun.ac.za



changes in the autophagy variables as well as the transient time-dependent behaviour of autophagy intermediates in two cell lines. Taking advantage of controlling $J$, we perform proteomic analysis on cells with a known increase in autophagosome flux using two means of autophagy induction to identify novel markers that correlated with $J$. We then further investigate the underlying mechanism of autophagy, and explore the vesicle dynamics as well as the effects of cell size on autophagosome flux.

## 4.1 Measuring autophagosome flux

In our previous work we characterised $J$, $n_{\mathrm{A}}$, $n_{\mathrm{AL}}$ and $n_{\mathrm{L}}$ under basal and rapamycin-induced steady-state conditions. Fig. 4.1 shows a graphic illustration of the progress curve of the autophagy variables measured over time under basal and rapamycin induced conditions, where $J$ is calculated from the initial rate of increase of autophagosomes after the inhibition of fusion between autophagosomes and lysosomes with 400 nM bafilomycin $\mathrm{A}_1$ [50]. As part of the protocol development and validation, we performed a series of experiments to assess the reliability of our protocol by (i) measuring $J$ in ATG5-silenced autophagy (negative control), (ii) assessing the autophagy variables ($J$, $n_{\mathrm{A}}$, $n_{\mathrm{AL}}$ and $n_{\mathrm{L}}$) using another fluorescent lysosomal marker, namely red fluorescent protein conjugated to Lysosomal-associated membrane protein 1 (RFP-LAMP1), and (iii) comparing our approach to a recently developed ratiometric autophagy flux probe.

Stellenbosch University https://scholar.sun.ac.za



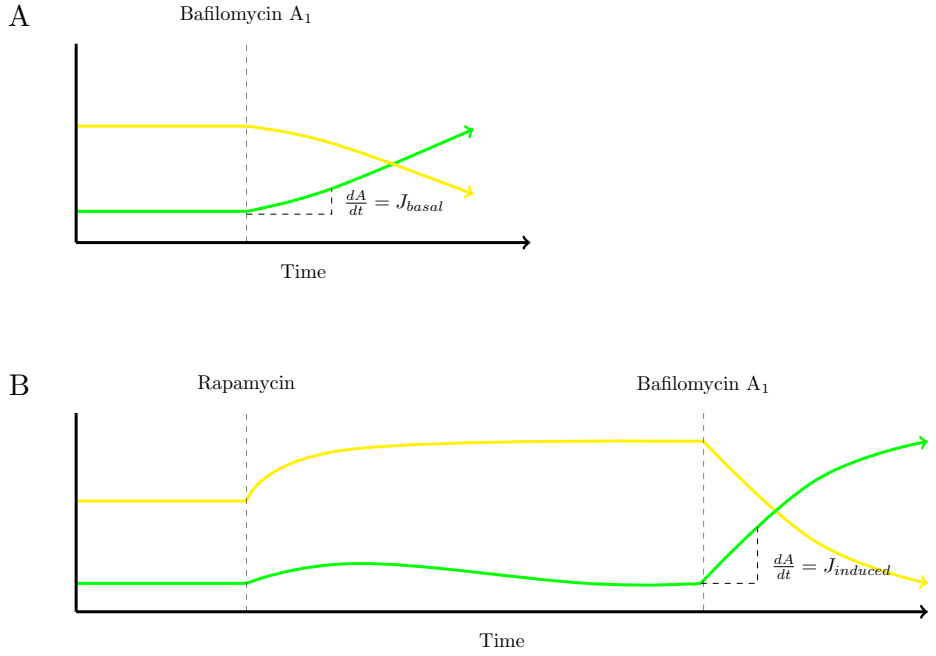


**Figure 4.1:** Graphic illustration of measuring autophagosome flux under basal and induced conditions. The time dependent changes in autophagosomes (—) and autolysosomes (—) are measured in (A) basal and (B) rapamycin-induced states.

**Negative control.** Autophagy was suppressed through ATG5 silencing that limits the formation of the ATG5:ATG12 complex, thereby disrupting autophagosome synthesis [140]. Autophagy was silenced in Mouse Embryonic Fibroblast (MEF) cells that stably express GFP-LC3 using ATG5_L siRNA (Qiagen, # SI02633946) and Lipofectamine® 3000 (Thermo Fisher Scientific, # L3000001) according to the manufacturer's instructions. Two days after transfection was performed, there was a significant decrease in ATG12:ATG5 protein levels as assessed by western blot analysis (Fig. 4.2A). In keeping with our protocol, cells were patterned on fibronectin disc shapes and $n_{\mathrm{A}}$, $n_{\mathrm{AL}}$ and $n_{\mathrm{L}}$ were measured over time in the absence and presence of 400 nM bafilomycin $\mathrm{A}_1$ under basal conditions. Silencing of ATG5 resulted in a 68.9% decrease in $J$ compared to the non-silenced control (Fig. 4.2B).

Stellenbosch University https://scholar.sun.ac.za



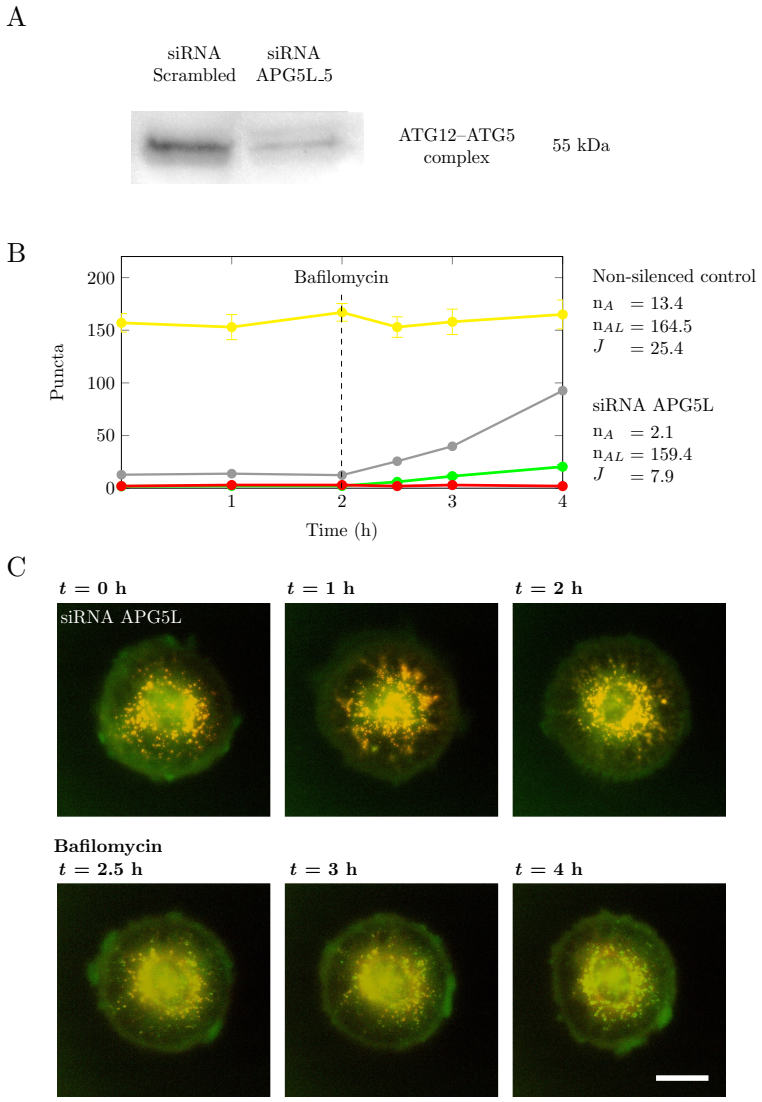


**Figure 4.2:** Measuring autophagosome flux in autophagy-silenced cells. (A) Western blot analysis of ATG12-ATG5. (B) The transient time dependent behaviour of autophagosomes (●), autolysosomes (●) and lysosomes (●) in autophagy silenced MEF cells and autophagosomes in control cells (●). Cells were treated with 400 nM bafilomycin $A_1$ at 2 h to measure the autophagosome flux. (C) Representative images of autophagy-silenced MEF cells. ($n = 5$). Scale bar: 20 $\mu$m.

**Lysosomal markers.** Our protocol made use of LysoTracker, a fluorescent acidotrophic dye used to distinguish between the autophagosomes, autolysosomes and lysosomes. Since bafilomycin $A_1$ disrupts autophagy through the deacidification of

Stellenbosch University https://scholar.sun.ac.za



lysosomes, it can lead to LysoTracker diffusing out of lysosomes and result in unreliable data. To assess the degree to which bafilomycin $A_1$ potentially can effect LysoTracker signal and $J$ measurement, we repeated our protocol using MEFs stably expressing GFP-LC3 and RFP-LAMP1 and co-stained with LysoTracker blue. Cells were assessed under non-inducing conditions and treated with 400 nM bafilomycin $A_1$ and monitored for 4 h. Both LysoTracker blue and RFP-LAMP1 had similar $n_A$, $n_{AL}$ and $n_L$ values at steady state (Fig. 4.3A and B). Determining $J$ using LysoTracker blue and RFP-LAMP1 also yielded similar results when using the 30 min post inhibition time point (Fig. 4.3A and B). However, after 1 h of bafilomycin $A_1$ treatment the LysoTracker blue puncta count was notably lower than that of the RFP-LAMP1 puncta count (Fig. 4.3C), the result of the diminishing pH gradient. Taken together, the use of LysoTracker to measure $J$, $n_A$, $n_{AL}$ and $n_L$ generates reliable measurements at least up until 1 h after the addition of bafilomycin $A_1$.

Stellenbosch University https://scholar.sun.ac.za



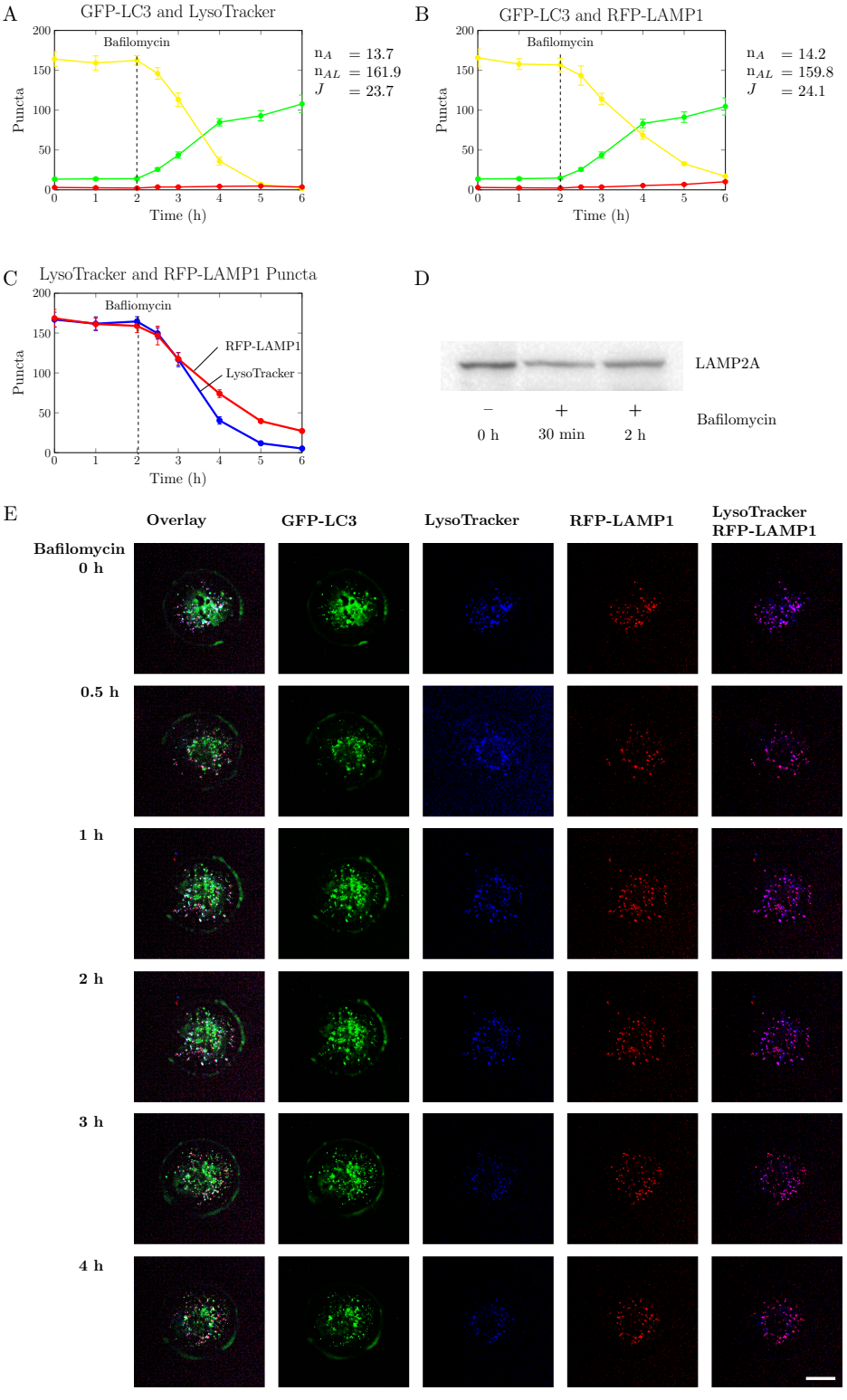


**Figure 4.3:** Measuring autophagosome flux using LysoTracker blue and LAMP1-RFP in MEF cells stably expressing GFP-LC3. Assessing the number of autophagosomes (●), autolysosomes (●) and lysosomes (●) over time using LysoTracker blue (A) and LAMP1-RFP (B). (C) Graph showing the total number of LysoTracker blue and LAMP1-RFP puncta over time in cells. (D) Western blot images of LAMP2A. (E) Deconvolved representative images of MEF cells expressing both GFP-LC3 and RFP-LAMP1 and co-stained with LysoTracker blue. ($n = 5$). Scale bar: 20 $\mu$m.

Stellenbosch University https://scholar.sun.ac.za



**Autophagic flux probe.** In recent years there has been a growing interest in developing new/novel techniques to measure autophagy activity. One of the most recent techniques developed to assess autophagy flux is based on the GFP-LC3-RFP-LC3ΔG ratio-metric probe developed by Kaizuka *et al.* [120]. The probe is cleaved by ATG4 proteases into equal amounts of GFP-LC3 and RFP-LC3ΔG. GFP-LC3 is degraded by the autophagy machinery, whilst RFP-LC3ΔG remains in the cytosol. Therefore, the ratio of GFP to RFP is used to compare the autophagy degradative capacity between treatments. To compare this technique to our approach, we transiently transfected wild-type MEF cells with GFP-LC3-RFP-LC3ΔG plasmid using Lipofectamine® 3000, and treated the cells under basal and induced conditions using 25 nM rapamycin (Fig. 4.1). Despite an increase in autophagosome flux of 25.4 A/hr/cell to 105.4 A/hr/cell after rapamycin treatment, no significant changes were observed in the ratio of red/green fluorescent signal over time (Fig. 4.4). A possible reason for this is that the plasmid is not expressed strongly enough to detect changes in red/green fluorescent signal. This is an inherent challenge when using plasmids, which often require optimisation in order to achieve sufficient fluorescence signal for experimental purposes. It also highlights the potential drawback of our approach, since live-cell imaging of wild-type cells, such as primary isolated cells, would require these cells to be transfected with GFP-LC3 and/or RFP-LAMP1 plasmids in order to assess $J$. A possible means to circumvent challenges associated with plasmid-based techniques would be to fix cells at specific time points and stain them using immunofluorescent techniques.

Stellenbosch University https://scholar.sun.ac.za



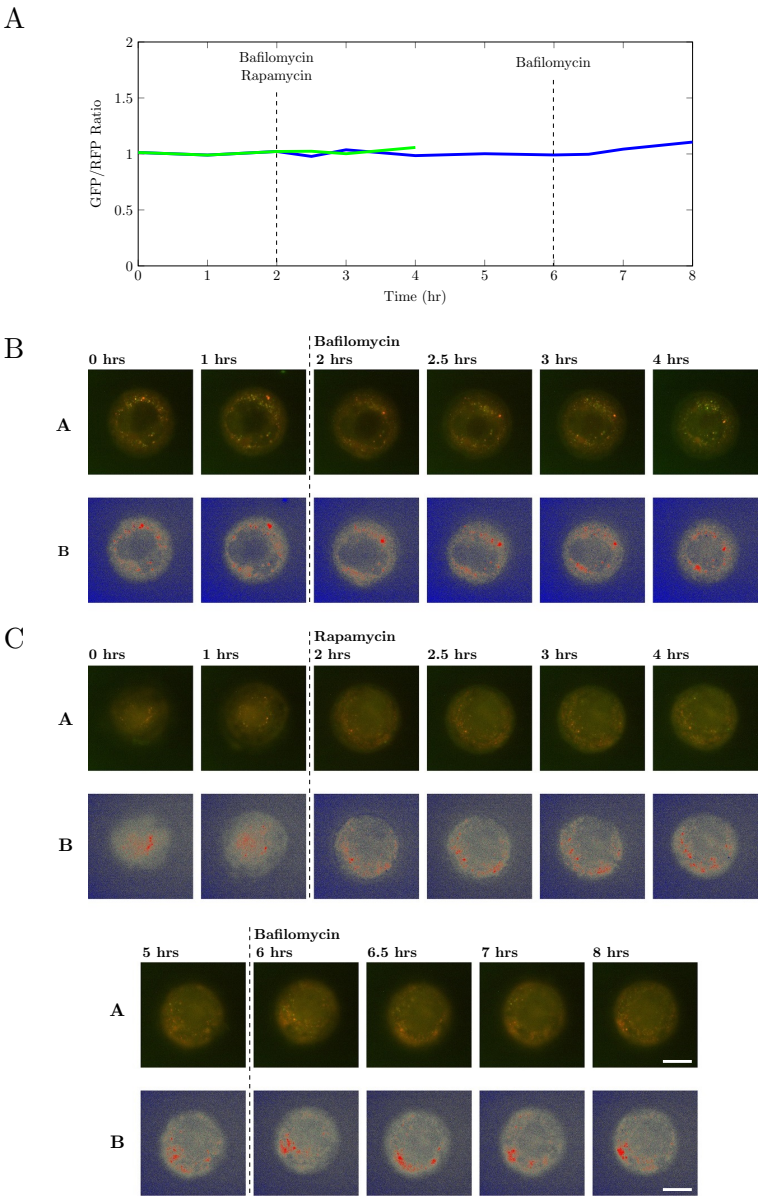


**Figure 4.4:** Measuring autophagy activity using GFP-LC3-RFP-LC3ΔG probe. (A) Ratio of red/green fluorescent signal over time of basal autophagy activity (—) in cells treated with 400 nM bafilomycin $A_1$ at 2 h, and induced autophagy activity (—) in cells treated with 25 nM rapamycin at 2 h and 400 nM bafilomycin $A_1$ at 6 h. (B and C) Representative images of basal and rapamycin induced autophagy activity. Top: raw representative images; bottom: representative hot-cold look up table (LUT) images of the ratio between red/green fluorescent signal. ($n = 5$). Scale bar: 20 $\mu$m.

Stellenbosch University https://scholar.sun.ac.za



Taken together, our results demonstrate that LysoTracker can be used as a suitable lysosomal marker within the given time frame when assessing autophagosome flux. Compared to other autophagy activity probes, the direct assessment of autophagosomes over time in the presence and absence of autophagosome/lysosome fusion inhibitors sensitively detects small changes in the autophagy vesicular pathway.

## 4.2 Drug screening

In light of autophagy's cytoprotective properties, we set out to screen selected autophagy modulating drugs with the aim of characterising the autophagy response in terms of $v_A$, the rate of autophagosome synthesis[1], and $n_{\mathrm{A}}$, $n_{\mathrm{AL}}$ and $n_{\mathrm{L}}$ after 24 h treatment. The reason for treating cells for 24 h with the respective drugs, rather than 6 h as previously described in our protocol (Fig. 4.1), was to maximise the probability for a steady state to be established. Then, using selected concentrations of the respective drug that elicits an response we assessed the time depended behaviour of the autophagy intermediates. Drugs that can either selectively target autophagy regulatory complexes/proteins or can indirectly regulate autophagy were selected on the basis of their clinical importance and modulating capacity (table 4.1).

### 4.2.1 Dose-response screening

Drug screening was performed on MEF and HeLa cells stably expressing GFP-LC3 and co-stained with LysoTracker red. Our first approach was to perform a fixation-based drug screening of MEF cells on a high-content analysis system based at Nelson Mandela Metropolitan University (NMMU). The fixation-based method was not without its inherent challenges, and we therefore developed an in-house live-cell "high-content" method to screen selected drugs in HeLa cells, and

[1] As discussed further on, we could not be absolutely sure that steady state had been reached and, consequently, we could not be sure that the rate at which $n_{\mathrm{A}}$ increased after bafilomycin $\mathrm{A}_1$ treatment was actually equal to $J$. For this reason we introduced the symbol $v_A$ for the observed rate of autophagosome synthesis.

Stellenbosch University https://scholar.sun.ac.za



**Table 4.1:** Autophagy modulating drugs.

| | Treatment | Target | Effect on autophagy | References |
|---|---|---|---|---|
| Direct modulation | MRT67307 | ULK | ↓ | [66, 212] |
| | Rapamycin | mTOR | ↑ | [117, 218, 231] |
| | Metformin | AMPK | ↑ | [235, 278] |
| | Dorsomorphin | AMPK | ↑ and ↓ | [99, 264] |
| Indirect modulation | 3-Methyladenine | PI3K | ↓ | [108, 233, 275] |
| | Lithium chloride | IMPase | ↑ | [91, 230] |
| | Rilmenidine | Imidazoline | ↑ | [224, 274] |
| | Spermidine | Acetyltransferase | ↑ | [55, 204, 213] |
| | FBS | Nutrient abundance | ↑ | [96, 196, 218] |

to assess the time-dependent behaviour of the autophagy variables of both MEF and HeLa cells. In this section, we will report the results of the two approaches and discuss the generated data.

#### 4.2.1.1 Fixation-based drug screening

Our first approach was to characterise the autophagy drug response of selected drugs by screening fixed MEF GFP-LC3 cells after 24 h treatment. The rate of autophagosome synthesis, $v_A$, was calculated from the difference in $n_{\mathrm{A}}$ between cells treated with and without bafilomycin $\mathrm{A}_1$ after 24 h treatment with the selected drugs.

**Experimental work flow.** Screening plates were assembled by attaching a coverslip (thickness 1 $\approx$ 0.13 to 0.16 mm) (Ted Pella, # 260462) to a 96 well bottomless frame plate (Separations, # 4TI-0224/F) using a non-toxic silicone elastomer "glue" (AMT, # SM420). After the coverslip was secured to the plate, it was briefly irradiated with UV. Approximately $20 \times 10^3$ MEF cells were seeded into a well and left overnight to adhere to the plate in culture medium. The following day the culture medium was treated for 24 h with a medium containing 25 nM LysoTracker red and the respective drugs. To determine $v_A$, cells were treated

Stellenbosch University https://scholar.sun.ac.za



with 400 nM bafilomycin $A_1$ for an additional 30 min. Cells were fixed using 4% paraformaldehyde (Sigma, # P6148) solution mixed with culture medium in a 1:1 ratio and stained for 5 min with Hoechst (Sigma, # 63493). The 96 well plates were imaged using the ImageXpress Micro XLS Widefield high-content analysis system and the images exported to Fiji for analysis as described in Section 3.7.

**Screening results** . Fig. 4.5 shows the drug dose-dependent changes of $v_A$, $n_{\mathrm{A}}$, $n_{\mathrm{AL}}$ and $n_{\mathrm{L}}$ in MEF GFP-LC3 cells. Analysis of the data shows that rapamycin, spermidine, dorsmorphin, rilmenidine and FBS treatments exhibited modulation ranges whereas mrt67307, metformin and LiCl had no effect on autophagy after 24 h. 3-Methyladenine inhibited autophagy at all the concentrations screened. Data is further discussed and contextualised in Section 4.2.1.3.

We are unable to verify whether or not the autophagy system was at steady state at 24 h and therefore we can only say that the rate of increase in $n_{\mathrm{A}}$ as measured here represents $v_A$. To accurately measure $J$ would require the dynamic assessment of $n_{\mathrm{A}}$, $n_{\mathrm{AL}}$ and $n_{\mathrm{L}}$ over time to verify whether or not the autophagy system is in steady state. Thus, the fixation approach described here is not ideally suited for assessing $J$ in cells. There are two potential improvements one can make to verify whether or not the autophagy system is in steady state. One is to fix cells at selected time points to assess changes in $n_{\mathrm{A}}$, $n_{\mathrm{AL}}$ and $n_{\mathrm{L}}$, and if the number of autophagy intermediates does not change over time, it would indicate that the autophagy system is at steady state and therefore that $v_A$ equals $J$. Two, to measure $v_A$ at selected time points in cells fixed before and after bafilomycin $A_1$ treatment, and if $v_A$ remains constant it would indicate that the autophagy is also at steady state.

There is a notable difference in $n_{\mathrm{AL}}$ and $n_{\mathrm{L}}$ between fixation-based imaging (Fig. 4.5) and live-cell imaging (Fig. 4.8). Here paraformaldehyde was used as fixative, which forms cross-links both within and between proteins, particularly between lysine residues. Consequently, the fixation process results in limited damage to the tertiary structure of the proteins that may account for the loss in GFP fluorescent signal. The partial loss of GFP signal from the fixation process com-

Stellenbosch University https://scholar.sun.ac.za



bined with the exposure of autolysosomal GFP to the luminal acidic environment and proteolytic enzymes can result in further, if not the complete, quenching of GFP signal. The loss in the GFP signal results in higher $n_{\mathrm{L}}$ and lower $n_{\mathrm{AL}}$. Since the fixation process only accounts for the partial loss in GFP signal from autophagosomes, we can reasonably assume that $n_{\mathrm{A}}$ is unaffected and that the calculation of $v_A$ is correct. Also, considering that $n_{\mathrm{L}}$ usually makes up about 1–5 puncta of the LysoTracker pool, adding $n_{\mathrm{AL}}$ and $n_{\mathrm{L}}$ together would represent a more realistic $n_{\mathrm{AL}}$.

Stellenbosch University https://scholar.sun.ac.za



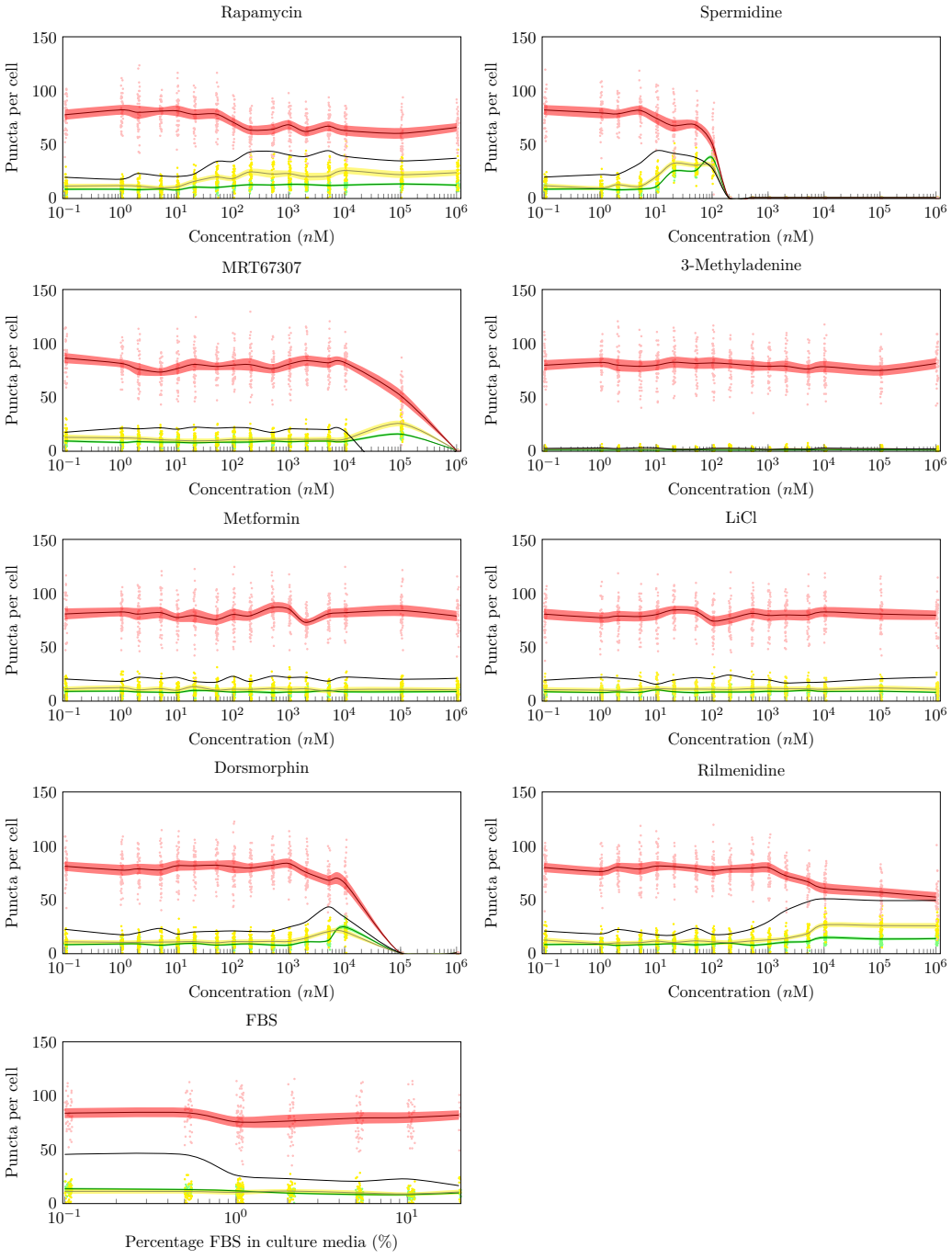


**Figure 4.5:** Fixation based screening of autophagy modulating drugs in the MEF GFP-LC3 cell line. The autophagy drug response assessed after 24 h treatment by measuring the autophagy variables; autophagosomes (●), autolysosomes (●) and lysosomes (●), and the rate of autophagosome synthesis (—). The error band depicts the standard error of the mean (SEM) of autophagosomes (■), autolysosomes (■) and lysosomes (■). ($n$ = 40).

Stellenbosch University https://scholar.sun.ac.za



#### 4.2.1.2 Live-cell based drug screening

In light of the aforementioned limitations of using the fixation approach, we set out to develop a small in-house drug screening protocol that would allow for "high-content" image acquisition using Carl Zeiss LSM780 confocal microscopy (Carl Zeiss, Germany). The new approach is structured around assessing the autophagy intermediates over time and verifying whether or not the autophagy system is at steady state and then measuring $J$. There were several challenges associated with adapting the confocal microscope for high throughput image acquisition. The mobility of the objective was the greatest restraint when developing live-cell screening protocol since the manoeuvrability of the objective is limited to a small area and it requires the microscope objective to be submerged in oil for image acquisition, which in turns further limits its area of movement as result of the oil spreading too thin. We designed a compact microscope slide that would allow for the minimal travel distance of the microscope objective between wells using CAD software (Fig. 4.6A) that consisted of 12 wells in a 25 mm x 19 mm frame which was machined from non-toxic acetal sheet (Maizy, # P500).

We screened the drugs for changes in $n_{\mathrm{A}}$, $n_{\mathrm{AL}}$, $n_{\mathrm{L}}$ and $v_A/J$ in HeLa cells using the live cell-based approach, and thereafter assessed the time-dependent behaviour of the autophagy intermediates in both MEF and HeLa cells in its approach to steady state. The transient time-dependent behaviour of the autophagy intermediates of the MEF cells was also used to infer whether or not the $v_A$ measured in the previous section could be equated to $J$.

Stellenbosch University https://scholar.sun.ac.za



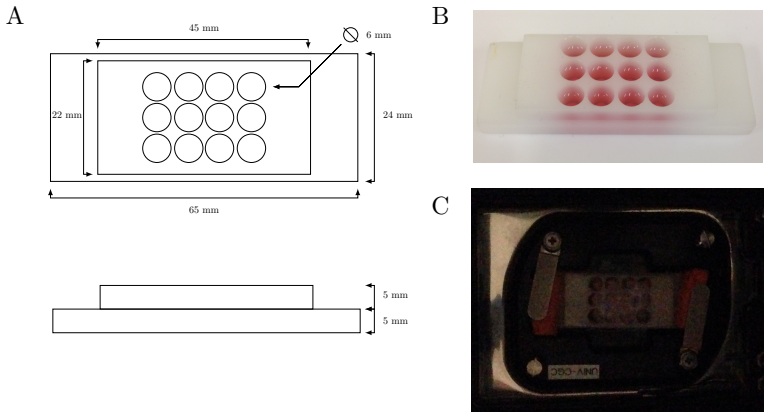


**Figure 4.6:** Custom-machined microscope slides for high content live-cell imaging. (A) CAD design of the microscope slide. (B) Microscope slide machined from acetal containing culture medium. (C) Microscope slide encased in the incubation chamber of the Carl Zeiss LSM780 confocal microscope.

**Experimental work flow.** Slides were assembled by attaching a coverslip (thickness ≈ 0.13–0.16 mm) (Fisherbrand, # 12544C) to our self-fabricated slide using a non-toxic silicone elastomer "glue" (AMT, # SM420). After the coverslip was secured to the slide, it was briefly irradiated with UV. The drug response screening was performed on approximately $40 \times 10^3$ HeLa cells seeded per well and left overnight to attach to the coverslip in culture medium. The following day the culture medium was refreshed and treated with drugs for 24 h, followed by 30 min bafilomycin $A_1$-treatment. To visualize autolysosomes and lysosomes, culture medium was supplemented with 25 nM LysoTracker red 2 h prior to imaging. The slide was placed in the heated chamber of the microscope maintained at 5% $CO_2$. Cells were imaged at three time points, 1 h apart, to assess the time-dependent changes in $n_{\mathrm{A}}$, $n_{\mathrm{AL}}$ and $n_{\mathrm{L}}$. To measure $v_A$, cells were treated for 30 min with 400 nM bafilomycin $A_1$. If there was no net change in the autophagy intermediates over time (Fig. 4.7), it indicated that the autophagy system was at steady state and therefore $v_A = J$.

Approximately $15 \times 10^3$ MEF cells and $40 \times 10^3$ HeLa cells were seeded per well and left overnight to attach in culture medium for the respective experiments. The time-dependent behaviour was assessed in both MEF and HeLa cells. After the

Stellenbosch University https://scholar.sun.ac.za



cells had attached, the culture medium was refreshed with medium supplemented with 25 nM LysoTracker red 2 h prior to imaging. The slide was placed into the heated chamber, supplied with 5% $CO_2$, that encased the microscope objective. An LCI "Plan-Apochromat"63x/1.4 Oil DIC M27 objective was used for image acquisition with an Argon multiline laser 25 mW at 488 nm and 514 nm with MBS 488/561/633 beam splitters with a GaAsP detector 32+2 PMT. Track filters were set at 490–597 nm for GFP and 566–690 nm for LysoTracker red. Laser power and master gain were chosen for 488 nm (GFP) and 514 nm (LysoTracker red) and were set to ensure optimal signal to noise ratio with no pixel saturation. Cell positions were recorded and used with the loop function to automatically acquire images in z-stacks with 1 $\mu$m step width of all cells. Images were acquired every hour for three time points and then treated with the respective drugs and imaged for nine hours with 1 h intervals. As before, to measure $v_A/J$, cells were treated for 30 min with 400 nM bafilomycin $A_1$ at the 11 h time point.

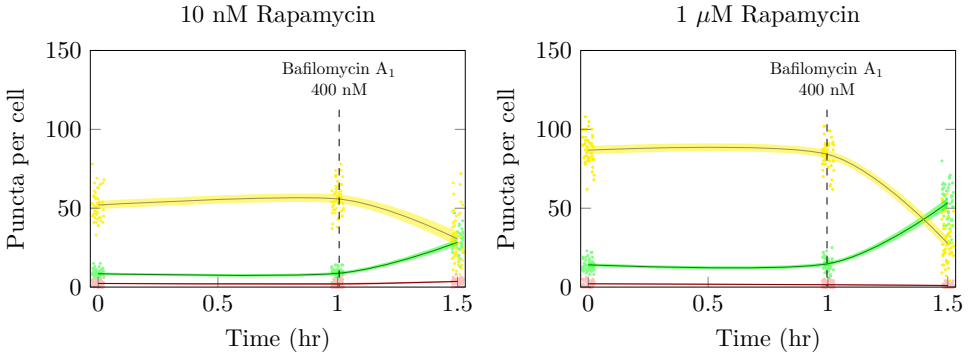


**Figure 4.7:** Verifying if the autophagy system is at steady state in HeLa GFP-LC3 cells after 24 h treatment with 10 nM and 1 $\mu$M rapamycin; autophagosomes (●), autolysosomes (●) and lysosomes (●). No net change is observed in the autophagy intermediates over time (0 – 1 h) indicating that the autophagy system is at steady state before measuring $J$. The error band shows the standard error of the mean (SEM) of autophagosomes (■), autolysosomes (■) and lysosomes (■). ($n = 50$).

**Live-cell drug screening results.** Fig. 4.8 shows the drug dose-dependent changes in $v_A$, $n_{\mathrm{A}}$, $n_{\mathrm{AA}}$ and $n_{\mathrm{L}}$ in HeLa GFP-LC3 cells. As before, $v_A$ was cal-

Stellenbosch University https://scholar.sun.ac.za



culated from the increase in $n_{\mathrm{A}}$ after bafilomycin $\mathrm{A}_1$ treatment. Analysis of the data shows that rapamycin, spermidine, 3-methyladenine, LiCl, dorsmorphin, rilmenidine and FBS were able to modulate autophagy, while metformin had no effect on autophagy in HeLa cells. MRT67307 was the only drug that was able to inhibit autophagy at the concentrations screened. The drug screening data is further contextualised in Section 4.2.1.3.

Live-cell imaging allowed us to measure the autophagy intermediates over time before using bafilomycin $\mathrm{A}_1$, thereby enabling us to verify whether or not the autophagy system was at steady state before measuring $v_A$. No changes were observed in $n_{\mathrm{A}}$ and $n_{\mathrm{AL}}$ over the time course of imaging the cells, indicating that the autophagy system was steady state prior to inhibiting the fusion of autophagosomes and lysosomes, and therefore that $v_A = J$. However, comparing $v_A$ after 24 h and 9 h treatments (experiments used to investigate the time-dependent behaviour of autophagy on page 90) reveals that despite the fact there was no net change in $n_{\mathrm{A}}$ and $n_{\mathrm{AL}}$, indicating that autophagy was at steady state, $J$ at 9 h was not equal to $J$ at 24 h (except for rapamycin and spermidine treated cells). Thus, we cannot confidently say that the $v_A$ measured equals $J$. This is discussed further on page 91.

Stellenbosch University https://scholar.sun.ac.za



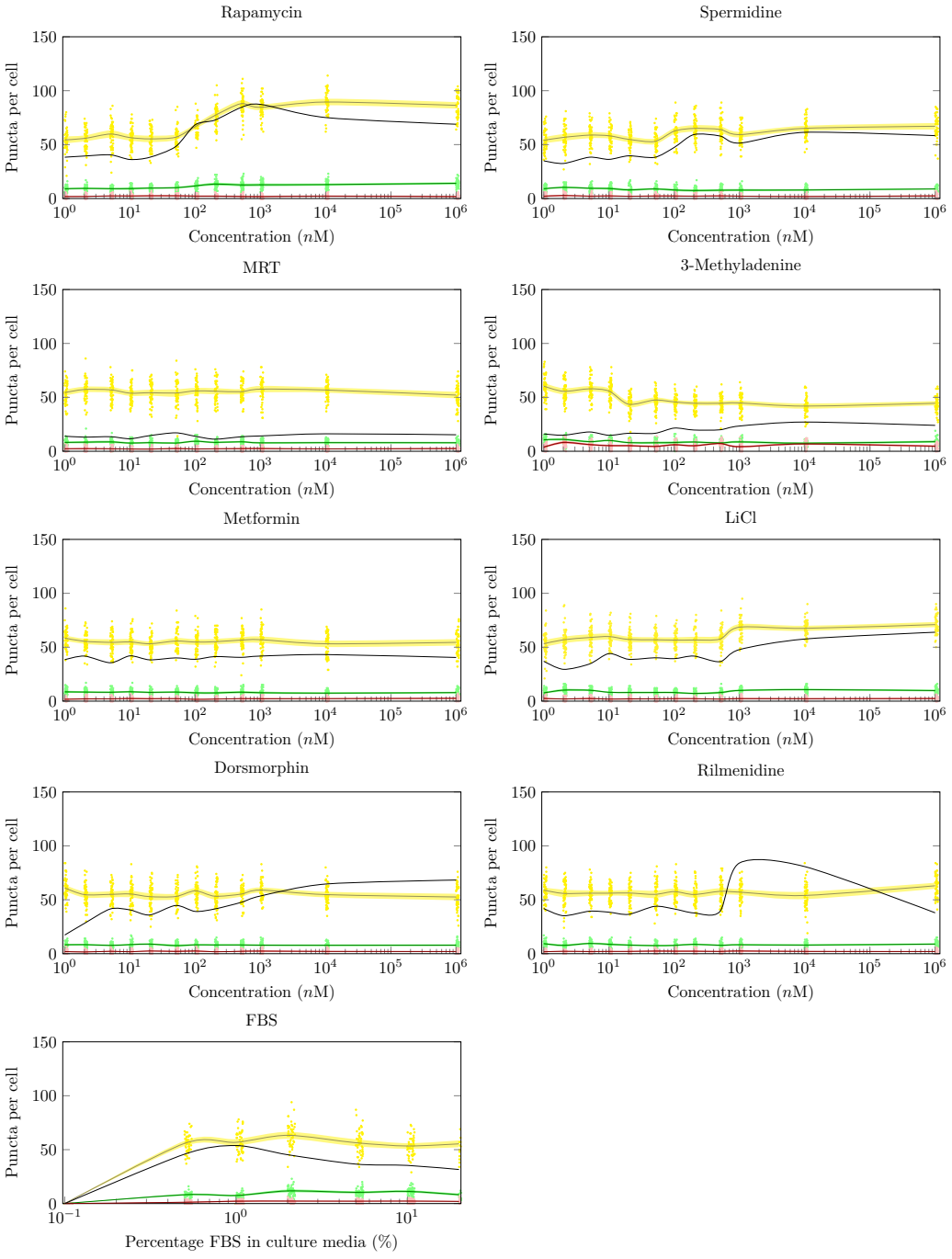


**Figure 4.8:** Live-cell screening of autophagy modulating drugs in HeLa GFP-LC3 cells. The autophagy drug response assessed after 24 h treatment; autophagosomes (●), autolysosomes (●) and lysosomes (●), and the rate of autophagosome synthesis (—). The error band depicts the SEM of autophagosomes (■), autolysosomes (■) and lysosomes (■). ($n = 50$).

Stellenbosch University https://scholar.sun.ac.za



#### 4.2.1.3 Modulation of autophagy

In the previous sections, we characterised the drug dose-response of the autophagy system. The data generated revealed important pharmacodynamic properties of the autophagy system and, more importantly with respect to autophagy-targeting therapies, that it is possible to finely modulate autophagy.

The success of our approach to characterise the dose-response profile lies in accurate measurement of the autophagosome flux/synthesis rate and the complete pool size of the autophagy intermediates at steady state over a wide drug concentration range. The dose-response curves (Figs. 4.5 and 4.8) can be used to identify important pharmacodynamic properties that would allow developing safe and effective autophagy targeting therapies. There have been only a few comprehensive drug screening experiments to identify and (re)classify autophagy modulators [120, 163, 172, 238], also using a fluorescence microscopy-based high-throughput screening platform to evaluate large libraries of pharmaceutical. The most popular method utilised to assess autophagic activity was by measuring the change in the abundance of autophagosomes, either by measuring the overall fluorescence signal from cells or by directly counting the number of autophagosomes, before and after treatment with a fusion inhibitor [163, 172, 238]. In contrast to our results, these studies did not distinguish between the autophagy intermediates and they did not quantify flux, but rather expressed it as a fraction of $n_{\mathrm{A}}$ after bafilomycin treatment and $n_{\mathrm{A}}$ before treatment. The duration of bafilomycin $\mathrm{A}_1$-treatment used to determine flux was greater than 2 h and varied among screenings experiments, and thus may affect the flux data since it allows more time for feedback mechanisms to affect autophagy compared to our approach, which was only 30 min. Another method used for screening was the ratiometric probe developed by Kaizuka *et al.* [120]. Although it does not require fusion inhibitors to measure flux, it is unable to quantify autophagosome flux as a rate.

Generally, the initial stage of screening is performed on all compounds using a high concentration to identify potential modulators, which are then screened using a range of concentrations to determine the dose-response curve. Dose-response screenings found in the literature are often limited to three or four concentrations

Stellenbosch University https://scholar.sun.ac.za



[163, 172, 238]. The risk of using a small number of concentrations is that important characteristics such as maximum achievable autophagy activity/flux may go unnoticed. For instance, the data generated by Kaizuka *et al.* [120] suggests that the maximum autophagy flux was achieved using 0.1 $\mu$M rapamycin in HeLa cells. In comparison, although we also found that autophagy was enhanced with 0.1 $\mu$M rapamycin, we could show that this was not the maximum achievable activity/flux, which was only reached at 1 $\mu$M rapamycin. Another advantage of using a large concentration range is that it can be used to determine the minimum concentration required to induce autophagy. Here we found that rapamycin was able to start inducing autophagy from $\pm$ 20 nM. Together, these properties can be used to determine the therapeutic range, which is the range between the minimum concentration at which a drug elicits a response and the maximum concentration required to maximumly induced autophagy, in the case of rapamycin: 20 nM $\rightarrow$ 1 $\mu$M. Figs. 4.5 and 4.8 shows that drugs not only differ in their therapeutic range, but that these therapeutic ranges differ between cell lines. Characterising drugs in terms of their therapeutic ranges in various cell lines has major implications for developing efficient autophagy targeting therapies.

In addition to the minimum and maximum concentrations, another advantage of using a broad concentration range is that it allows us to determine at which concentrations toxicity may occur. Although we did not explicitly quantify cell death, we did observe morphological changes associated with apoptosis (blebbing, cell shrinkage and chromatin condensation) at higher concentrations of several drugs. This can be used to determine the maximum tolerated concentration that will produce the desired effect without unacceptable toxicity. For instance, spermidine already starts to enhance autophagy in MEF at 2 nM, reaches maximum $J$ at 10 nM and remains safely upregulated up to 100 nM, but thereafter all cells die. This is in contrast to HeLa cell, where autophagy started to respond with 50 nM spermidine and reaches maximum $J$ at 200 nM, whereafter it remains upregulated with no cell death (Figs. 4.5 and 4.8). The maximum tolerated concentration, together with therapeutic range, would allow us to score the drugs according to their therapeutic index; which is a comparison of the concentration of a therapeu-

Stellenbosch University https://scholar.sun.ac.za



tic drug required to yield a therapeutic effect, to the concentration that causes toxicity. Similar toxicity analyses have been performed in research when evaluating potential autophagy modulators [163]. Undoubtedly these factors play an important role in comprehensively assessing drug responses and in moving drug development (therapy) from *in vitro* experiments to *in vivo* and clinical studies.

The most notable feature of our drug screening (Figs. 4.5 and 4.8) is the use of small concentration increments to measure autophagosome flux, which allowed us to characterise the dose-response with high resolution. While it is common to use three or four concentrations used for screening, Kaizuka *et al.* [120] did perform detail screening of serum withdrawal in HeLa cells using their ratiometric probe. They reported that FBS started to induce autophagy at 2% FBS (% of culture) and reached maximum $J$ at 1% FBS, which is nearly identical to our findings, the only difference being that our cells died at 0% FBS where theirs did not. A possible explanation is that they supplemented the culture medium with selected amino acids. It is worth noting that the FBS screening experiments of Kaizuka *et al.* [120] were performed over several hours allowing for generation of transient profiles.

Another drawback with using three/four concentrations for drug screening is that they need to be carefully selected based on cell types and drugs in order to determine the autophagy modulation capacity of drugs. Although this in itself may not have any serious consequences, it does, however, make it a laborious task to perform. Here the concentration ranges were purposefully kept the same so that we could fully characterise the dose-response, easily set screening plates, and easily compare differences in the pharmacodynamic properties (e.g. the effective and toxic concentration) of the selected drugs. Moreover, using a standardised concentration range also affects the visualization of high content screening data. This would be most beneficial for the visualization and interpretation of high throughput screening data of large drug libraries spanning a broad range of concentrations and cell types.

Our drug screening (Figs. 4.5 and 4.8) can be further enhanced by using drug response curve models. A dose-response model describes the response in $J$ to

Stellenbosch University https://scholar.sun.ac.za



exposure to a specific drug in a cell/tissue-specific manner as a function of the drug concentration. The Hill equation can serve as a good starting point to model concentration dependent effects of a drug on $J$;

$$J = J_{\text{basal}} + (J_{max} - J_{\text{basal}}) \cdot \frac{d^{\eta}}{K_d^h + d^h} \tag{4.1}$$

where $d$ is drug concentration, $J_{\text{basal}}$ is the baseline autophagosome flux and $J_{max}$ is the maximum induced flux. $K_d$ is the EC50, the concentration causing 50% of a maximum effect, and $h$ is the Hill coefficient that describes the steepness of the drug-response curve.

Dose-response models can range from very simple models, e.g. equation 4.1, to complex models which require multiple equations (e.g. drug response and cell death models). Fig. 4.9 shows a cartoon of a mathematical expression fitted to the experimental data (Fig. 4.5) to characterise the autophagy steady state drug response curves (rapamycin, spermidine and FBS).

Drug response curve models can aid in the characterisation of the pharmacodynamic properties of drugs in various cell types, which may allow us to determine the concentrations at which a drug will be safe and effective, especially with those with a narrow therapeutic index, for example, spermidine in MEF cells (Fig. 4.9). Moreover, expanding these models to include drug exposure patterns, for instance, continuous drug exposure (cell culture experiments), cyclic and intermittent drug exposure (pharmacotherapy), would allow effective modulation of autophagy. The characterisation of the autophagy steady state pharmacological properties as performed here presents a promising way forward in developing effective autophagy targeting therapies.

Stellenbosch University https://scholar.sun.ac.za



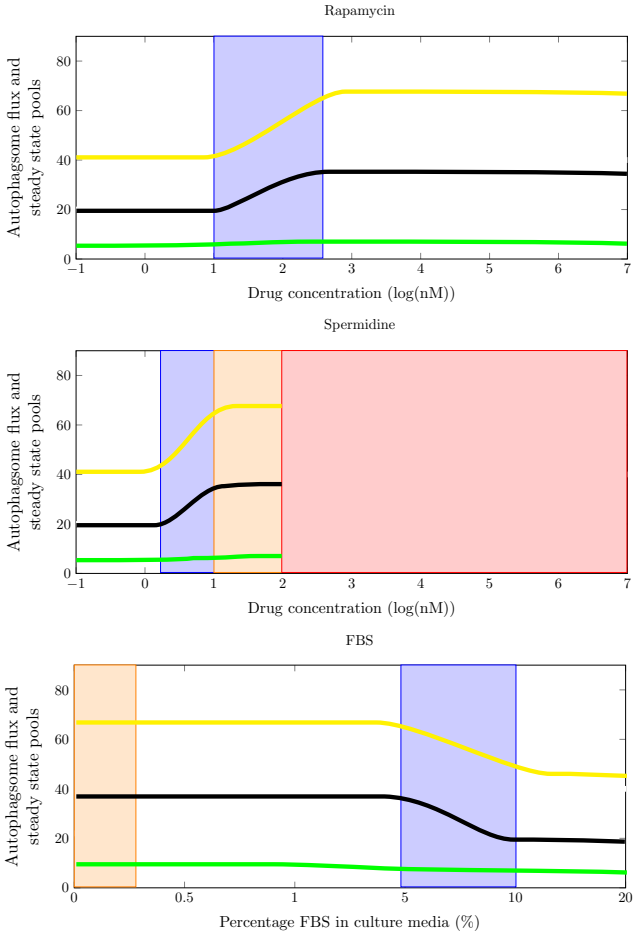


**Figure 4.9:** A cartoon of a dose–response model: mathematical expressions fitted to the experimental data (Fig. 4.5) to characterise the response curves of autophagosome (—), autolysosome (—) and autophagosome flux (—). These models (and raw data) can be used to determine important pharmacodynamic properties for the development autophagy targeting therapies: the therapeutic concentration range (), a range of concentrations wherein autophagy can be safely modulated, and the maximum tolerated dose (), the highest drug concentration (range) that will produce the desired effect without unacceptable toxicity. Toxic concentrations are also shown ().

#### 4.2.1.4 Fixation and live-cell imaging

**Limitations of using a fixed based method.** Screening of the 96 well plates using the ImageXpress Micro XLS Widefield allowed for the high content analysis, but it was not without its inherent challenges. Arguably, the greatest limitation

Stellenbosch University https://scholar.sun.ac.za



using a fixed based screening approach is that it does not allow for the real-time assessment of the autophagy system, making it difficult to verify whether or not the autophagy system is at steady state; it provides only a snapshot of the $n_{\mathrm{A}}$, $n_{\mathrm{AL}}$ and $n_{\mathrm{L}}$ at a single time and allows us to measure only $v_A$, not $J$. It is possible to modify the protocol by fixing cells at specific times in order to elucidate the time-dependent nature of the autophagy response. Nevertheless, the combination of the destructive nature of the fixation process and the acidicity of autolysosomes does result in inaccurate $n_{\mathrm{AL}}$ and $n_{\mathrm{L}}$, making it a less favourable approach.

**Advantages and disadvantages of live-cell imaging.** Our "high-content" live-cell based approach allowed us to measure the autophagy intermediates over time, which was not possible using the fixation method. Also, the refined method generated more reliable data of the autophagy intermediates counts since it is not destructive to the fluorophores compared to the fixation method that quenched the GFP signal. The addition of microscope stage control allowed for the automatic multi-layered image acquisition of all the positions. However, recording the positions used for image acquisition had to be done manually, a laborious task when compared to ImageXpress Micro XLS Widefield, which sets all the positions automatically. Moreover, the versatile design of our slide made it an ideal platform for use with the micro-patterning technique (page 107). Despite the success of our "high-content" live-cell based imaging approach, there still exist areas for further development such as automated image positioning and on the fly image analysis, which can be achieved by writing a macro for the Zen imaging software. Arguably the greatest advantage of this approach is that it allows for the dynamic assessment of autophagy over time in a "high-content" manner, making it an ideal approach to assess the transient time-dependent response of the autophagy system.

### 4.2.2 The transient time-dependent behaviour of autophagy

In the previous section, we characterised the drug dose-dependent response of autophagy. The next step was to characterise the transient time-dependent be-

Stellenbosch University https://scholar.sun.ac.za



haviour of autophagy. Continuing with the previous format, we set out to screen for the transient time-dependent behaviour of both MEF and HeLa cells with the selected drugs using a concentration that we know knew would elicit a response (Figs. 4.5 and 4.8). Drugs that did not bring about an autophagy response in either of the two cell lines were also included using what we deemed to be relatively high concentrations—in case there would be a "short-lived" autophagy response that were not able to observe when imaging after 24 h.

**Time dependent behaviour of autophagy in MEF and HeLa cells.** Figs. 4.10 and 4.11 show the quantitative analysis of the transient time-dependent behaviour of $n_{\mathrm{A}}$, $n_{\mathrm{AL}}$ and $n_{\mathrm{L}}$ of the respective treatments over a 9 h period. In the case of LiCl (MEF only) and metformin which did not elicit a response after 24 h, we used a 10 $\mu$m LiCl and 10 $\mu$M metformin for MEF cells and 1 $\mu$M metformin for HeLa cells. After 9 h of treatment the autophagosome synthesis rate was calculated from the initial rate of increase in $n_{\mathrm{A}}$ after the complete inhibition of fusion of autophagosomes and lysosomes with 400 nM bafilomycin $\mathrm{A}_1$.

Stellenbosch University https://scholar.sun.ac.za



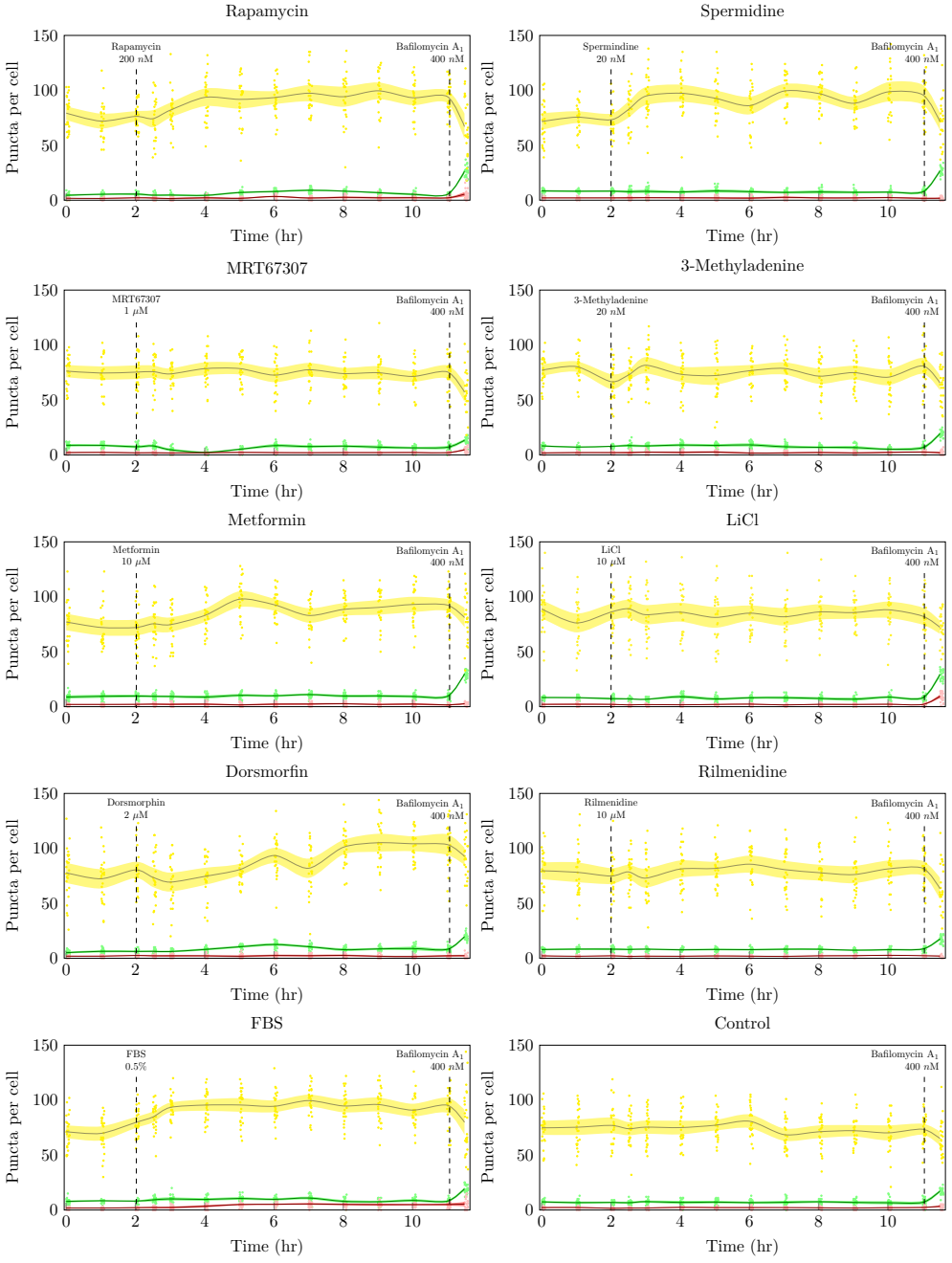


**Figure 4.10:** The transient time-dependent response of autophagosomes (●), autolysosomes (●) and lysosomes (●) in MEF GFP-LC3 cells. Autophagy intermediates were measured under basal conditions (0–2 h) and treated with the respective drugs/treatment at 2 h and monitored over a 9 h period. The fusion between autophagosome and lysosome was inhibited using 400 nM bafilomycin $A_1$ at the 11 h. The error band shows the SEM of autophagosomes (■), autolysosomes (■) and lysosomes (■).

$$(n = 20).$$

Stellenbosch University https://scholar.sun.ac.za



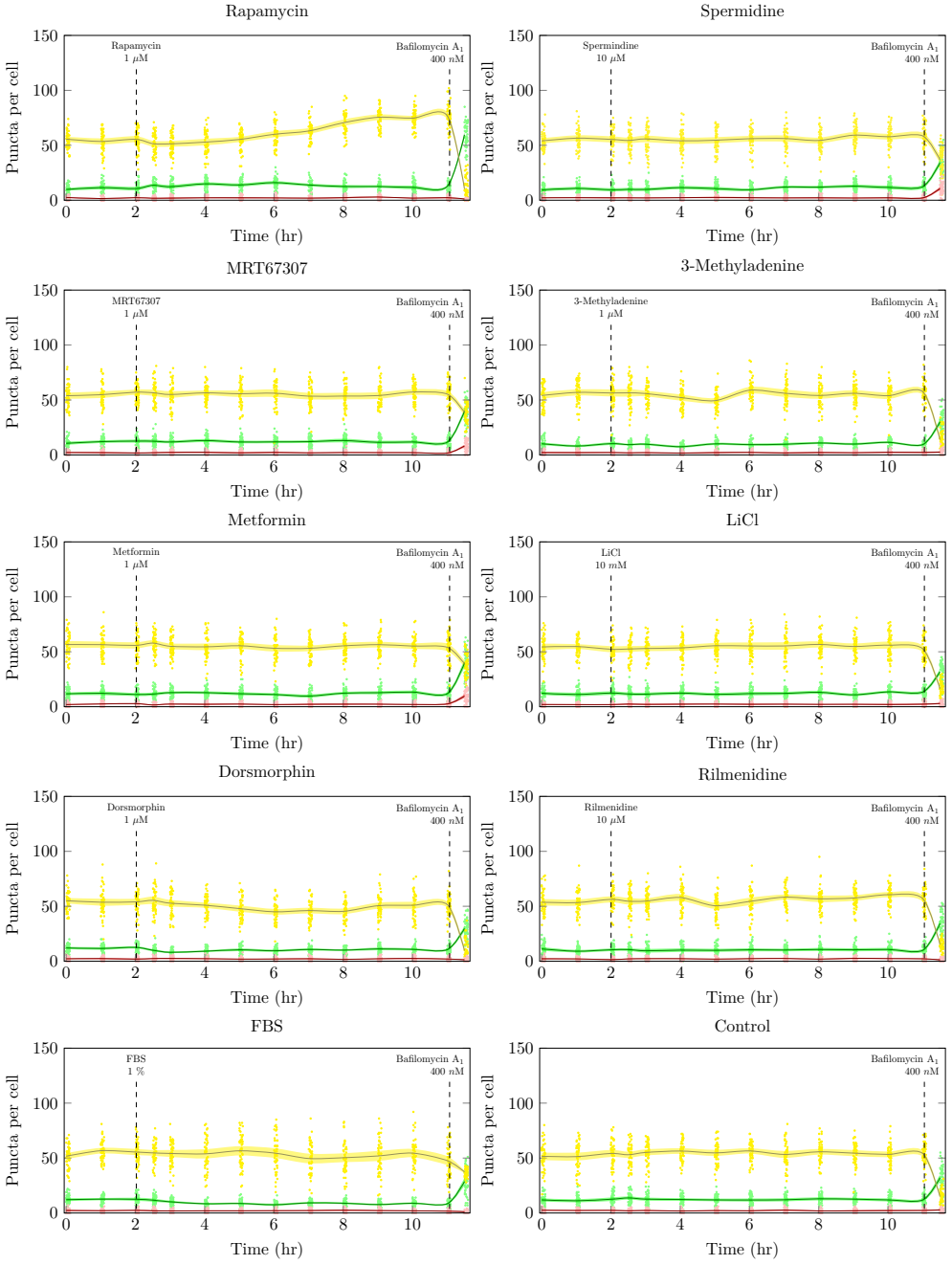


**Figure 4.11:** The transient time-dependent response of autophagosomes (●), autolysosomes (●) and lysosomes (●) in HeLa GFP-LC3 cells. Autophagy intermediates were measured under basal conditions (0–2 h) and treated with the respective drugs/treatment at 2 h and monitored over a 9 h period. The fusion between autophagosomes and lysosomes was inhibited using 400 nM bafilomycin $A_1$ at the 11 h. The error band depicts the SEM of autophagosomes (■), autolysosomes (■) and lysosomes (■). ($n = 50$).

Stellenbosch University https://scholar.sun.ac.za



**Establishing a new steady state.** The time-dependent analysis of the transient behaviour of $n_{\mathrm{A}}$ and $n_{\mathrm{AL}}$ shows that the autophagy system was at a steady state prior to measuring $v_A$, which therefore equals $J$. One would expect that $J$ measured at 9 h be the same as $J$ at 24 h, but despite the fact that $n_{\mathrm{A}}$ and $n_{\mathrm{AL}}$ remained constant over time, there were significant differences in $J$ at these two time points (Table 4.2). One reason for this could be that autophagy responds to acute induction/inhibition in two phases, an initial response followed by a long-term alteration/regulation of autophagy. Another reason could be that using autophagic intermediates to verify whether or not steady state has been established has inherent limitations, in particular that $n_{\mathrm{A}}$ does not change much upon intervention. Although $n_{\mathrm{AL}}$ is potentially a better assessor of the autophagic steady state, for neither $n_{\mathrm{A}}$ not for $n_{\mathrm{AL}}$ a 1 h interval is sufficient for ascertaining whether the system is at steady state. This is especially the case where the transition in autophagy activity occurs over long period (here, greater than 24 h). Measuring $v_A$ over time is a more reliable means to verify if the autophagy system is at steady state. Based on the data, we can confidently say that rapamycin- and spermidine-induced autophagy is at steady state after 4–6 h treatment in MEF cells since $v_A$ is similar at both 9 h and 24 h time points. In comparison, for HeLa cells this was only achieved with rapamycin (Table 4.2).

Stellenbosch University https://scholar.sun.ac.za



**Table 4.2:** The rate of autophagosome synthesis ($v_A$) measured at 9 h and 24 h in MEF and HeLa GFP-LC3 cells. $v_A$: $n_A$/hr/cell.

| | MEF | | HeLa | |
|---|---|---|---|---|
| | 9 h | 24 h | 9 h | 24 h |
| Rapamycin | 42.2 | 42.7 | 94.0 | 87.3 |
| Spermidine | 38.6 | 41.7 | 43.8 | 61.4 |
| MRT67307 | 12.8 | 20.1 | 56.6 | 14.2 |
| 3-Methyladenine | 25.6 | 1.1 | 41.6 | 23.4 |
| Metformin | 41.0 | 21.8 | 56.2 | 41.8 |
| LiCl | 42.8 | 17.1 | 37.2 | 63.9 |
| Dorsomorphin | 23.2 | 28.9 | 38.8 | 53.5 |
| Rilmenidine | 18.4 | 50.7 | 48.8 | 80.8 |
| FBS | 22.6 | 45.1 | 40.6 | 53.8 |
| Control | 20.6 | 22.3 | 40.2 | 35.4 |

### 4.2.3 Screening autophagosomes

Most of the strategies for modulating autophagy target autophagosome formation. However, targeting downstream processes has also been successful; for example, the inhibition of fusion sensitises tumour cells to chemotherapeutic agents. High concentrations of fusion inhibitors will of course completely prevent fusion of autophagosomes and lysosomes, but partial inhibition of fusion could potentially be used as as modulating strategy. To explore this possibility we incrementally inhibited fusion and assessed the time-dependent behaviour of autophagy.

MEF GFP-LC3 and HeLa GFP-LC3 were treated with 10 nM and 20 nM bafilomycin $A_1$ and the autophagy intermediates monitored for 9 h, at which time $J$ was measured using 400 nM bafilomycin $A_1$ as described in Section 4.2.1.2. Although treatment with 10 nM bafilomycin $A_1$ increased $n_A$ and decreased $n_{AL}$ it did not change the autophagosome flux in any of the two cell lines (Fig. 4.12). On the other hand, 20 nM bafilomycin $A_1$ further increased $n_A$ and decreased $n_{AL}$ in both cell lines, while increasing $J$ in MEF cells and decreasing $J$ in HeLa cells

Stellenbosch University https://scholar.sun.ac.za



(Fig. 4.12). This demonstrates two important points; first, that $J$ can continue unimpaired within a small degree of variation in the rate of fusion between autophagosomes and lysosomes, and second, that if the fusion rate decreases beyond a specific threshold it impairs autophagy activity. The exact mechanism responsible for the regulation of autophagy in response to a decrease in the rate of fusion remains unclear, but presumably involves the amino acid-sensing network.

Stellenbosch University https://scholar.sun.ac.za



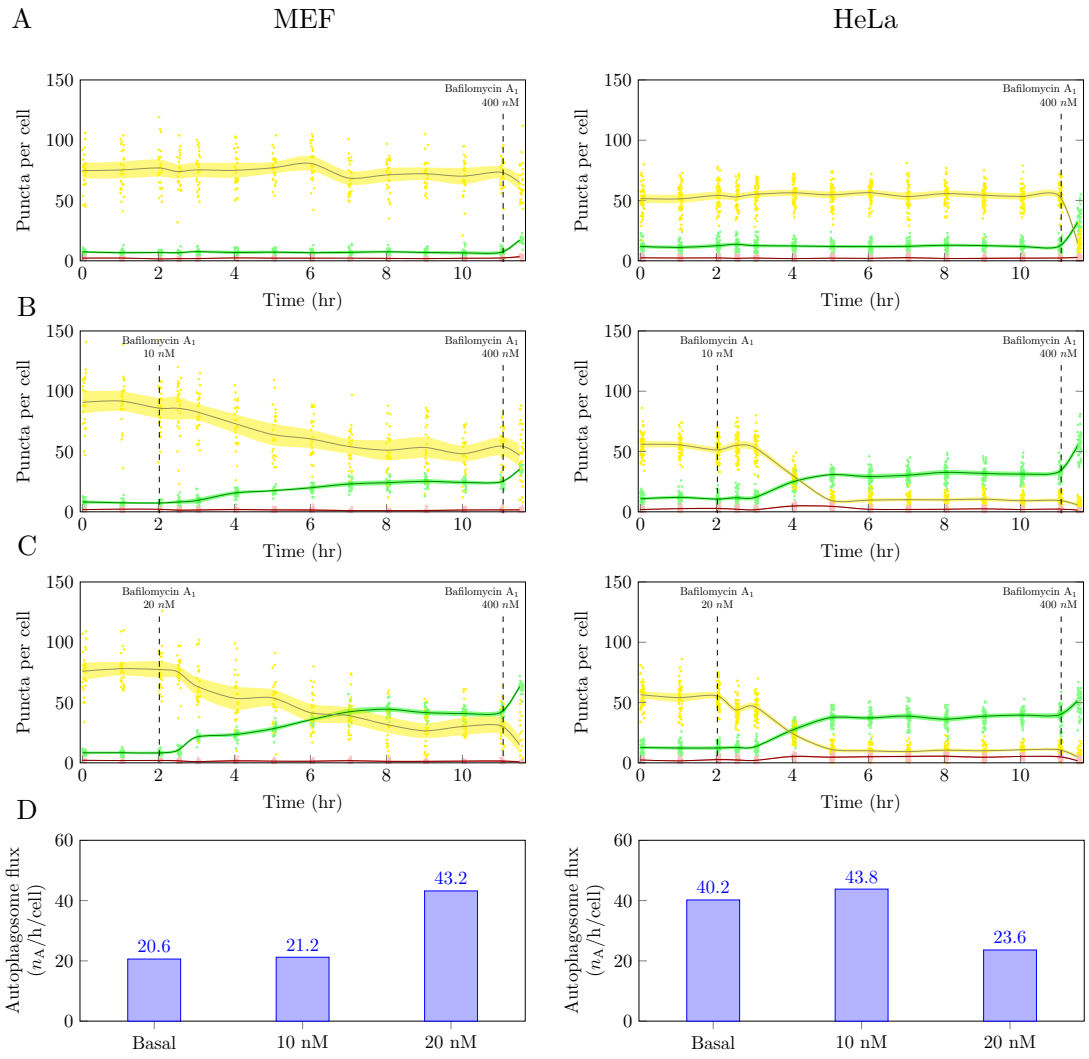


**Figure 4.12:** Manipulating the rate of fusion between autophagosomes and lysosomes. The change in the number of autophagosomes (●), autolysosomes (●) and lysosomes (●) over time under in MEF (left) and HeLa (right) cells. Pool sizes of the three autophagic intermediates under basal conditions (A) in MEF and HeLa cells. Partial inhibition of fusion between autophagosomes and lysosomes using 10 nM (B) and 20 nM (C) bafilomycin $A_1$ in MEF and HeLa cells. Complete inhibition of fusion at the 11 h with 400 nM bafilomycin $A_1$. (D) Quantification of $J$ under basal conditions and partial inhibition of fusion between autophagosomes and lysosomes using 10 nM and 20 nM bafilomycin $A_1$ in MEF and HeLa cells. MEF, $n = 20$, HeLa, $n = 50$.

Stellenbosch University https://scholar.sun.ac.za



## 4.3 Autophagosome flux markers

Considering the complexity of the autophagy process and cargo turnover, there is presently no single marker that can be used in a stand-alone assay to monitor autophagy in mammalian cells [140]. Although various autophagy markers for assessing general autophagy activity have been described in the literature, none of them directly indicate the rate at which the autophagy pathway proceeds. However, each of them does report on a particular feature of autophagy. For example, LC3, a structural component of autophagosomes, is used to assess autophagosome abundance, while p62, an autophagosome cargo receptor, is often used as a degradative marker. Taking advantage of controlling $J$, we set out to perform proteomic analysis on mTOR-dependent (rapamycin) and mTOR-independent (spermidine) induction of autophagy with similar incremental increases in $J$ to identify protein markers that correlate with flux. We chose two different induction methods to identify robust markers of autophagosome flux. We also included a partial inhibition group using a low concentration of bafilomycin $A_1$. Although the concentration of bafilomycin $A_1$ used to partially inhibit fusion does not affect $J$, it does increase the number of autophagosomes (see Section 4.2.3). Under both enhanced and partial inhibition conditions there was a higher $n_A$ compared to basal levels, and, consequently, increased levels of autophagosome membrane components. Thus, we used the partial inhibition group to filter out false positive protein markers identified using rapamycin and spermidine.

We performed proteomic analysis on MEF GFP-LC3 cells in which the autophagosome flux was increased by $\pm 25\%$ and $\pm 75\%$ after 12 h through mTOR-dependent and -independent induction using rapamycin (20 nM and 50 nM) and spermidine (100 nM and 500 nM) respectively. It is worth pointing out that when comparing the spermidine concentrations with the drug dose-response graphs, the concentrations used here resulted in cell death after 24 h. Preliminary data showed that after 12 h of spermidine exposure the autophagy system was at steady state and there was no cell death. Proteins were grouped into those that increased with $J$, those that decreased with $J$, those that remained constant with a change in $J$, and those directly involved in autophagy, especially in the transport

Stellenbosch University https://scholar.sun.ac.za



of autophagosomes (Fig. 4.13). An interaction network representation of identified autophagosome flux markers that increased and decreased with autophagosome is shown Fig. 4.14

Stellenbosch University https://scholar.sun.ac.za



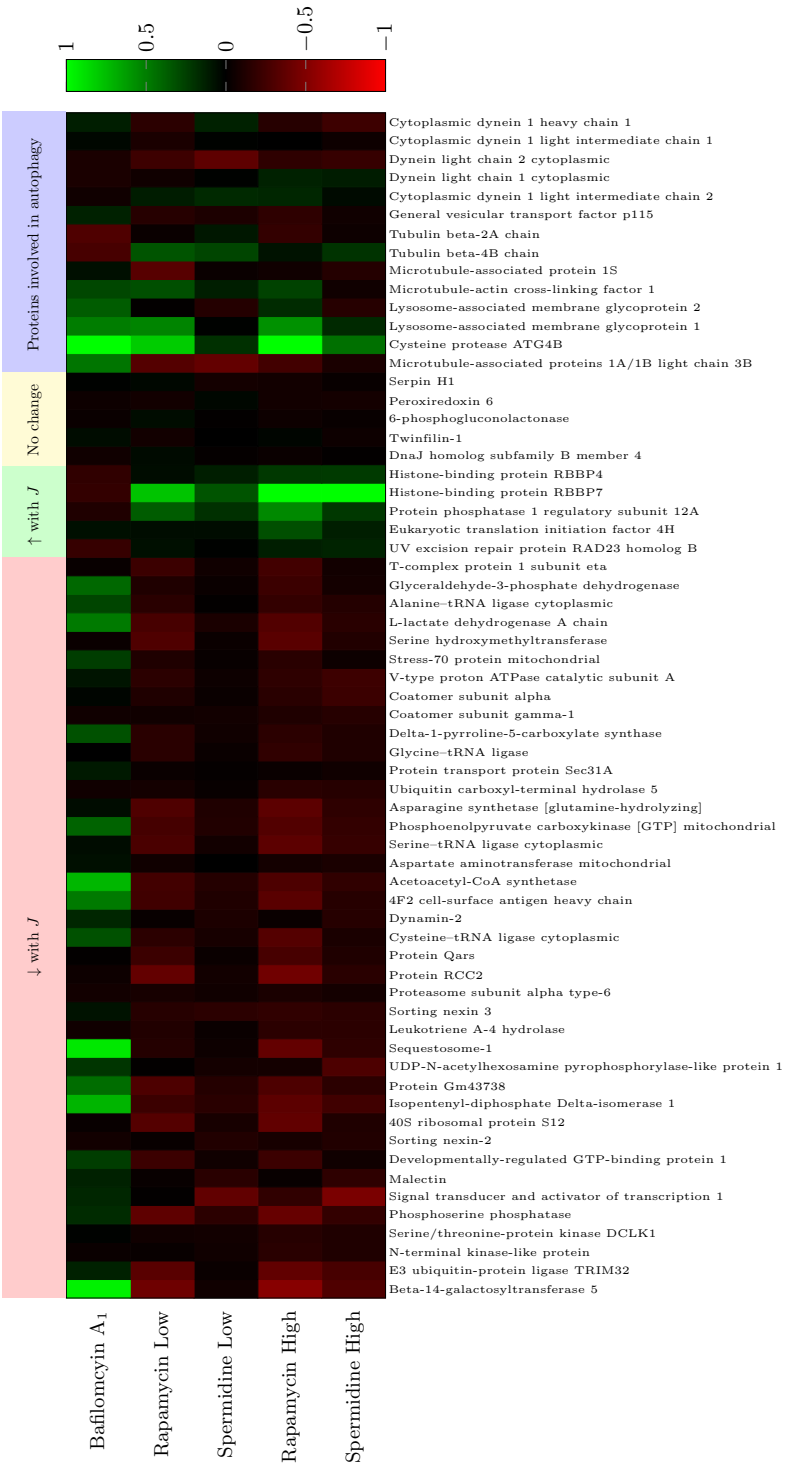


**Figure 4.13:** Heat map of protein markers identified using proteomic analysis of MEF GFP-LC3 cells with known autophagosome flux. Autophagosome flux was enhanced by 25% (low rapamycin and spermidine) and by 75% (high rapamycin and spermidine) to determine which proteins change with increasing autophagosome flux. Partial inhibition with bafilomycin $A_1$ was included to increase the number of autophagosomes and autolysosomes without changing the autophagosome flux, allowing us to distinguish markers that relate only to autophagosome flux. Protein markers are grouped into those who increase, decrease and remain the same with increasing autophagosome flux. Protein abundance is expressed as fold change relative to control.

Stellenbosch University https://scholar.sun.ac.za



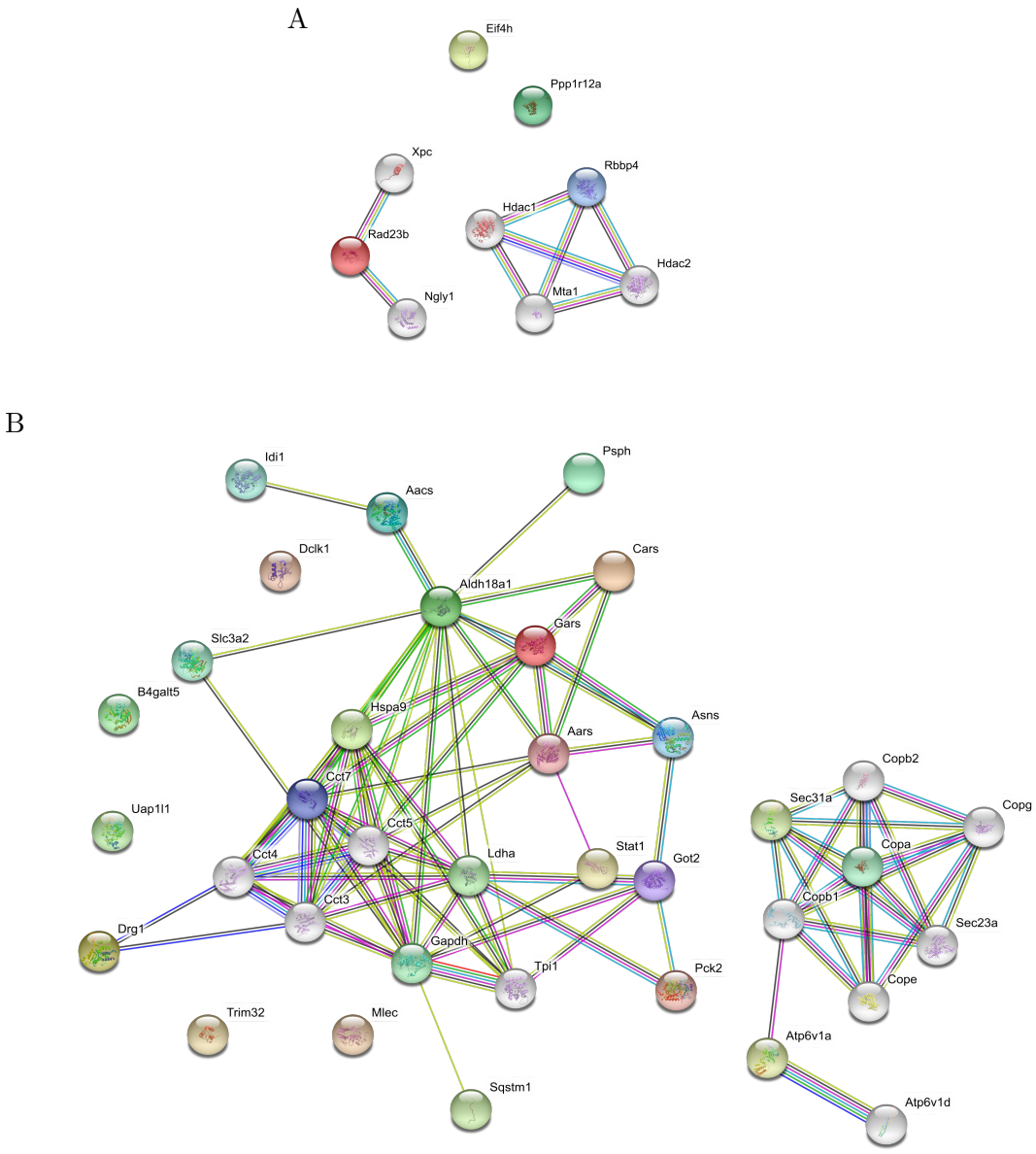


**Figure 4.14:** Network representation of autophagosome flux markers that increase (A) and decrease (B) with autophagosome flux. Coloured nodes: autophagosome flux markers; White nodes: proteins that interact with autophagosome flux markers. Node connection: known interactions from curated databases (—); experimentally determined interactions (—). Predicted interactions: gene neighbourhood (—); gene fusions (—); gene co-occurrence (—); text-mining (—); co-expression (—). Images generated using STRING database of known and predicted protein-protein interactions (https://string-db.org/).

Stellenbosch University https://scholar.sun.ac.za



**Cargo proteins as a measure of $J$.** Considering that autophagosome flux is a measure of its degradative activity, cargo proteins would intuitively make ideal markers of autophagosome flux. The majority of the potential biomarkers that were identified were cytosolic proteins that decrease with increasing $J$, suggesting that they form part of the cargo (Fig. 4.13). When assessing these proteins two major trends came to light, the first of which was the increase in abundance of these proteins when treated with bafilomycin $A_1$, and second the difference in the levels of these proteins between the rapamycin and spermidine groups despite their having similar autophagosome fluxes.

The apparent increase in many of these cytosolic proteins following partial inhibition of fusion stemmed from the increase in $n_A$. Under bafilomycin $A_1$-treated conditions there was no net change in cytoplasmic turnover, but the increase in $n_A$ (which is greater compared to induced conditions, see Fig. 4.12) led to an accumulation of undigested autophagy cargo. As a result, a greater abundance of these proteins was detected in the bafilomycin $A_1$ treated group compared to the other groups. Although one would intuitively think that cargo proteins would act as suitable indicators of autophagosome flux, since their abundance is dependent on the rate of autophagy, it was clear that this can be misleading. This was particularly relevant in the case of sequestosome-1, better known as p62, which is commonly used as a cargo marker for the clearance of proteins/aggregates due to its mediating role in cargo degradation [21, 140, 191, 209]. Indeed, many studies have shown that there is an abnormal accumulation of p62 with the loss of autophagy activity [72, 147]. However, we found that an increase in p62 can also occur with an increase in $n_A$ (typically associated with impaired autophagy) without any change in the autophagosome flux. Thus, a change in p62 can result from two distinct mechanisms, either a loss of function (decrease in autophagosome flux, and consequently, protein turnover) or a change in phenotype (change in the number of autophagy intermediates without a change in $J$), which makes it ill-suited as a flux marker. Ideally, autophagosome flux markers should only change with a change in flux. However, p62 is an important cargo marker that provides valuable information on cargo behaviour and should be used in combination with other

Stellenbosch University https://scholar.sun.ac.za



assays or protein markers to derive a complete picture of the autophagy system.

Another aspect that needs addressing is the difference in the abundance of cargo proteins despite the autophagosome flux being similar between the mTOR-dependent and -independent induced autophagy groups. Proteomic analysis revealed that the large majority of these proteins were more affected by mTOR-targeted induction of autophagy (Fig. 4.13). This is most likely as a result of an inherent increase in autophagosome size associated with mTOR-induced autophagy which further increases cytosolic turnover compared to mTOR-independent induction (see Fig. 4.15). This highlights the importance of distinguishing between autophagy machinery (and autophagosome flux) and cargo, and that cytosolic cargo turn requires equal attention.

**Autophagy machinery as a measure of $J$.** Since an increasing autophagosome flux would likely require more autophagy-related proteins in order to maintain high levels of autophagy activity, it is surprising that we did not find any autophagy-related proteins that increased proportionally with autophagosome flux (Fig. 4.13). In fact, expanding this criterion to include a broad range of proteins associated with autophagy, such as dynein motors and transport/fusion factors, did not reveal any correlation with autophagosome flux. This clearly shows that the abundance of autophagy proteins, such as Atg5, Atg7, LC3, etc., are not indicative of degradative activity. This has been noted by others and is the reason why these markers are assessed with and without bafilomycin $A_1$ over time to infer autophagy activity [140, 191, 226].

Further analysis of the proteomic data revealed several biomarkers that increased with autophagosome flux. This included histone-binding protein RBBP 4 and 7, eukaryotic translation initiation factor 4H and protein phosphatase 1 regulatory subunit 12A, all of which are related, in some way or another, to protein synthesis [221, 270]. The exact reason why these proteins increase remains unclear, but considering the increase in cytosolic protein turnover, it presumably relates to the inherent change in protein synthesis in order to replace degraded proteins, so as to not compromise cellular function and integrity. The advantage of using these

Stellenbosch University https://scholar.sun.ac.za



"protein synthesis" markers that reflect cargo turnover as a means to measure flux is that it circumvents the limitations of using cargo proteins associated with phenotypical changes. This raises the question of whether other markers associated with the protein synthesis, such as mRNA, could serve as potential markers for autophagosome flux and cytosolic cargo turnover.

**Loading controls for $J$.** Loading controls are an important part of immunodetection assays in that they compensate and correct for sample-to-sample variation. Standardising protein abundance using an internal control protein is the most commonly used method [45]. Ideally, the control protein should be unrelated to the autophagy process and must be present in all samples, so that reference protein abundance depends completely on sample concentration. Housekeeping proteins, such as actin and glyceraldehyde 3-phosphate dehydrogenase (GAPDH), are typically used as internal controls because they are constitutively expressed throughout all cells of an organism.

Proteomic analysis revealed that GAPDH decreases with an increase in autophagosome flux (Fig. 4.13). This has particular relevance in autophagy research, where GAPDH is used as loading control [4, 13, 101]. In the event of high autophagy activity, the increased rate of protein turnover leads to a decrease in GAPDH levels. If the abundance of the target protein is normalized to GAPDH, it would result in the reporting of higher target protein abundance. Therefore, it is advisable to avoid using cytosolic proteins as loading controls due to the potential impact of autophagy on their abundance, which includes many of the housekeeping proteins that are typically used. Nonetheless, proteomic analysis revealed two cytosolic proteins that could potentially serve as loading controls, namely 6-phosphogluconolactonase (6PGL), a cytosolic enzyme that catalyzes the third step of the pentose phosphate pathway [183] in all organsisms, and dnaj homolog subfamily B member 4, a chaperone protein involved in the folding of proteins [75]. Interestingly, the reasons why GAPDH is considered a good housekeeping protein for standardising protein abundance also applies to 6PGL, yet 6PGL is never used as internal control. Since there is no reason why 6GPL would

Stellenbosch University https://scholar.sun.ac.za



not make an ideal loading control (beyond what would relate to both GAPDH and 6PGL), GAPDH is most likely utilized is because it was the first of that class of housekeeping proteins to be used and there has been no reason to use another.

Intuitively, structural proteins such as tubulin and actin, and nuclear proteins such as histones and telomeres would serve as better loading controls since their abundance would most probably not be affected by autophagy activity. While both tubulin and actin are commonly used, and are gaining popularity as a loading control in autophagy research [14, 35, 145], the use of nuclear proteins seems to be non-existent. It is interesting to note that we did find some variation in tubulin and microtubule-associated proteins levels between treatments (Fig. 4.13). In addition to tubulin and actin, proteomic analysis revealed novel markers associated with the structural network that could potentially serve as loading controls: twinfilin-1, an actin monomer-binding protein conserved in mammals [262], and serpin H1, a collagen-binding protein that may act as a collagen-specific chaperone [216]. These markers may improve our standardisation of western blot analysis in the context of monitoring autophagy and autophagy-related processes *in vitro*, and potentially in samples derived from patients.

## 4.4 Autophagy system properties

The time-dependent analysis of MEF cells with the different drugs highlighted intriguing aspects of the autophagy system, such as the relationship between autophagy intermediates and cell size, and that the differential response to drugs was not only limited to changes in $v_A$ but in some cases changes in autophagosome size. These observations raise several questions about the underlying properties of autophagy. Can the overall autophagy degradative activity be finely controlled by including the targeting of autophagosome size? Does $J$ increase with cell size? In this section, we address these questions by investigating the underlying mechanism of autophagy, with emphasis on autophagosome dynamics and cell size/geometry.

Stellenbosch University https://scholar.sun.ac.za



### 4.4.1 Modulation of cargo flow through the autophagy pathway

Induction of autophagy through mTOR-dependent and -independent pathways using two different concentrations of rapamycin and spermidine led to a similar increase in $J$ after 9 h (Fig. 4.15). From the analysis of time-dependent changes in autophagosome size it became clear that there was an increase in autophagosomes size when treated with rapamycin, but not when treated with spermidine (Fig. 4.15). Although both may have similar $J$, the increase in autophagosome size in rapamycin-treated cells resulted in an increase in $J_{\text{vol}}$ that was 3.7 times higher than that in spermidine-treated cells. We also assessed cells subjected to FBS withdrawal, which mimics starvation-induced autophagy and occurs through the mTOR-dependent pathway. This induction resulted in a time-dependent autophagosome size profile comparable to that of rapamycin induced autophagy, but surprisingly, it did not result in an increase in $J$ after 9 h. However, the increase in autophagosomes as a result of FBS withdrawal leads an 8.3 fold increase in $J_{\text{vol}}$ compared to basal autophagy and surprisingly a 3.1 fold increase in $J_{\text{vol}}$ compared to spermidine-treated cells which had a higher $J$. The table in Fig. 4.15B shows that an increase in $J$ does not lead to a corresponding increase in $J_{\text{vol}}$. These findings suggest that $J_{\text{vol}}$ may present an additional, potentially even more sensitive, means to assess autophagy activity. Moreover, the induction of autophagy through FBS withdrawal resulted in an increase in $J$ after 24 h, suggesting that acute amino acid withdrawal can elicit a biphasic response.

Stellenbosch University https://scholar.sun.ac.za



A

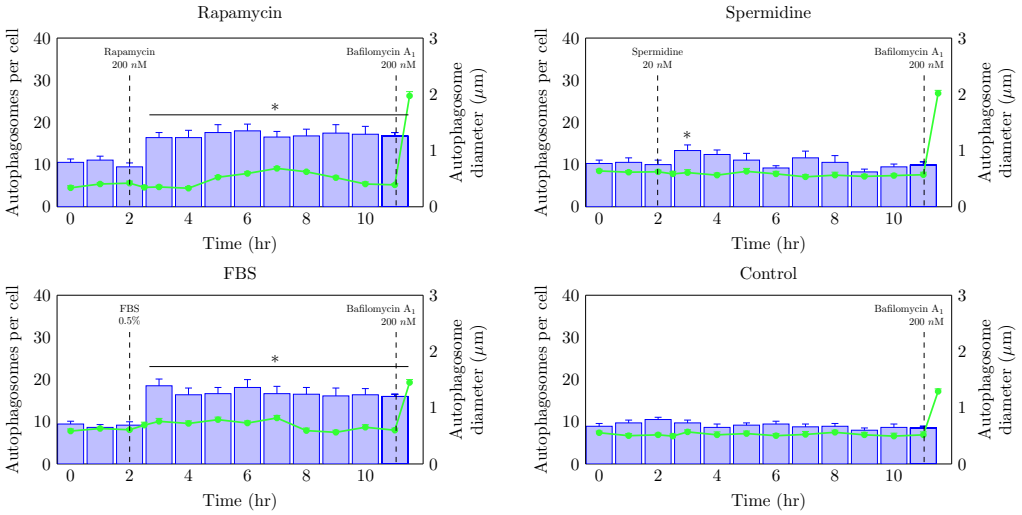


B

| | Unit | Rapamycin | Spermidine | FBS | Control |
|---|---|---|---|---|---|
| $J$ | A/hr/cell | 42.2 | 38.6 | 22.6 | 20.6 |
| $J_{vol}$ | fL/hr/cell | 229.7 | 62.2 | 163.5 | 19.5 |

| | Unit | Rapamycin | Spermidine | FBS | Control |
|---|---|---|---|---|---|
| $J$ | A/hr/cell | 42.7 | 41.7 | 45.1 | 22.3 |
| $J_{vol}$ | fL/hr/cell | 229.7 | 62.2 | 163.5 | 19.5 |

**Figure 4.15:** Modulation of cargo flow through the autophagy pathway. (A) Graphs showing the transient time-dependent behaviour of autophagosomes (●) and their corresponding diameter (□) over time in MEF cells. Cells were treated with the respective drugs/conditions at 2 h and fusion-inhibited at 11 h with 400 nM bafilomycin $A_1$. (B) Table depicting the autophagosome flux ($J$) and the rate of flow of cargo, the cytoplasmic volume degraded through autophagy ($J_{vol}$), under various treatment conditions for 9 h. * vs Baseline (0–2 h), $p < 0.05$ in MEF cells. ($n = 15$)

### 4.4.2 Using micro-patterning to control cell shape and dissect the autophagy process

MEF cells are highly proliferating and migrating cells that give rise to a large array of cell shapes/sizes and metabolic demands in a cell population. As a result MEF cell populations can exhibit a considerable degree of internal variability in autophagy activity. The resulting intercellular variation in cell populations can

Stellenbosch University https://scholar.sun.ac.za



mask the subtle differences between treatment groups. With the aim of further exploring the underlying mechanism of autophagy, such as the relationship between cell size and autophagosome flux, and how these changes in autophagosome flux can affect autophagosome trafficking, we used micro-patterning to manipulate cell size and shape. We could control cells with high precision to produce highly ordered cells. Fig. 4.16 shows that patterned cells are characterised by a highly organised tubulin network with a distinct distribution profile of autophagy intermediates, in contrast to non-patterned cells that presented an asymmetrical tubulin network with uneven distribution of autophagosomes and lysosomes throughout the cell.

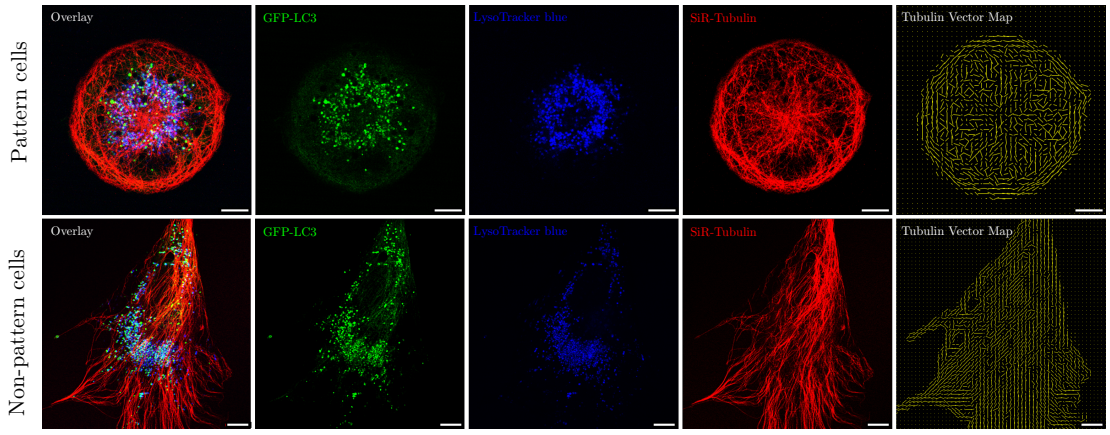


**Figure 4.16:** Precision control of cell size using micro-patterning. Micro-patterned cells (top) show a highly organised tubulin network with radial distribution of autophagy intermediates, while non-patterned cells (bottom) are characterized by an asymmetric tubulin arrangement with a non-uniform distribution profile of autophagy pathway intermediates. Autophagosomes (●), autolysosomes (●), lysosomes (●), tubulin network (—) and vector map (—) generated using OrientationJ in Fiji. Scale bar: 10 $\mu$m.

### 4.4.3 The relationship between autophagosome flux and cell size

One of the questions that can be asked about the systems properties of autophagy is whether or not $J$ is proportional to cell size. Here we assessed the relationship between $J$ and cell size using GFP-LC3 MEF cells that were patterned on disc

Stellenbosch University https://scholar.sun.ac.za



shapes with fixed diameters of 30, 40 and 50 $\mu$m, measuring their steady state $J$, $n_{\mathrm{A}}$, $n_{\mathrm{AL}}$ and $n_{\mathrm{L}}$ under both basal and rapamycin-induced conditions.

Patterns were printed onto coverslips as described in Section 3.5 and glued to 12-well slide plates using silicone elastomer. Once the cells adhered to the printed pattern, they were incubated in culture medium supplemented with 25 nM LysoTracker red to distinguish between autophagosomes, autolysosomes and lysosomes. We measured $J$, $n_{\mathrm{A}}$, $n_{\mathrm{AL}}$ and $n_{\mathrm{L}}$ at 6 h under both control and rapamycin-induced conditions. As before, $J$ was calculated from the initial increase in $n_{\mathrm{A}}$ after the inhibition of fusion between autophagosome and lysosome using 400 nM bafilomycin $\mathrm{A}_1$. Z-stack images were acquired of cells before and after bafilomycin $\mathrm{A}_1$ treatment for both basal and rapamycin treatment groups and the total number of $n_{\mathrm{A}}$, $n_{\mathrm{AL}}$ and $n_{\mathrm{L}}$ was quantified as described in Sections 3.6 and 3.7.

The data showed that not only autophagy intermediates increased with cell size, but that $J$ also increased proportionally to cell size (Fig. 4.17). Therefore, $J$ does not proceed at a fixed rate in cells, but rather in a dynamic fashion in relation to cell size (volume). Determination of rapamycin-induced autophagosome flux ($J_{\mathrm{induced}}$) showed a trend similar to that of basal autophagy, where $J_{\mathrm{induced}}$ increased proportionally with increasing cell size. When considering the relative change in $J$ ($J_{\mathrm{induced}}/J_{\mathrm{basal}}$) we found that smaller cell sizes (30 $\mu$m and 40 $\mu$m) were more sensitive to rapamycin ($\pm$2-fold increase) compared to 50 $\mu$m cell size ($\pm$1.5-fold increase).

Stellenbosch University https://scholar.sun.ac.za



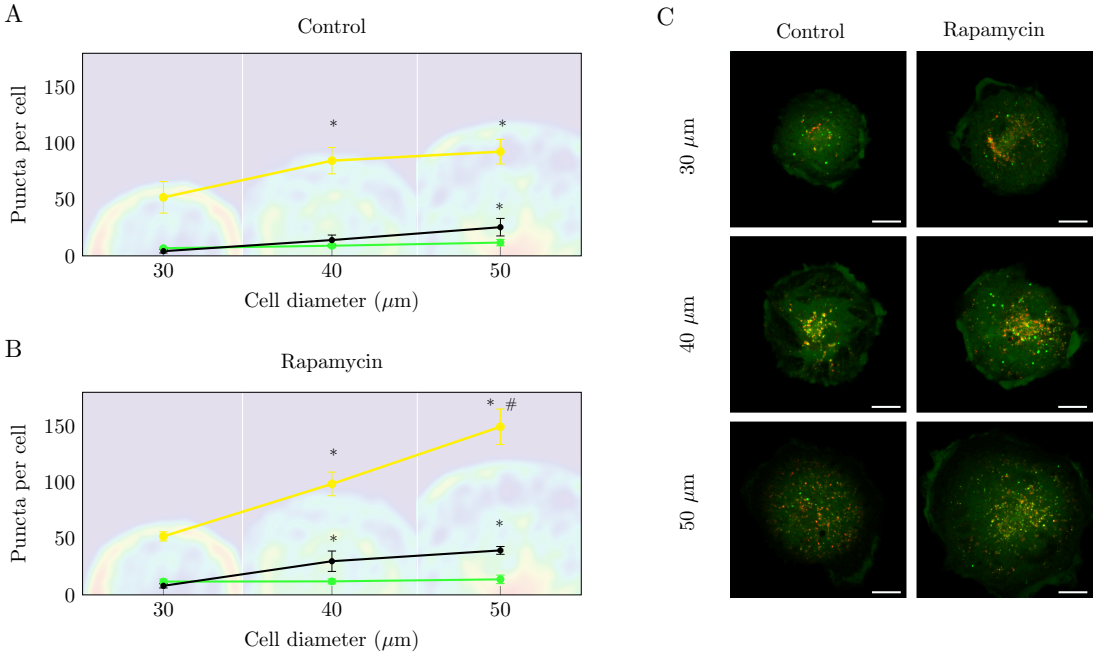


**Figure 4.17:** Cell size-dependent changes in autophagy variables. Autophagosomes (●), autolysosomes (●) and autophagosome flux (—) of MEF GFP-LC3 cells patterned on 30, 40 and 50 $\mu$m diameter disc shapes under basal and rapamycin-induced conditions. (A) Autophagosome flux variables under basal conditions. Density maps of the tubulin network are shown in the background of the respective cell size. (B) Enhanced autophagy after 6 h of treatment with 200 nM rapamycin. (C) Representative images of basal and rapamycin-induced autophagy after 6 h treatment. * vs 30 $\mu$m, $p < 0.05$, # vs 40 $\mu$m, $p < 0.05$.($n = 5$). Scale bar: 10 $\mu$m.

### 4.4.4 Tracking autophagosomes in non-patterned and patterned cells under control and enhanced autophagy conditions

Next we explored how the autophagosome tubulin-associated translocation rate and displacement distance in the cell responded to induction of autophagy as well as to partial inhibition of fusion between autophagosomes and lysosomes. As before, autophagy was induced through both mTOR-dependent and -independent pathways using rapamycin and spermidine respectively, using precision control of $J$ to achieve a similar $J$ with both inducers. A partial inhibition group was

Stellenbosch University https://scholar.sun.ac.za



also included using bafilomycin $A_1$ which had a similar $J$ to that of control (Section 4.2.3).

Live-cell imaging was used to perform tubulin network assessment of autophagosome trafficking behaviour. The tubulin network was visualised with an SiR-Tubulin kit (SpiroChrome, # CY-SC002) (SiR-Tubulin dye and Verapamil), while autophagosomes, autolysosomes and lysosomes were assessed using LysoTracker blue with GFP-LC3 stably expressed in MEF cells. Cells were patterned on coverslips and maintained in culture medium containing 0.1 $\mu$M SiR-Tubulin, 10 $\mu$M Verapamil and 25 nM LysoTracker blue, and treated with 200 nM rapamycin, 20 nM spermidine and 10 nM bafilomycin $A_1$ for 6 h. Raw image series were acquired and the trafficking behaviour of autophagosomes was assessed as described in Sections 3.6 and 3.7.

The autophagosome translocation rate and displacement analysis revealed distinct differences between treatment groups in patterned cells, while non-patterned cells exhibited an irregular profile due to large variation within treatment groups (Fig. 4.19A). Induction of autophagy in non-patterned cells led to significant increases in autophagosome translocation rate upon treatment with spermidine, while it did not change after induction with rapamycin. Autophagosomal displacement showed significant differences between spermidine and bafilomycin $A_1$ treatment groups only in non-patterned cells. On the other hand, patterned cells displayed distinct differences between non-induced (control and bafilomycin $A_1$ group) and induced autophagy (rapamycin and spermidine) treatment groups. To our surprise, we observed a significant decrease in both autophagosome displacement and translocation rate (Fig. 4.19). Further analysis of the tubulin network revealed that autophagosomes consistently associated with tubulin, and were thus actively transported along the tubulin network. These data suggest that an increased $J$, which is accompanied primarily by an increase in autolysosomes, leads to a decrease in autophagosome translocation rate and displacement, potentially as a result of tubulin network crowding effects. Moreover, overall autophagosome size appears to be larger in the rapamycin-treated cells, compared to autophagosomes observed in the other groups (Fig. 4.18), which is in agreement with our earlier

Stellenbosch University https://scholar.sun.ac.za



findings. Assessment of the low versus high velocity transport tracks in patterned and non-patterned cells shows that there are no regional preferences for increased or decreased rate of transport (Fig. 4.19B), suggesting that cell size and tubulin network organisation is unlikely to be involved in the regional translocation rate and displacement behaviour of autophagosomes.

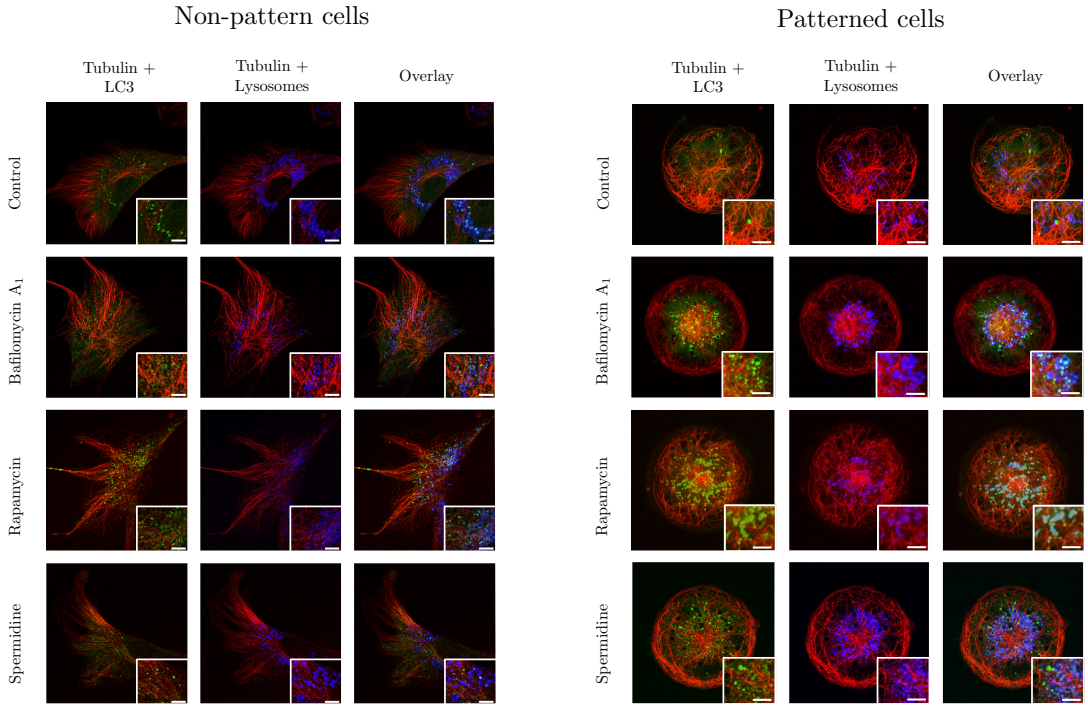


**Figure 4.18:** Representative micrographs of non-patterned and patterned cells showing autophagy pathway intermediates and the tubulin network.

Stellenbosch University https://scholar.sun.ac.za



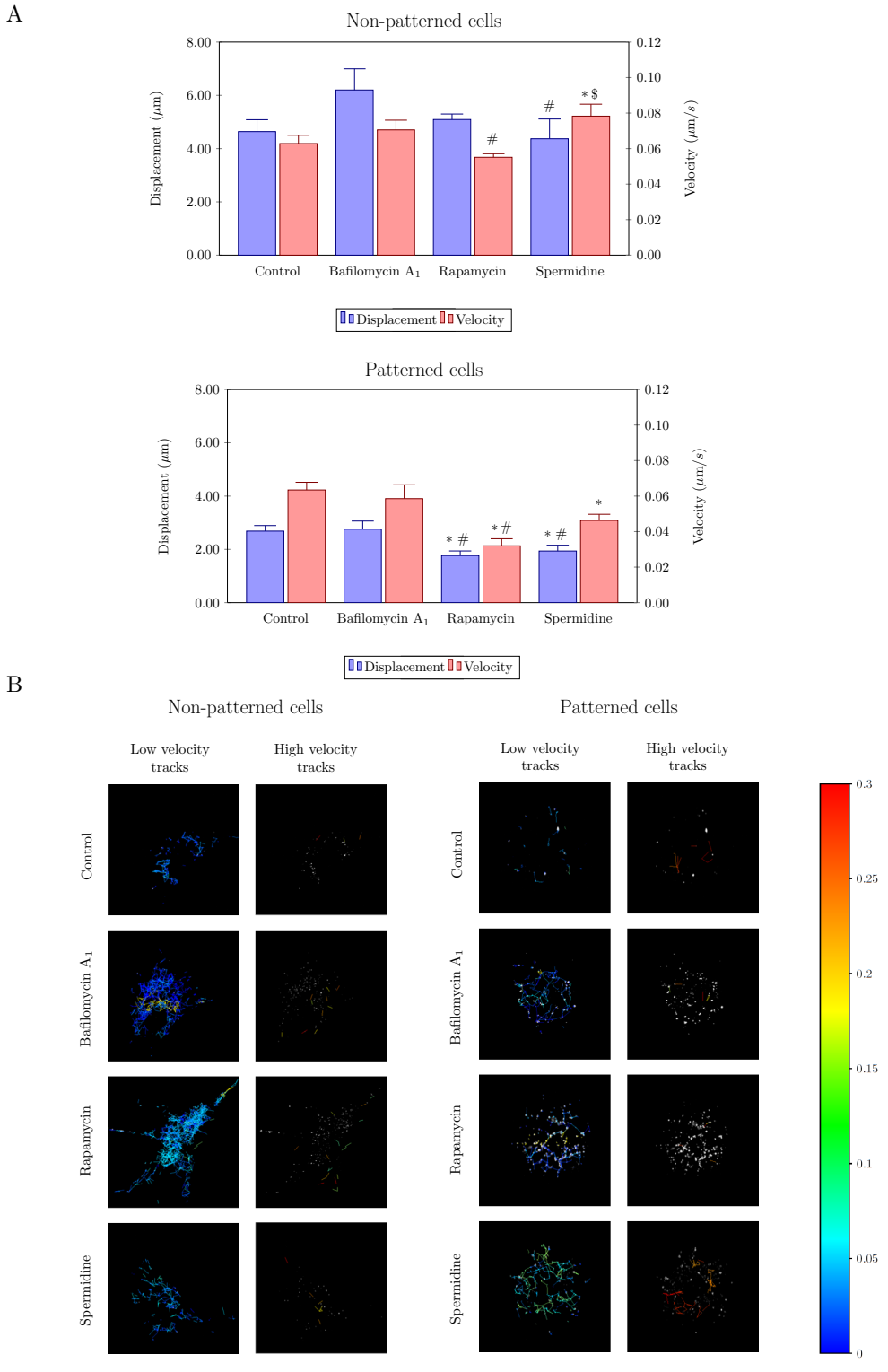


**Figure 4.19:** Changes in translocation rate and displacement of GFP-LC3 positive puncta under basal and induced conditions. (A) Graphs showing the changes in displacement and translocation rate of GFP-LC3 positive puncta after induction through mTOR dependent (200 nM rapamycin) and independent (20 nM spermidine) pathway, and after partial inhibition of fusion between autophagosomes and lysosomes (10 nM bafilomycin $A_1$). (B) Representative micrographs of low and high velocity transport tracks of non-patterned and patterned cells. * vs Control, $p < 0.05$; # vs bafilomycin $A_1$, $p < 0.05$. ($n = 5$).

Stellenbosch University https://scholar.sun.ac.za

# Chapter 5

# Modelling and Supply-Demand Analysis of Autophagy Vesicle Dynamics

This chapter, presented here an article in preparation, describes the experimental procedure to measure the synthesis and turnover of autophagosomes, autolysosomes and lysosomes. The data were used to construct a model of autophagy and to perform supply and demand analysis of autophagosomes. While the minimal model presented here was developed during my MSc-study (Sections 5.4 and 5.5 are directly from my MSc thesis), the supply and demand analysis of autophagosomes and the related experiments described in Section 5.6 form part of the PhD-study.

## 5.1 Abstract

Macroautophagy (autophagy) is an intracellular degradation pathway that is essential for homeostasis and survival during periods of cellular stress and metabolic perturbations. It is a well-orchestrated process that involves the coordination of more than 30 proteins. Abnormalities such as a reduction in the capacity for autophagic degradation or excessive degradation can have deleterious effects on the cell, most evident in human pathologies such as neurodegeneration and cancer. An

Stellenbosch University https://scholar.sun.ac.za



effective strategy for studying complex cellular processes such as autophagy is to build computational models rooted in biological data, that may serve as *in silico* tools to analyse the regulation, control and behaviour of these cellular processes. However, only a few such autophagic models are described in the literature, and even fewer of these are rooted in biological data. Here we present the development of a data-derived kinetic model of autophagic vesicle dynamics that describes the stepwise transition of phagophore to autolysosome in a mammalian system.

We used fluorescence-based microscopy techniques and live cell imaging to measure the synthesis and turnover of autophagosomes, lysosomes and autolysosomes in single cells. Our model provided a close fit to the experimental data and its stepwise construction allowed a deeper understanding of the contribution of each step to the autophagic process. The data also allowed us to perform a supply-demand analysis around autophagosomes, from which the elasticity coefficients of the supply and demand with respect to autophagosomes could be calculated; these results clearly showed that under basal conditions the autophagosome flux is controlled by the supply processes that form autophagosomes.

## 5.2 Introduction

Macroautophagy, referred to hereafter as autophagy, is an evolutionarily conserved process that degrades and recycles cellular components. Autophagy is a tightly regulated process that plays an essential role in cell metabolism and proteostasis, and when deregulated can have deleterious effects on the cell. Autophagy, in particular its deregulation, has been implicated in several diseases, which has made autophagy an attractive therapeutic target. However, the effective and precise modulation of such a complex process remains a challenge, especially since the dynamics of autophagy has proved to be difficult to study experimentally. In order to be able to modulate autophagy we need to understand how the different steps in the autophagic pathway contribute to its behaviour.

Computational modelling is a powerful tool for studying complex systems such as autophagy. The goal of computational modelling is to simulate the behaviour

Stellenbosch University https://scholar.sun.ac.za



of the system based on the known properties of the system components, so as to analyse the regulation, control and behaviour of reaction networks that underlie cellular processes. A successful computational model can provide valuable insight and serve as a complement to experimental studies. There are only a few computational models of autophagy in the literature that model unique aspects of the autophagic process such as vesicle dynamics, regulatory pathways and crosstalk between autophagy and apoptosis. The major problem with these models is that they are often based on data obtained with outdated techniques that result in inaccurate or estimated autophagy vesicle counts and flux measurements. We recently described a method to characterise the dynamics of autophagy in terms of its complete steady-state autophagy vesicle pool size, autophagosome flux and transition times for the respective pools [50]. This method addresses the limitations of current techniques, and yields experimental data that allows the construction of a computational model of the dynamics of autophagy.

The autophagic pathway is a series of stepwise transformations of membrane-bound vesicles accompanied by a flow of cytoplasmic material, which is degraded during the process. We previously defined autophagosome flux as the rate of turnover of autophagomes in steady state [168]. This definition of autophagosome flux is similar to that of metabolic flux used in metabolic control analysis studies, where it refers to the rate of turnover of metabolites in steady state [92, 119]. A number of techniques exist are routinely used to measure the autophagic activity, such Western blot analysis, fluorescence and transmission electron microscopy [191]. Although with these techniques it is possible to assess whether or not autophagic activity is occurring, and whether it has increased or decreased, they are not well suited to express the autophagic activity as a rate, which is required to measure autophagosome flux. However, our recently developed method generates the data necessary to characterise and model the autophagic process in terms of its steady state pool size, autophagosome flux and transition time in a single cell [50].

This fluorescence microscopy driven technique measures the autophagosome flux based on the quantitative assessment of the number of autophagosomes, auto-

Stellenbosch University https://scholar.sun.ac.za



lysosomes and lysosomes over time. Inhibiting the fusion of autophagosomes and lysosomes with bafilomycin $A_1$ at steady state and measuring the initial rate of accumulation of autophagosomes allows the steady-state autophagosome flux to be calculated. In addition to quantifying the autophagosome flux, this method also quantifies the time-dependent behaviour of the autophagy system during the transition period in which a steady state is established. Here we describe the development of a data-driven kinetic model that simulates the time-course behaviour of the autophagic vesicles during the autophagy process. Our plan was to begin with a model of the autophagic process using the simplest possible rate equations, and then, step by step, expand the network scheme and modify the kinetics so as to achieve a good fit to our experimental data. Such an approach allowed us to develop a deeper understanding of the contribution of each part of the autophagic network to its time-dependent behaviour. In the discussion section we will assess and discuss implications of our model and compare its strength with published computer based models and highlight key differences.

## 5.3 Methods and Materials

### 5.3.1 Computer simulations

The kinetic model of autophagy described here is based on the experimental data shown in the Fig. 5.1, data that was obtained in a study described in [50]. The model was developed using PySCeS (the Python Simulator for Cellular Systems [206], a console-based simulation platform written in the Python programming language that makes use of the Scientific Libraries for Python (SciPy) and Numerical Python (NumPy) libraries. These libraries are collections of mathematical algorithms for scientific applications. PySCeS parses an input file and converts it into a model object that can simulate the time-dependent behaviour and calculate the steady-state numbers of the different autophagic vesicles.

Stellenbosch University https://scholar.sun.ac.za



### 5.3.2 Experimental studies

The experimental procedure is based on our recently-described protocol for measuring the autophagosome flux [50]. In short, the protocol is based on a fluorescence microscopy technique with which the changes with time in the number of autophagosomes, autophagolysosomes and lysosomes are quantitatively measured in a single cell. The autophagosome flux is quantified as the rate of increase in the number of autophagosomes after complete inhibition of the fusion of autophagosomes and lysosomes with bafilomycin $A_1$ when the autophagic system is in steady state. The flux was measured in the basal steady-state, in the steady state that obtained after induction of autophagy with rapamycin, and in the steady-state that obtained after partial inhibition with bafilomycin $A_1$. The latter two modulations allowed us to respectively calculate the demand and supply elasticities with respect to the number of autophagosomes.

#### 5.3.2.1 Cell culture

Mouse Embryonic Fibroblast (MEF) cells that stably express GFP light chain 3 (LC3) protein were maintained in Dulbecco's modified Eagle's medium (DMEM) (Life Technologies, #41-965-039), supplemented with 10% fetal bovine serum (Biochrom, #S-0615) and penicillin-streptomycin (Life Technologies, #15-140-122).

#### 5.3.2.2 Chemicals

400 nM Bafilomycin $A_1$ (LKT Laboratories Inc., # B-0025) was used as autophagosome and lysosome fusion inhibitor and 25 nM Rapamycin (Sigma-Aldrich, # R-0395) as autophagy inducer. Lysotracker Red (Thermo Fisher, # L-7528) fluorescence probe was used to identify autophagic vesicles using live cell imaging.

#### 5.3.2.3 Microscopy

Cells were seeded onto CYTOO micro-patterned slides with large fibronectin disc shapes (CYTOO, #10-003-10). Fluorescence microscopy was performed with an

Stellenbosch University https://scholar.sun.ac.za



Olympus IX81 wide-field microscope, suited for live cell imaging, using a 60X oil immersion objective. Image stacks were captured using an automated z-stack and stage control. Autophagic vesicles (autophagosomes, lysosomes, autolysosomes) were measured over time in the presence and absence of Rapamycin (25 nM) and bafilomycin $A_1$ (400 nM).

#### 5.3.2.4 Image Analysis

The image processing and deconvolution was performed using Cell R and images analysed with ImageJ (http://rsbweb.nih.gov/ij/download.html) with a modified WatershedCounting3D plug-in [71] and custom Python script data extraction automation.

## 5.4 Results

Table 5.4 shows the steady-state values of basal and rapamycin-induced autophagic variables as obtained by the experimental measurements described in [50]. Fig. 5.1 shows how autophagic vesicles change over time under basal and rapamycin-induced conditions. The time-course after partial inhibition with bafilomycin $A_1$ is shown in Fig. 5.4.

**Table 5.1:** Functional variables of autophagy for basal and rapamycin (25 nM) induced autophagy in MEF cells (A: autophagosomes; AL: autolysosomes; L: lysosomes). Derived variables are shown in italics.

| **Variable** | Unit | Basal | Induced |
|---|---|---|---|
| Autophagosome flux, $J$ | A/h/cell | 25.4 | 105.4 |
| Number of autophagosomes, $n_{\mathrm{A}}$ | A/cell | 13 | 17 |
| Number of autolysosomes, $n_{\mathrm{AL}}$ | AL/cell | 165 | 251 |
| Number of lysosomes, $n_{\mathrm{L}}$ | L/cell | 1 | 1 |
| *Autophagosomal transition time*, $\tau_{\mathrm{A}}$ | h | 0.53 | 0.16 |
| *Autophagolysosomal transition time*, $\tau_{\mathrm{AL}}$ | h | 6.7 | 2.4 |

Stellenbosch University https://scholar.sun.ac.za



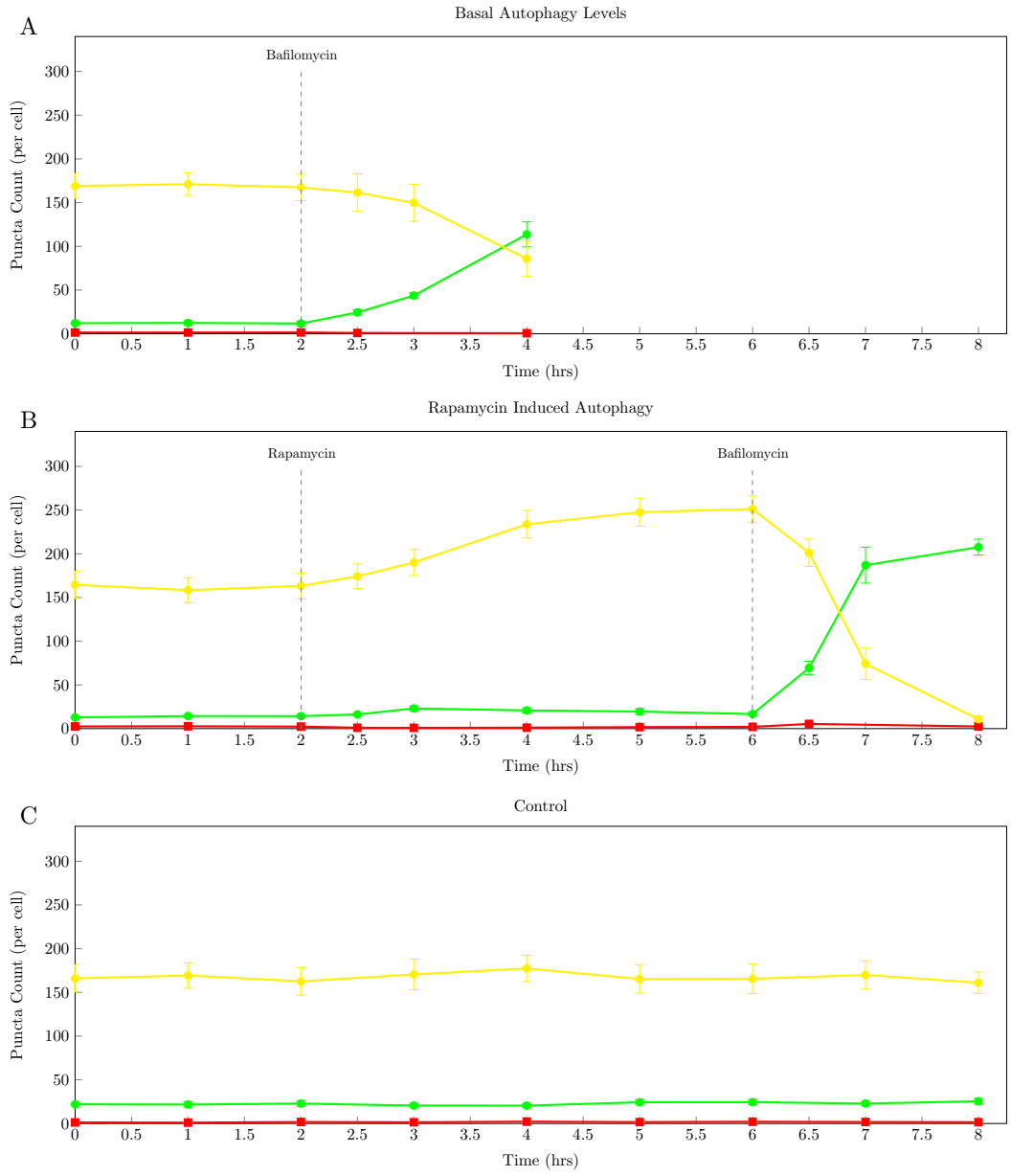


**Figure 5.1:** The changes in autophagosomes (●), autolysosomes (●) and lysosomes (●) over time. (A) Pool sizes of the three autophagic intermediates under basal conditions (0 - 2 h) and after inhibition of fusion with 400 nM bafilomycin $A_1$ at 2 h; (B) Enhanced autophagy after 25 nM rapamycin treatment at 2 h and after inhibition of fusion with 400 nM bafilomycin $A_1$ at 6 h; (C) Control: pool sizes of the three autophagic intermediates under basal conditions (0 - 8 h). (n = 10).

Stellenbosch University https://scholar.sun.ac.za



## 5.5 The kinetic model

Fig. 5.2 shows three representations of the autophagic pathway. The simplest representation (Fig. 5.2A) accounts for the formation of autophagosomes (A), fusion with lysosomes (L) to form autolysosomes (AL), and degradation of autolysosomal cargo to amino acids (AA); this served as our starting point in the modelling process. We subsequently extended this pathway to include the biogenesis and degradation of lysosomes (Fig. 5.2B) and the mTOR/pmTOR system (Fig. 5.2C).

PySCeS input files for the process networks shown in Fig. 5.2 described the stoichiometry and kinetics of the steps in the autophagic pathway (see appendix 5.9). Each step in the autophagic pathway was treated as a reaction of which the reactants are the autophagic intermediate vesicles. All reactions were considered to be irreversible and product-insensitive since it is accepted that autophagosomes cannot convert back to phagophores, and autolysosomes cannot not convert back to autophagosomes and lysosomes. For each reaction a rate equation with mass-action kinetics was defined, and all parameters and intermediates were initialised. The autophagy vesicles were quantified in terms of number of counted puncta in a single cell. The input file also included events that simulate (i) partial or complete inhibition of the fusion of autophagosomes and lysosomes, and (ii) the induction of the autophagic system upon treatment with rapamycin as seen in the experimental data (Fig. 5.1).

We started with a minimal model (Fig. 5.2A) using the simplest possible kinetics to describe the reaction rates. At first all reaction equations were considered to be first-order with respect to all species:

$$\begin{aligned} v_1 &= k_1 \cdot n_{\mathrm{P}} \\ v_2 &= k_2 \cdot n_{\mathrm{A}} \cdot n_{\mathrm{L}} \\ v_3 &= k_3 \cdot n_{\mathrm{AL}} \end{aligned}$$

The ‘concentrations’ in these rate equations are quantified in terms of number of vesicles per cell.

Stellenbosch University https://scholar.sun.ac.za



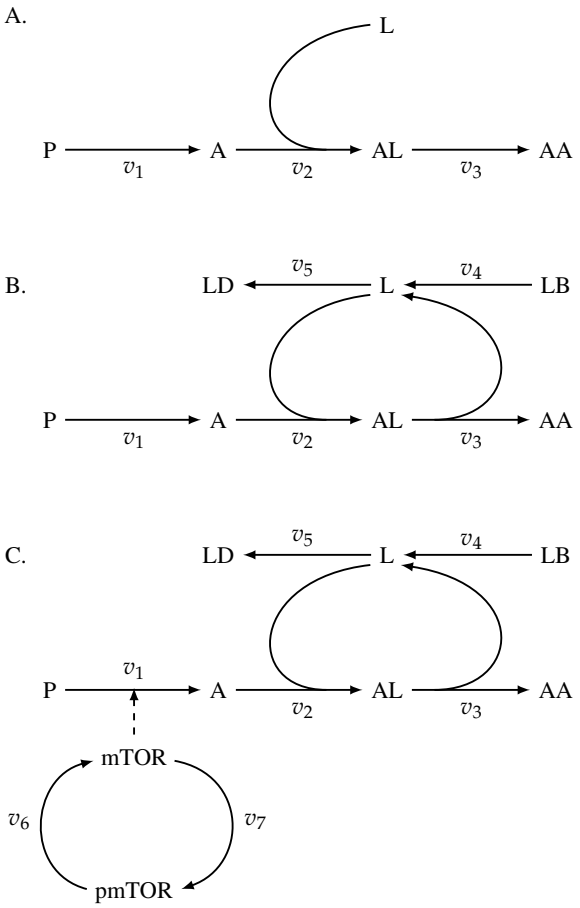


**Figure 5.2:** Network representation of the autophagy process: (A) describes the synthesis of autophagosomes, fusion with lysosomes, the formation of autolysosomes with the subsequent release of amino acids. The number of phagophores $n_{\mathrm{P}}$ and the number of lysosomes $n_{\mathrm{L}}$ are fixed parameters in this model. In (B) the biogenesis and degradation of lysosomes are incorporated, turning $n_{\mathrm{L}}$ into a variable. In (C) the network is extended to include the mTOR/pmTOR cycle, with mTOR incorporated into the rate equation for step 1. P: phagophores, A: autophagosomes, AL: autolysosomes, AA: amino acids, L: lysosomes, LB: lysosome precursor, LD: lysosome degradation product. In the kinetic models of (B) and (C) LB and LD are dummy variables necessary for defining the models.

The experimentally determined basal flux of 25.4 autophagosomes/hour/cell was simulated by setting the kinetic parameters of the rate reactions as follows: $n_{\mathrm{P}} = 1$, $n_{\mathrm{L}} = 1$, $[AA] = 0$, $k_1 = 25.4\ \mathrm{h}^{-1}$, $k_2 = 25.4/13\ \mathrm{n}^{-1}.\mathrm{h}^{-1}$, $k_3 = 25.4/165\ \mathrm{h}^{-1}$. The initial values of $n_{\mathrm{A}}$ and $n_{\mathrm{AL}}$ were set to zero. The reasoning behind the chosen

Stellenbosch University https://scholar.sun.ac.za



parameter values is as follows:

- Since the first step in the pathway was considered to be irreversible and insensitive to downstream events, it completely determines the steady-state autophagosome flux under all conditions. With $n_{\mathrm{P}} = 1$, the initial rate of $v_1$ was set to 25.4 autophagosomes/hour/cell by making $k_1 = 25.4$ h$^{-1}$.

- The rates $v_2$ and $v_3$ were now fixed at 25.4 autophagosomes/hour/cell. This allowed $n_{\mathrm{A}}$ to be set at its experimentally-determined basal steady-state value of 13 by setting $k_2$ to 25.4/13 n$^{-1}$.h$^{-1}$, calculated from $v_2 = 25.4 = k_2(13)(1)$.

- Similarly, to set $n_{\mathrm{AL}}$ to its experimentally-determined basal steady-state value of 165, $k_3$ was set to 25.4/165 h$^{-1}$, calculated from $v_3 = 25.4 = k_3(165)(1)$.

The time-dependent behaviour of the system was simulated with PySCeS using the above parameters. The *inhibition of fusion* between autophagosomes (A) and lysosomes (L) by bafilomycin $A_1$ was simulated by creating an event that set $k_2$ to zero at 2 h. Fig. 5.3 A shows the simulated data of basal conditions and indicates a good fit to the experimental data up to 30 min after bafilomycin $A_1$ treatment. After that there are unknown processes that change the rates of autophagosome formation and autophagosome degradation which our model (and all the extensions discussed below) could not account for.

After *induction of autophagy* by rapamycin a new experimental steady-state autophagosome flux of 105.4 autophagosomes/hour/cell was established. This was simulated by increasing the value of $n_{\mathrm{P}}$ from 1 to 105.4/25.4 at $t = 2$ h (calculated from $v_1 = k_1 \cdot n_{\mathrm{P}} = (25.4)(105.4/25.4)$). As above, the inhibition of fusion by bafilomycin $A_1$ was simulated by setting $k_2$ to zero at $t = 6$ h. Fig. 5.3 B shows how the rapamycin-induced simulated curves compare to the experimental data. Although the new steady-state autophagosome flux was by design a perfect fit (the slopes following inhibition of fusion were equal for both simulated and experimental data), the steady-state values for $n_{\mathrm{A}}$ and $n_{\mathrm{AL}}$ were higher than the experimental

Stellenbosch University https://scholar.sun.ac.za



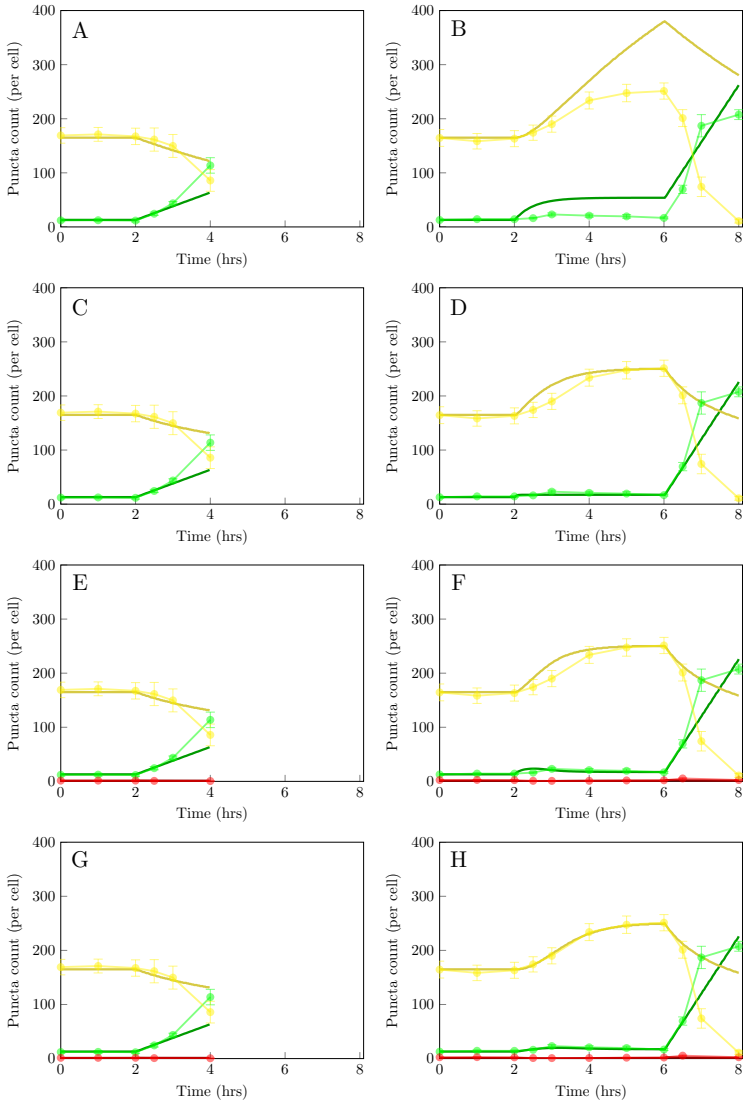


**Figure 5.3:** Overlaying the simulation curves on experimental data. Left-hand graphs show the determination of basal flux; right-hand graphs show the determinations of induced flux. (A,B) the minimal model of autophagy in Fig. 5.2 A with first-order rate equations; (C,D) the minimal model of autophagy in Fig. 5.2 A with higher-order rate equations; (E,F) the minimal model expanded to include lysosomal formation and degradation (Fig. 5.2 B); (G,H) further addition of the mTOR/pmTOR system (Fig. 5.2 C). The autophagosomal (–), autolysosomal, (–), and lysosomal (–) simulated behaviour, superimposed on experimental data (Fig. 5.1).

values: $n_{\mathrm{A}} = 54$ instead of 17, $n_{\mathrm{AL}} = 385$ instead of 251. The only way to lower these values without affecting the basal and induced flux was by adjusting the

Stellenbosch University https://scholar.sun.ac.za



kinetic orders of $n_{\mathrm{A}}$ and $n_{\mathrm{AL}}$ in the rate equations for $v_2$ and $v_3$ respectively. We therefore introduced terms for these kinetic orders in our rate equations as follows:

$$\begin{aligned} v_1 &= k_1 \cdot n_{\mathrm{P}} \\ v_2 &= k_2 \cdot n_{\mathrm{A}}^{h2} \cdot n_{\mathrm{L}} \\ v_3 &= k_3 \cdot n_{\mathrm{AL}}^{h3} \end{aligned}$$

These modifications to our equations of course required us to recalculate $k_2$ and $k_3$ as $k_2 = 25.4/13^{h_2}$ and $k_2 = 25.4/165^{h_3}$. By trial and error we settled on the values of $h_2 = 5$ and $h_3 = 3.4$, which lowered $n_{\mathrm{A}}$ and $n_{\mathrm{AL}}$ to the required values of 17 and 251 respectively. These modifications to our minimal model brought the simulation very close to the experimental profile (Fig. 5.3D). Although the effect on the simulation of basal autophagosome flux was negligible (compare Fig. 5.3C to Fig. 5.3A), the decrease in $n_{\mathrm{AL}}$ in the 30 min period after bafilomycin $\mathrm{A}_1$-treatment was slightly better approximated with the incorporation of $h_2$ and $h_3$.

Our simulation still did not match the experimental profile in the two-hour period after induction with rapamycin, during which $n_{\mathrm{A}}$ nearly doubled to 23 autophagosomes/cell and then decreased to its new steady-state value of 17. This initial increase in $n_{\mathrm{A}}$ after induction was accompanied by a slower increase in $n_{\mathrm{AL}}$. The only way to introduce this effect into the simulation was by making the lysosome pool a variable as in the extended scheme in Fig. 5.2B. It was important that not only regeneration of lysosomes in step 3 was included, but also de novo biogenesis and degradation of lysosomes (steps 4 and 5), which allows $n_{\mathrm{L}}$ to vary independently from $n_{\mathrm{AL}}$ (without these steps $n_{\mathrm{L}}$ and $n_{\mathrm{AL}}$ form a moiety-conserved cycle that would have forced their sum to be constant, something that is clearly

Stellenbosch University https://scholar.sun.ac.za



not true in the cell).

$$\begin{aligned} v_1 &= k_1 \cdot n_{\mathrm{P}} \\ v_2 &= k_2 \cdot n_{\mathrm{A}}^{h2} \cdot n_{\mathrm{L}} \\ v_3 &= k_3 \cdot n_{\mathrm{AL}}^{h3} \\ v_4 &= k_4 \cdot n_{\mathrm{LB}} \\ v_5 &= k_5 \cdot n_{\mathrm{L}} \end{aligned}$$

The kinetic properties of steps 4 and 5 had to be set to values that ensured both that $n_{\mathrm{L}}$ returned to a value of 1 in the induced steady state and that the initial increase in $n_{\mathrm{A}}$ after induction (and the concomitant decrease in $n_{\mathrm{L}}$ and slower increase in $n_{\mathrm{AL}}$) occurred during the two hours after induction. The first criterion was satisfied if, at an $n_{\mathrm{LB}}$-value of 1, $k_4 = k_5$. Note that in steady state, $v_1 = v_2 = v_3$, which implies that $v_4 = v_5$ (for $n_{\mathrm{L}}$ to be in steady state), and therefore that $k_4(1) = k_5 n_{\mathrm{L}}$. For $n_{\mathrm{L}}$ to be 1 in steady state, $k_4$ therefore had to equal $k_5$. By trial and error we found that the second criterion was satisfied when $k_4 = k_5 = 80$.

Fig. 5.3F shows that, although we could now simulate the initial overshoot of $n_{\mathrm{A}}$ after induction, it was too fast. This was due to our making the induction event instantaneous, whereas in reality it would be a slower process that depends on the rate of dephosphorylation of pmTOR to mTOR, which is the protein complex that activates autophagy. We therefore incorporated the pmTOR/mTOR cycle into our model (Fig. 5.2C):

$$\begin{aligned} v_1 &= k_1 \cdot n_{\mathrm{P}} \cdot n_{\mathrm{mTOR}} \\ v_2 &= k_2 \cdot n_{\mathrm{A}}^{h2} \cdot n_{\mathrm{L}} \\ v_3 &= k_3 \cdot n_{\mathrm{AL}}^{h3} \\ v_4 &= k_4 \\ v_5 &= k_5 \cdot n_{\mathrm{L}} \\ v_6 &= k_6 \cdot n_{\mathrm{pmTOR}} \\ v_7 &= k_7 \cdot n_{\mathrm{mTOR}} \end{aligned}$$

Stellenbosch University https://scholar.sun.ac.za



In the rate equation for $v_1$ mTOR appears as a reactant, so that the rate of autophagy depends linearly on $n_{\mathrm{mTOR}}$. This served our purpose, but is probably too simple and a more realistic rate equation will be developed in the future.

With $n_{\mathrm{P}} = 1$ and $n_{\mathrm{mTOR}} = 1$ the set $k_1$-value of 25.4 ensured the correct basal autophagosome flux. But, instead of increasing $n_{\mathrm{P}}$ by a factor of 105.4/25.4 to simulate induction, we now had to ensure that $n_{\mathrm{mTOR}}$ increased with time from a value of 1 to 105.4/25.4 (with $n_{\mathrm{P}}$ now reset to its original value of 1.0). The simplest way of ensuring a pre-induction steady-state $n_{\mathrm{mTOR}}$-value of 1 was to set $k_6$ to 1 and $k_7$ to 105.4/25.4, while initialising $n_{\mathrm{mTOR}}$ to 1 and $n_{\mathrm{pmTOR}}$ to 25.4/105.4. With these values $v_6 = v_7$, and the mTOR/pmTOR cycle was in steady state. To simulate induction by rapamycin $n_{\mathrm{mTOR}}$ had to increase from 1 to 105.4/25.4. Because the mTOR/pmTOR cycle is a moiety-conserved cycle, i.e., the sum of $n_{\mathrm{mTOR}}$ and $n_{\mathrm{pmTOR}}$ is constant, switching the $k_7/k_6$ ratio from 105.4/25.4 to 25.4/105.4 would switch $n_{\mathrm{mTOR}}$ and $n_{\mathrm{pmTOR}}$ to 105.4/25.4 and 1 respectively, so that $n_{\mathrm{mTOR}}$ would increase by the required factor of 105.4/25.4. This switch in $k_7/k_6$ was done by multiplying $k_6$ with the factor $(105.4/25.4)^2$.

We now had to also multiply $k_6$ and $k_7$ by the same time-scaling factor to simulate the rate of the induction process itself, i.e., the time taken for $n_{\mathrm{mTOR}}$ to change from 1.0 to 105.4/25.4. A factor of 0.08 (determined by trial and error) gave the desired result. Fig 5.3G and H show that with all these extensions of and modifications to our simple model we now had a near-perfect simulation of our experimental data for both basal and induced autophagy.

## 5.6 Supply and demand analysis of autophagy

The model of autophagy described here is a simple linear pathway of which we defined the first step to be insensitive to downstream intermediates; this forced the control of autophagosome flux in the model to reside in the first step. In reality, autophagy is a complex process that involves the recruitment of more than 30 proteins in a highly organised manner to give rise to the functional units of the autophagy pathway, which in turn are regulated by amino acid availability (the

Stellenbosch University https://scholar.sun.ac.za



end product of the autophagy process) and energy abundance.

In the traditional sense, computational modelling of metabolic processes requires the isolation of all of the enzymes/proteins involved in the pathway experimentally in order to study their kinetic properties separately from one another. However, applying this approach to characterise the enzymes/proteins involved in autophagy process would be impractical (if not impossible) due to the complexity of interactions in assembling autophagosomes, and of the subsequent events such as fusion with lysosomes to form autolysosomes. This is where the supply-demand analysis framework of Hofmeyr and Cornish-Bowden [94] comes into its own in that it does not require information on the kinetics or activity of the enzymes/proteins involved the in the pathway. All that is required is the ability to perturb the activities of the processes that synthesise and degrade a chosen intermediate in a pathway. By reducing the autophagy process to a supply-demand system in which autophagosome synthesis (supply) and autophagosome degradation (demand) are linked by the autophagosome pool, it is possible to determine the control of the supply and demand blocks over the steady-state flux and concentration of autophagosomes by measuring the response of these steady-state variables to small perturbations in the supply and demand. Above we described how to measure steady-state responses to rapamycin induction of autophagy. However, we also needed to determine how the autophagic steady state responded to perturbations of the demand for autophagosomes. This was achieved by partially inhibiting the fusion of autophagosomes with lysosomes, waiting until a new steady-state was established, and then measuring the flux as before by complete inhibition of fusion with bafilomycin $A_1$. Fig. 5.4 shows the experiments with basal conditions and partial inhibitions with 10 nM and 20 nM bafilomycin $A_1$.

Stellenbosch University https://scholar.sun.ac.za



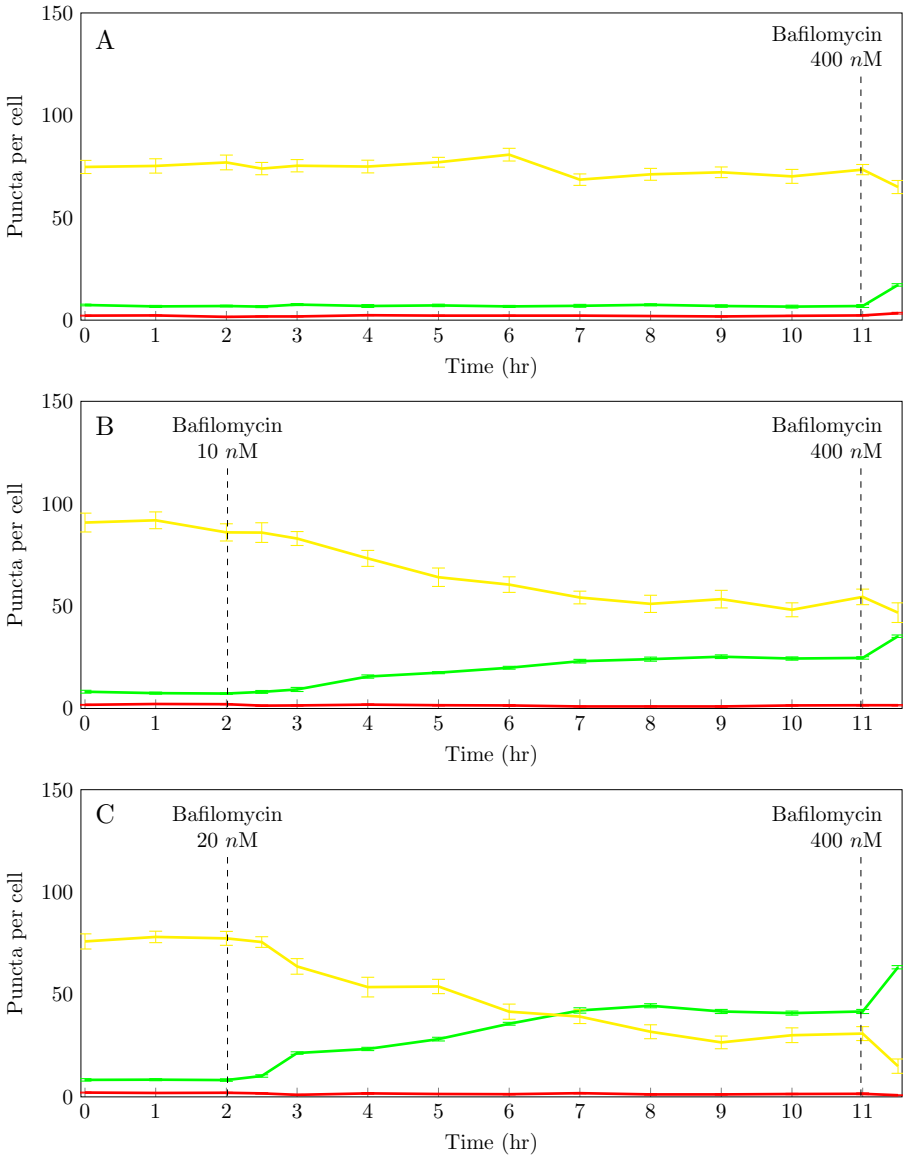


**Figure 5.4:** The transient time-dependent changes in autophagosomes (●), autolysosomes (●) and lysosomes (●). (A) Pool sizes of the three autophagic intermediates under basal conditions (0–11 h) and after inhibition of fusion with 400 nM bafilomycin $A_1$ at 11 h; (B,C) Partial inhibition of autophagosome/lysosome fusion with 10 nM and 20 nM bafilomycin $A_1$ treatment at 2 h and after inhibition of fusion with 400 nM bafilomycin $A_1$ at 11 h. (n = 40).

Fig. 5.5 shows the so-called co-responses [93] of the steady-state autophago-

Stellenbosch University https://scholar.sun.ac.za



some flux and autophagosome pool size as measured by fluorescence microscopy in response to perturbation of the supply and demand of autophagosomes. The slopes of the tangents to the supply and demand rate characteristics at the steady-state point (Fig. 5.5) are equal to the so-called supply and demand elasticity coefficients. An elasticity coefficient quantifies the sensitivity of a rate $v$ to a perturbation a variable $x$ that directly affects this rate, and is mathematically defined as

$$\varepsilon_x^v = \frac{\partial \ln v}{\partial \ln x} \tag{5.1}$$

The perturbation of the autophagosome supply by rapamycin allows the calculation of the demand elasticity from the concomitant co-response of autophagosome flux and autophagosome pool size; similarly, the perturbation in the autophagosome demand by bafilomycin $A_1$ allows the calculation of the demand elasticity.

From the values of the supply and demand elasticities the flux- and concentration-control coefficients can be calculated. A control coefficient quantifies the sensitivity of a steady-state variable such as a flux or concentration with respect to a perturbation is the activity of a step in the system, and is mathematically defined as:

$$C_{v_i}^X = \frac{\partial \ln X}{\partial \ln v_i} \tag{5.2}$$

where $X$ is a flux $J$ or a concentration, here $n_{\mathrm{A}}$.

The flux-control coefficients can be expressed in terms of supply and demand elasticities [94], and calculated as follows:

$$\begin{aligned} C_{v_{\mathrm{supply}}}^J &= \frac{\varepsilon_{n_{\mathrm{A}}}^{v_{\mathrm{supply}}}}{\varepsilon_{n_{\mathrm{A}}}^{v_{\mathrm{demand}}} - \varepsilon_{n_{\mathrm{A}}}^{v_{\mathrm{supply}}}} = \frac{1,15}{1,15-0} = 1 \\ C_{v_{\mathrm{demand}}}^J &= \frac{\varepsilon_{n_A}^{v_{\mathrm{demand}}}}{\varepsilon_{n_{\mathrm{A}}}^{v_{\mathrm{demand}}} - \varepsilon_{n_{\mathrm{A}}}^{v_{\mathrm{supply}}}} = \frac{0}{1,15-0} = 0 \end{aligned}$$

The concentration-control coefficients can also be expressed in terms of supply and demand elasticities [94], and calculated as follows:

$$\begin{aligned} C_{v_{\mathrm{supply}}}^{n_{\mathrm{A}}} &= \frac{1}{\varepsilon_{n_{\mathrm{A}}}^{v_{\mathrm{demand}}} - \varepsilon_{n_{\mathrm{A}}}^{v_{\mathrm{supply}}}} = \frac{1}{1,15-0} = 0.87 \\ C_{v_{\mathrm{demand}}}^{n_{\mathrm{A}}} &= \frac{-1}{\varepsilon_{n_{\mathrm{A}}}^{v_{\mathrm{demand}}} - \varepsilon_{n_{\mathrm{A}}}^{v_{\mathrm{supply}}}} = \frac{-1}{1,15-0} = -0.87 \end{aligned}$$

Stellenbosch University https://scholar.sun.ac.za



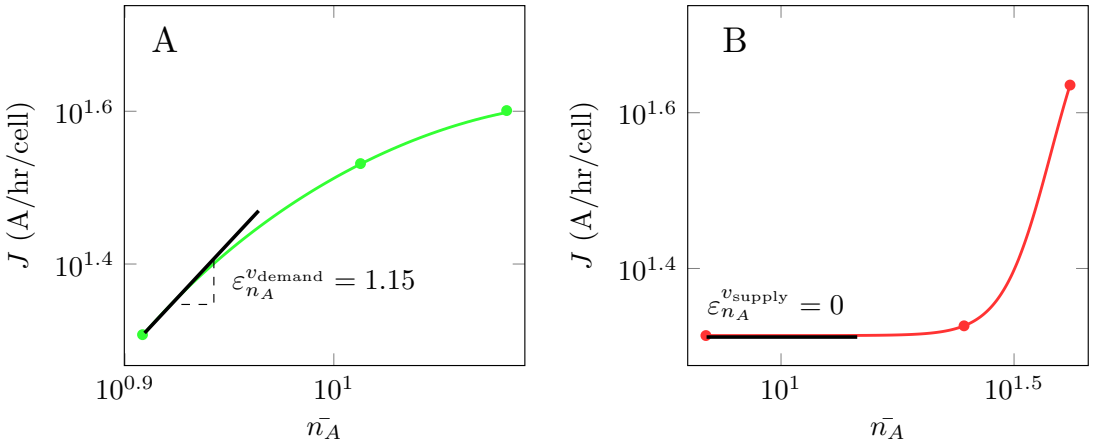


**Figure 5.5:** Co-response of the steady-state autophagosome flux and autophagosome pool size in response to perturbation of the supply and demand of autophagosome. (A) Log-log demand rate characteristic determined by increasing the supply of autophagosomes with rapamycin; (B) Log-log supply rate characteristic determined by perturbing the demand of autophagosomes with bafilomycin $A_1$. The slopes of the tangents to the supply (–) and demand (–) rate characteristics at the steady-state point are the elasticities of the supply and demand rates with respect to autophagosomes. (n = 40).

From the calculated flux-control coefficients one can see that flux through the autophagy pathway is, in agreement with our model, completely determined by the autophagosome supply. The distribution of flux and concentration control around the steady state can be visualised by plotting the intersection of the supply and demand co-responses in Fig. 5.5 in logarithmic space, as shown in Fig. 5.6. These curves are also known as log-log rate characteristics. Comparing equal fold-changes in the supply and demand clearly shows that flux control resides in the supply of autophagosomes, while the regulation of autophagosome number resides in the demand. The steepness of the slope of the demand (here $-1.15$) determines the degree of homeostatic regulation of autophagosome number, since the steeper the slope of the demand rate characteristic, the narrower the magnitude of variation in autophagosome number, and the better the homeostatic maintenance of autophagosomes.

Stellenbosch University https://scholar.sun.ac.za



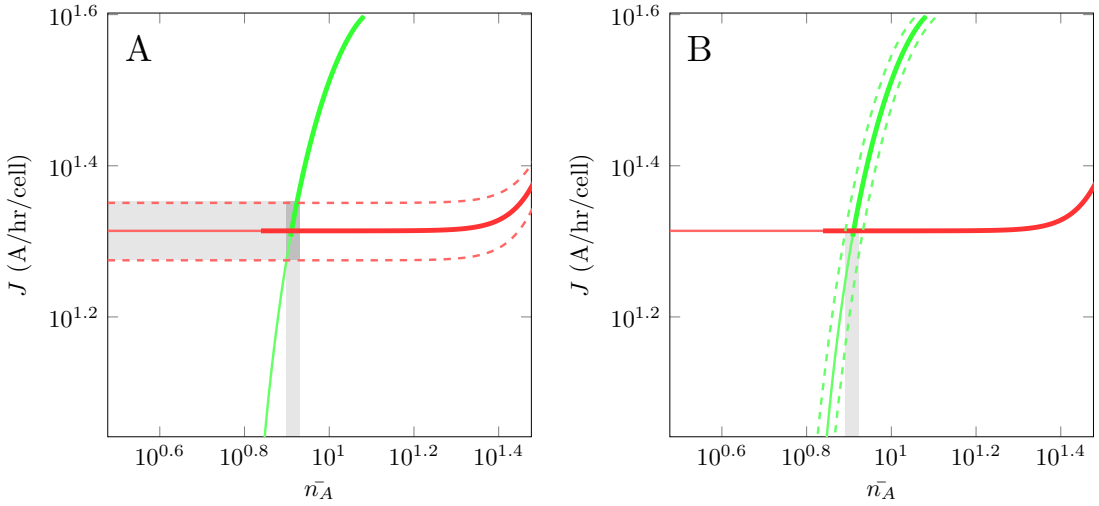


**Figure 5.6:** The rate characteristics of a supply–demand system plotted in log-log space, showing the steady state where the supply (–) and demand (–) rate characteristics intersect; $J$ is the steady-state autophagosome flux, and $\bar{n_{\mathrm{A}}}$ is the steady-state autophagosome concentration. The thick lines are the experimental curves from Fig. 5.5, while the thin lines are hypothetical extrapolations. The dotted lines show a fixed percentage increase or decrease in supply (A) and demand (B) of autophagosomes. The shaded regions show the magnitude of the responses in $J$ and $\bar{n_{\mathrm{A}}}$.

## 5.7 Discussion

The autophagy process is characterised by the formation and degradation of autophagic vesicles in the cytoplasm. It is an essential process that maintains cellular integrity and proteostasis by lysosome-mediated degradation of damaged proteins and organelles. Thus, deregulation of autophagy can result in a variety of pathological conditions. Although the regulation and the molecular machinery of the autophagy pathway is increasingly understood, the control of the pathway activity remains challenging. Why is this important? An increasing number of studies have produced promising results with regard to treating neurodegenerative diseases through modulation of autophagy [224]. But, to finely manipulate the autophagic process for therapeutic purposes, we need to know which processes control the autophagosome flux, and a computational model of autophagy can assist in developing effective manipulation strategies.

Stellenbosch University https://scholar.sun.ac.za



A well-defined model of the autophagic system needs to be rooted in experimental data that not only reflects steady-state characteristics, but also the dynamic nature of the autophagic system when it is in transit between steady states. This requires the continuous assessment of the autophagic process in live cells, and should quantitatively distinguish between the pool sizes of the different autophagic vesicles. Our fluorescence microscopy method allows the characterization of the autophagic system in terms of (i) the steady state pool size of the various autophagic intermediates ($n_{\mathrm{A}}$, $n_{\mathrm{AL}}$ and $n_{\mathrm{L}}$), (ii) the autophagosome flux, $J$, and (iii) the transition time, $\tau$, for the respective autophagic vesicle pools ($\tau_{\mathrm{A}}$ and $\tau_{\mathrm{AL}}$). The experimentally-determined time-dependent behaviour of these autophagic variables provided a strong foundation for the construction of the computational model of autophagy described above. Although at this stage it is only a minimal model, it already reflects more accurately the dynamics of autophagy as compared to other models in literature

There are a few studies in the literature that describe computer models and simulations of various aspects of the autophagic system. Choi and co-workers [78–81] developed several comprehensive models of the autophagic system with the aim to unravel the underlying mechanism of autophagy and its role in disease pathologies. These models were used to investigate various aspects of autophagy, such as its basic dynamics and oscillatory behaviour, its involvement in the transition from cell death to life, and its role in cellular quality control. Although these models provide the opportunity to investigate the relationship between autophagy activity and the corresponding cellular changes, they do not satisfactorily provide a quantitative account of the dynamic nature of autophagy generally observed in experiments. These models are often based on a theoretical framework and parameterised with data derived from isotopic labelling techniques from the late 1980's and onwards. Although stable isotope labelling is an effective tool for flux analysis and provides a solid base for a computational modelling, it is less suited for the autophagic pathway as it reveals little about how the autophagic variables, such as autophagosome flux and pool sizes of autophagic vesicles, depend on network parameters.

Stellenbosch University https://scholar.sun.ac.za



Recently, Brady and co-workers [22] and MacKeigan and co-workers [175] made use of fluorescence microscopy to measure the synthesis and turnover of autophagic vesicles over time in a single cell in the presence and absence of an autophagic inducer and inhibitor. Brady *et al.* focused their model on the dynamic interaction of the vesicles themselves: fusion of autophagosomes with either lysosomes or autolysosomes, autolysosomes fusing with autolysosomes or lysosomes, etc. MacKeigan *et al.* investigated a model centred around the reactions required for the isolation of the membrane for the formation of autophagic vesicles, including some of the regulatory processes governing the formation of phagophores and how they affect autophagic vesicle dynamics. Although these studies distinguished themselves from other studies in the literature in that they model the dynamic nature of the autophagic vesicles, certain factors were not considered. First, they did not confirm that the autophagic system was at a steady state prior to measuring flux. At steady state the rate of autophagosome synthesis equals the rate of its degradation, and the rate of autolysosome synthesis equals the rate of its degradation; the autophagosome flux therefore equals any of the individual rates. If the number of autophagosomes/autolysosomes per cell remains constant, the system is in steady state. Fluctuations in the autophagosome/autolysosome number over time indicate that the system is not in a steady state, but rather in a transition phase between steady states. Measuring the rate of autophagosome synthesis during the transition phase will not represent the flux. Second, these studies did not accurately distinguish between the different autophagic vesicles, and could therefore not quantify their respective pool sizes. It is generally assumed that GFP-LC3-II puncta/dots indicate autophagosomes, but it is becoming ever more evident that GFP-LC3-II puncta do not represent autophagosomes only. Newly formed autolysosomes are still able to emit green fluorescence as the GFP is not immediately quenched. These factors all influence the accuracy of characterizing autophagic variables and the concomitant computational model derived from the data.

The advantage of starting with a minimal model and then, step by step, expanding the network scheme and modifying the kinetics, allowed us a greater understanding of the role that each part plays in the autophagic model. One such

Stellenbosch University https://scholar.sun.ac.za



aspect that we need to address is the use of variable kinetic orders in the rate equations for the formation and degradation of autolysosomes in order to achieve our experimentally autophagosome and autolysosome steady state values. This suggests that processes are influenced by other factors. One can only speculate at this point what these factors could represent. For instance, step 2 represents the fusion of autophagosomes with lysosomes which requires a multitude of factors such as those processes that are associated with the translocation of vesicles, tethering proteins, microtubules [181] and dynein motors [58], and a number of fusion proteins [280]. The incorporation of such factors in the model and simulations would be of great interest since they have been suggested to form part of the pathogenesis of diseases [109, 134, 143, 181, 203, 217]. The here described model could form a platform for the inclusion of such data.

The PySCeS metabolic control analysis module can be used to calculate the control and elasticity coefficients of a steady state. However, our kinetic model of autophagy does not allow us to draw confident conclusions about the control of autophagosome flux and concentrations of autophagic vesicles, since we defined the first step to be insensitive to downstream intermediates which automatically confers flux control to the first step in the scheme. However, the experimental supply and demand analysis allowed us to determine the elasticities of supply and demand rate with respect to autophagosomes and calculate the flux and concentration control coefficients without needing any enzymes/proteins to be isolated and characterised, and regardless of feedback mechanisms (for instance amino acid feedback on mTOR) and moiety conservation (autolysosomes and lysosomes pool). By plotting the rate characteristics together we could visualise the distribution of flux and concentration control around the steady state, providing insight about system behaviour around the steady state, and showing that in our experimental system the supply of autophagosomes controls the flux.

Although the kinetic model presented here is a simplification of the autophagy process, it still provided an excellent fit to the experimental data. It will serve as a good starting point for future work, where we plan not only to validate the kinetic model with experimental data of autophagy other than that what was used

Stellenbosch University https://scholar.sun.ac.za



here to parameterise our model, but also to expand the model by including other autophagy regulators such as amino acid feedback, as well as the factors that are involved with the translocation of the autophagic vesicles, namely microtubules and dynein motors. Such an expanded model could serve as a starting point for understanding autophagy in different cell types in healthy and diseased states.

## 5.8 Acknowledgements

The authors acknowledge financial support from the South African National Research Foundation (NRF), the Medical Research Council (MRC) and the Cancer Association South Africa (CANSA). Any opinion, findings, and conclusions or recommendations expressed in this material are those of the authors, and therefore the NRF, MRC and CANSA does not accept any liability in regard thereto.

## 5.9 PySCeS-input files

### 5.9.1 Minimal model of autophagy

```
# Autophagy model

#           L
#           |
# P ---> A ---> AL ---> AA

# P:  phagophores
# A:  autophagosomes
# L:  lysosomes
# AL: autolysosomes

FIX: P L AA

R1: P = A         k1*P

R2: A + L = AL    k2*(A**h2)*L

R3: AL = AA       k3*AL**h3

#Init
```

Stellenbosch University https://scholar.sun.ac.za



```
P  = 1.0
AA = 0.0
L  = 1.0

#InitPar
h2 = 5.0
h3 = 3.4
k1 = 25.4
k2 = 25.4/(13.0**5.0)
k3 = 25.4/(165.0**3.4)

#InitVar
A  = 13.0
AL = 165.0

# Event 1 - Simulating Rapamycin Induction
Event: Induction, _TIME_ > 2, 0 {P = 105.4/25.4}
# Event 2 - Simulating Inhibiton with Bafilomycin A1
Event: Inhibition, _TIME_ > 6, 0 {k2 = 0.0}
```

### 5.9.2 Extended model of autophagy

```
# Extended autophagy model

#            LD <----  L <---- LB
#                 |        |
#       P  ---> A ---> AL ---> AA
#           ^
#        -> T  -
#       |       |
#        - pT <-

# P:  supply of autophagosomes which is controlled by T/pT
# A:  autophagosomes
# L:  lysosomes
# AL: autolysosomes
# AA: amino acids
# pT: phosphorylated mTOR
# T:  mTOR
# LD: lysosome degradation
# LB: lysosome biosynthesis

FIX: P AA LB LD
```

Stellenbosch University https://scholar.sun.ac.za



```
R1: P = A          k1*P*T

R2: A + L = AL     k2*L*A**h2

R3: AL = AA + L    k3*AL**h3

R4: LB = L         k4*LB

R5: L = LD         k5* L

R6: pT = T         k6*pT

R7: T = pT         k7*T

#Init
P  = 1.0
LB = 1.0
D  = 0.0
LD = 0.0
AA = 0.0

#InitPar
h2 = 5.0
h3 = 3.4
k1 = 25.4
k2 = 25.4/(13.0**5.0)
k3 = 25.4/(165.0**3.4)
k4 = 80.0
k5 = 80.0
k6 = 0.08*1.0
k7 = 0.08*(105.4/25.4)

#InitVar
A  = 13.0
AL = 165.0
L  = 1.0
pT = 105.4/25.4
T  = 1.0

# Event 1 - Simulating Rapamycin Induction
Event: Induction, _TIME_ > 2, 0 {k6 = 0.08*(105.4/25.4)*(105.4/25.4)}
# Event 2 - Simulating Inhibition with Bafilomycin A1
Event: Inhibition, _TIME_ > 6, 0 {k2 = 0.0}
```

Stellenbosch University https://scholar.sun.ac.za

# Chapter 6

# Measuring autophagy *ex vivo* at organ level

It is well known that autophagy occurs in all cells and tissues of the mammalian system, that it proceeds at different rates and responds differently when induced, such as during periods of nutrient starvation [189]. Although western blot analysis of isolated tissue provides valuable information on autophagy proteins, it reveals little about cell specific distribution. The interrogation of tissue with light and specific fluorescent labels has become an increasingly attractive and powerful research tool to better understand and assess autophagy. Harvesting and sectioning of tissue limits the interrogation of autophagy to a single plane. To fully understand the role of autophagy on tissue physiology and its role in disease progression, it is important to characterise the distribution of autophagy not only in a cell specific manner but also in the context of an entire organ.

The CLARITY technique makes tissues transparent and so enhances the study of neuronal circuits by improving deep tissue imaging of whole brain samples [37]. In this part of the study, as proof of concept to achieve single cell resolution of autophagy pathway intermediates, we aimed to clear brain tissue and perform immunofluorescence on autophagy-related proteins, with the emphasis on generating 3D-data to characterise autophagy in the brain. In doing so, we also aimed to develop an economical and effective approach to clearing multiple brain sam-

Stellenbosch University https://scholar.sun.ac.za



ples concomitantly within a reasonable amount of time using limited reagents and clearing solution. The goal was to use readily available materials in a common laboratory setting in combination with the 3D-printing of specifically designed components suitable for rodent brain tissue processing.

## 6.1 CLARITY

CLARITY is a technique that embeds proteins and nucleic acids into a hydrogel matrix, allowing for removal of light scattering lipids using detergents (Fig. 6.1). The first step involves infusion of the brain tissue with a paraformaldehyde and acrylamide mixture which captures proteins and DNA in their native form. Paraformaldehyde facilitates the attachment of proteins and DNA to acrylamide and is necessary to establish linkages between the cellular components and the acrylamide monomer which is then polymerized into a gel. While cellular components are held firmly in place, lipids can be washed from the gel with an ionic detergent through passive diffusion or actively using electrophoretic methods [37]. Both passive and active clearing methods rely on lipid-collecting sodium dodecyl sulphate (SDS) micelles to diffuse into the tissue and remove the lipids, rendering it transparent. Passive clearing, as the name suggests, relies on passive diffusion of the SDS micelles into the hydrogel-embedded tissue by incubating it in clearing solution until it becomes transparent. Electrophoretic tissue clearing takes advantage of the ionic charge on the SDS, which actively draws the ionic SDS micelles through hydrogel-embedded tissue for faster clearing using an electric field. The lipophilic properties of micelles which form in the detergent solution clears the hydrogel-embedded tissue by picking up lipids as they pass through the gel leaving the majority of non-lipid components unaffected. The removal of light scattering lipids makes the hydrogel-embedded tissue transparent while cellular components retain original spatial position.

As part of our aim to characterise autophagy, we set out to design and 3D print passive and active clearing stations for tissue processing.

Stellenbosch University https://scholar.sun.ac.za



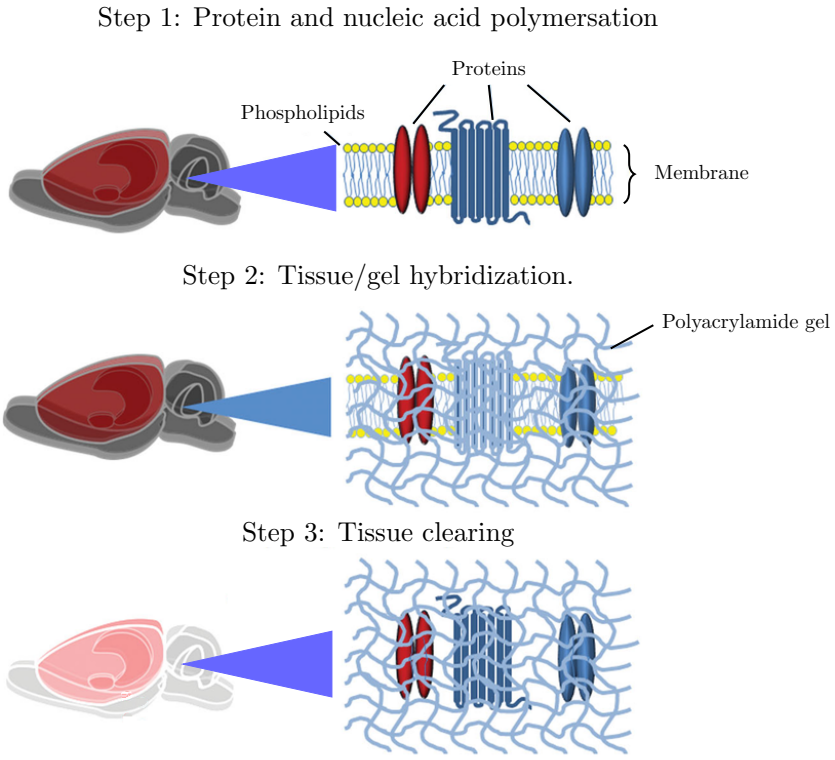


**Figure 6.1:** A schematic representation of the clearing process of brain tissue using CLARITY. (Step 1) The tissue is infused with a paraformaldehyde and acrylamide mixture, capturing proteins and nucleic acids. (Step 2) The polymerisation of the mixture forms a matrix wherein proteins and nucleic acids are embedded. (Step 3) Lipids are removed from the gel using detergents, rendering the brain transparent. Adapted from Rojczyk-Golebiewska *et al.* [223].

## 6.2 Tissue processing and imaging

In this section, we describe the protocol for infusing hydrogel into brain tissue and clearing it using a self-designed passive and active clearing station. Our goal was to first clear whole brain tissue and assess the achievable resolution, i.e., identify autophagosomes and lysosomes using fluorescence dyes. Our second goal was to perform immunostaining on brain slices in order to visualise autophagy-related proteins. The reason for using brain slices is to overcome the inherent challenges of antibody penetration into the hydrogel-embedded tissue. Therefore, brain tissue

Stellenbosch University https://scholar.sun.ac.za



was sectioned into 1 mm slices to achieve a more uniform immunofluorescence staining. From the data we could then infer whether or not it was possible to assess autophagy intermediates in the brain and form a global picture of their distribution, and also identify potential pitfalls of this approach.

**Hydrogel preparation and tissue embedding.** The hydrogel solution (4% Acrylamide (Sigma, # 01697), 0.25% Thermal initiator VA-044 (Wako-chem, # 27776-21-2), 4% paraformaldehyde (Sigma, # P6148) in PBS, adjusted to pH 7.6) was prepared freshly on the day of tissue harvesting. Thermal initiator VA-044 acted as the source of free radicals for the polymerisation of the hydrogel. At low temperature (4°C) the initiator is inert, allowing for the hydrogel monomers to infuse uniformly into the tissue during incubation. At higher temperatures (>30°C) the initiator molecule decomposes and generates free radicals which initiate polymerization of the acrylamide monomer.

For this study GFP-LC3 transgenic mice were used. Ethical approval was granted through the Division of Research and Development at Stellenbosch University (SUACUD15-00023). GFP-LC3 transgenic mice were housed at room temperature with an approximate humidity of about 50% and a 12 hr light/dark cycle. GFP-LC3 transgenic mice were culled by cervical dislocation and perfused briefly with PBS to remove blood cells as much as possible to prevent their incorporation into the hydrogel matrix, since they could act as a source of autofluorescence. Once the brain had been harvested, it was placed in a 50 mL falcon tube containing approximately 15 mL hydrogel solution and incubated for two days at 4°C. Thereafter, isopropanol was added to the brain/hydrogel tube to create an oxygen barrier between the solution and the air. Oxygen acts as a free radical quencher that can inhibit acrylamide polymerization. The tube was placed in a heated bath for three hours at 38°C to allow for the polymerisation of the hydrogel matrix. The brain was then removed, and the excess gel gently removed using tissue paper. Brain tissue was then either sliced into sections or kept whole for clearing. Brain tissue was sliced into 1 mm sections using the brain matrix slicer (Fig. 6.2), which was designed with Blender (https://download.blender.org/release/Blender2.79),

Stellenbosch University https://scholar.sun.ac.za



an open-source 3D computer graphics software toolset. The brain matrix slicer was 3D printed using PLA filament and a MakerBot Replicator Z18 3D Printer.

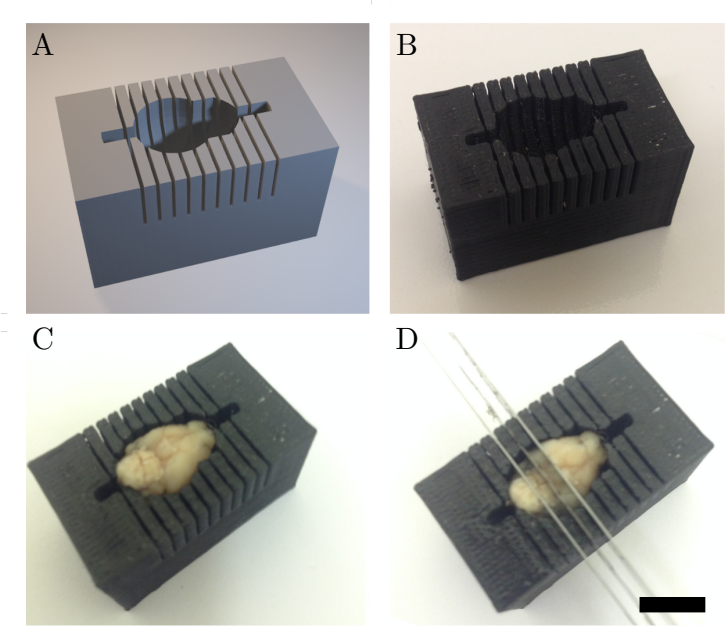


**Figure 6.2:** 3D-printed brain matrix slicer. (A) 3D model of the brain matrix slicer created with Blender. (B) Brain matrix slicer printed with a MakerBot Replicator Z18 3D Printer using PLA filament. (C) Mouse brain fitted in the matrix slicer. (D) Sectioning brain into 2 mm slices using razor blades. Scale bar: 1 cm.

**Passive clearing.** Brain slices and whole brains were cleared passively by placing them in 5 mL falcon tubes containing 40 mL of clearing solution (200 mM Boric acid (Sigma, # B6768), 4% SDS, adjusted to pH 8.5) and incubated in a water bath at 38°C until the tissue becomes transparent. To reduce the time required for passive clearing, brain tissue was placed in a cage that fitted inside the falcon tube which was connected to a reservoir containing 500 mL clearing solution (Fig. 6.3). Clearing solution was continuously circulated through the tube using a pump (AQUA Maxi 104). The cage was printed from PLA filament on a MakerBot Replicator Z18 3D Printer. Mesh was glued to the cage

Stellenbosch University https://scholar.sun.ac.za



and attached to the lid of the falcon tube using a non-toxic silicone elastomer "glue" (AMT, # SM420). Clearing solution pH was monitored daily using pH strips (Sigma, # P4536) and refreshed either weekly or once the pH was below 7, until the tissue became completely transparent. The STL file of the passive clearing cage (Fig. 6.3A) can be found at (https://drive.google.com/open?id=1fP7fnCExLzNlKsbcZH0CH0dqM8ODfzq6).

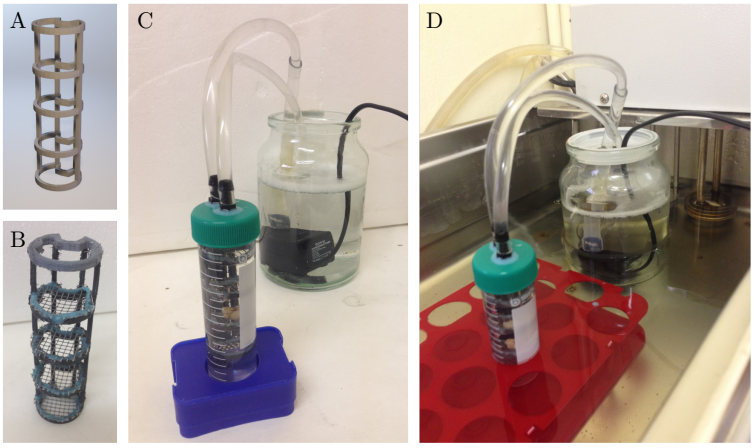


**Figure 6.3:** CLARITY passive clearing system. (A) 3D model of the CLARITY passive clearing tray designed with Blender. (B) CLARITY passive clearing tray printed with MakerBot Replicator Z18 3D Printer using PLA filament. (C) Fully assembled CLARITY passive clearing system. (D) CLARITY passive clearing station in a water bath.

Fig. 6.4 shows the clearing of a brain slice and a whole brain over time using passive clearing. The 1 mm brain slices were transparent after two weeks of incubation in clearing solution. The whole brain required between 1–2 months of incubation in clearing solution to become transparent. Over the time course of passively clearing the tissue it swelled to approximately 1.5 times its original size. This is a common effect of tissue clearing and results from the hydrophilic properties of the gel. Swelling of the hydrogel-embedded tissue can be advantageous since it increases pore size in the hydrogel allowing for deeper antibody penetration. After the staining step, the samples were incubated in mounting media that made

Stellenbosch University https://scholar.sun.ac.za



the tissue even more transparent and caused it to shrink back to its anatomical size.

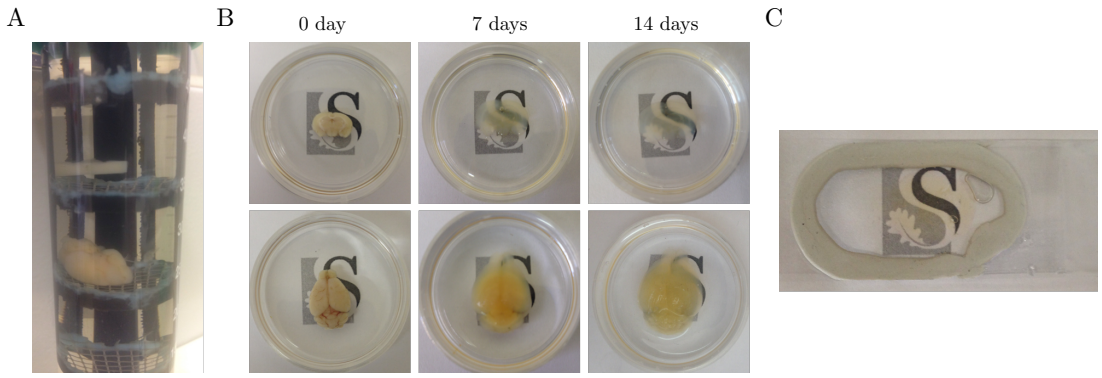


**Figure 6.4:** Passive clearing of brain slices and whole tissue. (A) Passive clearing of brain tissue. (B) Clearing of a brain slice and whole brain over time. (C) Brain slice mounted between a coverslip and glass slide filled with mounting media for confocal imaging.

**Active clearing.** Passive clearing of tissue with SDS micelles is a slow process, which can be accelerated by taking advantage of the ionic charge of the SDS micelles. By placing an electric field over the tissue, the negatively-charged micelles can be actively drawn through the hydrogel-embedded tissue, increasing the speed at which whole tissue samples are cleared. We designed a chamber based on the design of Chung and Deisseroth [37], that fitted into a 50 mL falcon tube housing a removable cage inbetween two platinum wires (Sigma, # 349402). A whole brain was placed between the platinum wires inside the cage. A constant voltage of 15 V electric current was applied over the platinum wires encasing the brain using Power Pac 1000 (Bio-Rad). The clearing solution temperature was kept at 38°C. The pH of the clearing solution was monitored every day using pH strips (Sigma, # P4536) and refreshed either once the pH was below 7 or after one week, until the tissue became completely transparent. Applying an electrical field can cause the generation of $H^+$ ions causing the solution to become more acidic and generate heat that can damage the brain tissue. It is important to have a

Stellenbosch University https://scholar.sun.ac.za



strong continuous stream of clearing solution circulating through the chamber to avoid build-up of harmful by-products that can cause damage to the brain. The STL file of the active clearing cage (Fig. 6.5A) can be downloaded at (https://drive.google.com/open?id=1fP7fnCExLzNlKsbcZHOCHOdqM8ODfzq6).

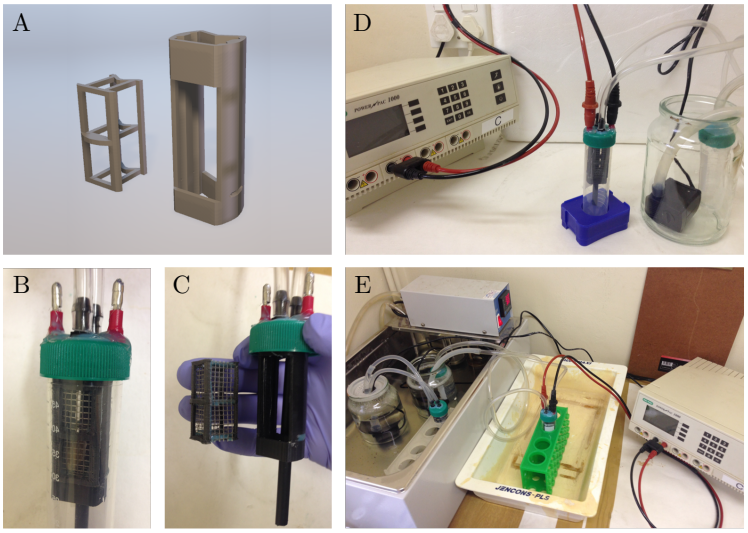


**Figure 6.5:** CLARITY active clearing system. (A) 3D model of the CLARITY active clearing tray designed with Blender. (B and C) CLARITY active clearing tray 3D-printed using PLA filament. (D) Fully assembled CLARITY active clearing system with falcon tube, power supply and clearing solution reservoir. (E) CLARITY experimental set-up with clearing solution reservoir in a heated water bath and the falcon tube placed in spill container.

Fig. 6.6 shows the active and passive clearing of a whole brain. After 4 days of clearing the brain with the two methods, the actively-cleared brain was considerably lighter than the passively-cleared brain. However, after one week of clearing, the actively-cleared brain became yellowish with signs of tissue damage (black marks). Although the active clearing produced better results at day 4, excess clearing using electrophoresis therefore resulted in tissue damage and discolouring that can affect imaging penetration depth. This is a common problem when using active clearing [37]. It is possible to circumvent these problems by fine adjustments in voltage settings and the flow rate of clearing solution, as well as by combining

Stellenbosch University https://scholar.sun.ac.za



active with passive clearing—first actively clearing for 2–4 days followed by passive clearing. Since the passively-cleared brain was sufficiently transparent for fluorescence imaging, we decided to continue using it for all subsequent experiments.

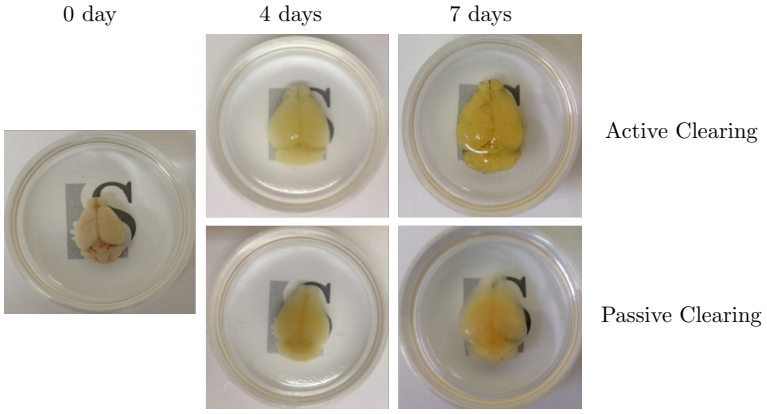


**Figure 6.6:** Whole brain samples cleared using passive and active clearing. Top: actively-cleared brain tissue using 15 V at day 4 and 7; Bottom: passively-cleared brain at day 4 and 7.

**Tissue storing.** Once the brain samples were transparent, they were washed by incubating the tissue in washing solution (0.1% Tween 20 (Sigma, # P1379) in PBS, pH 7.6 (PBS-T)) overnight for small tissues such as brain slices or for two days for large samples such as whole brain tissue at room temperature. At this point, the brain tissue could be refrigerated in PBS-T supplemented with 0.02% sodium azide ($NaN_3$) (Sigma, # S2002) for later use.

### 6.2.1 Staining and imaging of large brain tissue.

Our first goal was to stain a whole mouse brain using fluorescent dyes to assess the achievable resolution when imaging a large sample. After clearing the brain and washing it with PBS-T for two days, it was incubated in 2 mL Nissl staining solution for three days; the staining solution consisted of Nissl stain (Thermo Fisher Scientific, # N21480) in a 1:100 ratio with PBS-T. Thereafter the brain was washed overnight in PBS-T and incubated in the mounting solution (85%

Stellenbosch University https://scholar.sun.ac.za



glycerol (Sigma, # G5516) in de-ionized water) for one day. Thereafter the brain was placed in the imaging chamber (Fig. 6.4C) filled with mounting solution.

A Zeiss light sheet Z.1 microscope (Carl Zeiss, Germany) was used to image the cerebellum. Light sheet microscopy is a fluorescence microscopy technique that focuses a laser light sheet in the direction perpendicular to the sample, illuminating one thin slice of the sample at a time. The advantage of this technique is that it allows rapid image acquisition with little to no sample photobleaching, while producing high resolution images. Multiple z-stacks were acquired using a Plan-Apochromat 5x/0.16 M27 objective with a step with of 10 $\mu$m. An Argon multiline laser at 488 nm was used for image acquisition with appropriate beam splitters and a GaAsP detector 32+2 PMT. The sample was illuminated from both the right and left side in the chamber. The laser power and gain were set individually for the right and left side illumination to achieve the optimal signal/noise ratio. After image acquisition, the raw right/left illuminated images were stitched together using the Zen 2011 imaging software.

**Cerebellum anatomy.** Due to limited access to the light sheet microscope, only one mouse cerebellum was acquired instead of the whole brain. Therefore, we decided to focus on the mouse cerebellum, which has distinct cell populations such as the purkinje cells, with known autophagy activity. Fig. 6.7 shows the gross anatomy of the cerebellum. The cerebellum plays an important role in motor control. It does not initiate movement, but rather contributes to coordination and precision of movement by integrating input from sensory systems to fine-tune motor activity.

Stellenbosch University https://scholar.sun.ac.za



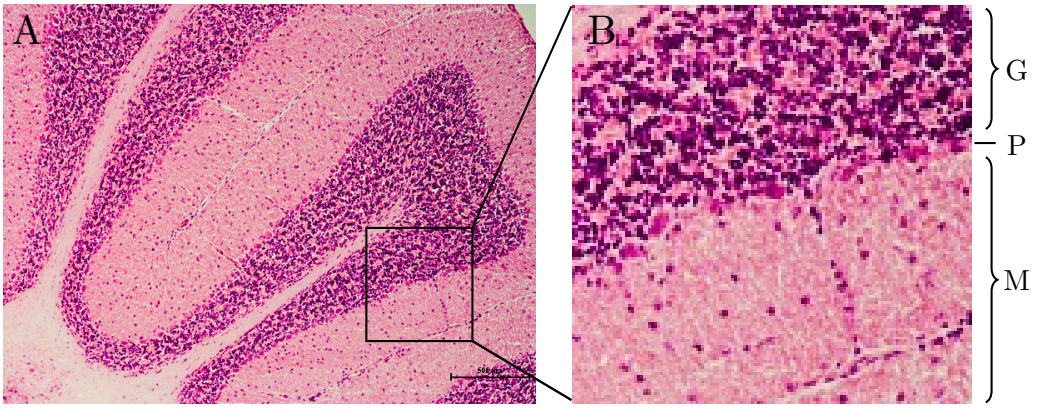


**Figure 6.7:** Histology of the cerebellum. (A) An overview of the cerebellar cortex showing the granular and molecular layers within the complex folia. (B) A zoomed-in image of the cerebellar cortex illustrating the molecular layer (M), a layer of Purkinje cells (P) and the granular layer (G).

**Imaging results.** Fig. 6.8 shows micrographs of cleared mouse cerebellum acquired using a light sheet microscope, with which the whole cerebellum could be 3D-imaged, revealing the overall spatial arrangement of the molecular and granular layers of the cerebellum as well as the nuclei of individual cells. While nuclei were readily detected in the periphery of the tissue, the centre was not stained due to poor penetration of Nissl stain through the whole tissue. This is a common challenge associated with staining large tissue samples [245]. While it possible to achieve uniform staining with small molecule probes, such as Nissl and Hoechst, through longer periods of incubation, permeabilization is required for immunohistochemistry [245]. Nonetheless, because we wanted to assess image resolution capacity when imaging large tissues, the images generated were sufficient for further analysis.

From the images acquired, we were able to identify individual nuclei of cells in the whole cerebellum. Nuclei were near the limit of the resolving capability of the 5x objective. Considering that autophagosomes can be smaller by a factor of 50 compared to nuclei, it makes it impractical to quantify autophagy intermediates in a whole brain when using the 5x objective. Although the light sheet microscope is equipped with higher magnifying objectives that might allow to achieve the

Stellenbosch University https://scholar.sun.ac.za



desired resolution, it requires the brain to be sectioned for imaging with 20x and 40x objectives. For the next step, a confocal microscope with a 40x objective was used for the image acquisition of mouse brain slices immunofluorescently stained for autophagy-related proteins.

### 6.2.2 Immunofluorescence staining of brain slices.

In the previous section, we showed that we were able to stain and image a whole cerebellum using a fluorescent tracer probe. However, since no such probes are available to visualize autophagosomes, we used antibody-based staining of 1 mm mouse cerebellum brain slices. After the brain slices were cleared and washed with PBS-T, they were stained with primary antibodies by incubating the slices in 100 $\mu$L of antibody solution (0.02% $NaN_3$ in PBS-T, supplemented with the respective antibody in a 1:50 ratio) in an Eppendorf tube for one week on a bench-top shaker at room temperature. To assess autophagy in brain tissue we used anti-rabbit LC3 (Cell Signalling, # 2775S), anti-mouse p62 (Abcam, # ab56416) and anti-rabbit LAMP2 (Abcam, # ab18528). After incubation with primary antibodies, brain tissue was washed with PBS-T overnight and incubated in 100 $\mu$L secondary antibody solution (0.02% $NaN_3$ in PBS-T, supplemented with the respective secondary antibody in a 1:50 ratio) for one week. Secondary antibodies used include anti-rabbit Alexa Fluor 488 (Thermo Fisher Scientific, # A11001) and anti-mouse Alexa Fluor 688 (Thermo Fisher Scientific, # A21235). Thereafter the brain tissue was washed in PBS-T overnight. To stain nuclei, brain slices were incubated overnight using Hoechst (Sigma, # 63493) in a 1:100 ratio in PBS-T. The brain tissue was washed with PBS-T overnight and then incubated in mounting solution until the next day. Brain tissue was then mounted between a glass slide and cover-slip using a putty-like adhesive (Prestik) and filled with mounting solution (Fig. 6.4C).

Brain slices were imaged using a Carl Zeiss LSM780 (Carl Zeiss, Germany) confocal microscope, which has the advantage of being able to produce high-resolution z-stack images of brain slices with no specific modifications required. CLARITY slides were placed on the microscope stage with the coverslip side facing the ob-

Stellenbosch University https://scholar.sun.ac.za



jective. Raw image stacks were acquired using a 10x (EC Plan-Neofluar 10x/0.3 M27) and a 40x (LD Plan-Nuofluar 40x/0.6 Corr M27) objective with 1–5 $\mu$m step width between image frames depending on the objective. Lasers strength illumination/excitation outputs were chosen using an Argon multiline laser 25 mW at 488 nm and 514 nm to ensure an optimal signal/noise ratio with minimal saturation using a GaAsP detector 32+2 PMT. Images were processed using Zen 2011 imaging software

**Imaging results.** The passive clearing design used here did not damage the delicate samples and allowed us to interrogate the intact brain structures using immunofluorescence labelling. Figs. 6.9 and 6.10 show the results of a cerebellum slice stained for autophagy markers. The autophagy vesicles can be distinguished in a manner similar to the approach described in Chapter 4 by immunostaining for autophagosomes and lysosomes using LC3 and LAMP2 antibodies respectively. However, since both LC3 and LAMP2 antibodies were rabbit-derived they could not be used together, and therefore separate immunostaining experiments were performed. p62 was also included in experiments since it is valuable marker for autophagy cargo.

LC3 and LAMP2 puncta were distributed throughout all three cell layers of the cerebellum, with the highest abundance of puncta observed in the molecular layer. In contrast, while p62 aggregates were also present in all three cell layers, they were more abundant in the granular layer compared to the Purkinje cell and molecular layers. The data suggest that autophagy activity indeed differs between neuronal cell types [171]. The few studies in the literature that assessed autophagy in the cerebellum [5, 248, 263] most commonly used western blot analysis of LC3 and p62 protein [5, 248, 263], which has the inherent limitation that it only allows the measurement of LC3 and p62 protein levels in brain regions and cannot discriminate between cell types. On the other hand, both fluorescence and electron microscopy have also been used to assess autophagy at a single cell level in brain tissue, allowing for the characterisation of autophagy in different cell types [5, 248]. However, limitations in the experimental set-up restricts sample interrogation to

Stellenbosch University https://scholar.sun.ac.za



a single plane.The data we generated using CLARITY allowed us to quantify the complete number of autophagy pathway intermediates in the cerebellum.

The cell structure of Purkinje cells is clearly visible in Fig. 6.9 due to the fluorescence signal in the cytoplasm. This may result from either high levels of cytoplasmic LC3 or of the intrinsic background associated with these specific cell lines. Regardless of the background noise observed, we were able to identify autophagosomes inside the cells. The well-defined Purkinje cells do give the impression that many of the LC3 and p62 puncta are not associated with cells since they are located outside the Purkinje cells. The molecular layer contains mostly the axons of the cells from the granular layer and the dendrites of Purkinje cells. However, glial cells are also found in the molecular layer, which provides support and insulation for surrounding neurons. Staining for nuclei highlighted glial cells residing between the Purkinje cell dendrites and granular cell-derived axons (Fig. 6.9). Fig. 6.9 also shows the small neuronal cells densely localized together in the granular layer consists. While glial cells had more LC3 puncta than Purkinje cells, further investigation is needed to ascertain whether this also translates in into higher autophagosome flux in glial cells.

The high degree of autofluorescence observed originated mostly from blood vessels, which is an inherent problem in the use of CLARITY [37, 257]. Although it does make the images aesthetically more pleasing, the autofluorescence overpowers the fluorescence signal of p62 under low magnification making it difficult to detect. It was only under high magnification that p62 signal became apparent. Moreover, the strong autofluorescence makes it difficult to separate true p62 signal from background noise using threshold techniques. One possible way of removing autofluorescence would be to treat tissue with hydrogen peroxide to quench autofluorescence and then perform immunofluorescent staining.

### 6.2.3 Conclusion

We have shown that it is possible to detect autophagy pathway intermediates using immunohistochemistry in cleared brain tissue and characterise their overall spatial arrangement. Moreover, analysis of LC3, p62 and LAMP2 puncta distribution

Stellenbosch University https://scholar.sun.ac.za



revealed that autophagy occurs throughout the cerebellum cortex, and with regard to characterising autophagy in the brain, that autophagy differs between cell layers. This approach presents a promising way forward for assessing autophagy activity in whole organs. Although we were able to clear and stain whole brain tissue, uniform staining of cellular components and resolving fine structures remained challenging. Here, the recently-developed mouse model (GFP-LC3-RFP-LC3ΔG probe) may be useful to assess autophagy in whole organs [120]. Nevertheless, immunostaining of sectioned brain tissue provides a practical method to assess autophagy activity in brain tissue while keeping the three-dimensional neuronal arrangement. Such an approach would be important for unravelling autophagy's role in the progression of diseases in the context of whole organs and would aid in developing autophagy-targeting therapies. Taken together, it may be possible to measure the autophagosome flux and pool sizes, transferring the previously described method in Chapter 4 to a tissue screening approach.

Stellenbosch University https://scholar.sun.ac.za



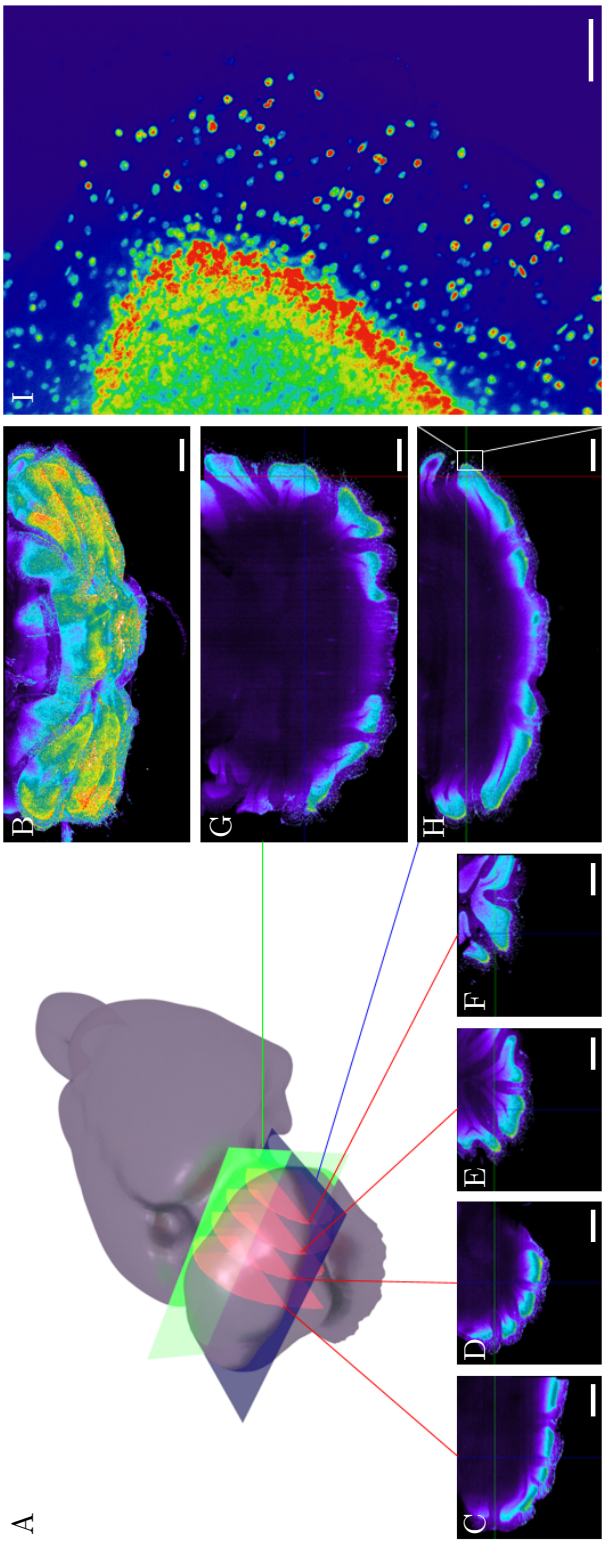


**Figure 6.8:** Fluorescence micrographs of a mouse cerebellum stained with Nissl. (A) An illustration of a mouse brain with hypothetical cross-sectional slices in the X, Y and Z axes. The micrograph is converted to index colour images using a hot-cold colour lookup table. (B) A maximum intensity projection of the mouse cerebellum. Representative images in the X (C, D, E and F), Y (H) and Z (G) axis are shown. (I) A region of interest in image slice 295 showing the molecular and granular layer of the mouse cerebellum. (B–H) Scale bar: 1 mm; (I) Scale bar: 100 $\mu$m

Stellenbosch University https://scholar.sun.ac.za



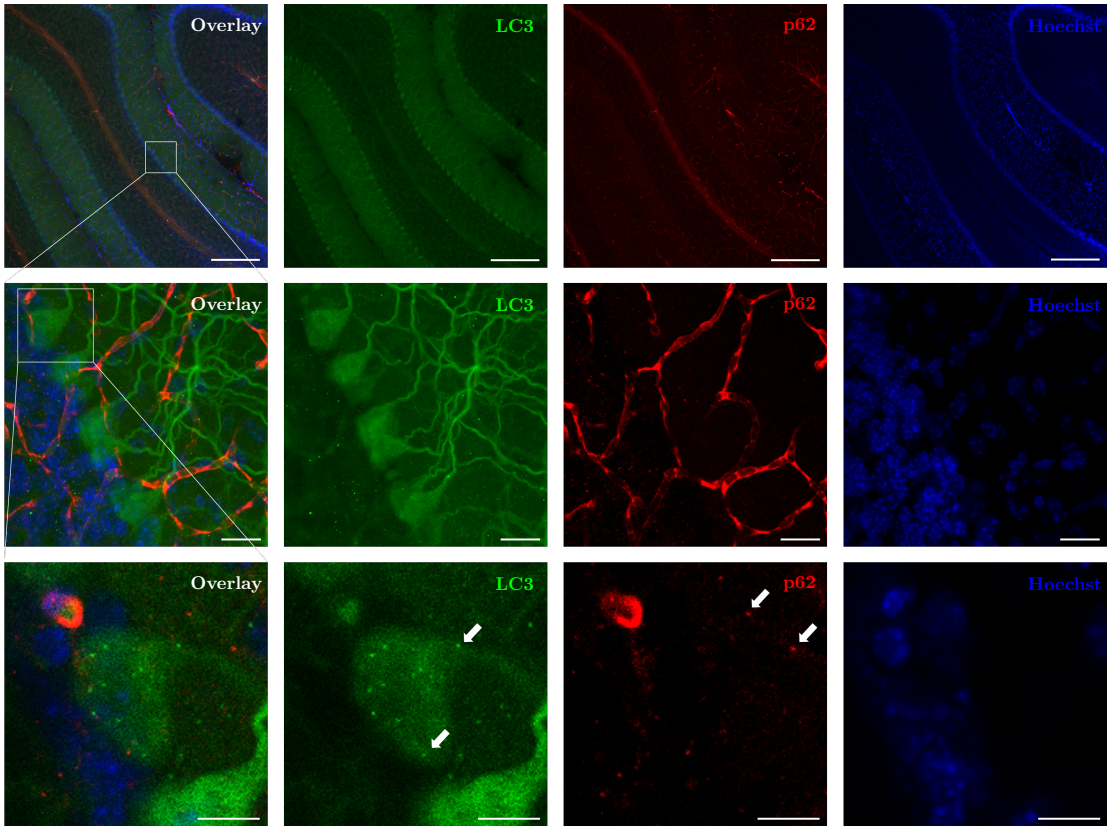


**Figure 6.9:** Achieving single cell resolution in mouse cerebellum stained with LC3, p62 and Hoechst. Top; overview of a single layer micrograph of cerebellum acquired using the 10x objective. Scale bar: 200 $\mu$m. Middle; maximum intensity projection of 27 image layers showing granular layer (left), Purkinje cell layer (middle) and molecular layer (right) using the 40x objective. Autofluorescence from blood vessels can be seen in the red channel. Scale bar: 20 $\mu$m. Bottom; a zoomed in area of one of the layers showing LC3 (autophagosomes) and p62 aggregates inside Purkinje cells. Scale bar: 10 $\mu$m.

Stellenbosch University https://scholar.sun.ac.za



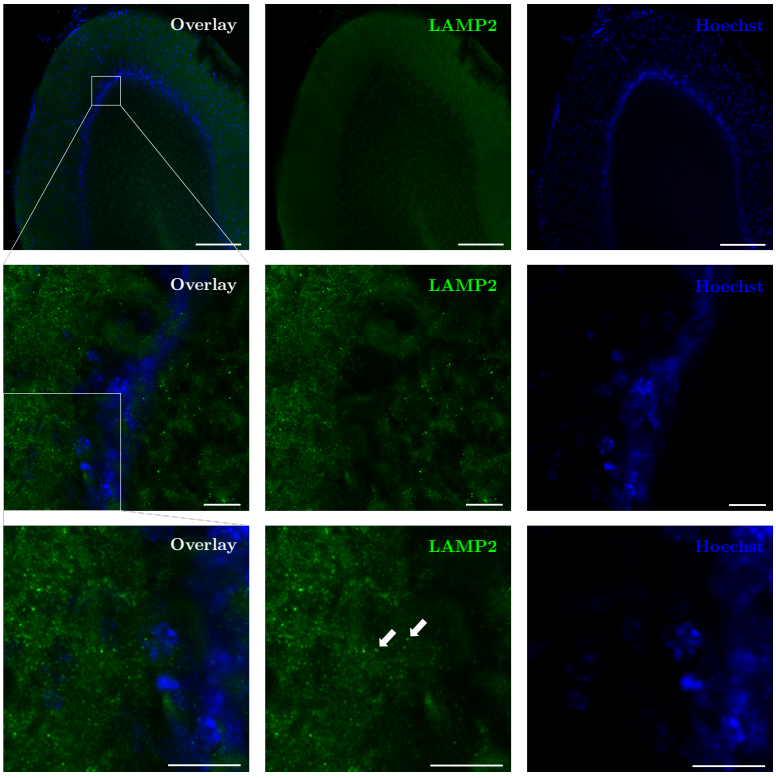


**Figure 6.10:** Achieving single cell resolution in mouse cerebellum stained for LAMP2 and nuclei. Top; an overview of mouse cerebellum acquired using the 10x objective. Scale bar: 200 $\mu$m. Middle; a single layer showing molecular layer (left), Purkinje cell layer (middle) and granular layer (right) using the 40x objective. Scale bar: 20 $\mu$m. Bottom; a zoomed in area showing LAMP2 puncta. Scale bar: 20 $\mu$m.

Stellenbosch University https://scholar.sun.ac.za

# Chapter 7

# General discussion

## 7.1 Introduction

Despite advances in unravelling the mechanistic behaviour of autophagy and its molecular defects in pathologies, there still remains confusion around which tools and systems should be used to assess the dynamics of autophagy accurately and in a way that allows for better screening of drugs and subsequent fine-tuning of autophagy in a clinical setting.

We distinguish between the vesicular machinery of the autophagy system and the cargo that is being degraded within this system. Autophagosome flux is the rate of flow along the vesicular pathway, whereas cargo clearance is the rate of cargo degradation within the vesicular system. We developed a technique that accurately measures the autophagosome flux based on counting the autophagy intermediates over time, and then at steady state blocking the fusion of autophagosomes and lysosomes and calculating the autophagosome flux from the initial rate of increase in the autophagosomes. In light of the clinical importance of being able to accurately modulate autophagy, the aim of this study was to evaluate the reliability and flexibility of this technique, and its practicality as a tool in assessing autophagosome flux in cells at basal level, as well as when treated with known autophagy inducers.

Our first aim was to assess the reliability and flexibility of our technique. This

Stellenbosch University https://scholar.sun.ac.za



included setting up a suitable negative control and evaluating alternative probes for measuring the autophagosome flux. Our second aim was to use our approach to perform high-throughput screening of several known autophagy modulating drugs in two cell lines, as well as to characterize the transient time-dependent response of the autophagy system. Our data showed that we could characterise the drug-dose autophagy response in different cell lines, making it possible to finely control autophagy activity. However, using fluorescence probes and high-resolution imaging platforms to distinguish between structures on a micrometre scale would still be difficult to implement practically in a clinical setting. To be successful, autophagy-targeting therapies would require the clinician and doctors to be able to easily and accurately assess autophagy, and adjust it according to the pathology and degree of deviation from normal behaviour. With this in mind our third goal was to identify novel biomarkers that can be used as measurable indicators of autophagosome flux collected at a single time point without requiring a labour-intense microscope setup.

Arguably the greatest advantage of live cell imaging is that it reveals the dynamic nature of cellular components, providing real time data on the inner workings of the cell. Often in autophagy research the main goal is to determine the role of autophagy in disease and the potential therapeutic effect of manipulating autophagy, while the more integrated aspects of autophagy are overlooked. Our fourth goal was to tease out some of the underlying mechanism of autophagy. Data generated by these studies provided context and contributed to our understanding of the system as a whole, and thereby allowed us to generate new testable hypotheses that could aid the improvement of autophagy-targeting interventions.

Finally, we aimed to bridge the gap between *in vitro* and *in vivo* studies by characterising autophagy in the brain through a microscopy approach. Promising results in pre-clinical trials has made autophagy an attractive target for treating neurodegenerative diseases. However, because of the inherent limitations of the imaging techniques used up to now, little is known about the overall distribution of autophagy activity in the brain and how it affects the progression of diseases. Recently, a technique was developed that transforms intact tissue into

Stellenbosch University https://scholar.sun.ac.za



a gel-hybrid form that can be imaged using fluorescence microscopy. We evaluated this fluorescence-hydrogel imaging technique to see whether it could resolve autophagy intermediates in brain tissue at a single cell level.

## 7.2 Measuring autophagosome flux

Our fluorescence microscopy-based approach allows for the numerical quantification of autophagosome flux and the autophagy pathway intermediates. It centres around distinguishing between and measuring the total pool sizes of autophagosomes, autolysosomes and lysosomes over time, which allows us to characterise the autophagy steady-state and time-dependent behaviour. This approach proved to be a powerful tool to characterise autophagy due to its versatility, sensitivity and quantitative capabilities.

Despite the usefulness of our approach, it is not without its challenges. Our method relies on measuring the autophagosomes, autolysosomes and lysosomes pool sizes over time in the presence and absence of a fusion inhibitor, such as bafilomycin $A_1$. Bafilomycin $A_1$ acts by inhibiting the membrane-bound V-ATPase proton-pump in autolysosomes and lysosomes; this leads to the de-acidification of the lumen of these vesicles, which prevents the fusion of lysosomes with autophagosomes. Thus, when using acidotrophic fluorescent dyes such as LysoTracker, the signal is quenched in the presence of bafilomycin $A_1$. Despite this, we have shown that there is a time window after bafilomycin $A_1$ treatment during which reliable data can be obtained. This window was determined by comparing the transient time-dependent behaviour of the autophagy intermediates using both LysoTracker and RFP-LAMP1 (Fig. 4.3). Its duration is likely to differ between the cell lines and the concentration of LysoTracker used, and it would therefore be advisable to measure this time window with fluorescently-tagged lysosomal markers. Considering the labour-intensiveness of this task, one may ask why then use acidotrophic dyes at all? Arguably the greatest advantage of using acidotrophic dyes is that it allows for effortless and uniform fluorescent labelling of autolysosomes and lysosomes throughout cell population in living cells, due to the inherent properties of

Stellenbosch University https://scholar.sun.ac.za



the probe. Moreover, it allows for the acquisition of high-contrast images, making it ideal for automated and highly accurate puncta counting. When it comes to the automated analysis of large data sets generated by high-throughput screening this is critical.

The use of fluorescent probes has gained popularity because of the ease with which they selectively label organelles, in contrast to plasmid-based techniques which can be both challenging and laborious. To label autophagosomes with fluorescently-tagged structural proteins requires cells to be transfected with appropriate vectors. There are many obstacles associated with plasmid- or virus-based cell transfection: low transfection efficiency, reduced cell viability following transfection, and non-reproducible transfection results. These obstacles would pose serious problems for measuring autophagic variables in primary cell lines which are known to be difficult to transfect. Here we made use of cell lines that stably express GFP-LC3 in order to circumvent many of these challenges. Nevertheless, the heterogeneous expression of GFP-LC3 throughout the cell population remains an inherent obstacle. The level of GFP-LC3 expression directly relates to the accuracy of detecting autophagosomes and autolysosomes [191]. In some instances, little or no GFP signal could be detected, which made it impossible to identify autophagosomes. The inhomogeously-distributed signal further complicated image analysis, rendering simple threshold algorithms problematic and in some cases impractical. Even the more sophisticated threshold functions, such as the adaptive threshhold algorithm used in our studies to detect puncta, are not unproblematic. Considering the importance of LC3 in autophagy, a potential means to achieve sufficient GFP signal throughout the whole population would be to knock out the endogenous LC3 gene so that only GFP-LC3 is expressed.

Another aspect that needs to be discussed is the potential risk of misidentifying whether the autophagy system is at steady state in cases where the transition occurs very slowly (Table 4.2). We found that with most of the drugs screened there was a slow temporal response, which when measuring the autophagy intermediates over a period of three hours showed no net change, thus suggesting that the autophagy system was in steady state. Drug screening performed by Kaizuka

Stellenbosch University https://scholar.sun.ac.za



*et al.* [120] with the autophagic flux probe showed that the autophagy response can occur over days. Therefore, verifying whether it is at steady state using hourly intervals may be insufficient when the response is slow. It is important to keep these intrinsic properties of the autophagy system in mind, namely that not all autophagy modulating drugs cause a response on the same time scale, and adjust the time intervals at which puncta are counted accordingly.

Recent advances in molecular techniques have led to the development of novel probes for assessing autophagy activity, such as the GFP-LC3-RFP-LC3ΔG probe by Kaizuka *et al.* [120]. This probe is used to assess autophagic flux by expressing the abundance of GFP and RFP signal as a ratio. There are a number of advantages associated with using GFP-LC3-RFP-LC3ΔG probe. First, it relies on the average fluorescence intensity of cells to estimate autophagy activity, and therefore does not require high resolving imaging platforms, making it ideal for high-content analysis/drug discovery platforms such as cytometry. Second, it allows continual assessment of autophagy activity without requiring the inhibition of fusion, thus making it simpler to characterize the transition of the autophagy system to a new steady state. Despite these advantages it cannot be used to quantify autophagy activity as a rate and, compared to our approach, is limited in its ability to resolve small changes in autophagy activity (Fig. 4.4).

Another method for assessing autophagy activity is based on monitoring the decay of cytosolic proteins [260]. Although this only indirectly correlates with autophagy degradative activity, it remains one of the most accurate means of measuring this property. This method uses cytosolic photo-activatable fluorescent probes, that, once activated, can be used to estimate the autophagy activity by measuring the rate of decay of the fluorescence signal in the cytoplasm. From this data the turnover rate of the cytosolic protein pool or, more accurately, of the fluorescent protein pool, can be calculated and used to compare treatment interventions. Although this technique does allow for the direct assessment of cytosolic protein turnover, which is at the core of many autophagy-disease related studies, it does not discriminate between cytosolic protein degradation via autophagy and via the ubiquitin-proteasome pathway. Another disadvantage is that this

Stellenbosch University https://scholar.sun.ac.za



approach provides no information on the autophagy pathway intermediates and their transient time-dependent behaviour. Let us consider the following example to highlight these disadvantages. During the initial stages of disease progression, where the rate of autophagosome and lysosome fusion decreases, the autophagosome flux is unaffected because the rate of autophagosome synthesis controls the flux (see Chapter 5) until the point where fusion impairment becomes so severe that it leads to autophagy arrest. While in the early stages of the disease there are measurable changes in the autophagy machinery, e.g., an accumulation in autophagosomes, the cytosolic protein turnover remains indistinguishable from that of normal cells. This can be particularly important in a clinical setting where the accumulation of autophagosomes could potentially be used to identify the early stages of a disease where treatment can prevent irreversible failure. Thus, using cytosolic fluorescent probes in isolation is inadequate to characterise the full extent of the role of autophagy in disease progression.

As discussed earlier, our method for the measurement of the autophagosome flux and the autophagy intermediates is not without its limitations, but these can be lessened by combining our approach with other probes. Combining our approach with cytosolic photo-activatable fluorescent probes should generate a more complete picture of the autophagy system, enabling us to determine the rate of cytosolic protein turnover (cargo flux) as well as the rate along the vesicular pathway (autophagosome flux). Ideally this could be done by measuring both the rate of decay of the cytosolic photo-activatable fluorescent probe and the time-dependent changes in autophagy intermediate pool sizes. This would be the best-case scenario, but given the difficulties of using cytosolic photo-activatable fluorescent probes it would not be trivial to combine them with our approach in a single experiment. One could potentially scale down the use of cytosolic fluorescent probes by only measuring their rate of decay at two or three key time points, but this would be sub-optimal. The second possibility is to combine our approach with the GFP-LC3-RFP-LC3$\Delta$G autophagic flux probe (Fig. 7.1). This probe would allow us to easily monitor autophagy activity under low magnification in order to characterise the transitioning profile, and whether the system is at steady state

Stellenbosch University https://scholar.sun.ac.za



using the ratio of GFP/RFP. LysoTracker blue and GFP-LC3 from the GFP-LC3-RFP-LC3ΔG construct could then be used to determine the complete autophagy intermediate pool sizes at selected times points at high magnification, and once the autophagy system is at steady state, measure the autophagosome flux accurately.

The first will generate a more complete picture of the autophagy system, enabling us to determine the rate of cytosolic protein turnover (cargo flux) as well as the rate along the vesicular pathway (autophagosome flux). Ideally this would be accomplished by measuring both the rate of decay of cytosolic photo-activatable fluorescent probe and the time-dependent changes in autophagy intermediate pool sizes. This would be the best-case scenario, but given the nature of experimental set-up of using cytosolic photo-activatable fluorescent probes it would be difficult to combine them with our approach in a single experiment. One could potentially scale down the use of cytosolic fluorescent probes by only measuring their rate of decay at two or three key time points, but this would be sub-optimal. The second, although it may not directly measure cytosolic turnover, does provide a rough indication of cytosolic turnover that could be easily incorporated into our workflow (Fig. 7.1). The GFP-LC3-RFP-LC3ΔG probe would allow us to easily monitor autophagy activity under low magnification in order to characterise the transitioning profile, and whether the system is at steady state using the ratio of GFP/RFP. LysoTracker blue and GFP-LC3 from the GFP-LC3-RFP-LC3ΔG construct could then be used to determine the complete autophagy intermediate pool sizes at selected times points at high magnification, and once the autophagy system is at steady state, measure the autophagosome flux accurately.

Stellenbosch University https://scholar.sun.ac.za



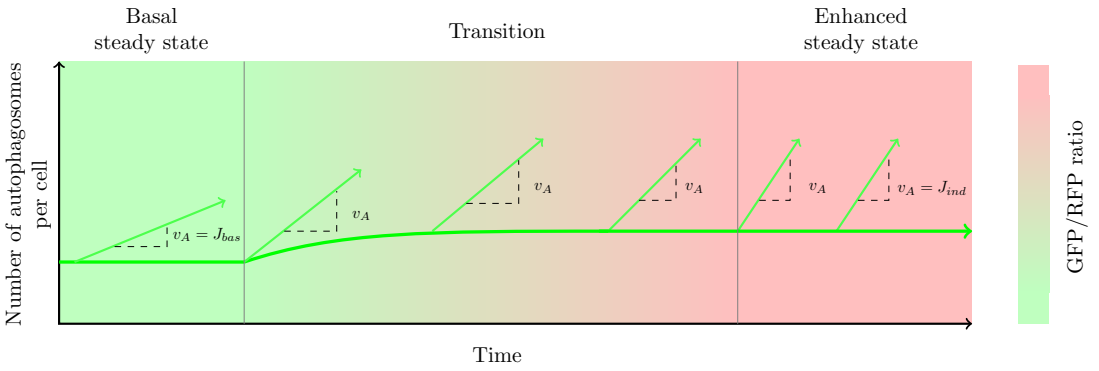


**Figure 7.1:** An illustration of using our approach in combination with the GFP-LC3-RFP-LC3ΔG probe to effortlessly assess autophagy. The autophagic flux probe allows for the assessment of autophagy activity over time using the GFP/RFP ratio, while the complete autophagy intermediates pool size is measured using GFP-LC3 and LysoTracker blue. The graph also shows the change in the rate of autophagosome synthesis, $v_A$, over time from basal steady state to the new enhanced steady state which can easily be assessed using the autophagic flux probe.

## 7.3 Modulating autophagy

The success of autophagy-targeting therapies depends on the accurate characterisation of autophagy modulating drugs. Dose-responses can be used to determine the required dose to achieve a desired effect as well as the therapeutic index for a drug, thereby determining the efficacy and safety of a drug.

We have shown that our approach allows us to accurately measure autophagosome flux (not merely pool size) in response to a range of autophagy modulating drugs, which can be used to generate detailed dose-response curves. From the data generated (Figs. 4.5 and 4.8 show the raw data and Fig. 4.9 show a cartoon dose-response model fitted to selected drugs) we were able to describe possible therapeutic ranges in terms of minimum and maximum effective concentrations between autophagy activity can be modulated. In addition, the maximum tolerated and toxic concentrations can also be identified to avoid possible unwanted side effects. Here, future cytotoxicity screenings will be of value.

Although screening autophagy modulating drugs in itself is not novel [120, 163,

Stellenbosch University https://scholar.sun.ac.za



172], what sets our work apart is that we characterise the dose-response profile in terms of autophagosome flux/synthesis rate and the complete pool size of the autophagy intermediates with high precision at steady state over a wide range of concentrations. Although we have screened fewer drugs compared to others [120, 163, 172], the level of characterisation achieved may be the most detailed description of these drugs available to date. The characterisation of the autophagy steady state and dose response as performed here presents a promising way forward for identifying best suitable autophagy modulators.

Fig. 7.2 shows our conceptualisation of developing and fine tuning the control of autophagy. Screening large drug libraries using a wide concentration range with high precision would allow for the scoring of drugs according to their therapeutic index in a cell/tissue (and disease state) specific manner. This would allow us to determine concentrations required to achieve a maximal effect, thereby enabling to offset deviation in autophagy by either enhancing (neurodegeneration) or decreasing (cancer) autophagy while avoiding adverse effects on other cells/tissues. Furthermore, data generated can be used to create dose-response models to design treatment interventions using a combination of drugs at their minimal dosages to achieve maximal efficiency.

Stellenbosch University https://scholar.sun.ac.za



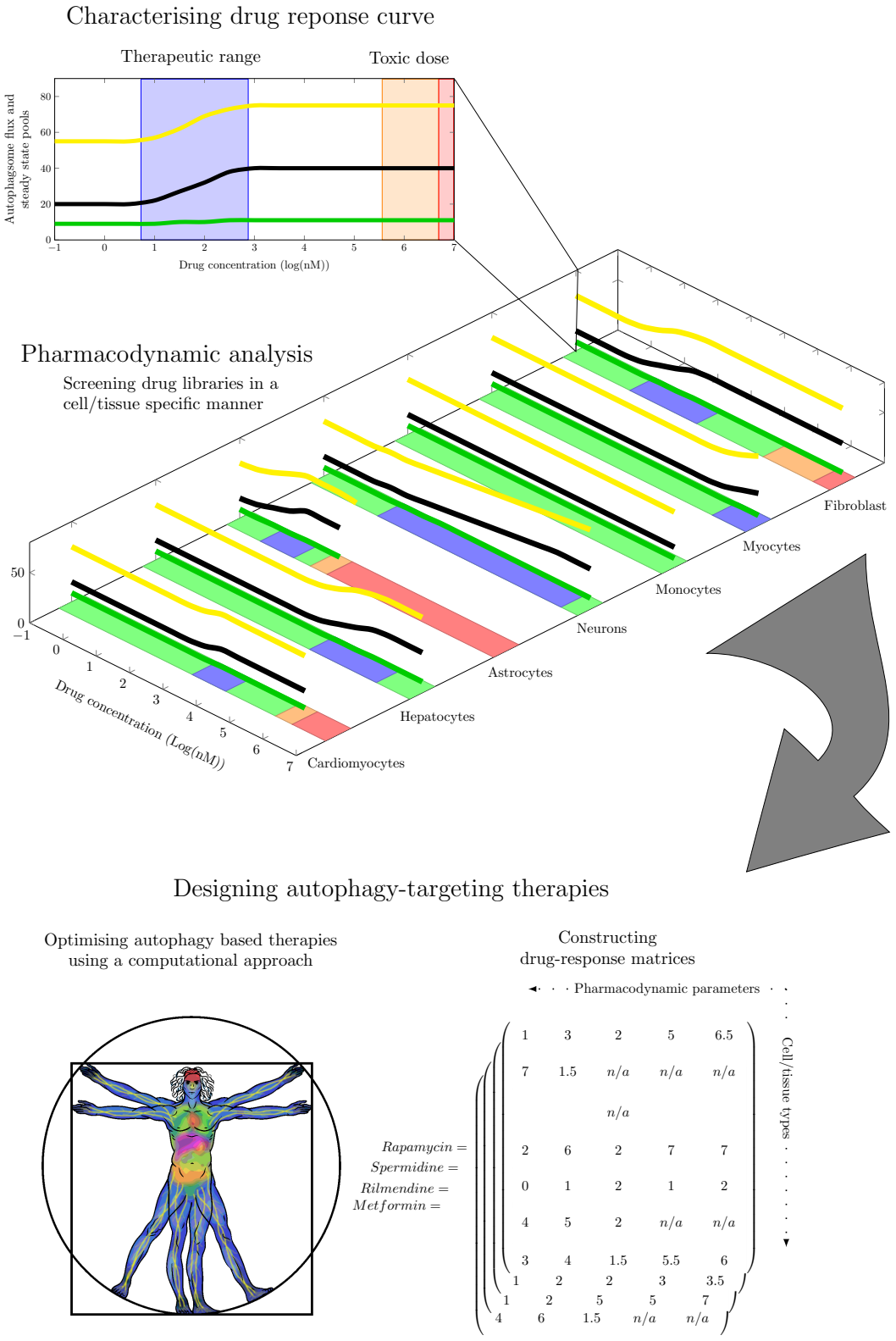


**Figure 7.2:** Conceptualisation of developing autophagy modulating therapies using our approach. Pharmacodynamic analysis of autophagy modulating drugs allows for the identification of the therapeutic concentration range (□), where it is possible to safely modulate autophagy, as well as determining the concentration that would lead to adverse effects. Pharmacodynamic analysis of autophagy modulating drugs in key cell types is a critical aspect for developing therapies. These pharmacodynamic parameters in combination with a computational approach will further aid in the optimisation (and patient-centred approach) of autophagy targeting therapies. (Hypothetical data shown).

Stellenbosch University https://scholar.sun.ac.za



## 7.4 Autophagosome flux markers

Targeting autophagy in a clinical setting requires clinicians and clinician scientists to be able to easily assess autophagy activity in patients. Despite the usefulness of our microscopy-based approach, it remains a challenging and laborious task to implement in a clinical setting. For instance, one of the greatest foreseen difficulties would be the ability to consistently and uniformly label the autophagy intermediates in primary cells using plasmids for live cell imaging. In such cases biomarkers may present a more promising method as a measurable indicator for autophagosome flux.

There are a number of biomarkers that are routinely used in western blot analysis to assess autophagy activity both *in vitro* and *in vivo*. These biomarkers are however inherently unsuitable to assess autophagosome flux, as they usually reflect on the abundance of autophagy components rather than autophagosome flux. One of the most accepted and predominately recommended techniques to assess flux relies on comparing relative changes in LC3 protein levels in the presence and absence of autophagosome/lysosome fusion inhibitors, such as bafilomycin $A_1$, to infer whether or not autophagy activity has changed. Although this approach indicates autophagy activity, it remains limited in its capacity to reflect autophagosome flux based on a single point.

Taking advantage of a controlled autophagosome flux, we used proteomic analysis to reveal autophagosome flux biomarkers by using both mTOR-dependent and -independent induced autophagy with similar incremental increases in autophagosome flux in order to identify autophagosome flux markers (Fig. 4.13). Although proteomics has been used in the past to create an autophagy interaction network [17] and to elucidate its role in diseases [19, 132], it has never been employed to identify autophagosome flux biomarkers.

In light of the role of autophagy in cytosolic turnover, it is not surprising that most of the biomarkers that we identified were cytosolic proteins that decreased with increasing autophagosome flux. Such markers would be an ideal indicator of autophagy as they directly relate to cargo turnover, which is at the core of autophagy-targeting therapies. However, many of these markers were influenced

Stellenbosch University https://scholar.sun.ac.za



by phenotypical changes of autophagy, i.e., an increase in the number of autophagosomes while flux remained unchanged. Proteins associated with protein synthesis, on the other hand, were unaffected by these phenotypical changes and increased with flux. The exact reason why these proteins increased remain unclear, but presumably it relates to proteostasis. This raises the question of whether other components of protein synthesis, such as mRNA, could serve as measurable indicators of autophagosome flux.

Taken together, the biomarkers identified in this study may serve as suitable starting points for developing assays that can be used in a clinical setting to assess autophagosome flux and cytosolic turnover. Future work would require extensive testing of these markers to determine their effectivity in reporting on autophagosome flux and cytosolic turnover. If shown to be specific and reliable, these biomarkers would allow clinicians to easily measure autophagy activity and compare it to databases for screening, diagnoses and therapeutic interventions.

## 7.5 Autophagy system properties: cell size and vesicle dynamics

Over the past two decades, we have learnt much about the molecular machinery of the autophagy system and its regulatory network in the mammalian system. An increasing number of studies have shown that targeting autophagy presents a promising way forward in treating various diseases such neurodegeneration [25, 203, 240] and cancer [100, 112, 243, 265], while other studies [120, 163, 172], including ours, have developed increasingly accurate tools to measure autophagy activity and characterise autophagy-modulating drugs that would enable us to control autophagy more effectively. Nevertheless, some aspects of the underlying mechanism of autophagy, such as the change in vesicle behaviour response to induction, are often overlooked. The study of these fundamental properties can be used to create or improve existing computational models of autophagy which could then further deepen our understanding of the autophagy process. Here we took advantage of our experimental data to expand our understanding of the systemic

Stellenbosch University https://scholar.sun.ac.za



properties of autophagy, with a focus on autophagosome size, cell size and vesicle translocation rate.

### 7.5.1 A contribution to autophagy degradative capacity through autophagosome size?

The time-dependent analysis of rapamycin-treated cells revealed an increase in autophagosome size compared with spermidine-treated cells. As a result, although both rapamycin- and spermidine-treated cells had similar fluxes, treatment with rapamycin increased the cytoplasmic protein turnover considerably. This suggests that autophagic protein turnover can be modulated over and above simply increasing flux. The modulation of cytosolic cargo turnover in yeast model systems through autophagosome size and flux has been suggested previously [115], but accurate assessment remained a challenge. Using our approach we were able to accurately quantify both autophagosome size and autophagosome flux, which allowed us to derive a measure of cytosolic cargo turnover (Fig. 4.15). This may make future studies of the interplay between these two components more efficacious, especially where the pathology lies in cargo recognition.

Our data showed that inducing autophagy through the mTOR-dependent pathway leads to a bimodal response in autophagy, while the mTOR-independent pathway mainly affects autophagosome flux (Fig. 4.15). We know that the amount of PtdIns3P recruited to the phagophore site contributes to the regulation of autophagosome size [27]. This may explain why the induction of autophagy via mTOR resulted in a bimodal response because the recruitment of PtdIns3P is regulated by mTOR activity via the ULK complex [63]. In comparison, spermidine, which is thought to induce autophagy through EP300 acetyltransferase [194], changes the overall acetylproteome, increasing the rate of autophagosomes synthesis [213]. This requires further attention in future studies, especially when screening drugs for efficiency and magnitude of autophagy induction since it highlights two major cellular control systems for fine-tuning autophagy activity.

Stellenbosch University https://scholar.sun.ac.za



### 7.5.2 Autophagosome flux and cell size

The cytoprotective role of autophagy in cells stems, at least in part, from continual cytoplasmic turnover, which prevents the build-up of unused as well as potentially deleterious proteins and organelles [34, 100, 187]. It is well established that autophagy occurs at different rates in all cells in the mammalian system [189], presumably to meet the cell-specific metabolic and proteostatic demands. Considering this important function of autophagy, one of the questions asked about the autophagy system relates to whether or not it proceeds in relation to cell size (cytoplasmic volume). As trivial as it may seem, investigating the relationship between autophagy activity and cell size is challenging, since comparing autophagy activity of two cell types with different sizes would inherently be flawed by differences in the inherent cell-specific autophagy activity. In our study, in order to dissect the relationship between autophagosome flux and cells size, we purposefully utilized a micro-patterning approach to control and standardize cell size. Our data shows that autophagy activity increases with increasing cell size, indicating that it does not proceed at a single or fixed rate (Fig. 4.15). Therefore, cell size is a contributing factor in the regulation of autophagy.

### 7.5.3 Autophagosome trafficking

At the core of the autophagy machinery lies the encapsulation of cargo into autophagosomes which are dynein-dependently transported along the tubulin network to the perinuclear region where they fuse with lysosomes for degradation. [111, 192]. Despite the fact that most of the research in the autophagy field is directed towards the autophagy machinery, particularly autophagosome formation and its implications in diseases, the trafficking behaviour of autophagosomes is usually overlooked even though it plays an important functional role. Taking advantage of being able to finely control autophagy and cell shape, we assessed autophagosome trafficking behaviour under various conditions that resulted in an increase in autophagosome and autolysosome abundance.

Our results showed that equal induction of autophagy with rapamycin and

Stellenbosch University https://scholar.sun.ac.za



spermidine led to a similar increase in autophagosomes flux and the respective autophagy intermediates pool sizes. Induction of autophagy led to a decrease in rate of autophagosome translocation and displacement compared to control in the rate of tubulin-associated translocation of autophagosomes and how far in the cell they are displaced relative to the control. Due to the overall increase in the autophagy intermediates after induction, it is reasonable to conjecture that the decrease in the autophagosome translocation rate is a result of the tubulin network becoming congested. However, despite the increase in autophagosomes following partial inhibition with bafilomycin $A_1$ (where autophagosome flux was equal to control) (Fig. 4.12), there was no change in the autophagosome translocation rate and displacement (Fig. 4.19). The reason for the decrease in autophagosome translocation rate and displacement with induction of autophagy remains unclear. The formation of autophagosomes and the translocation thereof is an energy-requiring process [63, 169]. A decrease in localized ATP seems an unlikely cause for the decrease in translocation rate, since enhanced autophagy may increase metabolite substrate generation which contributes to an energetically favourable environment [169]. Moreover, "congestion" or "crowding" on the tubulin network *per se* also seems unlikely since the autophagosome translocation rate in the partial inhibition group was the same as that of the control, while having considerably more autophagosomes being translocated on the tubulin network.

Considering that autophagosome translocation rate is linked to the rate of autophagosomes being processed (synthesis → translocation → fusion with lysosomes), we speculate that the decrease in the autophagosome translocation rate stems from less cytoskeleton motor protein, primarily dynein, binding to autophagosomes. We reason that under enhanced autophagy conditions there is greater flux of dynein motors towards the perinuclear region resulting in the reduction of available motors in the periphery for translocating autophagosome. This deserves to be further studied.

The efficient translocation of organelles is essential in all eukaryotic cells. For example, single point mutations in dynein motors or their regulatory machinery result in a range of neurological diseases in humans, such as Alzheimer's disease

Stellenbosch University https://scholar.sun.ac.za



[167, 185]. Even more so, mutations in dynein motors have also been shown to impair autophagic clearance of aggregate-prone proteins [217]. In these cases, malfunctioning of autophagy is due to a knock-on effect of impaired dynein function, which renders autophagy-modulating drugs ineffective. This scenario is similar in cases where a dysfunctional microtubule network is the source of defective autophagy. However, knowing the defect in the pathology provides new avenues for developing effective therapies. It could well be that in these cases the use of gene therapy in combination with autophagy modulating drugs could serve as an effective tool to replace dysfunctional motors (or any other defective components) while enhancing the clearance of protein build-up, thereby aiding in recovery.

### 7.5.4 Conclusion

Taken together, through a series of experiments, we found several highly relevant phenomena concerning the underlying mechanism of autophagy. The first finding is that autophagy can be modulated through both the synthesis rate of autophagosomes and the regulation of autophagosome size. The second finding is that autophagy activity and its responsiveness to drugs is closely linked to cell size. The third finding is that the induction of autophagy through rapamycin and spermidine decreases the autophagosome translocation rate and displacement. These studies deepen our understanding of the autophagy system, so providing a context for interpreting experimental data and developing more accurate computational models of autophagy.

## 7.6 Supply and demand analysis of autophagy

To finely manipulate autophagy for therapeutic purposes requires a deeper understanding of underlying principles and the degree of control regulatory mechanisms exert over autophagosome flux. A main aim of the work described in this thesis was to determine whether the control of autophagosome flux lies with the synthesis of or the demand for autophagosomes. We previously constructed a minimal model of autophagy that closely fitted our experimental data. However, at this

Stellenbosch University https://scholar.sun.ac.za



stage of the development of our kinetic model of autophagy, we could not draw confident conclusions about the control of autophagosome flux and concentrations of autophagic vesicles.

Taking advantage of the framework of supply and demand analysis [94] we were able to experimentally determine the elasticity coefficients of supply and demand rate with respect to autophagosome number. For these elasticity coefficients we could calculate the flux- and concentration-control coefficients without needing any enzymes/proteins to be isolated and characterised, and regardless of feedback mechanisms (for instance amino acid feedback on mTOR) and moiety conservation (autolysosomes and lysosomes pool). By plotting the combined log-log rate characteristics we could visualise the distribution of flux- and concentration-control around the steady state, providing insight about system behaviour under normal physiological conditions. This approach presents a promising way forward in characterising autophagy in diseased cells that would guide the development of effective autophagy-targeting therapies.

## 7.7 Paving the way towards assessing autophagy *in vivo*

The important role of autophagy in pathology has generated extensive research to develop autophagy targeting therapies, especially for neurodegenerative diseases where the loss of autophagy function results in the build-up of toxic compounds, and ultimately neuronal death [176, 240, 260]. Yet, little is known about the distribution of autophagy throughout the brain under normal physiological conditions and how it impacts disease progression in the three-dimensional neuroanatomical context. The success of these therapies depend on an in-depth understanding of the precise role of autophagy on a cellular level and whole organ level.

Recently, novel techniques that allow for live cell imaging of *in vivo* neurons have been developed [95, 241]. Despite their benefits, their spacial resolution and capacity to label proteins of interest still pose serious limits. An advanced tissue-clearing technique, termed CLARITY, captures cellular components *in situ* in

Stellenbosch University https://scholar.sun.ac.za



an optically transparent hydrogel matrix, enabling three-dimensional imaging of whole brain tissue to assess the organisational distribution of autophagy markers in the overall global context of the brain.

We developed a relatively simple and cost-effective solution to brain tissue clearing, utilising materials readily available in a basic laboratory setting that also caters for 3D printing of sample chambers. It satisfactorily cleared tissue samples for fluorescence microscopy without causing damage to their delicate features, allowing brain tissue to be visualised in a three-dimensional neuroanatomical context. More importantly with regard to autophagy, we were able to achieve single cell resolution in these samples, identifying autophagy pathway intermediates such as autophagosomes and lysosomes as well as protein cargo. These results demonstrate that autophagic flux analysis *in vivo* with high precision as demonstrated in Chapter 4 is indeed possible.

## 7.8 Concluding remarks

The major focus on autophagy in recent years, driven by the hope of exploiting it for therapeutic purposes, has led to the development of novel tools and techniques to assess this process. The method described and applied here allows for the quantification of autophagosome flux and its steady state intermediates in a reliable manner. The capacity to detect small changes in the autophagy variables makes it an ideal method for characterising autophagy-modulating drugs. Furthermore, its design makes it suitable for high-throughput platforms and is flexibile enough to accommodate a wide range of probes. Data generated by this method, in combination with a computational approach, can contribute to our understanding of the autophagy system and its role in healthy cells and disease progression, and so guide the development of safe and effective autophagy-targeting therapies.

Despite the usefulness of our approach, it remains a challenging task to implement it in a clinical setting. The biomarkers identified in this study may serve as a starting point for developing assays that are more suitable in a clinical setting to assess autophagosome flux and cytosolic turnover. Future work would require

Stellenbosch University https://scholar.sun.ac.za



extensive testing of these markers to determine their robustness on reporting autophagosome flux and cytosolic turnover. If shown to be specific and reliable, it would allow clinicians to easily measure the autophagy activity for screening, diagnostic and therapeutic interventions.

In-depth understanding of the precise role of autophagy in healthy and disease states on both a cellular level and whole organ level would be important to the success of autophagy targeting therapies. This is particularly relevant in the case of neurodegenerative diseases, where the loss of autophagy function results in the build-up of toxic compounds that begin in one particular region and spread throughout the brain. Here we showed that advanced fluorescence-hydrogel imaging techniques may present a useful tool to characterise autophagy in the brain with single cell resolution. This may guide in the selection of drugs based on their regional effects on autophagy for precision targeting.

Stellenbosch University https://scholar.sun.ac.za

# Bibliography

[1] Abedin, M. J., Wang, D., McDonnell, M. A., Lehmann, U. and Kelekar, A. [2007] "Autophagy delays apoptotic death in breast cancer cells following DNA damage" *Cell Death Differ.* **14**, 500–510.

[2] Aita, V. M., Liang, X. H., Murty, V., Pincus, D. L., Yu, W., Cayanis, E., Kalachikov, S., Gilliam, T. C. and Levine, B. [1999] "Cloning and genomic organization of Beclin 1, a candidate tumor suppressor gene on chromosome 17q21" *Genomics* **59**, 59–65.

[3] Alirezaei, M., Kemball, C. C., Flynn, C. T., Wood, M. R., Whitton, J. L. and Kiosses, W. B. [2010] "Short-term fasting induces profound neuronal autophagy" *Autophagy* **6**, 702–710.

[4] Alirezaei, M., Kiosses, W. B., Flynn, C. T., Brady, N. R. and Fox, H. S. [2008] "Disruption of neuronal autophagy by infected microglia results in neurodegeneration" *PloS one* **3**, e2906.

[5] Alves, S., Cormier-Dequaire, F., Marinello, M., Marais, T., Muriel, M.-P., Beaumatin, F., Charbonnier-Beaupel, F., Tahiri, K., Seilhean, D., El Hachimi, K. *et al.* [2014] "The autophagy/lysosome pathway is impaired in sca7 patients and sca7 knock-in mice" *Acta neuropathologica* **128**, 705–722.

[6] Amaravadi, R. K., Yu, D., Lum, J. J., Bui, T., Christophorou, M. A., Evan, G. I., Thomas-Tikhonenko, A. and Thompson, C. B. [2007] "Autophagy

Stellenbosch University https://scholar.sun.ac.za



inhibition enhances therapy-induced apoptosis in a Myc-induced model of lymphoma" *J. Clin. Invest.* **117**, 326.

[7] Amaya, C., Fader, C. M. and Colombo, M. I. [2015] "Autophagy and proteins involved in vesicular trafficking" *FEBS letters* **589**, 3343–3353.

[8] Antonioli, M., Di Rienzo, M., Piacentini, M. and Fimia, G. M. [2017] "Emerging mechanisms in initiating and terminating autophagy" *Trends in biochemical sciences* **42**, 28–41.

[9] Arrasate, M., Mitra, S., Schweitzer, E. S., Segal, M. R. and Finkbeiner, S. [2004] "Inclusion body formation reduces levels of mutant huntingtin and the risk of neuronal death" *Nature* **431**, 805–810.

[10] Atkinson, D. E. and Walton, G. M. [1967] "Adenosine triphosphate conservation in metabolic regulation rat liver citrate cleavage enzyme" *J. Biol. Chem.* **242**, 3239–3241.

[11] Avni, D., Glucksam, Y. and Zor, T. [2012] "The Phosphatidylinositol 3-kinase (PI3k) inhibitor LY294002 modulates cytokine expression in macrophages via p50 nuclear factor kappa B inhibition, in a PI3k-independent mechanism" *Biochemical Pharmacology* **83**, 106–114.

[12] Axe, E. L., Walker, S. A., Manifava, M., Chandra, P., Roderick, H. L., Habermann, A., Griffiths, G. and Ktistakis, N. T. [2008] "Autophagosome formation from membrane compartments enriched in phosphatidylinositol 3-phosphate and dynamically connected to the endoplasmic reticulum" *J. Cell Biol.* **182**, 685–701.

[13] Bachar-Wikstrom, E., Wikstrom, J. D., Ariav, Y., Tirosh, B., Kaiser, N., Cerasi, E. and Leibowitz, G. [2013] "Stimulation of autophagy improves endoplasmic reticulum stress–induced diabetes" *Diabetes* **62**, 1227–1237.

[14] Baldo, B., Soylu, R. and Petersén, Å. [2013] "Maintenance of basal levels of autophagy in huntington's disease mouse models displaying metabolic dysfunction" *PLoS One* **8**, e83050.

Stellenbosch University https://scholar.sun.ac.za



[15] Bampton, E. T. W., Goemans, C. G., Niranjan, D., Mizushima, N. and Tolkovsky, A. M. [2005] "The dynamics of autophagy visualized in live cells: from autophagosome formation to fusion with endo/lysosomes" *Autophagy* **1**, 23–36.

[16] Bandyopadhyay, D., Cyphersmith, A., Zapata, J. A., Kim, Y. J. and Payne, C. K. [2014] "Lysosome transport as a function of lysosome diameter" *PloS one* **9**, e86847.

[17] Behrends, C., Sowa, M. E., Gygi, S. P. and Harper, J. W. [2010] "Network organization of the human autophagy system" *Nature* **466**, 68–76.

[18] Bellot, G., Garcia-Medina, R., Gounon, P., Chiche, J., Roux, D., Pouysségur, J. and Mazure, N. M. [2009] "Hypoxia-induced autophagy is mediated through hypoxia-inducible factor induction of BNIP3 and BNIP3L via their BH3 domains" *Mol. Cell. Biol.* **29**, 2570–2581.

[19] Bihan, M.-C. L., Bigot, A., Jensen, S. S., Dennis, J. L., Rogowska-Wrzesinska, A., Lainé, J., Gache, V., Furling, D., Jensen, O. N., Voit, T., Mouly, V., Coulton, G. R. and Butler-Browne, G. [2012] "In-depth analysis of the secretome identifies three major independent secretory pathways in differentiating human myoblasts" *Journal of proteome research* **77**, 344–356.

[20] Birgisdottir, Å. B., Lamark, T. and Johansen, T. [2013] "The LIR motif–crucial for selective autophagy" *J Cell Sci* **126**, 3237–3247.

[21] Bjorkoy, G. [2005] "p62/SQSTM1 forms protein aggregates degraded by autophagy and has a protective effect on huntingtin-induced cell death" *J. Cell Biol.* **171**, 603–614.

[22] Börlin, C. S., Lang, V., Hamacher-Brady, A. and Brady, N. R. [2014] "Agent-based modeling of autophagy reveals emergent regulatory behavior of spatio-temporal autophagy dynamics" *Cell Commun Signal* **12**, 56.

[23] Botti, J., Djavaheri-Mergny, M., Pilatte, Y. and Codogno, P. [2006] "Autophagy signaling and the cogwheels of cancer" *Autophagy* **2**, 67–73.

Stellenbosch University https://scholar.sun.ac.za



[24] Brugarolas, J., Lei, K., Hurley, R. L., Manning, B. D., Reiling, J. H., Hafen, E., Witters, L. A., Ellisen, L. W. and Kaelin, W. G. [2004] "Regulation of mTOR function in response to hypoxia by REDD1 and the TSC1/TSC2 tumor suppressor complex" *Genes Dev.* **18**, 2893–2904.

[25] Caia, Z. and Yanb, L.-J. [2013] "Rapamycin, autophagy, and Alzheimer's disease" *J. Biochem. Pharmacol. Res.* **1**, 84–90.

[26] Carew, J. S., Nawrocki, S. T., Kahue, C. N., Zhang, H., Yang, C., Chung, L., Houghton, J. A., Huang, P., Giles, F. J. and Cleveland, J. L. [2007] "Targeting autophagy augments the anticancer activity of the histone deacetylase inhibitor SAHA to overcome Bcr-Abl–mediated drug resistance" *Blood* **110**, 313–322.

[27] Carlsson, S. R. and Simonsen, A. [2015] "Membrane dynamics in autophagosome biogenesis" *J Cell Sci* **128**, 193–205.

[28] Carpi, N., Piel, M., Azioune, A. and Fink, J. [2011] "Micropatterning on glass with deep uv" *Nature Protocol Exchange* **10**.

[29] Chalkiadaki, A. and Guarente, L. [2012] "Sirtuins mediate mammalian metabolic responses to nutrient availability" *Nature Reviews Endocrinology* **8**, 287–296.

[30] Chen, D., Fan, W., Lu, Y., Ding, X., Chen, S. and Zhong, Q. [2012] "A mammalian autophagosome maturation mechanism mediated by tecpr1 and the atg12-atg5 conjugate" *Mol. Cell* **45**, 629–641.

[31] Chen, Y., McMillan-Ward, E., Kong, J., Israels, S. J. and Gibson, S. B. [2007] "Oxidative stress induces autophagic cell death independent of apoptosis in transformed and cancer cells" *Cell Death Differ.* **15**, 171–182.

[32] Cheong, H., Lindsten, T., Wu, J., Lu, C. and Thompson, C. B. [2011] "Ammonia-induced autophagy is independent of ULK1/ULK2 kinases" *Proc. Natl. Acad. Sci. U.S.A.* **108**, 11121–11126.

Stellenbosch University https://scholar.sun.ac.za



[33] Chin, R. M., Fu, X., Pai, M. Y., Vergnes, L., Hwang, H., Deng, G., Diep, S., Lomenick, B., Meli, V. S., Monsalve, G. C., Hu, E., Whelan, S. A., Wang, J. X., Jung, G., Solis, G. M., Fazlollahi, F., Kaweeteerawat, C., Quach, A., Nili, M., Krall, A. S., Godwin, H. A., Chang, H. R., Faull, K. F., Guo, F., Jiang, M., Trauger, S. A., Saghatelian, A., Braas, D., Christofk, H. R., Clarke, C. F., Teitell, M. A., Petrascheck, M., Reue, K., Jung, M. E., Frand, A. R. and Huang, J. [2014] "The metabolite $\alpha$-ketoglutarate extends lifespan by inhibiting ATP synthase and TOR" *Nature* **510**, 397–401.

[34] Choi, A. M., Ryter, S. W. and Levine, B. [2013] "Autophagy in human health and disease" *N. Engl. J. Med.* **368**, 651–662.

[35] Choi, Y. J., Park, Y. J., Park, J. Y., Jeong, H. O., Kim, D. H., Ha, Y. M., Kim, J. M., Song, Y. M., Heo, H.-S., Yu, B. P., Chun, P., Moon, H. R. and Chung, H. Y. [2012] "Inhibitory effect of mTOR activator MHY1485 on autophagy: suppression of lysosomal fusion" *PLoS ONE* **7**, 43418.

[36] Chourasia, A. H., Tracy, K., Frankenberger, C., Boland, M. L., Sharifi, M. N., Drake, L. E., Sachleben, J. R., Asara, J. M., Locasale, J. W., Karczmar, G. S. *et al.* [2015] "Mitophagy defects arising from BNip3 loss promote mammary tumor progression to metastasis" *EMBO reports* **16**, 1145–1163.

[37] Chung, K. and Deisseroth, K. [2013] "CLARITY for mapping the nervous system" *Nature methods* **10**, 508–513.

[38] Ciechomska, I., Goemans, G., Skepper, J. and Tolkovsky, A. [2009] "Bcl-2 complexed with Beclin-1 maintains full anti-apoptotic function" *Oncogene* **28**, 2128–2141.

[39] Clark, S. L. [1957] "Cellular differentiation in the kidneys of newborn mice studied with the electron microscope" *J. Biophys. Biochem. Cytol.* **3**, 349–362.

[40] Cook, K. L., Wärri, A., Soto-Pantoja, D. R., Clarke, P. A., Cruz, M. I., Zwart, A. and Clarke, R. [2014] "Chloroquine Inhibits Autophagy to Poten-

Stellenbosch University https://scholar.sun.ac.za



tiate Antiestrogen Responsiveness in ER+ Breast Cancer" *Clinical Cancer Research* **20**, 3222–3232.

[41] Criollo, A., Niso-Santano, M., Malik, S. A., Michaud, M., Morselli, E., Mariño, G., Lachkar, S., Arkhipenko, A. V., Harper, F., Pierron, G., Rain, J.-C., Ninomiya-Tsuji, J., Fuentes, J. M., Lavandero, S., Galluzzi, L., Maiuri, M. C. and Kroemer, G. [2011] "Inhibition of autophagy by TAB2 and TAB3" *EMBO J.* **30**, 4908–4920.

[42] Cuervo, A. M., Bergamini, E., Brunk, U. T., Dröge, W., Ffrench, M. and Terman, A. [2005] "Autophagy and aging: the importance of maintaining "clean" cells" *Autophagy* **1**, 131–140.

[43] Cuervo, A. M., Stefanis, L., Fredenburg, R., Lansbury, P. T. and Sulzer, D. [2004] "Impaired degradation of mutant $\alpha$-synuclein by chaperone-mediated autophagy" *Science* **305**, 1292–1295.

[44] de Duve, C. and Wattiaux, R. [1966] "Functions of lysosomes" *Annu. Rev. Physiol.* **28**, 435–492.

[45] Degasperi, A., Birtwistle, M. R., Volinsky, N., Rauch, J., Kolch, W. and Kholodenko, B. N. [2014] "Evaluating strategies to normalise biological replicates of western blot data" *PloS one* **9**, e87293.

[46] Del Roso, A., Vittorini, S., Cavallini, G., Donati, A., Gori, Z., Masini, M., Pollera, M. and Bergamini, E. [2003] "Ageing-related changes in the in vivo function of rat liver macroautophagy and proteolysis" *Exp. Gerontol.* **38**, 519–527.

[47] Denk, W. and Horstmann, H. [2004] "Serial block-face scanning electron microscopy to reconstruct three-dimensional tissue nanostructure" *PLoS biology* **2**, e329.

[48] Devasagayam, T., Tilak, J., Boloor, K., Sane, K. S., Ghaskadbi, S. S. and Lele, R. [2004] "Free radicals and antioxidants in human health: current status and future prospects" *Japi* **52**, 794–804.

Stellenbosch University https://scholar.sun.ac.za



[49] Diao, J., Liu, R., Rong, Y., Zhao, M., Zhang, J., Lai, Y., Zhou, Q., Wilz, L. M., Li, J., Vivona, S. *et al.* [2015] "ATG14 promotes membrane tethering and fusion of autophagosomes to endolysosomes" *Nature* **520**, 563.

[50] du Toit, A., Hofmeyr, J.-H. S., Gniadek, T. J. and Loos, B. [2018] "Measuring autophagosome flux" *Autophagy* **14**, 1060–1071 PMID: 29909716.

[51] Durán, R., MacKenzie, E., Boulahbel, H., Frezza, C., Heiserich, L., Tardito, S., Bussolati, O., Rocha, S., Hall, M. and Gottlieb, E. [2013] "HIF-independent role of prolyl hydroxylases in the cellular response to amino acids" *Oncogene* **32**, 4549–4556.

[52] Durán, R. V., Oppliger, W., Robitaille, A. M., Heiserich, L., Skendaj, R., Gottlieb, E. and Hall, M. N. [2012] "Glutaminolysis activates Rag-mTORC1 signaling" *Mol. Cell.* **47**, 349–358.

[53] Egan, D. F., Chun, M. G. H., Vamos, M., Zou, H., Rong, J., Miller, C. J., Lou, H. J., Raveendra-Panickar, D., Yang, C.-C., Sheffler, D. J., Teriete, P., Asara, J. M., Turk, B. E., Cosford, N. D. P. and Shaw, R. J. [2015] "Small molecule inhibition of the autophagy kinase ulk1 and identification of ulk1 substrates." *Molecular cell* **59**, 285–297.

[54] Egan, D. F., Shackelford, D. B., Mihaylova, M. M., Gelino, S., Kohnz, R. A., Mair, W., Vasquez, D. S., Joshi, A., Gwinn, D. M., Taylor, R. *et al.* [2011] "Phosphorylation of ULK1 (hATG1) by AMP-activated protein kinase connects energy sensing to mitophagy" *Science* **331**, 456–461.

[55] Eisenberg, T., Knauer, H., Schauer, A., Büttner, S., Ruckenstuhl, C., Carmona-Gutierrez, D., Ring, J., Schroeder, S., Magnes, C., Antonacci, L., Fussi, H., Deszcz, L., Hartl, R., Schraml, E., Criollo, A., Megalou, E., Weiskopf, D., Laun, P., Heeren, G., Breitenbach, M., Grubeck-Loebenstein, B., Herker, E., Fahrenkrog, B., Fröhlich, K.-U., Sinner, F., Tavernarakis, N., Minois, N., Kroemer, G. and Madeo, F. [2009] "Induction of autophagy by spermidine promotes longevity" *Nat. Cell. Biol.* **11**, 1305–1314.

Stellenbosch University https://scholar.sun.ac.za



[56] Eisenberg, T., Schroeder, S., Andryushkova, A., Pendl, T., Küttner, V., Bhukel, A., Mariño, G., Pietrocola, Eisenberg, T., Schroeder, S., Andryushkova, A., Pendl, T., K uttner, V., Bhukel, A., Mariño, G., Pietrocola, F., Harger, A., Zimmermann, A., Moustafa, T., Sprenger, A., Jany, E., B uttner, S., Carmona-Gutierrez, D., Ruckenstuhl, C., Ring, J., Reichelt, W., Schimmel, K., Leeb, T., Moser, C., Schatz, S., Kamolz, L., Magnes, C., Sinner, F., Sedej, S., Fr ohlich, K. U., Juhasz, G., Pieber, T. R., Dengjel, J., Sigrist, S. J., Kroemer, G. and Madeo, F. [2014] "Nucleocytosolic depletion of the energy metabolite acetyl-coenzyme a stimulates autophagy and prolongs lifespan" *Cell Metab.* **19**, 431–444.

[57] Eng, C. H., Yu, K., Lucas, J., White, E. and Abraham, R. T. [2010] "Ammonia derived from glutaminolysis is a diffusible regulator of autophagy" *Science Signaling* **3**, 31.

[58] Eschbach, J. and Dupuis, L. [2011] "Cytoplasmic dynein in neurodegeneration" *Pharmacol. Ther.* **130**, 348–363.

[59] Eskelinen, E.-L., Cuervo, A. M., Taylor, M. R., Nishino, I., Blum, J. S., Dice, J. F., Sandoval, I. V., Lippincott-Schwartz, J., August, J. T. and Saftig, P. [2005] "Unifying nomenclature for the isoforms of the lysosomal membrane protein LAMP-2" *Traffic* **6**, 1058–1061.

[60] Fader, C. M., Sánchez, D. G., Mestre, M. B. and Colombo, M. I. [2009] "TI-VAMP/VAMP7 and VAMP3/cellubrevin: two v-SNARE proteins involved in specific steps of the autophagy/multivesicular body pathways" *Biochimica et Biophysica Acta (BBA)-Molecular Cell Research* **1793**, 1901–1916.

[61] Fan, W., Nassiri, A. and Zhong, Q. [2011] "Autophagosome targeting and membrane curvature sensing by barkor/atg14 (l)" *Proceedings of the National Academy of Sciences* **108**, 7769–7774.

[62] Farré, J.-C. and Subramani, S. [2016] "Mechanistic insights into selective autophagy pathways: lessons from yeast" *Nature reviews Molecular cell biology* **17**, nrm–2016.

Stellenbosch University https://scholar.sun.ac.za



[63] Feng, Y., He, D., Yao, Z. and Klionsky, D. J. [2013] "The machinery of macroautophagy" *Cell Res.* **24**, 24–41.

[64] Fracchiolla, D., Sawa-Makarska, J., Zens, B., de Ruiter, A., Zaffagnini, G., Brezovich, A., Romanov, J., Runggatscher, K., Kraft, C., Zagrovic, B. *et al.* [2016] "Mechanism of cargo-directed Atg8 conjugation during selective autophagy" *Elife* **5**.

[65] Galluzzi, L., Baehrecke, E. H., Ballabio, A., Boya, P., Bravo-San Pedro, J. M., Cecconi, F., Choi, A. M., Chu, C. T., Codogno, P., Colombo, M. I. *et al.* [2017] "Molecular definitions of autophagy and related processes" *The EMBO journal* **36**, 1811–1836.

[66] Galluzzi, L., Bravo-San Pedro, J. M., Levine, B., Green, D. R. and Kroemer, G. [2017] "Pharmacological modulation of autophagy: therapeutic potential and persisting obstacles" *Nat. Rev. Drug Discovery* **16**, 487.

[67] Galluzzi, L., Bravo-San Pedro, J. M., Vitale, I., Aaronson, S. A., Abrams, J. M., Adam, D., Alnemri, E. S., Altucci, L., Andrews, D., Annicchiarico-Petruzzelli, M. and others. [2015] "Essential versus accessory aspects of cell death: recommendations of the NCCD 2015" *Cell Death Differ.* **22**, 58–73.

[68] Geng, J. and Klionsky, D. J. [2008] "The Atg8 and Atg12 ubiquitin-like conjugation systems in macroautophagy" *EMBO Rep.* **9**, 859–864.

[69] Giaccia, A. J., Simon, M. C. and Johnson, R. [2004] "The biology of hypoxia: the role of oxygen sensing in development, normal function, and disease" *Genes & Development* **18**, 2183–2194.

[70] Giatromanolaki, A., Koukourakis, M. I., Koutsopoulos, A., Chloropoulou, P., Liberis, V. and Sivridis, E. [2011] "High Beclin 1 expression defines a poor prognosis in endometrial adenocarcinomas" *Gynecol. Oncol.* **123**, 147–151.

Stellenbosch University https://scholar.sun.ac.za



[71] Gniadek, T. J. and Warren, G. [2007] "WatershedCounting3D: A new method for segmenting and counting punctate structures from confocal image data" *Traffic* **8**, 339–346.

[72] González-Rodríguez, Á., Mayoral, R., Agra, N., Valdecantos, M., Pardo, V., Miquilena-Colina, M., Vargas-Castrillón, J., Iacono, O. L., Corazzari, M., Fimia, G. *et al.* [2014] "Impaired autophagic flux is associated with increased endoplasmic reticulum stress during the development of NAFLD" *Cell death and disease* **5**, e1179.

[73] Guo, J. Y., Xia, B. and White, E. [2013] "Autophagy-mediated tumor promotion" *Cell* **155**, 1216–1219.

[74] Gutierrez, M. G., Munafó, D. B., Berón, W. and Colombo, M. I. [2004] "Rab7 is required for the normal progression of the autophagic pathway in mammalian cells" *Journal of cell science* **117**, 2687–2697.

[75] Hageman, J., van Waarde, M. A., Zylicz, A., Walerych, D. and Kampinga, H. H. [2011] "The diverse members of the mammalian hsp70 machine show distinct chaperone-like activities" *Biochemical Journal* **435**, 127–142.

[76] Haigis, M. C. and Sinclair, D. A. [2010] "Mammalian sirtuins: biological insights and disease relevance" *Annual Review of Pathological Mechanical Disease* **5**, 253–295.

[77] Han, D., Williams, E. and Cadenas, E. [2001] "Mitochondrial respiratory chain-dependent generation of superoxide anion and its release into the intermembrane space" *Biochem. J.* **353**, 411–416.

[78] Han, K., Kim, J. and Choi, M. [2014] "Computer simulations unveil the dynamics of autophagy and its implications for the cellular quality control" *J. Biol. Syst.* **22**, 659–675.

[79] Han, K., Kim, J. and Choi, M. [2014] "Quantitative indices of autophagy activity from minimal models" *Theoretical Biology and Medical Modelling* **11**, 31.

Stellenbosch University https://scholar.sun.ac.za



[80] Han, K., Kim, J. and Choi, M. [2015] "Autophagy mediates phase transitions from cell death to life" *Heliyon* **1**, e00027.

[81] Han, K., Kwon, H. W., Kang, H., Kim, J., Lee, M.-S. and Choi, M. [2012] "Dynamics of macroautophagy: Modeling and oscillatory behavior" *Physica A* **391**, 686–692.

[82] Hanada, T., Noda, N. N., Satomi, Y., Ichimura, Y., Fujioka, Y., Takao, T., Inagaki, F. and Ohsumi, Y. [2007] "The Atg12-Atg5 conjugate has a novel E3-like activity for protein lipidation in autophagy" *J. Biol. Chem.* **282**, 37298–37302.

[83] Hara, T., Nakamura, K., Matsui, M., Yamamoto, A., Nakahara, Y., Suzuki-Migishima, R., Yokoyama, M., Mishima, K., Saito, I. and Okano, H. [2006] "Suppression of basal autophagy in neural cells causes neurodegenerative disease in mice" *Nature* **441**, 885–889.

[84] Hara, T., Takamura, A., Kishi, C., Iemura, S.-i., Natsume, T., Guan, J.-L. and Mizushima, N. [2008] "FIP200, a ULK-interacting protein, is required for autophagosome formation in mammalian cells" *J. Cell Biol.* **181**, 497–510.

[85] Harder, L. M., Bunkenborg, J. and Andersen, J. S. [2014] "Inducing autophagy: a comparative phosphoproteomic study of the cellular response to ammonia and rapamycin" *Autophagy* **10**, 339–355.

[86] Hardie, D. G., Ross, F. A. and Hawley, S. A. [2012] "AMPK: a nutrient and energy sensor that maintains energy homeostasis" *Nat. Rev. Mol. Cell. Biol.* **13**, 251–262.

[87] Harding, H. P., Zhang, Y., Zeng, H., Novoa, I., Lu, P. D., Calfon, M., Sadri, N., Yun, C., Popko, B., Paules, R. *et al.* [2003] "An integrated stress response regulates amino acid metabolism and resistance to oxidative stress" *Molecular cell* **11**, 619–633.

Stellenbosch University https://scholar.sun.ac.za



[88] Hasegawa, J., Iwamoto, R., Otomo, T., Nezu, A., Hamasaki, M. and Yoshimori, T. [2016] "Autophagosome–lysosome fusion in neurons requires inpp5e, a protein associated with joubert syndrome" *The EMBO journal* **35**, 1853–1867.

[89] He, C. and Klionsky, D. J. [2009] "Regulation mechanisms and signaling pathways of autophagy" *Annu. Rev. Genet.* **43**, 67–93.

[90] Heilbronn, L. K. and Ravussin, E. [2003] "Calorie restriction and aging: review of the literature and implications for studies in humans" *Am. J. Clin. Nutr.* **78**, 361–369.

[91] Heiseke, A., Aguib, Y., Riemer, C., Baier, M. and Schätzl, H. M. [2009] "Lithium induces clearance of protease resistant prion protein in prion-infected cells by induction of autophagy" *J. Neurochem.* **109**, 25–34.

[92] Hofmeyr, J.-H. S. [2001] "Metabolic control analysis in a nutshell" in *Proceedings of the 2nd International Conference on systems Biology* pp. 291–300.

[93] Hofmeyr, J.-H. S. and Cornish-Bowden, A. [1996] "Co-response analysis: a new experimental strategy for metabolic control analysis" *J. Theor. Biol.* **182**, 371–380.

[94] Hofmeyr, J.-H. S. and Cornish-Bowden., A. [2000] "Regulating the cellular economy of supply and demand" *FEBS Lett.* **476**, 47–51.

[95] Hong, G., Diao, S., Chang, J., Antaris, A. L., Chen, C., Zhang, B., Zhao, S., Atochin, D. N., Huang, P. L., Andreasson, K. I., Kuo, C. J. and Dai, H. [2014] "Through-skull fluorescence imaging of the brain in a new near-infrared window." *Nature photonics* **8**, 723–730.

[96] Hosokawa, N., Hara, T., Kaizuka, T., Kishi, C., Takamura, A., Miura, Y., Iemura, S.-i., Natsume, T., Takehana, K., Yamada, N. and others. [2009] "Nutrient-dependent mTORC1 association with the ULK1–Atg13–FIP200 complex required for autophagy" *Mol. Biol. Cell* **20**, 1981–1991.

Stellenbosch University https://scholar.sun.ac.za



[97] Hotamisligil, G. S. [2010] "Endoplasmic reticulum stress and the inflammatory basis of metabolic disease" *Cell* **140**, 900–917.

[98] Houtkooper, R. H., Pirinen, E. and Auwerx, J. [2012] "Sirtuins as regulators of metabolism and healthspan" *Nat. Rev. Mol. Cell. Biol.* **13**, 225–238.

[99] Hu, M., Huang, H., Zhao, R., Li, P., Li, M., Miao, H., Chen, N. and Chen, M. [2014] "AZD8055 induces cell death associated with autophagy and activation of AMPK in hepatocellular carcinoma" *Oncology reports* **31**, 649–656.

[100] Huang, J. and Klionsky, D. J. [2007] "Autophagy and human disease" *Cell Cycle* **6**, 1837–1849.

[101] Huang, S.-P., Chien, J.-Y. and Tsai, R.-K. [2015] "Ethambutol induces impaired autophagic flux and apoptosis in the retina" *Disease models & mechanisms* pp. dmm–019737.

[102] Hutson, N. and Mortimore, G. E. [1982] "Suppression of cytoplasmic protein uptake by lysosomes as the mechanism of protein regain in livers of starved-refed mice" *J. Biol. Chem.* **257**, 9548–9554.

[103] Inoki, K., Li, Y., Zhu, T., Wu, J. and Guan, K.-L. [2002] "Tsc2 is phosphorylated and inhibited by akt and suppresses mtor signalling" *Nature cell biology* **4**, 648.

[104] Inokuchi-Shimizu, S., Park, E. J., Roh, Y. S., Yang, L., Zhang, B., Song, J., Liang, S., Pimienta, M., Taniguchi, K., Wu, X., Asahina, K. and others. [2014] "TAK1-mediated autophagy and fatty acid oxidation prevent hepatosteatosis and tumorigenesis" *J. Clin. Invest.* **124**, 3566–3578.

[105] Irvine, G. and El-Agnaf, O. [2008] "Suppression of basal autophagy in neural cells causes neurodegenerative disease in mice" *Mol. Med.* **14**, 1.

[106] Itakura, E., Kishi, C., Inoue, K. and Mizushima, N. [2008] "Beclin 1 forms two distinct phosphatidylinositol 3-kinase complexes with mammalian Atg14 and UVRAG" *Mol. Biol. Cell* **19**, 5360–5372.

Stellenbosch University https://scholar.sun.ac.za



[107] Itakura, E., Kishi-Itakura, C. and Mizushima, N. [2012] "The hairpin-type tail-anchored SNARE syntaxin 17 targets to autophagosomes for fusion with endosomes/lysosomes" *Cell* **151**, 1256–1269.

[108] Iwai-Kanai, E., Yuan, H., Huang, C., Sayen, M. R., Perry-Garza, C. N., Kim, L. and Gottlieb, R. A. [2008] "A method to measure cardiac autophagic flux in vivo" *Autophagy* **4**, 322–329.

[109] Iwata, A., Riley, B. E., Johnston, J. A. and Kopito, R. R. [2005] "HDAC6 and microtubules are required for autophagic degradation of aggregated huntingtin" *J. Biol. Chem.* **280**, 40282–40292.

[110] Jäger, S., Bucci, C., Tanida, I., Ueno, T., Kominami, E., Saftig, P. and Eskelinen, E.-L. [2004] "Role for Rab7 in maturation of late autophagic vacuoles" *J. Cell. Sci.* **117**, 4837–4848.

[111] Jahreiss, L., Menzies, F. M. and Rubinsztein, D. C. [2008] "The itinerary of autophagosomes: from peripheral formation to kiss-and-run fusion with lysosomes" *Traffic* **9**, 574–587.

[112] Janku, F., McConkey, D. J., Hong, D. S. and Kurzrock, R. [2011] "Autophagy as a target for anticancer therapy" *Nature Reviews Clinical Oncology* **8**, 528–539.

[113] Jiang, P. and Mizushima, N. [2013] "Autophagy and human diseases" *Cell Res.* **24**, 69–79.

[114] Jin, H. and Lei, J. [2014] "A mathematical model of cell population dynamics with autophagy response to starvation" *Math. Biosci.* **258**, 1–10.

[115] Jin, M. and Klionsky, D. J. [2014] "Regulation of autophagy: modulation of the size and number of autophagosomes" *FEBS letters* **588**, 2457–2463.

[116] Jung, C. H., Jun, C. B., Ro, S.-H., Kim, Y.-M., Otto, N. M., Cao, J., Kundu, M. and Kim, D.-H. [2009] "ULK-Atg13-FIP200 complexes mediate mTOR signaling to the autophagy machinery" *Mol. Biol. Cell* **20**, 1992–2003.

Stellenbosch University https://scholar.sun.ac.za



[117] Jung, C. H., Ro, S.-H., Cao, J., Otto, N. M. and Kim, D.-H. [2010] "mtor regulation of autophagy" *FEBS Lett* **584**, 1287–1295.

[118] Kabeya, Y., Mizushima, N., Ueno, T., Yamamoto, A., Kirisako, T., Noda, T., Kominami, E., Ohsumi, Y. and Yoshimori, T. [2000] "LC3, a mammalian homologue of yeast Apg8p, is localized in autophagosome membranes after processing" *EMBO J.* **19**, 5720–5728.

[119] Kacser, H., Burns, J. and Fell, D. [1995] "The control of flux: 21 years on" *Biochem. Soc. Trans.* **23**, 341–366.

[120] Kaizuka, T., Morishita, H., Hama, Y., Tsukamoto, S., Matsui, T., Toyota, Y., Kodama, A., Ishihara, T., Mizushima, T. and Mizushima, N. [2016] "An autophagic flux probe that releases an internal control" *Mol. Cell* **17**, 835–849.

[121] Kapuy, O., Vinod, P. K., Mandl, J. and Bánhegyi, G. [2013] "A cellular stress-directed bistable switch controls the crosstalk between autophagy and apoptosis" *Mol. BioSyst.* **9**, 296–306.

[122] Karanasios, E., Stapleton, E., Manifava, M., Kaizuka, T., Mizushima, N., Walker, S. A. and Ktistakis, N. T. [2013] "Dynamic association of the ULK1 complex with omegasomes during autophagy induction" *J Cell Sci* **126**, 5224–5238.

[123] Kato, H., Takahashi, S.-I., Takenaka, A., Funabiki, R., Noguchi, T. and Naito, H. [1989] "Degradation of endogenous proteins and internalized asialofetuin in primary cultured hepatocytes of rats" *Int. J. Biochem.* **21**, 483–495.

[124] Kaushik, S., Rodriguez-Navarro, J. A., Arias, E., Kiffin, R., Sahu, S., Schwartz, G. J., Cuervo, A. M. and Singh, R. [2011] "Autophagy in hypothalamic agrp neurons regulates food intake and energy balance" *Cell metabolism* **14**, 173–183.

Stellenbosch University https://scholar.sun.ac.za



[125] Khaminets, A., Behl, C. and Dikic, I. [2016] "Ubiquitin-dependent and independent signals in selective autophagy" *Trends in cell biology* **26**, 6–16.

[126] Kihara, A., Kabeya, Y., Ohsumi, Y. and Yoshimori, T. [2001] "Beclin–phosphatidylinositol 3-kinase complex functions at the trans-Golgi network" *EMBO reports* **2**, 330–335.

[127] Kihara, A., Noda, T., Ishihara, N. and Ohsumi, Y. [2001] "Two distinct VPS34 phosphatidylinositol 3–kinase complexes function in autophagy and carboxypeptidase Y sorting in Saccharomyces Cerevisiae" *J. Cell Biol.* **152**, 519–530.

[128] Kim, D.-H., Sarbassov, D. D., Ali, S. M., King, J. E., Latek, R. R., Erdjument-Bromage, H., Tempst, P. and Sabatini, D. M. [2002] "mTOR interacts with raptor to form a nutrient-sensitive complex that signals to the cell growth machinery" *Cell* **110**, 163–175.

[129] Kim, D.-H., Sarbassov, D. D., Ali, S. M., Latek, R. R., Guntur, K. V. P., Erdjument-Bromage, H., Tempst, P. and Sabatini, D. M. [2003] "Gbetal, a positive regulator of the rapamycin-sensitive pathway required for the nutrient-sensitive interaction between raptor and mtor." *Molecular cell* **11**, 895–904.

[130] Kim, J., Kim, Y. C., Fang, C., Russell, R. C., Kim, J. H., Fan, W., Liu, R., Zhong, Q. and Guan, K.-L. [2013] "Differential regulation of distinct VPS34 complexes by AMPK in nutrient stress and autophagy" *Cell* **152**, 290–303.

[131] Kim, J., Kundu, M., Viollet, B. and Guan, K.-L. [2011] "AMPK and mTOR regulate autophagy through direct phosphorylation of ULK1" *Nat. Cell. Biol.* **13**, 132–141.

[132] Kim, Y., Islam, N., Moss, B. J., Nandakumar, M. P. and Marten, M. R. [2011] "Autophagy induced by rapamycin and carbon-starvation have distinct proteome profiles in aspergillus nidulans" *Biotechnology and bioengineering* **108**, 2705–2715.

Stellenbosch University https://scholar.sun.ac.za



[133] Kimball, S. R. and Jefferson, L. S. [2006] "Signaling pathways and molecular mechanisms through which branched-chain amino acids mediate translational control of protein synthesis" *J Nutr* **136**, 227S–231S.

[134] Kimura, S., Noda, T. and Yoshimori, T. [2008] "Dynein-dependent movement of autophagosome mediates effiicient encounters with lysosomes" *Cell Struct. Funct.* **33**, 109–122.

[135] Kimura, T., Jain, A., Choi, S. W., Mandell, M. A., Schroder, K., Johansen, T. and Deretic, V. [2015] "Trim-mediated precision autophagy targets cytoplasmic regulators of innate immunity" *J Cell Biol* **210**, 973–989.

[136] Kimura, T., Mandell, M. and Deretic, V. [2016] "Precision autophagy directed by receptor regulators–emerging examples within the trim family" *J Cell Sci* **129**, 881–891.

[137] Kirisako, T., Ichimura, Y., Okada, H., Kabeya, Y., Mizushima, N., Yoshimori, T., Ohsumi, M., Takao, T., Noda, T. and Ohsumi, Y. [2000] "The reversible modification regulates the membrane-binding state of Apg8/Aut7 essential for autophagy and the cytoplasm to vacuole targeting pathway" *J. Cell Biol.* **151**, 263–276.

[138] Klionsky, D., Abdelmohsen, K., Abe, A., Abedin, M., Abeliovich, H., Acevedo Arozena, A., Adachi, H., Adams, C., Adams, P., Adeli, K. *et al.* [2016] "Guidelines for the use and interpretation of assays for monitoring autophagy autophagy" *Autophagy* **12**, 1–222.

[139] Klionsky, D. J., Abdalla, F. C., Abeliovich, H., Abraham, R. T., Acevedo-Arozena, A., Adeli, K., Agholme, L., Agnello, M., Agostinis, P., Aguirre-Ghiso, J. A. *et al.* [2012] "Guidelines for the use and interpretation of assays for monitoring autophagy" *Autophagy* **8**, 445–544.

[140] Klionsky, D. J., Abeliovich, H., Agostinis, P., Agrawal, D. K., Aliev, G., Askew, D. S., Baba, M., Baehrecke, E. H., Bahr, B. A., Ballabio, A., Bamber, B. A., Bassham, D. C. and others. [2008] "Guidelines for the use and

Stellenbosch University https://scholar.sun.ac.za



interpretation of assays for monitoring autophagy in higher eukaryotes" *Autophagy* **4**, 151–175.

[141] Klionsky, D. J., Eskelinen, E.-L. and Deretic, V. [2014] "Autophagosomes, phagosomes, autolysosomes, phagolysosomes, autophagolysosomes... wait, i'm confused" *Autophagy* .

[142] Knævelsrud, H., Søreng, K., Raiborg, C., Håberg, K., Rasmuson, F., Brech, A., Liestøl, K., Rusten, T. E., Stenmark, H., Neufeld, T. P. *et al.* [2013] "Membrane remodeling by the PX-BAR protein SNX18 promotes autophagosome formation" *J Cell Biol* **202**, 331–349.

[143] Köchl, R., Hu, X. W., Chan, E. Y. and Tooze, S. A. [2006] "Microtubules facilitate autophagosome formation and fusion of autophagosomes with endosomes" *Traffic* **7**, 129–145.

[144] Koga, H., Martinez-Vicente, M., Macian, F., Verkhusha, V. V. and Cuervo, A. M. [2011] "A photoconvertible fluorescent reporter to track chaperone-mediated autophagy" *Nat. Commun.* **2**, 386.

[145] Kogot-Levin, A., Saada, A., Leibowitz, G., Soiferman, D., Douiev, L., Raz, I. and Weksler-Zangen, S. [2016] "Upregulation of mitochondrial content in cytochrome c oxidase deficient fibroblasts" *PloS one* **11**, e0165417.

[146] Komatsu, M., Waguri, S., Chiba, T., Murata, S., Iwata, J.-i., Tanida, I., Ueno, T., Koike, M., Uchiyama, Y., Kominami, E. and others. [2006] "Loss of autophagy in the central nervous system causes neurodegeneration in mice" *Nature* **441**, 880–884.

[147] Komatsu, M., Waguri, S., Koike, M., Sou, Y.-s., Ueno, T., Hara, T., Mizushima, N., Iwata, J.-i., Ezaki, J., Murata, S. and others. [2007] "Homeostatic levels of p62 control cytoplasmic inclusion body formation in autophagy-deficient mice" *Cell* **131**, 1149–1163.

[148] Komatsu, M., Waguri, S., Ueno, T., Iwata, J., Murata, S., Tanida, I., Ezaki, J., Mizushima, N., Ohsumi, Y., Uchiyama, Y., Kominami, E., Tanaka, K.

Stellenbosch University https://scholar.sun.ac.za



and Chiba, T. [2005] "Impairment of starvation-induced and constitutive autophagy in Atg7-deficient mice" *J. Cell Biol.* **169**, 425–434.

[149] Komatsu, M., Wang, Q. J., Holstein, G. R., Friedrich, V. L., Iwata, J.-i., Kominami, E., Chait, B. T., Tanaka, K. and Yue, Z. [2007] "Essential role for autophagy protein Atg7 in the maintenance of axonal homeostasis and the prevention of axonal degeneration" *Proc. Natl. Acad. Sci. U.S.A.* **104**, 14489–14494.

[150] Korolchuk, V. I. and Rubinsztein, D. C. [2011] "Regulation of autophagy by lysosomal positioning" *Autophagy* **7**, 927–928.

[151] Kroemer, G., Mariño, G. and Levine, B. [2010] "Autophagy and the integrated stress response" *Mol. Cell.* **40**, 280–293.

[152] Kuma, A., Hatano, M., Matsui, M., Yamamoto, A., Nakaya, H., Yoshimori, T., Ohsumi, Y., Tokuhisa, T. and Mizushima, N. [2004] "The role of autophagy during the early neonatal starvation period" *Nature* **432**, 1032–1036.

[153] Lagouge, M., Argmann, C., Gerhart-Hines, Z., Meziane, H., Lerin, C., Daussin, F., Messadeq, N., Milne, J., Lambert, P., Elliott, P. and et al. [2006] "Resveratrol improves mitochondrial function and protects against metabolic disease by activating SIRT1 and PGC-1" *Cell* **127**, 1109–1122.

[154] Lamark, T. and Johansen, T. [2012] "Aggrephagy: Selective Disposal of Protein Aggregates by Macroautophagy" .

[155] Lamb, C. A., Yoshimori, T. and Tooze, S. A. [2013] "The autophagosome: origins unknown, biogenesis complex" *Nature reviews Molecular cell biology* **14**, 759.

[156] Lee, I. H., Cao, L., Mostoslavsky, R., Lombard, D. B., Liu, J., Bruns, N. E., Tsokos, M., Alt, F. W. and Finkel, T. [2008] "A role for the NAD-dependent deacetylase sirt1 in the regulation of autophagy" *Proc. Natl. Acad. Sci. U.S.A.* **105**, 3374–3379.

Stellenbosch University https://scholar.sun.ac.za



[157] Lee, I. H. and Finkel, T. [2009] "Regulation of autophagy by the p300 acetyltransferase" *J. Biol. Chem.* **284**, 6322–6328.

[158] Lee, J. V., Carrer, A., Shah, S., Snyder, N. W., Wei, S., Venneti, S., Worth, A. J., Yuan, Z.-F., Lim, H.-W., Liu, S. and others. [2014] "Akt-dependent metabolic reprogramming regulates tumor cell histone acetylation" *Cell Metab.* **20**, 306–319.

[159] Lee, J. W., Park, S., Takahashi, Y. and Wang, H.-G. [2010] "The association of ampk with ulk1 regulates autophagy" *PloS one* **5**, e15394.

[160] Levine, B. and Klionsky, D. J. [2004] "Development by self-digestion: molecular mechanisms and biological functions of autophagy" *Dev. Cell.* **6**, 463–477.

[161] Levine, B. and Kroemer, G. [2008] "Autophagy in the pathogenesis of disease" *Cell* **132**, 27–42.

[162] Li, J., Yang, D., Wang, W., Piao, S., Zhou, J., Saiyin, W., Zheng, C., Sun, H. and Li, Y. [2015] "Inhibition of autophagy by 3-ma enhances il-24-induced apoptosis in human oral squamous cell carcinoma cells." *Journal of experimental & clinical cancer research : CR* **34**, 97.

[163] Li, Y., McGreal, S., Zhao, J., Huang, R., Zhou, Y., Zhong, H., Xia, M. and Ding, W.-X. [2016] "A cell-based quantitative high-throughput image screening identified novel autophagy modulators" *Pharmacol. Res.* **110**, 35–49.

[164] Liang, C., Feng, P., Ku, B., Dotan, I., Canaani, D., Oh, B.-H. and Jung, J. U. [2006] "Autophagic and tumour suppressor activity of a novel Beclin1-binding protein UVRAG" *Nat. Cell. Biol.* **8**, 688–698.

[165] Liang, C., Lee, J.-s., Inn, K.-S., Gack, M. U., Li, Q., Roberts, E. A., Vergne, I., Deretic, V., Feng, P., Akazawa, C. *et al.* [2008] "Beclin1-binding UVRAG targets the class C Vps complex to coordinate autophagosome maturation and endocytic trafficking" *Nature cell biology* **10**, 776.

Stellenbosch University https://scholar.sun.ac.za



[166] Liang, X. H., Jackson, S., Seaman, M., Brown, K., Kempkes, B., Hibshoosh, H. and Levine, B. [1999] "Induction of autophagy and inhibition of tumorigenesis by beclin 1" *Nature* **402**, 672–676.

[167] Lipka, J., Kuijpers, M., Jaworski, J. and Hoogenraad, C. C. [2013] "Mutations in cytoplasmic dynein and its regulators cause malformations of cortical development and neurodegenerative diseases" .

[168] Loos, B., du Toit, A. and Hofmeyr, J.-H. S. [2014] "Defining and measuring autophagosome flux–concept and reality" *Autophagy* **10**, 2087–2096.

[169] Loos, B., Engelbrecht, A.-M., Lockshin, R. A., Klionsky, D. J. and Zakeri, Z. [2013] "The variability of autophagy and cell death susceptibility: Unanswered questions" *Autophagy* **9**, 1270–1285.

[170] Lu, J., He, L., Behrends, C., Araki, M., Araki, K., Wang, Q. J., Catanzaro, J. M., Friedman, S. L., Zong, W.-X., Fiel, M. I. *et al.* [2014] "NRBF2 regulates autophagy and prevents liver injury by modulating Atg14L-linked phosphatidylinositol-3 kinase iii activity" *Nature communications* **5**, 3920.

[171] Lumkwana, D., du Toit, A., Kinnear, C. and Loos, B. [2017] "Autophagic flux control in neurodegeneration: Progress and precision targeting—where do we stand?" *Progress in neurobiology* **153**, 64–85.

[172] Luu, K., Luty, W. and Kumar, A. [2015] "Hts profiling method for autophagy-modulators: Mix-and-read autophagy and cell viability dyes enable simple, rapid high-throughput screening" *Genetic Engineering & Biotechnology News* **35**, 12–13.

[173] Mackeh, R., Lorin, S., Ratier, A., Mejdoubi-Charef, N., Baillet, A., Bruneel, A., Hamai, A., Codogno, P., Pous, C. and Perdiz, D. [2014] "Reactive oxygen species, AMP-activated protein kinase, and the transcription cofactor p300 regulate $\alpha$-tubulin acetyltransferase-1 ($\alpha$TAT-1/MEC-17)-dependent microtubule hyperacetylation during cell stress" *J. Biol. Chem.* **289**, 11816–11828.

Stellenbosch University https://scholar.sun.ac.za



[174] Mariño, G., Pietrocola, F., Eisenberg, T., Kong, Y., Malik, S. A., Andryushkova, A., Schroeder, S., Pendl, T., Harger, A., Niso-Santano, M. *et al.* [2014] "Regulation of autophagy by cytosolic acetyl-coenzyme A" *Mol. Cell.* **53**, 710–725.

[175] Martin, K. R., Barua, D., Kauffman, A. L., Westrate, L. M., Posner, R. G., Hlavacek, W. S. and MacKeigan, J. P. [2013] "Computational model for autophagic vesicle dynamics in single cells" *Autophagy* **9**, 74–92.

[176] Martinez-Vicente, M., Talloczy, Z., Wong, E., Tang, G., Koga, H., Kaushik, S., de Vries, R., Arias, E., Harris, S., Sulzer, D. and Cuervo, A. M. [2010] "Cargo recognition failure is responsible for inefficient autophagy in Huntington's disease" *Nat Neurosci* **13**, 567–576.

[177] Mathew, R., Karantza-Wadsworth, V. and White, E. [2007] "Role of autophagy in cancer" *Nat. Rev. Cancer* **7**, 961–967.

[178] Matsui, Y., Takagi, H., Qu, X., Abdellatif, M., Sakoda, H., Asano, T., Levine, B. and Sadoshima, J. [2007] "Distinct roles of autophagy in the heart during ischemia and reperfusion roles of AMP-activated protein kinase and Beclin 1 in mediating autophagy" *Circ. Res.* **100**, 914–922.

[179] Matsunaga, K., Morita, E., Saitoh, T., Akira, S., Ktistakis, N. T., Izumi, T., Noda, T. and Yoshimori, T. [2010] "Autophagy requires endoplasmic reticulum targeting of the pi3-kinase complex via atg14l" *The Journal of cell biology* **190**, 511–521.

[180] Matsunaga, K., Saitoh, T., Tabata, K., Omori, H., Satoh, T., Kurotori, N., Maejima, I., Shirahama-Noda, K., Ichimura, T., Isobe, T. *et al.* [2009] "Two Beclin 1-binding proteins, Atg14l and Rubicon, reciprocally regulate autophagy at different stages" *Nat. Cell. Biol.* **11**, 385–396.

[181] Matsuyama, S. S. and Jarvik, L. F. [1989] "Hypothesis: microtubules, a key to Alzheimer disease" *Proc. Natl. Acad. Sci. U.S.A.* **86**, 8152–8156.

Stellenbosch University https://scholar.sun.ac.za



[182] McEwan, D. G., Popovic, D., Gubas, A., Terawaki, S., Suzuki, H., Stadel, D., Coxon, F. P., de Stegmann, D. M., Bhogaraju, S., Maddi, K. *et al.* [2015] "PLEKHM1 regulates autophagosome-lysosome fusion through HOPS complex and LC3/GABARAP proteins" *Molecular cell* **57**, 39–54.

[183] Miclet, E., Stoven, V., Michels, P. A., Opperdoes, F. R., Lallemand, J.-Y. and Duffieux, F. [2001] "Nmr spectroscopic analysis of the first two steps of the pentose-phosphate pathway elucidates the role of 6-phosphogluconolactonase" *Journal of Biological Chemistry* .

[184] Milani, M., Rzymski, T., Mellor, H. R., Pike, L., Bottini, A., Generali, D. and Harris, A. L. [2009] "The role of atf4 stabilization and autophagy in resistance of breast cancer cells treated with bortezomib" *Cancer research* **69**, 4415–4423.

[185] Millecamps, S. and Julien, J.-P. [2013] "Axonal transport deficits and neurodegenerative diseases" *Nature Reviews Neuroscience* **14**, 161.

[186] Mindell, J. A. [2012] "Lysosomal acidification mechanisms" *Annual review of physiology* **74**, 69–86.

[187] Mizushima, N., Levine, B., Cuervo, A. M. and Klionsky, D. J. [2008] "Autophagy fights disease through cellular self-digestion" *Nature* **451**, 1069–1075.

[188] Mizushima, N., Noda, T. and Ohsumi, Y. [1999] "Apg16p is required for the function of the Apg12p–Apg5p conjugate in the yeast autophagy pathway" *EMBO J.* **18**, 3888–3896.

[189] Mizushima, N., Yamamoto, A., Matsui, M., Yoshimori, T. and Ohsumi, Y. [2003] "In vivo analysis of autophagy in response to nutrient starvation using transgenic mice expressing a fluorescent autophagosome marker" *Mol. Biol. Cell* **15**, 1101–1111.

[190] Mizushima, N. and Yoshimori, T. [2007] "How to interpret LC3 immunoblotting" *Autophagy* **3**, 542–545.

Stellenbosch University https://scholar.sun.ac.za



[191] Mizushima, N., Yoshimori, T. and Levine, B. [2010] "Methods in mammalian autophagy research" *Cell* **140**, 313–326.

[192] Monastyrska, I., Rieter, E., Klionsky, D. J. and Reggiori, F. [2009] "Multiple roles of the cytoskeleton in autophagy" *Biological Reviews* **84**, 431–448.

[193] Morozova, K., Clement, C. C., Kaushik, S., Stiller, B., Arias, E., Ahmad, A., Rauch, J. N., Chatterjee, V., Melis, C., Scharf, B. *et al.* [2016] "Structural and biological interaction of hsc-70 protein with phosphatidylserine in endosomal microautophagy" *Journal of Biological Chemistry* **291**, 18096–18106.

[194] Morselli, E., Mariño, G., Bennetzen, M. V., Eisenberg, T., Megalou, E., Schroeder, S., Cabrera, S., Bénit, P., Rustin, P., Criollo, A. *et al.* [2011] "Spermidine and resveratrol induce autophagy by distinct pathways converging on the acetylproteome" *J. Cell Biol.* **192**, 615–629.

[195] Mortimore, G. E. and Poso, A. R. [1987] "Intracellular protein catabolism and its control during nutrient deprivation and supply" *Annu. Rev. Nutr.* **7**, 539–568.

[196] Mortimore, G. E. and Schworer, C. M. [1977] "Induction of autophagy by amino-acid deprivation in perfused rat liver" *Nature* **270**, 174–176.

[197] Motoi, Y., Shimada, K., Ishiguro, K. and Hattori, N. [2014] "Lithium and autophagy" *ACS chemical neuroscience* **5**, 434–442.

[198] Nair, U., Jotwani, A., Geng, J., Gammoh, N., Richerson, D., Yen, W.-L., Griffith, J., Nag, S., Wang, K., Moss, T. *et al.* [2011] "SNARE proteins are required for macroautophagy" *Cell* **146**, 290–302.

[199] Nakagawa, I., Amano, A., Mizushima, N., Yamamoto, A., Yamaguchi, H., Kamimoto, T., Nara, A., Funao, J., Nakata, M., Tsuda, K., Hamada, S. and Yoshimori, T. [2004] "Autophagy defends cells against invading group A Streptococcus." *Science (New York, N.Y.)* **306**, 1037–1040.

Stellenbosch University https://scholar.sun.ac.za



[200] Nakaso, K., Yoshimoto, Y., Nakano, T., Takeshima, T., Fukuhara, Y., Yasui, K., Araga, S., Yanagawa, T., Ishii, T. and Nakashima, K. [2004] "Transcriptional activation of p62/A170/ZIP during the formation of the aggregates: possible mechanisms and the role in lewy body formation in Parkinson's disease" *Brain Res.* **1012**, 42–51.

[201] Nazio, F., Strappazzon, F., Antonioli, M., Bielli, P., Cianfanelli, V., Bordi, M., Gretzmeier, C., Dengjel, J., Piacentini, M., Fimia, G. M. *et al.* [2013] "mTOR inhibits autophagy by controlling ULK1 ubiquitylation, self-association and function through AMBRA1 and TRAF6" *Nat. Cell. Biol.* **15**, 406–416.

[202] Nguyen, T. N., Padman, B. S., Usher, J., Oorschot, V., Ramm, G. and Lazarou, M. [2016] "Atg8 family LC3/GABARAP proteins are crucial for autophagosome–lysosome fusion but not autophagosome formation during PINK1/Parkin mitophagy and starvation" *J Cell Biol* **215**, 857–874.

[203] Nixon, R. A. [2007] "Autophagy, amyloidogenesis and Alzheimer disease" *J. Cell. Sci.* **120**, 4081–4091.

[204] Noro, T., Namekata, K., Azuchi, Y., Kimura, A., Guo, X., Harada, C., Nakano, T., Tsuneoka, H. and Harada, T. [2015] "Spermidine ameliorates neurodegeneration in a mouse model of normal tension glaucoma" *Investigative Ophthalmology & Visual Science* **56**, 5012–5019.

[205] Novikoff, A. B. [1959] "The proximal tubule cell in experimental hydronephrosis" *J. Biophys. Biochem. Cytol.* **6**, 136–138.

[206] Olivier, B. G., Rohwer, J. M. and Hofmeyr, J.-H. S. [2005] "Modelling cellular systems with PySCeS" *Bioinformatics* **21**, 560–561.

[207] Olsvik, H. L., Lamark, T., Takagi, K., Larsen, K. B., Evjen, G., Øvervatn, A., Mizushima, T. and Johansen, T. [2015] "Fyco1 contains a c-terminally extended, lc3a/b-preferring lc3-interacting region (lir) motif required for ef-

Stellenbosch University https://scholar.sun.ac.za



ficient maturation of autophagosomes during basal autophagy" *Journal of Biological Chemistry* **290**, 29361–29374.

[208] Pandey, U. B., Nie, Z., Batlevi, Y., McCray, B. A., Ritson, G. P., Nedelsky, N. B., Schwartz, S. L., DiProspero, N. A., Knight, M. A., Schuldiner, O. *et al.* [2007] "HDAC6 rescues neurodegeneration and provides an essential link between autophagy and the UPS" *Nature* **447**, 860–864.

[209] Pankiv, S., Clausen, T. H., Lamark, T., Brech, A., Bruun, J.-A., Outzen, H., Øvervatn, A., Bjørkøy, G. and Johansen, T. [2007] "p62/SQSTM1 binds directly to Atg8/LC3 to facilitate degradation of ubiquitinated protein aggregates by autophagy" *J. Biol. Chem.* **282**, 24131–24145.

[210] Papandreou, I., Lim, A., Laderoute, K. and Denko, N. [2008] "Hypoxia signals autophagy in tumor cells via AMPK activity, independent of HIF-1, BNIP3, and BNIP3L" *Cell Death Differ.* **15**, 1572–1581.

[211] Patel, P. K., Shirihai, O. and Huang, K. C. [2013] "Optimal dynamics for quality control in spatially distributed mitochondrial networks" *PLoS computational biology* **9**, e1003108.

[212] Petherick, K. J., Conway, O. J., Mpamhanga, C., Osborne, S. A., Kamal, A., Saxty, B. and Ganley, I. G. [2015] "Pharmacological inhibition of ulk1 blocks mtor-dependent autophagy" *J. Biol. Chem.* pp. jbc–C114.

[213] Pietrocola, F., Lachkar, S., Enot, D. P., Niso-Santano, M., Bravo-San Pedro, J. M., Sica, V., Izzo, V., Maiuri, M. C., Madeo, F., Mariño, G. and Kroemer, G. [2015] "Spermidine induces autophagy by inhibiting the acetyltransferase ep300." *Cell death and differentiation* **22**, 509–516.

[214] Proikas-Cezanne, T., Takacs, Z., Dönnes, P. and Kohlbacher, O. [2015] "WIPI proteins: essential PtdIns3P effectors at the nascent autophagosome" *J Cell Sci* **128**, 207–217.

[215] Qu, X., Yu, J., Bhagat, G., Furuya, N., Hibshoosh, H., Troxel, A., Rosen, J., Eskelinen, E.-L., Mizushima, N., Ohsumi, Y. *et al.* [2003] "Promotion of

Stellenbosch University https://scholar.sun.ac.za



tumorigenesis by heterozygous disruption of the Beclin 1 autophagy gene" *J. Clin. Invest.* **112**, 1809.

[216] Ragelle, H., Naba, A., Larson, B. L., Zhou, F., Prijić, M., Whittaker, C. A., Del Rosario, A., Langer, R., Hynes, R. O. and Anderson, D. G. [2017] "Comprehensive proteomic characterization of stem cell-derived extracellular matrices" *Biomaterials* **128**, 147–159.

[217] Ravikumar, B., Acevedo-Arozena, A., Imarisio, S., Berger, Z., Vacher, C., O'Kane, C. J., Brown, S. D. and Rubinsztein, D. C. [2005] "Dynein mutations impair autophagic clearance of aggregate-prone proteins" *Nat. Genet.* **37**, 771–776.

[218] Ravikumar, B., Vacher, C., Berger, Z., Davies, J. E., Luo, S., Oroz, L. G., Scaravilli, F., Easton, D. F., Duden, R., O'Kane, C. J. and Rubinsztein, D. C. [2004] "Inhibition of mTOR induces autophagy and reduces toxicity of polyglutamine expansions in fly and mouse models of Huntington disease" *Nat. Genet.* **36**, 585–595.

[219] Roberts, D. J., Tan-Sah, V. P., Ding, E. Y., Smith, J. M. and Miyamoto, S. [2014] "Hexokinase-ii positively regulates glucose starvation-induced autophagy through TORC1 inhibition" *Mol. Cell.* **53**, 521–533.

[220] Rodriguez-Enriquez, S., Kim, I., Currin, R. T. and Lemasters, J. J. [2006] "Tracker dyes to probe mitochondrial autophagy (mitophagy) in rat hepatocytes" *Autophagy* **2**, 39–46.

[221] Rogers, G. W., Richter, N. J., Lima, W. F. and Merrick, W. C. [2001] "Modulation of the helicase activity of eif4a by eif4b, eif4h, and eif4f" *Journal of Biological Chemistry* **276**, 30914–30922.

[222] Rogov, V., Dötsch, V., Johansen, T. and Kirkin, V. [2014] "Interactions between autophagy receptors and ubiquitin-like proteins form the molecular basis for selective autophagy" *Molecular cell* **53**, 167–178.

Stellenbosch University https://scholar.sun.ac.za



[223] Rojczyk-Golebiewska, E., Palasz, A., Worthington, J. J., Markowski, G. and Wiaderkiewicz, R. [2015] "Neurolight–astonishing advances in brain imaging" *International Journal of Neuroscience* **125**, 91–99.

[224] Rose, C., Menzies, F. M., Renna, M., Acevedo-Arozena, A., Corrochano, S., Sadiq, O., Brown, S. D. and Rubinsztein, D. C. [2010] "Rilmenidine attenuates toxicity of polyglutamine expansions in a mouse model of Huntingtons disease" *Hum. Mol. Genet.* **19**, 2144–2153.

[225] Rubinsztein, D. C. [2006] "The roles of intracellular protein-degradation pathways in neurodegeneration" *Nature* **443**, 780–786.

[226] Rubinsztein, D. C., Cuervo, A. M., Ravikumar, B., Sarkar, S., Korolchuk, V., Kaushik, S. and Klionsky, D. J. [2009] "In search of an "autophagomometer"" *Autophagy* **5**, 585–589.

[227] Rubinsztein, D. C., DiFiglia, M., Heintz, N., Nixon, R. A., Qin, Z.-H., Ravikumar, B., Stefanis, L. and Tolkovsky, A. [2005] "Autophagy and its possible roles in nervous system diseases, damage and repair" *Autophagy* **1**, 11–22.

[228] Russell, R. C., Yuan, H.-X. and Guan, K.-L. [2013] "Autophagy regulation by nutrient signaling" *Cell Res.* **24**, 42–57.

[229] Sancak, Y., Bar-Peled, L., Zoncu, R., Markhard, A. L., Nada, S. and Sabatini, D. M. [2010] "Ragulator-Rag complex targets mTORC1 to the lysosomal surface and is necessary for its activation by amino acids" *Cell* **141**, 290–303.

[230] Sarkar, S., Floto, R. A., Berger, Z., Imarisio, S., Cordenier, A., Pasco, M., Cook, L. J. and Rubinsztein, D. C. [2005] "Lithium induces autophagy by inhibiting inositol monophosphatase" *J Cell Biol* **170**, 1101–1111.

[231] Sarkar, S., Ravikumar, B., Floto, R. A. and Rubinsztein, D. C. [2009] "Rapamycin and mTOR-independent autophagy inducers ameliorate toxicity of

Stellenbosch University https://scholar.sun.ac.za



polyglutamine-expanded huntingtin and related proteinopathies" *Cell Death Differ.* **16**, 46–56.

[232] Schleich, K., Warnken, U., Fricker, N., Öztürk, S., Richter, P., Kammerer, K., Schnölzer, M., Krammer, P. H. and Lavrik, I. N. [2012] "Stoichiometry of the cd95 death-inducing signaling complex: experimental and modeling evidence for a death effector domain chain model" *Molecular cell* **47**, 306–319.

[233] Seglen, P. O. and Gordon, P. B. [1982] "3-methyladenine: specific inhibitor of autophagic/lysosomal protein degradation in isolated rat hepatocytes" *Proc. Natl. Acad. Sci. U.S.A.* **79**, 1889–1892.

[234] Settembre, C., Fraldi, A., Medina, D. L. and Ballabio, A. [2013] "Signals from the lysosome: a control centre for cellular clearance and energy metabolism" *Nat. Rev. Mol. Cell. Biol.* **14**, 283–296.

[235] Shi, W., Xiao, D., Wang, L., Dong, L., Yan, Z., Shen, Z., Chen, S., Chen, Y. and Zhao, W. [2012] "Therapeutic metformin/AMPK activation blocked lymphoma cell growth via inhibition of mTOR pathway and induction of autophagy" *Cell Death and Disease* **3**, e275.

[236] Shibutani, S. T. and Yoshimori, T. [2014] "A current perspective of autophagosome biogenesis" *Cell Res.* **24**, 58.

[237] Shimobayashi, M. and Hall, M. N. [2014] "Making new contacts: the mTOR network in metabolism and signalling crosstalk" *Nat. Rev. Mol. Cell. Biol.* **15**, 155–162.

[238] Shu, C.-W., Liu, P.-F. and Huang, C.-M. [2012] "High throughput screening for drug discovery of autophagy modulators" *Combinatorial chemistry & high throughput screening* **15**, 721–729.

[239] Singh, R. and Cuervo, A. M. [2011] "Autophagy in the cellular energetic balance" *Cell Metab.* **13**, 495–504.

Stellenbosch University https://scholar.sun.ac.za



[240] Son, J. H., Shim, J. H., Kim, K.-H., Ha, J.-Y. and Han, J. Y. [2012] "Neuronal autophagy and neurodegenerative diseases" *Experimental & Molecular Medicine* **44**, 89–98.

[241] Stetter, C., Hirschberg, M., Nieswandt, B., Ernestus, R.-I., Heckmann, M. and Sirén, A.-L. [2013] "An experimental protocol for in vivo imaging of neuronal structural plasticity with 2-photon microscopy in mice." *Experimental & translational stroke medicine* **5**, 9.

[242] Stolz, A., Ernst, A. and Dikic, I. [2014] "Cargo recognition and trafficking in selective autophagy" *Nature cell biology* **16**, 495.

[243] Sui, X., Chen, R., Wang, Z., Huang, Z., Kong, N., Zhang, M., Han, W., Lou, F., Yang, J., Zhang, Q. *et al.* [2013] "Autophagy and chemotherapy resistance: a promising therapeutic target for cancer treatment" *Cell death & disease* **4**, e838.

[244] Sun, Q., Fan, W., Chen, K., Ding, X., Chen, S. and Zhong, Q. [2008] "Identification of Barkor as a mammalian autophagy-specific factor for Beclin 1 and class iii phosphatidylinositol 3-kinase" *Proc. Natl. Acad. Sci. U.S.A.* **105**, 19211–19216.

[245] Susaki, E. A. and Ueda, H. R. [2016] "Whole-body and whole-organ clearing and imaging techniques with single-cell resolution: toward organism-level systems biology in mammals" *Cell chemical biology* **23**, 137–157.

[246] Suzuki, K., Kirisako, T., Kamada, Y., Mizushima, N., Noda, T. and Ohsumi, Y. [2001] "The pre-autophagosomal structure organized by concerted functions of APG genes is essential for autophagosome formation" *EMBO J.* **20**, 5971–5981.

[247] Suzuki, K., Kubota, Y., Sekito, T. and Ohsumi, Y. [2007] "Hierarchy of Atg proteins in pre-autophagosomal structure organization" *Genes Cells* **12**, 209–218.

Stellenbosch University https://scholar.sun.ac.za



[248] Swart, C., Khoza, A., Khan, K., Roux, S., du Plessis, A. and Loos, B. [2017] "Investigating basal autophagic activity in brain regions associated with neurodegeneration using in vivo and ex vivo models." *Journal of Alzheimers Disease & Parkinsonism* .

[249] Tanaka, M., Kim, Y. M., Lee, G., Junn, E., Iwatsubo, T. and Mouradian, M. M. [2004] "Aggresomes formed by $\alpha$-synuclein and synphilin-1 are cytoprotective" *J. Biol. Chem.* **279**, 4625–4631.

[250] Tanaka, Y., Guhde, G., Suter, A., Eskelinen, E.-L., Hartmann, D., Lüllmann-Rauch, R., Janssen, P. M. L., Blanz, J., von Figura, K. and Paul, S. [2000] "Accumulation of autophagic vacuoles and cardiomyopathy in LAMP-2-deficient mice" *Nature* **406**, 902–906.

[251] Tanida, I., Minematsu-Ikeguchi, N., Ueno, T. and Kominami, E. [2005] "Lysosomal turnover, but not a cellular level, of endogenous LC3 is a marker for autophagy" *Autophagy* **1**, 84–91.

[252] Tasdemir, E., Maiuri, M. C., Galluzzi, L., Vitale, I., Djavaheri-Mergny, M., D'Amelio, M., Criollo, A., Morselli, E., Zhu, C., Harper, F. *et al.* [2008] "Regulation of autophagy by cytoplasmic p53" *Nat. Cell. Biol.* **10**, 676–687.

[253] Terman, A., Gustafsson, B. and Brunk, U. T. [2007] "Autophagy, organelles and ageing" *The Journal of Pathology* **211**, 134–143.

[254] Thoresen, S. B., Pedersen, N. M., Liestøl, K. and Stenmark, H. [2010] "A phosphatidylinositol 3-kinase class iii sub-complex containing VPS15, VPS34, Beclin 1, UVRAG and BIF-1 regulates cytokinesis and degradative endocytic traffic" *Exp. Cell Res.* **316**, 3368–3378.

[255] Tian, Y., Li, Z., Hu, W., Ren, H., Tian, E., Zhao, Y., Lu, Q., Huang, X., Yang, P., Li, X. *et al.* [2010] "C. elegans screen identifies autophagy genes specific to multicellular organisms" *Cell* **141**, 1042–1055.

[256] Tinevez, J.-Y., Perry, N., Schindelin, J., Hoopes, G. M., Reynolds, G. D., Laplantine, E., Bednarek, S. Y., Shorte, S. L. and Eliceiri, K. W. [2017]

Stellenbosch University https://scholar.sun.ac.za



"Trackmate: An open and extensible platform for single-particle tracking" *Methods* **115**, 80–90.

[257] Tomer, R., Ye, L., Hsueh, B. and Deisseroth, K. [2014] "Advanced clarity for rapid and high-resolution imaging of intact tissuesgy" *Nat. Protoc.* **9**, 1682–1697.

[258] Tracy, K., Dibling, B. C., Spike, B. T., Knabb, J. R., Schumacker, P. and Macleod, K. F. [2007] "BNIP3 is an RB/E2F target gene required for hypoxia-induced autophagy" *Mol. Cell. Biol.* **27**, 6229–6242.

[259] Tsuboyama, K., Koyama-Honda, I., Sakamaki, Y., Koike, M., Morishita, H. and Mizushima, N. [2016] "The ATG conjugation systems are important for degradation of the inner autophagosomal membrane" *Science* **354**, 1036–1041.

[260] Tsvetkov, A. S., Arrasate, M., Barmada, S., Ando, D. M., Sharma, P., Shaby, B. A. and Finkbeiner, S. [2013] "Proteostasis of polyglutamine varies among neurons and predicts neurodegeneration" *Nat. Chem. Biol.* **9**, 586–592.

[261] Uytterhoeven, V., Lauwers, E., Maes, I., Miskiewicz, K., Melo, M. N., Swerts, J., Kuenen, S., Wittocx, R., Corthout, N., Marrink, S.-J. *et al.* [2015] "Hsc70-4 deforms membranes to promote synaptic protein turnover by endosomal microautophagy" *Neuron* **88**, 735–748.

[262] Vartiainen, M. K., Sarkkinen, E. M., Matilainen, T., Salminen, M. and Lappalainen, P. [2003] "Mammals have two twinfilin isoforms whose subcellular localizations and tissue distributions are differentially regulated" *Journal of Biological Chemistry* **278**, 34347–34355.

[263] Vodret, S., Bortolussi, G., Jašprová, J., Vitek, L. and Muro, A. F. [2017] "Inflammatory signature of cerebellar neurodegeneration during neonatal hyperbilirubinemia in ugt1-/-mouse model" *Journal of neuroinflammation* **14**, 64.

Stellenbosch University https://scholar.sun.ac.za



[264] Vucicevic, L., Misirkic, M., Kristina, J., Vilimanovich, U., Sudar, E., Isenovic, E., Prica, M., Harhaji-Trajkovic, L., Kravic-Stevovic, T., Vladimir, B. *et al.* [2011] "Compound c induces protective autophagy in cancer cells through ampk inhibition-independent blockade of akt/mtor pathway" *Autophagy* **7**, 40–50.

[265] Wang, B.-S., Liu, Y.-Z., Yang, Y., Zhang, Y., Hao, J.-J., Yang, H., Wang, X.-M., Zhang, Z.-Q., Zhan, Q.-M. and Wang, M.-R. [2013] "Autophagy negatively regulates cancer cell proliferation via selectively targeting VPRBP" *Clin. Sci.* **124**, 203–214.

[266] Wang, H., Bedford, F. K., Brandon, N. J., Moss, S. J. and Olsen, R. W. [1999] "GABAA-receptor-associated protein links GABAA receptors and the cytoskeleton" *Nature* **397**, 69–72.

[267] Wang, X. J., Yu, J., Wong, S. H., Cheng, A. S. L., Chan, F. K. L., Ng, S. S. M., Cho, C. H., Sung, J. J. Y. and Wu, W. K. K. [2013] "A novel crosstalk between two major protein degradation systems: regulation of proteasomal activity by autophagy" *Autophagy* **9**, 1500–1508.

[268] Warr, M. R., Binnewies, M., Flach, J., Reynaud, D., Garg, T., Malhotra, R., Debnath, J. and Passegué, E. [2013] "FOXO3A directs a protective autophagy program in haematopoietic stem cells" *Nature* **494**, 323–327.

[269] Wauson, E. M., Dbouk, H. A., Ghosh, A. B. and Cobb, M. H. [2014] "G protein-coupled receptors and the regulation of autophagy" *Trends Endocrinol. Metab.* **25**, 274–282.

[270] Webb, J. D., Murányi, A., Pugh, C. W., Ratcliffe, P. J. and Coleman, M. L. [2009] "Mypt1, the targeting subunit of smooth-muscle myosin phosphatase, is a substrate for the asparaginyl hydroxylase factor inhibiting hypoxia-inducible factor (fih)" *Biochemical Journal* **420**, 327–336.

Stellenbosch University https://scholar.sun.ac.za



[271] Wei, Y., Chiang, W.-C., Sumpter, R., Mishra, P. and Levine, B. [2017] "Prohibitin 2 is an inner mitochondrial membrane mitophagy receptor" *Cell* **168**, 224–238.

[272] White, E. [2012] "Deconvoluting the context-dependent role for autophagy in cancer" *Nat. Rev. Cancer* **12**, 401–410.

[273] Wilkinson, D. S., Jariwala, J. S., Anderson, E., Mitra, K., Meisenhelder, J., Chang, J. T., Ideker, T., Hunter, T., Nizet, V., Dillin, A. *et al.* [2015] "Phosphorylation of LC3 by the Hippo kinases STK3/STK4 is essential for autophagy" *Molecular cell* **57**, 55–68.

[274] Williams, A., Sarkar, S., Cuddon, P., Ttofi, E. K., Saiki, S., Siddiqi, F. H., Jahreiss, L., Fleming, A., Pask, D., Goldsmith, P., O'Kane, C. J., Floto, R. A. and Rubinsztein, D. C. [2008] "Novel targets for huntington's disease in an mTOR-independent autophagy pathway" *Nat. Chem. Biol.* **4**, 295–305.

[275] Wu, Y.-T., Tan, H.-L., Shui, G., Bauvy, C., Huang, Q., Wenk, M. R., Ong, C.-N., Codogno, P. and Shen, H.-M. [2010] "Dual role of 3-methyladenine in modulation of autophagy via different temporal patterns of inhibition on class i and iii phosphoinositide 3-kinase." *The Journal of biological chemistry* **285**, 10850–10861.

[276] Wullschleger, S., Loewith, R. and Hall, M. N. [2006] "Tor signaling in growth and metabolism." *Cell* **124**, 471–484.

[277] Xia, P., Wang, J.-J., Zhao, B.-B. and Song, C.-L. [2013] "The role of Beclin-1 expression in patients with gastric cancer: a meta-analysis" *Tumor Biol.* **34**, 3303–3307.

[278] Xie, Z., Lau, K., Eby, B., Lozano, P., He, C., Pennington, B., Li, H., Rathi, S., Dong, Y., Tian, R., Kem, D. and Zou, M.-H. [2011] "Improvement of cardiac functions by chronic metformin treatment is associated with enhanced cardiac autophagy in diabetic OVE26 mice" *Diabetes* p. DB_100351.

Stellenbosch University https://scholar.sun.ac.za



[279] Xie, Z., Nair, U. and Klionsky, D. J. [2008] "Atg8 controls phagophore expansion during autophagosome formation" *Mol. Biol. Cell* **19**, 3290–3298.

[280] Yamamoto, A., Tagawa, Y., Yoshimori, T., Moriyama, Y., Masaki, R. and Tashiro, Y. [1998] "Bafilomycin A1 prevents maturation of autophagic vacuoles by inhibiting fusion between autophagosomes and lysosomes in rat hepatoma cell line, H-4-II-E cells" *Cell Struct. Funct.* **23**, 33–42.

[281] Yang, W., Hong, Y. H., Shen, X.-Q., Frankowski, C., Camp, H. S. and Leff, T. [2001] "Regulation of transcription by AMP-activated protein kinase" *J. Biol. Chem.* **276**, 38341–38344.

[282] Yang, Z. J., Chee, C. E., Huang, S. and Sinicrope, F. A. [2011] "The role of autophagy in cancer: Therapeutic implications" *Mol. Cancer Ther.* **10**, 1533–1541.

[283] Ylä-Anttila, P., Vihinen, H., Jokitalo, E. and Eskelinen, E.-L. [2009] "Monitoring autophagy by electron microscopy in mammalian cells" *Methods Enzymol.* **452**, 143–164.

[284] Yu, L., McPhee, C. K., Zheng, L., Mardones, G. A., Rong, Y., Peng, J., Mi, N., Zhao, Y., Liu, Z., Wan, F. and et al. [2010] "Termination of autophagy and reformation of lysosomes regulated by mTOR" *Nature* **465**, 942–946.

[285] Yu, W. H., Cuervo, A. M., Kumar, A., Peterhoff, C. M., Schmidt, S. D., Lee, J.-H., Mohan, P. S., Mercken, M., Farmery, M. R., Tjernberg, L. O. *et al.* [2005] "Macroautophagy: a novel $\beta$-amyloid peptide-generating pathway activated in Alzheimer's disease" *J. Cell Biol.* **171**, 87–98.

[286] Yuan, H.-X., Russell, R. C. and Guan, K.-L. [2013] "Regulation of PIK3C3/VPS34 complexes by m TOR in nutrient stress-induced autophagy" *Autophagy* **9**, 1983–1995.

[287] Yue, Z., Jin, S., Yang, C., Levine, A. J. and Heintz, N. [2003] "Beclin 1, an autophagy gene essential for early embryonic development, is a haploinsufficient tumor suppressor" *Proc. Natl. Acad. Sci. U.S.A.* **100**, 15077–15082.

Stellenbosch University https://scholar.sun.ac.za



[288] Zhang, H., Bosch-Marce, M., Shimoda, L. A., Tan, Y. S., Baek, J. H., Wesley, J. B., Gonzalez, F. J. and Semenza, G. L. [2008] "Mitochondrial autophagy is an HIF-1-dependent adaptive metabolic response to hypoxia" *J. Biol. Chem.* **283**, 10892–10903.

[289] Zhong, Y., Wang, Q. J., Li, X., Yan, Y., Backer, J. M., Chait, B. T., Heintz, N. and Yue, Z. [2009] "Distinct regulation of autophagic activity by atg14l and rubicon associated with beclin 1–phosphatidylinositol-3-kinase complex" *Nature cell biology* **11**, 468.